



**Universiteit
Leiden**
The Netherlands

Development of the cardiac conduction system and cardiac anatomy in relation to genesis and treatment of arrhythmias

Jongbloed, Monica Reina Maria

Citation

Jongbloed, M. R. M. (2006, May 31). *Development of the cardiac conduction system and cardiac anatomy in relation to genesis and treatment of arrhythmias*. Retrieved from <https://hdl.handle.net/1887/4426>

Version: Corrected Publisher's Version

License: [Licence agreement concerning inclusion of doctoral thesis in the Institutional Repository of the University of Leiden](#)

Downloaded from: <https://hdl.handle.net/1887/4426>

Note: To cite this publication please use the final published version (if applicable).

Development of the Cardiac Conduction System
and Cardiac Anatomy in Relation to
Genesis and Treatment of Arrhythmias

This thesis was prepared at the Department of Cardiology, Anatomy & Embryology and Radiology of the Leiden University Medical Center, Leiden, The Netherlands.

Copyright © 2006 Monique R.M. Jongbloed, Leiden, The Netherlands. All rights reserved. No part of this book may be reproduced or transmitted, in any form or by any means, without prior permission of the author.

Cover:

Figure: AMIRA 3-D reconstruction of an embryonic heart (E14.5)

Reconstruction made by M.R.M. Jongbloed and L.J. Wisse.

Cover layout and design by Evelien M. den Hartoog

Layout:

Buijten & Schipperheijn, Jan Nieuwenhuis

Printed by:

Buijten & Schipperheijn,

Amsterdam, The Netherlands

ISBN: 90-9020727-9

Development of the Cardiac Conduction System
and Cardiac Anatomy in Relation to
Genesis and Treatment of Arrhythmias

Proefschrift

ter verkrijging van
de graad van Doctor aan de Universiteit Leiden,
op gezag van de Rector Magnificus Dr. D.D. Breimer,
hoogleraar in de faculteit der Wiskunde en
Natuurwetenschappen en die der Geneeskunde,
volgens besluit van het College voor Promoties
te verdedigen op woensdag 31 mei 2006
klokke 15.15 uur

door

Monica Reina Maria Jongbloed

Geboren te Alkmaar
in 1972

Promotiecommissie

Promotores: Prof. Dr. M.J. Schalijs
Prof. Dr. A.C. Gittenberger-de Groot

Co-promotor: Prof. Dr. J.J. Bax

Referent: Prof. Dr. R.N.W. Hauer (Universitair Medisch Centrum, Utrecht)

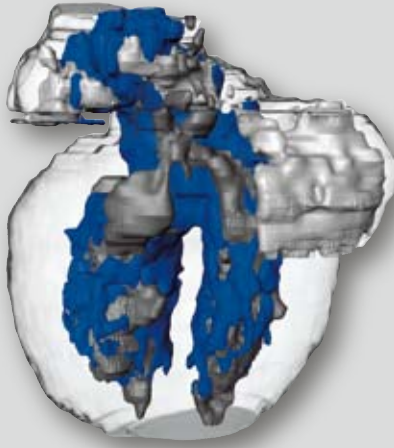
Overige leden: Prof. Dr. A.A.M. Wilde (Universiteit van Amsterdam)
Prof. Dr. E.E. van der Wall

Voor mijn ouders

Table of Contents

Chapter 1	General Introduction	9
Part I:	<i>Exploration of Cardiac Development and Anatomy in Relation to the Genesis of Clinical Arrhythmias</i>	59
Chapter 2	Embryonic Conduction Tissue: A Spatial Correlation with Adult Arrhythmogenic Areas. Transgenic CCS- <i>lacZ</i> Expression in the Cardiac Conduction System of Murine Embryos <i>J Cardiovasc Electrophysiol</i> 2004;15(3):349-355	61
Chapter 3	Development of the Right Ventricular Inflow Tract and Moderator Band; Possible Morphological and Functional Explanation for Mahaim Tachycardia <i>Circ Res</i> 2005;96(7):776-83	79
Chapter 4	Histology of Vascular-Myocardial Wall of Left Atrial Body after Pulmonary Venous Incorporation <i>Am J Cardiol</i> 2006 Mar 1;97(5):662-70	97
Part II:	<i>Exploration of Cardiac Anatomy using Different Imaging Techniques to Guide the Treatment of Arrhythmias</i>	113
Chapter 5	Multi-Slice CT of Pulmonary Vein Anatomy prior to Radiofrequency Catheter Ablation-Initial Experience <i>Radiology</i> 2005;243(3):702-9	115
Chapter 6	Clinical Applications of Intracardiac Echocardiography in Percutaneous Interventional Procedures <i>Heart</i> 2005;91(7):981-90	131
Chapter 7	Anatomical observations of the Pulmonary Veins with Intracardiac Echocardiography and Hemodynamic Consequences of Narrowing of Pulmonary Vein Ostial Diameters after Radiofrequency Catheter Ablation of Atrial Fibrillation <i>Am J Cardiol</i> 2004;93(10):1298-302	149

Chapter 8	Multi-slice Computed Tomography versus Intracardiac Echocardiography to Evaluate the Pulmonary Veins Prior to Radiofrequency Catheter Ablation of Atrial Fibrillation: A Head-to-head Comparison <i>J Am Coll Cardiol</i> 2005;45(3):343-50	163
Chapter 9	Non-invasive Visualization of the Cardiac Venous System Using Multi-Slice Computed Tomography <i>J Am Coll Cardiol</i> 2005;45(5):749-53	181
Chapter 10	Left Atrial tachycardia Originating from the Mitral Annulus-Aorta Junction <i>Circulation</i> 2004;110(20):3187-3192	193
	Summary & Conclusions	209
	Samenvatting en Conclusies	219
	List of Publications	229
	Acknowledgements	233
	Curriculum Vitae	237



Chapter

1

General Introduction

General Introduction

Cardiac arrhythmias are frequently encountered in clinical practice. Clinical mapping studies demonstrate that arrhythmias are often encountered at specific anatomical sites. In part I of this thesis, a developmental origin of clinical arrhythmias is hypothesized. The development of the heart and the cardiac conduction system cannot be seen as loose entities, but are narrowly related (**Figure 1**). As an introduction to this thesis therefore first cardiac development will be described shortly, where after the development of the cardiac conduction system is addressed. Subsequently anatomical predilection sites of the occurrence of clinical arrhythmias will be described in relation to cardiac development. Following on the description of the basics of cardiac development and the development of the cardiac conduction system, attention will be focused on current knowledge of clinical arrhythmias in adults in relation to cardiac anatomy, the treatment of these arrhythmias and imaging techniques used to visualise the substrate. These clinical issues will further be addressed in part II of the thesis.

10

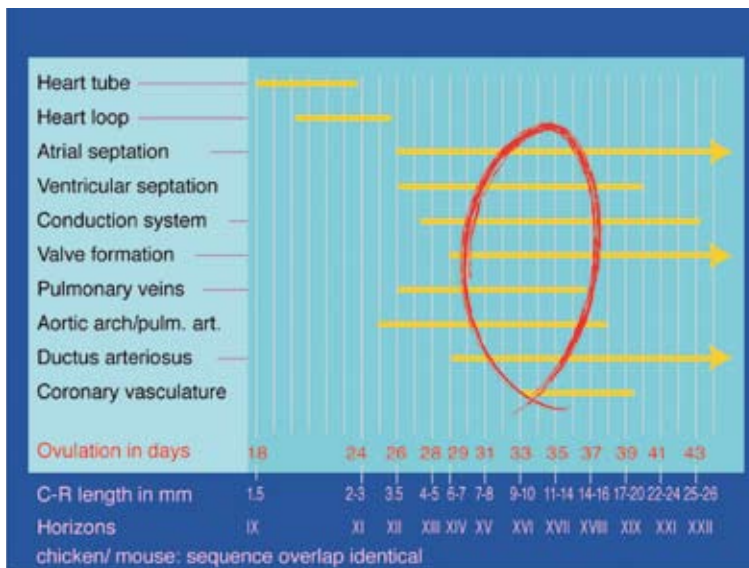


Figure 1

Schematic overview of the time span of development of the different cardiac components. Development of the cardiac conduction system is narrowly related to the development of the cardiac chambers and vascular system.

Short outline of cardiac development

In vertebrates, the heart is the first organ that is formed and becomes functional during early embryogenesis. Future cardiac cells arise in the epiblast lateral to the primitive streak, invaginate through the streak and migrate during gastrulation in rostro-lateral direction to bilateral areas of the lateral plate mesoderm¹⁻³. The lateral mesoderm separates in somatic and splanchnic epithelial layers; the (asymmetric) bilateral splanchnic mesoderm contains the cardiac precursors cells, that migrate toward the embryonic midline and fuse to form the primitive myocardial heart tube, lined on the inside with endocardium that is separated from the myocardial outer layer by cardiac jelly^{4,5} (**Figure 2 a-c**). During further development of the heart tube, cells from the splanchnic mesoderm will continue to contribute to the dorsal (venous pole) of the heart. Cells from the anterior or secondary heart field will contribute to the arterial pole and right ventricle of the heart⁶. The heart tube is attached to the rest of the embryonic (non-cardiac) mesoderm via the dorsal mesocardium, which

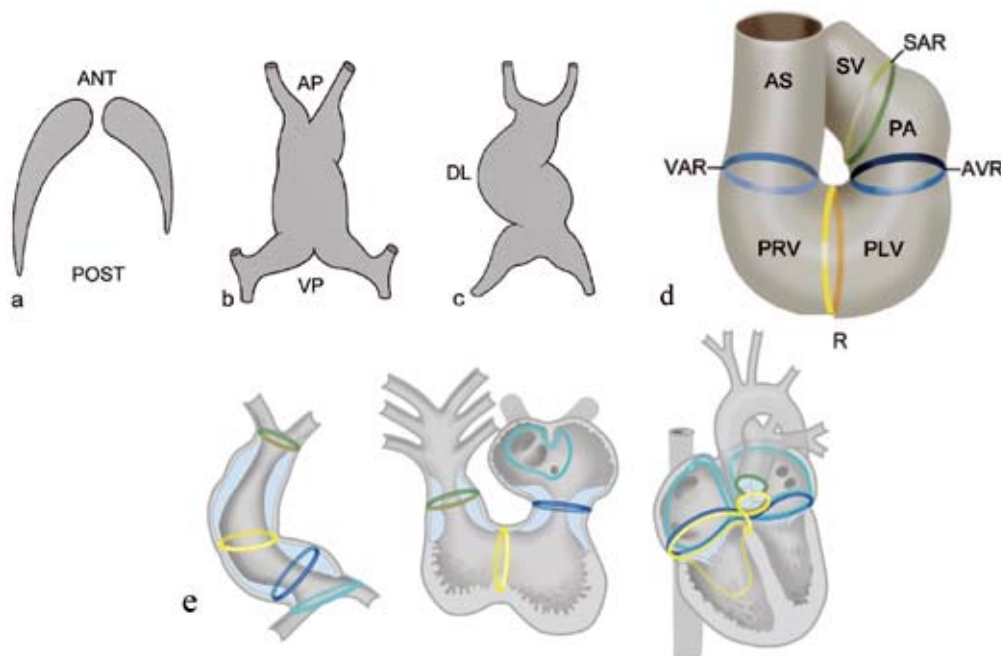


Figure 2

Schematic representation of the bilateral formation of the cardiogenic plates, which are derived from the splanchnic mesoderm (a). The bilateral plates fuse and from an initially straight heart tube (b), that start looping to the right (c-d). After looping, so-called transitional zones or rings can be recognised in the heart, that are positioned in between the putative cardiac chambers, being the sinu-atrial transition (SAR), the atrioventricular transition (AVR), the primary ring (PR) and the ventriculo-arterial transition (VAR). e. Position of these rings during further cardiac development. Ant: anterior, AP: arterial pole, AS: aortic sac, DL: dextral looping, PA: primitive atrium, PLV: primitive left ventricle, post: posterior, PRV: primitive right ventricle, SV: sinus venosus, VP: venous pole

Panel a-d from: Gittenberger-de Groot et al. *Pediatr Res*. 2005 Feb;57(2):169-76.

is disrupted during looping only leaving contact at the arterial and venous pole. After looping, the heart tube consists of several segments, being the left and right horn of the sinus venosus, the primitive atrium, the ventricular inlet segment and the ventricular outlet segment. These segments are divided by so-called transitional zones that connect at the inner curvature of the heart (**Figure 2d**)⁷.

Chamber differentiation occurs during further rightward looping of the heart tube, which results in positioning of the ventricles and the outflow tract of the heart in an anterior/ventral position, and of the atria in a dorsal/posterior position. Several genes/transcription factors that control chamber differentiation have been identified^{8,9}.

The sinus venosus becomes incorporated in the atrium and receives the venous inflow of the cardiac veins. The cardiac jelly becomes more concentrated at the AV junction and the outflow tract, sites where endocardial cushions and subsequently cardiac valves and membranous septa will form. Extracardiac neural crest cells migrate to the heart and play an important role in outflow tract septation^{10,11}. Myocardialisation of the walls of the caval and pulmonary veins presumably results from myocardium formation in the extracardiac mesenchyme¹². Migration of cardiomyocytes from the left atrium may also contribute to myocardialisation of the cardiac veins¹³. Cardiac septation and the formation of valves at the right and left AV junctions and in the right and left ventricular outflow tracts eventually results in the presence of a functional four chambered heart, that directs the separate systemic and pulmonary circulation of blood.

Development of the cardiac conduction system

The origin of the cells of the cardiac conduction system (CCS) has been the topic of interest of many studies in the last decade. Although the cells of the CCS were originally believed to be derived from the cardiac neural crest, a migratory cell population that arises at the embryonic neural plate at the level of the otic placode^{14,15}, retroviral lineage studies have demonstrated that the cardiomyocytes are the progenitor of the cardiac conduction cells in the embryonic heart¹⁶. Whether the cardiomyocytes that form CCS-tissue are derived from the division of differentiated (pre-specified) conduction cells (“*specification-model*”), or are recruited from a pool of multipotent (undifferentiated) cardiomyogenic cells (“*recruitment-model*”), is however still unclear¹⁷. Studies performed in chick embryos have demonstrated the development of both working myocardial cells and central and peripheral conduction cells from the same clone, and therefore strongly indicate that cells of the CCS originate from a common myogenic precursor in the embryonic tubular heart, i.e. a *bipotential myocardial cell population*, that is selectively recruited to the developing cardiac pace-making and conduction system^{16,18}. However, the mechanisms that determine the fate of the cardiomyocytes to become either a working myocardial cell or a cardiac conduction phenotype, are still unclear. The growth and differentiation factor Neuregulin has been

found to induce cardiomyocytes to a conduction system phenotype, as was demonstrated by the induction of ectopic CCS-lacZ expression after exposure to Neuregulin¹⁹. Furthermore, changes in electrical activation pattern supporting a critical role of Neuregulin in recruitment of cardiomyocytes to the cardiac pacemaking and conduction system have been observed. Recently, an interaction between Endothelin and Neuregulin has been suggested to promote the differentiation of the murine CCS²⁰.

Furthermore, the observation that a population of cardiac neural crest cells enters the heart at the venous pole and can be observed in the vicinity of putative elements of the cardiac conduction system, before they undergo a phase of apoptosis, has led to the hypothesis that these cells may be indirectly be involved in CCS differentiation^{21 22}.

Histology

Although in recent years several immunohistochemical and molecular markers of the developing CCS have been identified, the original descriptions of the developing CCS are based strictly on histological criteria as observed with light microscopy. Thirty years ago Viragh and Challice have described in great detail the developing CCS in mouse embryos²³⁻²⁶. From these studies it has become clear that the areas of putative CCS can be distinguished from the working myocardium based on histological criteria. In these studies cells of the developing CCS were characterized by a larger cell size, less developed and reduced number of myofibrils and a higher glycogen content than working cardiomyocytes.

The earliest sign of a morphologically specialized atrioventricular (AV) conduction pathway can be observed at embryological day (E) 9-10 in the mouse, and is located at the inner dorsal wall of the AV canal²³. During development the primordial AV node becomes structurally more compact. At stage E11 the primordia of both the sinu-atrial (SA) node (in the medio-anterior wall of the right superior caval vein) and the AV node can clearly be distinguished²⁵. Both these structures, as well as the AV bundle, develop simultaneously in the mouse heart, between E11-E12 (5-5.5 weeks in the human). At E13.5, all components of the CCS can be distinguished, with exception of the Purkinje fibers.

The AV node becomes interconnected with the His bundle that is located on the ridge of the interventricular septum²⁶. The left and right bundle branches extend down the subendocardial layers on both sides of the interventricular septum.

Insulation of the atrial myocardium from the ventricular myocardium occurs by development of the annulus fibrosus, that starts out by fusion of sulcus tissue with cushion tissue at the ventricular site of the AV junctional myocardium and moves the original atrioventricular myocardium to an atrial position²⁷. At E13-14 connective tissue begins to invade the AV sulcus and histological separation of the atria from the ventricles is initiated. Also, progressive insulation between the cells of the CCS and the ventricular working myocardium occurs, which however remains incomplete at the neonatal period²⁶.

The 4 ring theory of CCS development

Using the same histological criteria as Viragh and Challice to distinguish working myocardium from myocardium with more specialized features, the observation was made that after looping of the heart has started, 4 rings of tissue could be distinguished from the surrounding working myocardium, as described in 1976 by Wenink²⁸. These 4 rings are positioned at the above described transitional zones of the heart⁷, being the sino-atrial ring in between the sinus venosus segment and the primitive atrium, the atrioventricular ring in between the primitive atrium and primitive left ventricle, the primary ring or fold that separates the primitive left ventricle from the primitive right ventricle and the ventriculo-arterial ring at the junction of the primitive right ventricle with the truncus or putative outflow tract of the heart (**Figure 2d**). At these transitional zones, different staining properties of the myocardium, as well as size and chromatin distribution of the cells indicated the presence of primitive specialized tissue. The so-called “ring-theory”, hypothesizes that these 4 rings of “specialized” tissue are the precursors of the CCS. During further looping of the primitive heart tube these 4 rings come together in the inner curvature of the heart (**Figure 2e**), and during further differentiation of the heart part of the tissue loses its specialized character. What remains of the rings become the definitive elements of the mature cardiac conduction system. According to this theory the sino-atrial ring contributes to formation of the SA-node, both the SA-ring and AV-ring contribute to the AV-node, and the primary ring gives rise to the His bundle and bundle branches. This theory has since been the subject of discussion and controversy, which was renewed in recent years after the introduction of several immunohistochemical and molecular markers for CCS development.

Immunohistochemical markers of CCS development

In the past decades several immunohistochemical markers have been used to study the developing CCS. Although many of these markers have increased our understanding of CCS development, a limitation is that none of them is specific for cardiac conduction system only. In the nineties, the expression pattern of a **neurofilament-like protein** in the rabbit heart was used as marker for the developing CCS¹⁵. The presence of neurofilament-like protein was demonstrated in a ring at the sino-atrial and atrioventricular junctions and in ventricular components of the developing CCS, which were distributed in the ventricular subendocardium and connected to the AV ring¹⁵. The monoclonal antibody **HNK1**, originally used as a marker of neural crest cells during embryologic development, has been demonstrated to be expressed in the sinus venosus myocardium and in the developing CCS of several species, including rat, chick and human²⁹⁻³¹. HNK1 is predominantly expressed in the developing sino-atrial and atrioventricular CCS, and the expression pattern seems to correspond with rings described by Wenink. In human embryos, HNK1 stains the sino-atrial node, the internodal myocardium in the right atrium, the right atrioventricular AV ring with the posterior and anterior AV nodes, a retro aortic ring, the His bundle and the bundle branches. Furthermore, the myocardium surrounding the primitive pulmonary vein demonstrates transient staining²⁹ (**Figure 3**).

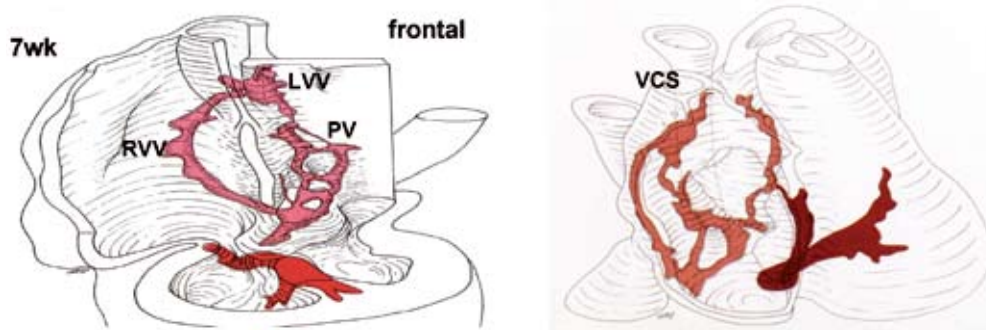


Figure 3
HNK1 expression in the human embryo. Explanation see text. LVV left venous valve, PV: primitive pulmonary vein, RVV: right venous valve, VCS: superior caval vein. From: Blom et al. *Circulation* 1999;99(6):800-806.

The neural tissue antigen **Gln2** is expressed in a single ring of tissue at the site of the primary ring in the early embryonic heart, which changes shape during development as a result of tissue remodelling underlying cardiac septation. This ring was hypothesized to eventually give rise to the atrioventricular CCS³².

The cell surface carbohydrate **PSA-NCAM** has been detected in ventricular trabeculae and the interventricular septum in the chick, in a pattern resembling the bundle branches and Purkinje fibers³³.

Molecular markers for CCS development

In recent years extensive study focusing on genetic determinants of cardiac conduction system formation has evolved. Study of transcription factors involved in cardiogenesis have made clear that regulation of myocardial differentiation into either a conductional or working myocardial phenotype is not dependant on a single gene, but is a multifactorial process during which several factors from different gene families contribute to the formation of the different subcompartments of this complex system. Molecular markers that have been used to delineate the developing cardiac conduction system include *minK-lacZ*, *CCS-lacZ*, *cGATA-6-lacZ*, *cardiac troponin I-lacZ*, *GATA-1*, the homeodomain transcription factor *Nkx2.5*, the recently described *Hop*, and the T-box transcription factors *Tbx2* and *Tbx3*, *Tbx5*. Furthermore, the expression pattern of several connexins in cardiac tissues has contributed to our understanding of the development and function of the CCS³⁴. Most of these transcription factors do not function in an autonomic matter, but interact with other factors, resulting in synergistic or repressing effects. The currently known molecular markers of CCS development are briefly described in the subheadings below.

The T-box family of transcription factors

In the developing heart the T-box transcription factors *Tbx2* and *Tbx3* are expressed in the cardiac inflow tract, the atrioventricular canal, the outflow tract and inner curvatures of

the heart. These factors presumably are transcriptional repressors of chamber formation, as both genes repress the genes *Nppa* (*ANF*) and *Cx40*, present in (a.o.) atrial working myocardium^{28 35 35 36}. In general, expression of *Tbx2* and *Tbx3* is mainly observed in putative slow conducting areas, but also in the His bundle and the proximal part of the bundle branches. The expression of *Tbx2* decreases from early foetal stages, whereas the expression of *Tbx3* increases. In the matured heart expression of *Tbx3* is observed in the SA node, AV node, but also in internodal myocardium, and in the His bundle and proximal bundle branches³⁵. Next to expression in part of the putative CCS, *Tbx3* expression is also observed in the atrioventricular cushions. Homozygous *Tbx3* mutant mice display a syndrome known in humans as *ulnarmammary syndrome*, and display early embryonic mortality, presumably due to severe compromise of the yolk sac³⁷. However, a significant cardiac conduction system phenotype has not been demonstrated in *Tbx3* knockout mice thus far^{37 38}. The T-box transcription factor *Tbx5* is also expressed in the developing central CCS, including the AV node, AV bundle and bundle branches, and is needed for correct morphogenesis and maturation of the CCS³⁹. Mice lacking *Tbx5* display a cardiac phenotype that resembles the syndrome known in humans as the *Holt-Oram syndrome*, including atrial septal defects and conduction system abnormalities⁸. *ANF* and *Cx40*, both expressed in cells of the (fast conducting) CCS are gene targets of *Tbx5*, and *Cx40* is abruptly in *Tbx5* mutated mice (*Tbx5*^{del/+}) mice³⁹.

Homeodomain transcription factors

The homeodomain transcription factor *Nkx2.5* is one of the earliest markers of the cardiac lineage, and is already expressed in the cardiogenic mesoderm⁴⁰. During cardiac development expression of *Nkx2.5* correlates with the recruitment of cells to the developing atrioventricular conduction system⁴¹. During development of the CCS, *Nkx2.5* expression is elevated in the differentiating atrioventricular conduction system, compared to expression in the adjacent working myocardium. In *Nkx2.5* haplo-insufficient mice, there is hypoplasia of the AV node and His bundle, and the number of peripheral Purkinje fibers is significantly reduced⁴². Cardiac phenotypes of mutations in *Nkx2.5* in mouse models resemble those in humans and include conduction defects⁴³.

Furthermore, *Nkx2.5* interacts with the *Cx40* promoter region, and mice lacking *Nkx2.5* demonstrate a significant decrease in *Cx40* expression⁴⁴. Furthermore, *Nkx2.5* can form a complex with the transcription factor *Tbx2*, that is able to *suppress ANF* promoter activity in the AV canal, which may be a mechanism that helps to regulate the sites of chamber formation in the developing heart⁴⁵. *Nkx2.5* can also bind to *Tbx5*, and both are essential components in the *activation* of the *ANF* gene.

The homeodomain transcription factor *Msx2*, a downstream target of Pax-3/splotch (which is a key player within early cardiac neural crest development), is expressed in the developing central CCS (but not the peripheral PF), in the chick. However, no abnormalities in the cardiac conduction have been observed in *Msx2* mutant mice^{46 47}.

Recently, expression of the homeobox gene *Hop* has been described. *Hop* is expressed strongly in the AV node, His bundle and bundle branches of the adult CCS and *Hop* null mice demonstrate conduction defects below the AV node, related to decreased expression of Cx40⁴⁸.

The GATA family of transcription factors/Zinc finger subfamilies

The GATA-family is a relatively small family of transcription factors, and for 3 of the 6 known vertebrate GATA transcription factors a role in cardiogenesis has been identified: *GATA4*, *GATA5* and *GATA6*⁴⁹. Expression of *GATA4* is present in both the adult and embryonic heart, and disruption results in cardiac dysmorphogenesis with early embryonic mortality⁵⁰. The large degree of interaction of the different transcription factors is again demonstrated in a recent study that demonstrated that, next to *Tbx3* and *Nkx2.5*, the *Cx40* promoter also is modulated by the cardiac transcription factor *GATA4*⁴⁴. *GATA4* is expressed in Purkinje fibers of the adult chick heart⁵¹. The *cGATA6* gene enhancer specifically marks components of the developing atrioventricular CCS and AV node^{52,53}, (but not the more distal components of the CCS) and expression of *cGATA6* remains visible in the mature CCS.

MinK/lacZ knock-in/ knock-out

The *minK* gene (also known as *IsK* and *KCNE1*) encodes a 129 amino-acid protein, that modifies electrical currents in the heart resulting from expression of the genes *HERG* and *KvLQT1*⁵⁴. Mutations in both *HERG* and *KvLQT1*, that encode the structural subunits for the channels involved in the cardiac delayed rectifier currents I_{Kr} and I_{Ks} , respectively, are the most common causes of congenital long-QT syndrome (LQTS)⁵⁴. Disruption of the *minK* gene and integration of the *lacZ* gene results in β -galactosidase expression under the control of endogenous *minK* regulatory elements, which has been used to study the expression pattern of *minK* in mice.

Disruption of the *minK* gene causes inner ear defects and QT interval prolongation (in bradycardic conditions), the combination of which is known in human as the *Jervell-and Lange-Nielsen syndrome*⁵⁵. *MinK* (-/-) myocytes lack the delayed rectifier current I_{Ks} and demonstrate significantly reduced I_{Kr} , which indicates a role of *minK* in modulating both rectifier currents⁵⁴. *MinK-lacZ* is expressed in the developing cardiac conduction system in murine embryos starting on E8.25⁵⁶.

CCS-lacZ insertional mutation

All the above genes have contributed to understanding the complex process of cardiac conduction system development. However, none of these genes are expressed in the entire, central and peripheral, CCS. In 2000, fortuitous insertion of a *lacZ* gene in the murine genome unexpectedly resulted in expression of *lacZ* in the (developing) conduction system of the heart. Although the gene was originally referred to as “*Engrailed2-lacZ*”, it should

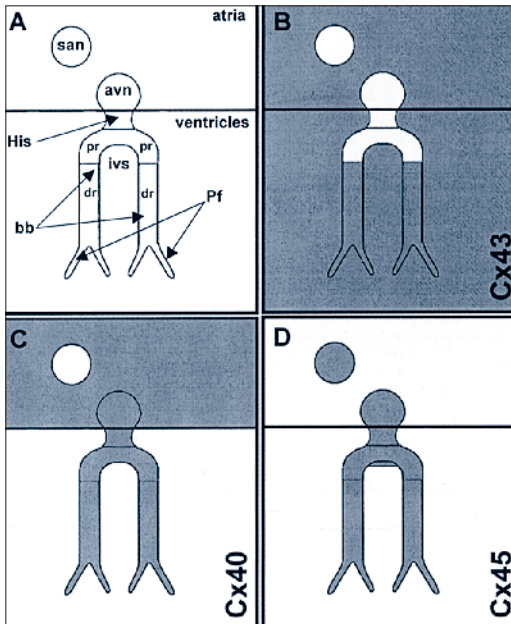


Figure 4

Schematic overview of the expression of connexin 40, 43 and 45 in the heart. avn: atrioventricular node, bb: bundle branches, dr: distal part of bundle branch, His: His bundle, ivs: interventricular septum, Pf: Purkinje fibers, pr: proximal part of bundle branch, san: sinu-atrial node, Adapted from: Miquerol et al. Novartis Foundation 2003: 80-94.

be emphasized that the transgene is most likely under the transcriptional control of a to date unidentified integration site and not by the *Engrailed2* regulatory elements included in the transgene proper (**Figure 4**). The gene was therefore renamed to cardiac conduction system (*CCS-lacZ*) by Fishman et al.¹⁹. Optical mapping studies performed in murine embryos demonstrated a clear correlation of electrical activation with *CCS-lacZ* expressing areas^{19,57}.

In this thesis the *CCS-lacZ* model was used to conduct anatomical studies of the developing CCS in relation to the expression of this marker (**Chapter 2, 3 and 10**).

Connexins expressed in cardiac conduction tissue

Myocardial cells of the heart are electrically connected via gap junctions. Gap junctions consist of 2 connexons, which are hexamers of transmembrane protein subunits called connexins⁵⁸, necessary for electrical and metabolic coupling between cells. In the heart, 3 major connexins have been identified: **Cx40**, expressed in fast conducting cardiac tis-

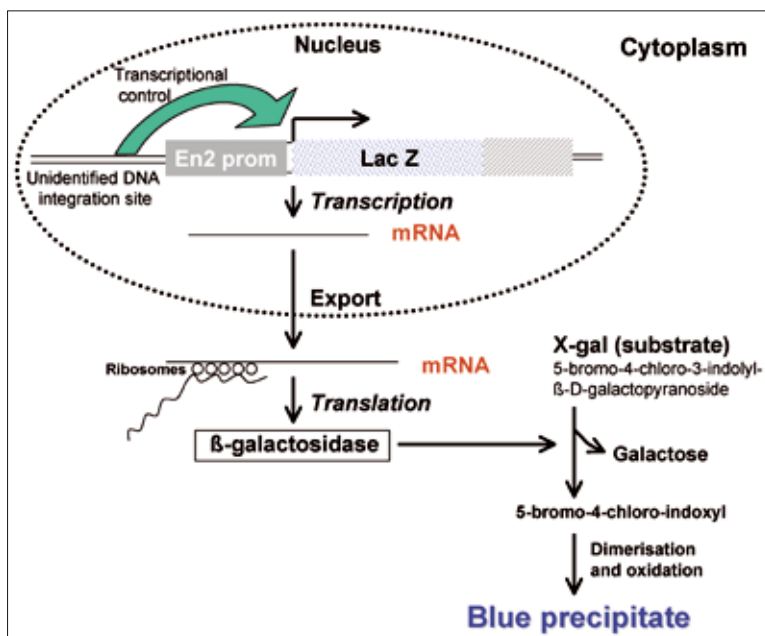


Figure 5

Simplified working scheme of the transgenic CCS-lacZ mouse model. The bacterial LacZ reporter gene was placed under the control of engrailed-2 promoter elements. Random integration of the construct in mouse genome resulted in β -galactosidase expression of the cardiac pacemaking and conduction system throughout the heart. As CCS-expression was not observed in a number of additional lines of mice harbouring the same transgenic construct, it is likely that the lacZ expression is under the transcriptional control of an unknown locus at the site of integration, rather than of the En-2 regulatory elements within the construct. Beta-galactosidase catalyses the conversion from X-gal to 5-bromo-4-chloro-indoxyl, which after non-enzymatic dimerisation and oxidation is visible as a blue precipitate in the cells in which the reporter gene is expressed.

sues and in the atria⁵⁹; **Cx43**, expressed in the slower conducting working myocardium of the atria and ventricles, and in the distal part of the conduction system⁶⁰; and **Cx45**, expressed in slow conducting pathways and in the myocardium of the primary heart tube^{61,62}. However, the expression of connexins in the heart is variable between different species, and varies during the different stages of development⁵⁹. A schematic overview of connexin expression in the heart is provided in **Figure 5**.

Cx40 can be detected starting from E9.5 in the mouse heart, when it is present first in the primitive atria and primitive left ventricle, later also in the primitive right ventricle, but not in the AV canal and interventricular septum. During further development, together with the development of the specialized CCS, expression becomes restricted to atrial myocytes, (but also appears to be present in the RVV of the embryonic sinus venosus), and the ventricular conduction system^{63,59}.

In adult species, Cx40 expression has also been demonstrated in the **sinus node** in rabbit⁶⁴, dog⁶⁵ and human⁶⁶, and in the **AV node** of several species, including rabbit⁶⁷, mouse⁶² and rat^{62,68,69}.

Cx40 deficiency results in sinoatrial conduction defects, significant decrease of conduction velocities in the atria, and conduction delay in the His bundle ⁶⁰. Cx40 knock-out mice display an increased incidence of inducible atrial arrhythmias, and significant conduction delay in infra-His and AV nodal conduction ⁷⁰⁻⁷³. Possibly Cx45 compensates partially for the lack of Cx40 in these mouse models ⁷⁴.

Cx43 is expressed in an inverse pattern of Cx40, and is first detected in the primitive ventricle at E9.5 and in the atria at E12.5. At later embryonic stages (E14.5 onward) Cx43 expression increases and is present in the adult ventricular (working) myocytes ⁷⁵⁻⁷⁶. Cx43 knockout mice die at birth because of developmental defects in the pulmonary outflow tract, presumably resulting from defective migration of cardiac neural crest cells to this region ⁷⁷. Cardiac specific deletion of Cx43 results in sudden cardiac death from spontaneous ventricular arrhythmias (at 2 months postnatal), which indicates an important role for Cx43 for maintenance of electrical stability in the heart ⁷⁸.

Cx45 is expressed already in all compartments of the linear heart tube (E8.5), including the inflow tract, AV canal and outflow tract. Expression of Cx45 decreases throughout development and in the adult mouse heart Cx45 is present in the AV node, His bundle, and surrounding the Purkinje fibers ⁶¹⁻⁶². Cx45 knockout mice demonstrate conduction block and die of heart failure at E10 ⁷⁹.

Development of the Embryonic ECG

The rhythmic heartbeat, that is characterized by sequential contraction of the atria and ventricles, is coordinated by a complex network of cells throughout the heart, the cardiac pacemaking and conduction system (CCS). In the adult heart, the slow conducting components of this system are the SA-node and AV-node; the fast conducting elements are the common bundle of His, the right and left bundle branches and the peripheral Purkinje fibers.

Peristaltic contraction of the tubular heart can be observed as early as 23 days post conception (dpc) in human (8.5 dpc in mouse), which results in propulsion of blood from the venous to the arterial pole of the heart ⁵. Sequential contraction of atria and ventricles can be observed as soon as cardiac looping starts, along with the occurrence of a surface ECG. Although a distinct SA-node primordium can only be detected at E11 in murine hearts ²⁵, pacemaker property is already present in the primitive heart tube in the sino-atrial region at the venous pole of the heart. Interestingly, the earliest pacemaker has been demonstrated at the site of the *left* atrium primordium, and during development shifts toward the right sinus primordium ⁸⁰⁻⁸¹. The change in activation pattern from base-to-apex to the mature apex-to-base pattern, that is needed for efficient ejection of blood from the ventricles in the outflow tracts of the heart, is a consequence of the development of the His-Purkinje

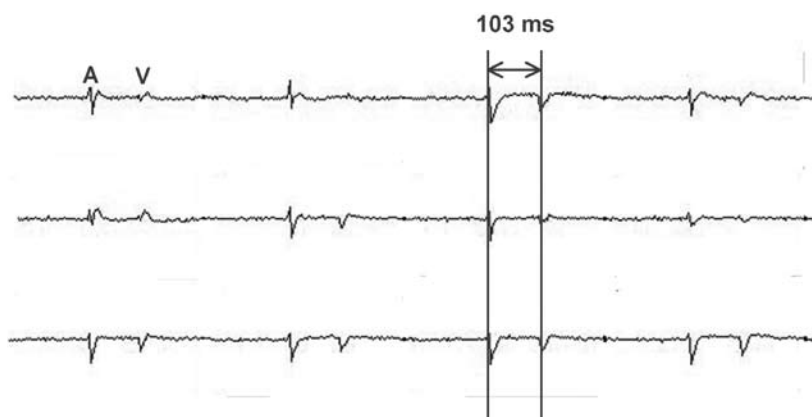


Figure 6
ECG recording of a murine embryo aged 10.5 days. The cardiac activation is characterised by 2 deflections representing atrial (A) and ventricular (V) activation, separated by a delay (103 ms).

system, and reflects the impulse propagation through this rapidly conducting system. This change occurs before ventricular septation has been completed^{57,82}.

It is generally accepted that, in order for the atrioventricular conduction axis to become functional, electrical isolation of the atria from the ventricles must occur, except at the site of the AV-node/His bundle. However, a typical electrogram characterised by a p-wave reflecting atrial activation, atrioventricular delay demonstrated by electrical silence on the ECG and a QRS-complex reflecting ventricular activation, can already be recorded from the embryo at early stages, when the fibrous isolation of the ventricles has not been completed yet (**Figure 6**), indicating that functional isolation between atria and ventricles may be present before anatomical isolation of the atria from the ventricles has been achieved.

Semantic issues regarding the definition of cardiac conduction system

Over the years, several controversies regarding semantics and different applications of definitions have been able to elicit strenuous discussions between researchers in the field of cardiac anatomy and development. One of these issues regards the question whether it is justified to name the tissues in the embryonic heart that are responsible for the embryonic ECG conduction tissue⁸³.

Discussions about the definitions of conduction system have in already 1910 led Aschoff and Monckeberg to describe 3 prerequisites that must apply to tissues in order to be designated “cardiac conduction tissue”. These criteria are 1) cells should be histologically distinct, 2) cells should be able to be followed from section to section in serially prepared

tissues and 3) the specialised cells should be insulated from the working myocardium by sheets of fibrous tissue^{84,85}. However, these criteria are not always compelling, as not all 3 criteria apply to all components of the CCS, such as the tissues of the SA and AV node, tissues that are generally accepted to be part of the cardiac pacemaking and conducting system.

Also, these adult criteria do not seem to apply to the developing cardiac conduction system since the embryonic heart already demonstrates sequential contraction of atria and ventricles regulating blood flow, concomitant with a mature surface ECG, well before the criteria of Aschoff and Monckeberg apply to these tissues.

Furthermore, several molecular markers and functional criteria are now available that help distinguish working myocardium from myocardium that displays a more specialized phenotype, before fibrous insulation is achieved.

Therefore, throughout this thesis the CCS is regarded from a morphological point of view based on expression of genetic markers, in particular the *CCS-lacZ* construct. When referred to the developing cardiac conduction system, the entire cardiac pacemaking and conduction system is meant, which thus means not only the nodal tissues, nor only the fast conduction tissues, but the entire network of nodes, tracts and fibers responsible for the coordinated, and in some cases, uncoordinated contraction of the heart, that is reflected by the electrical registration on the surface ECG.

Development of the cardiac conduction system in relation to putative sites of clinical arrhythmias

It is well known from electrophysiological studies that the occurrence of clinical arrhythmias is related to anatomical predilection sites. Clinical mapping studies have demonstrated that ectopic pacemaker foci are preferentially encountered in specific parts of the right and left atrium. In the right atrium foci are often encountered in sinus venosus related areas, such as the crista terminalis^{86,87}, a structure related to the initiation/perpetuation of atrial flutter; and the ostia of the caval veins⁸⁸ and coronary sinus⁸⁹ as initiators of clinical arrhythmias. In the left atrium atrial fibrillation has been attributed to arrhythmogenic foci that originate from the pulmonary veins⁹⁰. Furthermore, the interatrial bundle of Bachmann and accessory pathways, such as present in Wolf-Parkinson White (WPW) Syndrome and Mahaim tachycardia, are anatomical structures important in cardiac conduction and arrhythmogenesis^{91,92}. Also, it has been demonstrated that the myocardium at the atrioventricular junction itself has specialized properties, and arrhythmias originating from both the tricuspid and mitral junction have been described^{93,94}. The question thus arises why these structures, which do not belong to the mature cardiac conduction system, are able to generate or sustain arrhythmias.

We hypothesized that an answer to this question may lie in the embryonic development of the cardiac conduction system. In the subheadings below specific anatomical sites that are related to arrhythmogenesis in human are described.

Internodal pathways

One of the areas of serious controversies over the last decades, lasting now for almost a century, is the existence of functional internodal tracts. These internodal tracts, inextricably bound up with the name James, have been described to run in the right atrium in between the SA node and the AV node. The pathways as described by James consist of 3 cellular tracts, distinguishable from the atrial myocardium based on histological study of atrial sections (stained mostly with Goldner Trichome): a *posterior pathway* along the crista terminalis, an *anterior pathway* which continues to the left atrium via Bachmann's bundle, and a *medial pathway* that runs in the interatrial septum. Specialized Purkinje-like and transitional cells could be demonstrated in these three pathways⁹⁵⁻⁹⁷. In the embryonic heart, internodal tracts have been distinguished from the atrial myocardium based on the expression pattern of the marker HNK1²⁹. In this study, HNK1 was detected in the right venous valve (the putative crista terminalis that will form the boundary between the trabeculated and smooth walled myocardium of the right atrium), corresponding to the posterior pathway as described by James; in the left venous valve, that in humans becomes incorporated in the interatrial septum; and in an anterior pathway consisting of the septum spurium (the fused anterior right and left venous valves), that could be followed towards the left atrium in a retro-aortic position⁹⁸.

Although tracts with different histological and immunohistochemical characteristics thus can be distinguished in the atria, the functionality of these tracts is yet to be determined. Results of several studies have suggested preferential spread of atrial activation in a fashion that may correspond to these pathways. For instance, optical mapping studies have demonstrated a non-radial spread of intra-atrial conduction in the rat, and the recorded conduction patterns were preferential in a pattern corresponding to the posterior and anterior pathways as described by James⁹⁹. However, whether this preferential conduction in the atria, as is observed in these regions, is due to the presence of specialized cells, or is merely an anisotropic organisation of tissue¹⁰⁰ remains to be determined. Studies in 1966 and 1967 have demonstrated that the administration of elevated levels of potassium induced electrical quiescence of the atrial myocardium, with the exception of cells specifically localized in the areas corresponding the internodal pathways^{101 102}. More recently, Racker demonstrated 3 bundles with unique potential and conduction capacities in dogs, that run in between the SA- and AV node, supporting the presence of specialized properties of cells in these areas¹⁰³.

Recent data of molecular studies also seem to indicate that the embryological sinus venosus is molecularly distinct from the surrounding working atrial myocardium^{56 63}. (Also see **Chapter 2** of this thesis).

The coronary sinus

Embryology of the coronary venous system

24 The coronary sinus develops from the sinus venosus segment of the embryonic heart. The sinus venosus has a paired origin and in the 4th week of development it exists of a left and right sinus horn connected by a small transversal part. Each sinus horn receives blood from 3 significant veins: the v. vitellinae/omphalomesenterica, the umbilical vein, and the vena cardinalis communis. During the 4th and 5th week of development, growth in favour of the right atrium, due to left-to-right shunting of the blood flow, causes the ostium of the sinus venosus in the atrium to shift to the right. During further development in humans the left umbilical vein and left vitellin vein obliterate, eventually also the left common cardinal vein. All that remains of the left sinus horn is the coronary sinus, and the oblique vein of Marshall (which is a remnant of the left cardinal vein). In the mouse, the left superior caval vein does not regress and persists into adult life. Due to the left to right shunting of the blood, the right sinus horn and concomitant veins enlarge, and will form the eventual caval veins^{104 105}. The right sinus horn incorporates into the atria and the major part will form the smooth walled part of the right atrium, bordered by the left and right venous valves. During embryology, the left venous valve is continuous with the posterior wall and the right pulmonary ridge in the posterior wall of the left atrium³⁰. In human, during further development, the left venous valve becomes incorporated in the interatrial septum. Part of the right venous valve forms together with the venous sinus septum (a ridge present at the medial atrial wall) the *Eustachian* valve, which covers the inferior caval vein. The part of the right venous valve ventral to where it fuses with the venous sinus septum forms the *Thebesian* valve, that covers the ostium of the coronary sinus¹⁰⁴. Inside the coronary sinus, at the level of insertion of the oblique vein of Marshall, the *valve of Vieussens* is present¹⁰⁶ (**Figure 7**). Anatomical studies describe large interindividual variations in the anatomy of the adult coronary venous system¹⁰⁶.

Pulmonary veins and sinus venosus

Since arrhythmogenic capacities have been attributed to the pulmonary veins, these structures have become an important subject of interest, both for those working in the clinical field of electrophysiology, and for those working in basic science. In the following sections the development of the pulmonary veins, along with controversies in this field, is described, followed by a short overview of morphological, molecular and electrophysiological data in relation to the (controversial) presence of specialized myocardium at the site of the pulmonary veins.

Development of the pulmonary veins

In the embryonic heart, the heart tube is initially attached to the foregut via the dorsal mesocardium. As described in the first paragraph, during development of the heart the



Figure 7
Valves in the coronary venous system. The ostium of the coronary sinus is bordered by the Thebesian valve, whereas more distal in the coronary sinus the valve of Vieussens can be found.
CS: coronary sinus, LA: left atrium, LV: left ventricle, RA: right atrium.

dorsal mesocardium between the arterial and venous pole regresses. A strand of endothelial cells remains, called the *mid-pharyngeal endothelial strand*, which remains connected to the endocardium at the sinu-atrial region of the heart tube³⁰. This strand thus runs in front of the foregut from the arterial pole towards the venous pole of the heart, and is part of the splanchnic vascular plexus surrounding the developing foregut and lungbuds³⁰. During further development a strand of partly lumenized endothelial cells runs all the way from the sinus venosus to the lung parenchyma in the developing splanchnic vascular plexus. This strand lumenized completely and connects the lung bud (that originates from the foregut endoderm) to the sinus venosus. As such the venous connection to the lungs precedes the formation of the lung arteries that connect to the sixth pharyngeal arch artery at the arterial pole. Endothelial precursors at the peripheral tip of the lumenized vein proliferate and lumenize as well, and will form the tributaries of the primitive pulmonary vein³⁰. The connection between the pulmonary vein and the lungs probably occurs around E12.5-E13 in the mouse (as demonstrated by the presence of Cardiac Troponin I-*LacZ* positive cardiac cells near the main bronchial cavity¹³), and has been observed even in earlier stages in the quail, as demonstrated by QH1 staining (that detects quail endothelial cells)³⁰. The pulmonary vein and its tributaries incorporate in the left atrium during development. The amount of incorporation eventually determines the number of ostia by which the pulmonary veins drain into the left atrium. Under-incorporation will result in single ostia (or even a separate pulmonary venous chamber, a so-called pulmonary sinus), whereas over-incorporation will give rise to additional branches draining directly into the left atrium.

Relation of the primitive pulmonary vein to the sinus venosus

Whether the single primitive pulmonary vein drains in the sinus venosus segment or in the atrial segment of the embryonic heart is a highly controversial issue and has been the subject of vivid discussion over the past decades.

Several early studies describe the drainage of the primitive pulmonary vein into the sinus venosus segment of the heart ¹⁰⁷ (results revised by Rammos et al. ¹⁰⁸) ¹⁰⁹, also, in reptiles ¹¹⁰, fish ¹¹¹, birds ¹¹² ¹¹³ and different species of non-human mammals ¹¹⁴ ¹¹⁵. More recent studies, some of which based on observations using immunohistochemical markers, support this drainage pattern in human, mouse, rat and chicken ²⁹⁻³¹ ¹¹⁶⁻¹¹⁸.

In contrast, other reports describe drainage of the primitive vein directly in the dorsal wall of the atrial segment ¹⁰⁷ ¹¹⁹ ¹¹⁹⁻¹²¹ ¹²¹ ¹²². Part of these controversies seem to rest on different application of definitions (especially how to define the sinus venosus), and different interpretation of possibly similar observations.

During development the transition between the primitive sinus venosus and the atrial segment is demarcated by a fold of tissue, the sinu-atrial fold, that, like sinus venosus tissue but in contrast to the atrial segment, expresses HNK1. When using this fold as border structure between the sinus venosus and the atrial segment in early stages, the primitive pulmonary vein does appear to drain in the left part of the sinus venosus ³⁰ ¹¹⁶ (**Figure 8**). The HNK1 positive myocardium surrounding the primitive pulmonary vein is continuous with the left venous valve, which has consistently been observed in chick, rat and human ³⁰ ³¹ ²⁹. During later stages, this left-sided myocardium loses its HNK1 positivity, in contrast to the right part of the sinus venosus, and is separated from the right atrium by the development of the interatrial septum, so that the primitive pulmonary vein becomes a left sided structure ³⁰. During atrial septation and incorporation of the sinus venosus in the left atrium, the sinuatrial fold in the left atrium disappears.

However, if the left and right venous valves are considered as the border structures that separate the sinus venosus from the atrial segment, the primitive pulmonary vein does not drain within this area. However, these valves are not present yet in early stages, when the

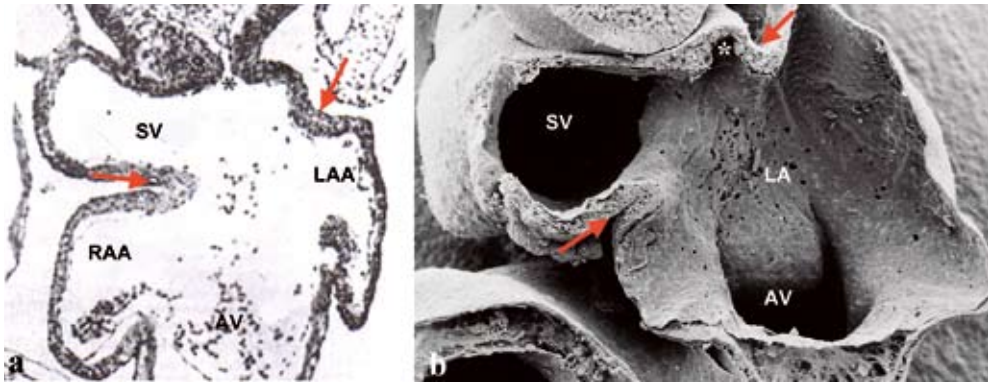


Figure 8

a. Transverse section through the sinus venosus and left and right atrial appendages of a chick embryo.

b. Electron microscopical picture at the same level. Arrows point at the sinu-atrial fold, which separates the sinus venosus from the atrial segment. The asterisk indicates the common pulmonary vein. AV: atrio-ventricular canal, LAA: left atrial appendage, RAA: right atrial appendage, SV: sinus venosus. Left panel adapted from: DeRuiter et al. *Anat. rec.*1995;243:84-92.

sinus venosus is still separated from the atrium by the sinu-atrial fold (**Figure 8**), but will develop in a later stage from this sinuatrial fold. Most authors do seem to agree that the right myocardial ridge of the common pulmonary vein is continuous with left venous valve, and that this structure forms the base of the atrial septum^{119 120}.

Results of studies of the Leiden Department of Anatomy & Embryology support a relation of the primitive pulmonary vein with the sinus venosus. To date however, neither a detailed description of the histological consequences of pulmonary vein incorporation for the structure of the left atrial wall, nor the presence of left sided sinus venosus in the human adult, has been described in literature yet.

The pulmonary veins, left atrium and arrhythmogenesis

Myocardialization of the pulmonary veins: development of a myocardial sleeve

The arrhythmogenic capacities of the pulmonary veins have been attributed to sleeves of myocardium that surround the pulmonary veins. Anatomical studies describe in detail the length and thickness of the veins^{123 124}. In general, the myocardial sleeves surrounding the left superior PV are the longest, whereas the sleeves surrounding the right inferior PV are shorter, and in some cases not present¹²³. These data correspond with the frequency of ectopic foci encountered in clinical mapping studies⁹⁰.

The mechanisms of the development of the myocardial sleeves of the pulmonary veins is not certain. The sleeves could develop due to a process of *myocardialisation*, i.e. growth of existing cardiomyocytes into mesenchyme, or *migration* of myocardial cells from the left atrial dorsal wall to the pulmonary veins¹³. Interestingly a wave of migration of cardiac cells from the sinu-atrial region is hypothesized to migrate to the lungs¹³. On the other hand, a process of *differentiation* or *recruitment* of cells from the mediastinal myocardium into cardiomyocytes seems a likely mechanism behind the secondary wave of myocardialisation responsible for the myocardium formation at the sites of the systemic and pulmonary veins^{12 12 13}. In the mouse, this secondary myocardialisation of the pulmonary veins has first been observed starting at E12.5^{12 13}.

An interest question that arises, is whether, and if so, why these myocardial sleeves possess specialized capacities responsible for the ectopic beats initiating and sustaining clinical tachycardias^{90 125}. The next paragraphs describe the results of several morphological and electrophysiological studies that support the presence of specialized characteristics of the myocardium surrounding the pulmonary veins.

Morphological studies indicative for the presence of specialized conduction cells in the pulmonary veins

Already in 1874, attention was drawn to possible independent pacemaking activity of the pulmonary veins by Brunton & Fayrer, who observed independent pulsation of the pulmonary veins in the otherwise mechanical silent hearts of rabbits and cats¹²⁶. In 1986, Masani studied the structure of the myocardial layer surrounding the pulmonary veins in rats, and

was able to demonstrate the presence of cells with clear cytoplasm, few myofibrils and round or oval mitochondria, that resembled sinus node pacemaker cells ¹²⁷.

More recently, Perez-Lugones et al have identified the presence of P cells, transitional cells and Purkinje cells in human pulmonary veins ¹²⁸. Interestingly, these cells were mainly found in the pulmonary veins of subjects with atrial fibrillation.

It has been hypothesized that deterioration or destruction of the primary pacemaker results in an atrial rhythm originating from these ectopic nodal foci ¹²⁹. Next to the pulmonary veins, cells resembling cardiac conduction cells have also been identified in the Eustachian ridge of cats ¹³⁰ and in Bachmann's bundle in dogs ⁹⁷.

28

Electrophysiological studies performed in pulmonary veins

Several studies have demonstrated distinct electrophysiological capacities of pulmonary veins as compared to the atria ¹³¹⁻¹³³. A greater degree of decremental conduction and shorter effective refractory periods have been observed in the myocardial sleeves of the pulmonary veins as compared to the myocardium of the atrium in patients with paroxysmal atrial fibrillation ^{134 135}.

Pulmonary venous cardiomyocytes have distinct electrophysiological properties compared to cardiomyocytes in the left atrium, with a reduced resting membrane potential, action potential amplitude, a smaller phase 0 upstroke velocity and a shorter duration of the action potential ¹³¹. In accordance with these findings, it has been demonstrated that the myocardium surrounding pulmonary veins has different ionic current properties in comparison to the left atrium. The inward-rectifier current is smaller in the pulmonary veins than in the left atrium, whereas the delayed rectifier currents are larger in the pulmonary vein than in the left atrium ¹³¹. These results are supported by a study of Chen et al., who distinguished 76% pacemaker cardiomyocytes and 24% non-pacemaker cardiomyocytes in pulmonary veins, with distinct action potentials and ionic current properties ¹³³.

The exact mechanism of the contribution of the pulmonary veins to arrhythmogenicity is not clear yet. Independent spontaneous pacemaker activity has been demonstrated in the pulmonary veins of guinea-pigs, rabbits and cats (125) ¹³⁶. Several other, more recent, reports also support *abnormal automaticity* or *enhanced pacemaker activity* in the pulmonary veins, with or without infusion of medication or pacing manoeuvres ¹³⁶⁻¹⁴⁰. Furthermore, independent atrial fibrillation has been demonstrated in the pulmonary veins ¹⁴¹.

Also, *enhanced triggered after-depolarisations*, sometimes in combination with spontaneous activity, has been supposed as the mechanism responsible for the arrhythmogenicity of the pulmonary veins ¹⁴²⁻¹⁴⁵.

The anisotropic arrangement of the myocardium may form the substrate for *re-entry* at this site, which may be important for maintenance of the arrhythmia once it has been initiated ¹⁴⁶. The cellular properties of the pulmonary venous cardiomyocytes mentioned above (reduced resting membrane potential, action potential amplitude, a smaller phase 0 upstroke

velocity and a shorter duration of the action potential), resulting in shorter refractoriness and slowed conduction, favour the occurrence of re-entry^{131 140 147 148}.

Molecular markers expressed in pulmonary veins

In accordance with findings of different electrophysiological properties of the pulmonary venous myocardium, differences in ion channel subunit expression have been observed in the pulmonary veins compared to the left atrial free wall. These differences include a greater abundance of the rapid delayed-rectifier α -subunit HERG, and of the slow delayed-rectifier α subunit KvLQT1, and lower abundance of the inward-rectifier subunit Kir2.3, which may underlie the differences in ionic currents observed between pulmonary veins and left atrial cardiomyocytes¹⁴⁹.

AV junction – accessory pathways/Mahaim fibers

In early embryonic stages, atrial and ventricular myocardium is continuous through the myocardium of the atrioventricular (AV) canal. In normal adult cardiac conduction, the AV conduction axis is the only functional atrioventricular conduction tract. AV re-entrant tachycardias are based on the presence of accessory myocardial bundles connecting atrial and ventricular tissue, thus bypassing the insulating function of the AV-groove. The most well known is the bundle of Kent, present in the Wolf-Parkinson White (WPW) syndrome¹⁵⁰.

Also, several arrhythmias have been described in literature that originate from the tricuspid and mitral junction^{93 94}. AV junctional cells surrounding both the tricuspid and mitral annuli resemble nodal cells in their cellular electrophysiology¹⁵¹

A special form of re-entrant tachycardia is Mahaim tachycardia, during which antidromic re-entrant tachycardia occurs over an accessory bundle with AV node like conduction properties. The proximal insertion often localized to the lateral, anterolateral or posterolateral tricuspid annulus and distal insertion into the right ventricular free wall or the right bundle branch¹⁵². To date there are two mouse models for WPW syndrome. Mutations in the gene **PRKAG2** (that encodes the gamma-2 subunit of the AMP-activated protein kinase) have been observed in patients with WPW-syndrome¹⁵³. Mice that carry a mutation in the **PRKAG2** gene display ventricular pre-excitation and a phenotype identical to humans with a familial form of ventricular pre-excitation¹⁵⁴. Patel et al. demonstrated the *postnatal* development of myocardial connections through the annulus fibrosus of the AV valves in mice over-expressing the **PRKAG2** mutation¹⁵⁵. The findings in these models seem to be associated with cardiac hypertrophy, accumulation of excessive amounts of cardiac glycogen, and disruption of the annulus fibrosus by glycogen filled cardiomyocytes¹⁵⁶.

Furthermore, deletion of the gene **ALK3** (which codes for the type 1a receptor for bone morphogenetic proteins) in the AV canal during development causes ventricular pre-excitation, which may indicate an important role of this gene in WPW syndrome^{157 158}.

However, no morphological or functional explanation for the long atriofascicular/ventricular accessory bundles as observed in Mahaim tachycardias has been described.

Treatment strategies for clinical arrhythmias related to specific anatomical sites

Atrial fibrillation, atrial tachycardia and atrial flutter

Atrial fibrillation is the most common arrhythmia encountered in clinical practice, with an increasing incidence and prevalence at higher age ¹⁵⁹. The lifetime risk for development of atrial fibrillation is 1 in 4 for men and women aged 40 years and older, even in the absence of related cardiac disease such as congestive heart failure or myocardial infarction ¹⁶⁰. Besides symptoms that affect the quality of life, there is a significant risk of thrombo-embolic complications (such as stroke), of heart failure and of death.

30 Idiopathic atrial fibrillation can be classified as follows: In *paroxysmal* atrial fibrillation, recurrent episodes of atrial fibrillation terminate spontaneously (usually within 48 hours) without medical intervention; *Persistent* atrial fibrillation does not terminate spontaneously but can be terminated by chemical or electrical cardioversion; In *permanent* atrial fibrillation chronic atrial fibrillation is continuously present and cannot (or is not attempted to) be converted by medical intervention.

Results of pharmacological treatment are often disappointing, adverse side effects of anti-arrhythmic medication are considerable and pro-arrhythmic effects may occur ¹⁶¹. Over the recent years, interest in non-pharmacological therapies for atrial fibrillation has increased. Besides the development of techniques focusing on rate-control such as His bundle abla-

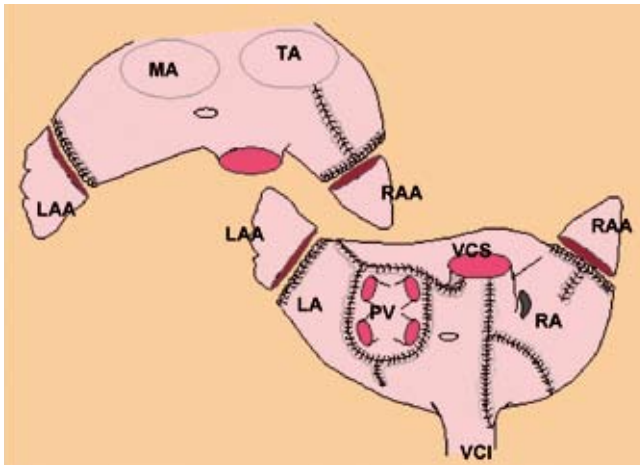


Figure 9

Schematic overview of the surgical MAZE procedure. Multiple incisions are made in the heart in order to eliminate the substrate for re-entry. LA: left atrium, LAA: left atrial appendage, MA: mitral annulus, PV: pulmonary veins, RA: right atrium, RAA: right atrial appendage, TA: tricuspid annulus, VCI: inferior caval vein, VSC: superior caval vein. Adapted from: Up to Date 2006: "MAZE procedure in atrial fibrillation".

tion, surgical techniques aimed at restoration of sinus rhythm have been developed. The most well known of these techniques is the surgical “MAZE” procedure, during which surgical atrial incisions create a network (resembling *mazes* of a net) that divide the atria in small segments, thus eliminating the substrate for re-entry¹⁶² (**Figure 9**). Several modifications of this technique are applied¹⁶³. In addition, intra-operative application of radiofrequency current and several-catheter based techniques have evolved. The observation that ectopic foci originating in the pulmonary veins can initiate atrial fibrillation^{90 125} has stimulated the development of percutaneous ablation strategies aimed at ablation at the site of the pulmonary veins. During these techniques, an ablation catheter is placed in the left atrium, usually by the transseptal approach. The initial ablation technique as proposed by the group of Haïssaguerre et al. was aimed at *focal elimination of arrhythmogenic ectopic foci* in the pulmonary veins^{90 125 164}. Arrhythmogenic veins can be recognised by the presence of (early) pulmonary vein potentials during sinus rhythm (**Figure 10**). The endpoint of this technique is the elimination of all pulmonary vein potentials. The advantage of this technique is that radiofrequency current is applied at only those sites in the pulmonary veins where arrhythmogenic activity is demonstrated. Disadvantages include the difficulty of mapping in patients with atrial fibrillation, necessitating cardioversion to sinus rhythm prior to the procedure; the difficulty of mapping intermittently firing foci; frequent recurrences of AF, necessitating re-ablation in approximately 41-69% of patients; long procedure-times due to extensive mapping; and a risk of pulmonary vein stenosis^{90 164-166}.

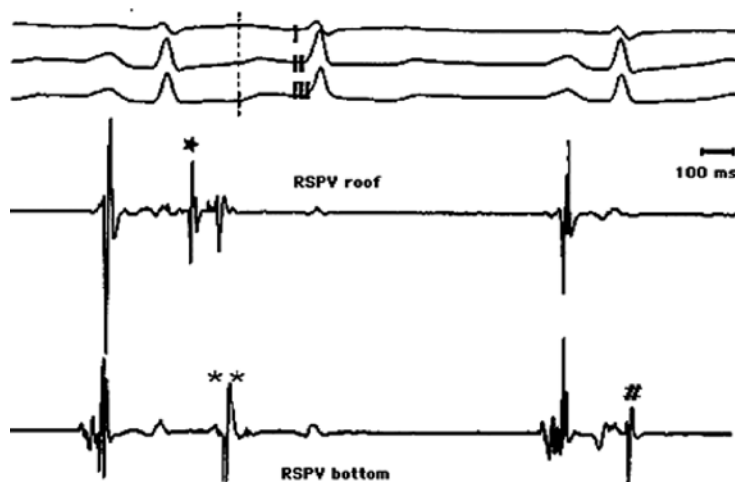


Figure 10

Pulmonary vein potentials during sinus rhythm. The upper 3 tracings are surface ECG lead I, II and III. The lower 2 recordings are derived from catheters positioned at the roof and bottom of the right superior pulmonary vein (RSPV). The first and third beats are sinus beats. The second beat, is an early ectopic beat originating from the roof of the RSPV, as indicated by the early pulmonary vein potential (asterisk). The bottom of the RSPV is passively activated later (**). # indicates a pulmonary vein potential from the bottom of the RSPV, without capture to the roof of the RSPV and to the atrium (“concealed” ectopic discharge). From: Haïssaguerre et al. *Circulation* 2000;101(12):1409-17.

Alternatively, *pulmonary vein isolation* can be performed, during which an attempt is made to achieve electrical isolation of the pulmonary veins from the left atrium by the application of circumferential ablation lesions at the ostia of the pulmonary veins. In general there are two methods by which pulmonary vein isolation is performed: First, *circumferential* pulmonary vein isolation, an anatomical approach during which electro-anatomical maps are used to locate the pulmonary veins and to guide the application of ablation lesion surrounding the pulmonary veins. This method was first proposed by the group of Carlo Pappone in Milan ¹⁶⁷. Next to disconnecting the trigger from the left atrium, it is believed that the substrate for atrial fibrillation is modified by the application of ablation lesions in the left atrium. Additional ablation lines connecting the ablation lines to anatomical landmarks, such as the left isthmus (between the left inferior pulmonary vein and the mitral annulus) are often made to prevent the occurrence of macro-reentrant circuits that may lead to left atrial flutter.

A second method of pulmonary vein isolation is *segmental* pulmonary vein isolation, during which a circular “lasso” catheter (first used by the group of Haissaguerre ¹⁶⁸) is placed at the orifice of a pulmonary vein, and is used to define the sites of pulmonary vein potentials and of electrical connections between pulmonary veins and the left atrium. Ablation at the sites of the connection at the pulmonary venous orifice is performed, aimed at achieving electrical isolation of the pulmonary veins from the left atrial body.

Recent publications stress the importance of complete electrical isolation, since incomplete electrical isolation of the pulmonary veins (either by resumption of conduction between the ablated areas, or due to residual conduction in pulmonary veins) may result in (late) recurrence of atrial fibrillation ¹⁶⁹⁻¹⁷². Furthermore, isolation of all pulmonary veins has been demonstrated to be more effective than selective pulmonary vein isolation ¹⁷³.

Advantages of complete (i.e. ablation of all pulmonary veins) pulmonary vein isolation are that extensive mapping is not necessary; “recurrent” foci are prevented by targeting all veins; and a reduced risk of pulmonary vein stenosis by targeting the application of radiofrequency current outside the orifice of the pulmonary veins. Disadvantages of this technique include the ablation of a significantly larger area, and long procedure-and fluoroscopy times due to difficult visualization of the pulmonary venous ostia.

Complete isolation of all four pulmonary veins from the left atrium has become the preferred approach for the treatment and prevention of both paroxysmal and persistent and permanent atrial fibrillation ¹⁷⁴. Results for patients with paroxysmal atrial fibrillation seem to be better than those for patients with persistent and permanent atrial fibrillation. In one large series of 251 patients 85% of patients with paroxysmal atrial fibrillation and 68% of patients with persistent/permanent AF were free of atrial fibrillation after RFCA ¹⁷⁵. In general, the outcome of circumferential ablation of the pulmonary veins seems to be better than the outcome of focal/segmental ablation of the pulmonary veins ^{173 176}, although a recent study reports better outcomes for segmental ablation ¹⁷⁷. However, in the latter study significant more patients with structural heart disease were included in the group receiving circumferential ablation. Differences in outcome may be due to patient selection.

Atrial fibrillation and atrial arrhythmias can also be related to other sites in the atria, such as the ostia of the coronary sinus and caval veins^{88 178 179} and the crista terminalis, and are accessible to local treatment by RFCA^{86 87 87}. Furthermore, in experimental animal models, the mitral annulus-aorta junction was found to be a source of arrhythmias¹⁸⁰⁻¹⁸². Atrial tachycardia has also been observed to originate at the posterior side of the left atrial appendage¹⁸³.

Ventricular tachycardia

Although most ventricular tachycardias are secondary to ischemia, several tachycardias are related to specific anatomical intracardiac sites, such as the right ventricular and left ventricular outflow tracts¹⁸⁴. RFCA of ventricular tachycardia is the treatment of choice in selected patients with hemodynamically stable VT^{185 186}. However, exact localization of catheters in relation to cardiac anatomy using fluoroscopy is difficult and time-consuming, in particular when small localized aneurysms as observed in arrhythmogenic right ventricular dysplasia (ARVD), are the targets of ablation. Furthermore, RFCA-procedures are associated with an increased risk of serious procedure-related complications^{185 187}, such as thrombo-embolic events or perforation with subsequent pericardial effusion (tamponade) due to catheter manipulation or – less often – the application of RF-current. The ability to monitor the occurrence of complications directly will potentially have beneficial effects on outcome¹⁸⁸.

Problems encountered with radiofrequency catheter ablation (of atrial fibrillation)

Visualisation of the substrate for ablation

As described above, results of catheter based ablation techniques are promising, but at the cost of long procedure times and serious procedure-related complications (described in detail below)¹⁶⁵. These issues are (in part) related to the fact that the ablation targets, the veno-atrial junctions and the pulmonary veins or their ostia, are not easily visualized using fluoroscopy alone. Furthermore, fluoroscopy does not allow identification of anatomical intracardiac structures accurately and cannot be used to verify adequate catheter-tissue contact and variations in wall thickness. Accurate catheter positioning can therefore be difficult and time-consuming, which may result in long-procedure and fluoroscopy times.

Variations in pulmonary venous anatomy

It has been long recognised that interindividual variations in the number of pulmonary veins and their insertion in the left atrium occur. Already in 1966, Nathan et al. described variations in number of pulmonary veins and the insertion in the left atrium¹⁸⁹. In several anatomical reports, based on observations in human autopsy hearts, common ostia have been observed in approximately 25% of examined hearts, most common on the left

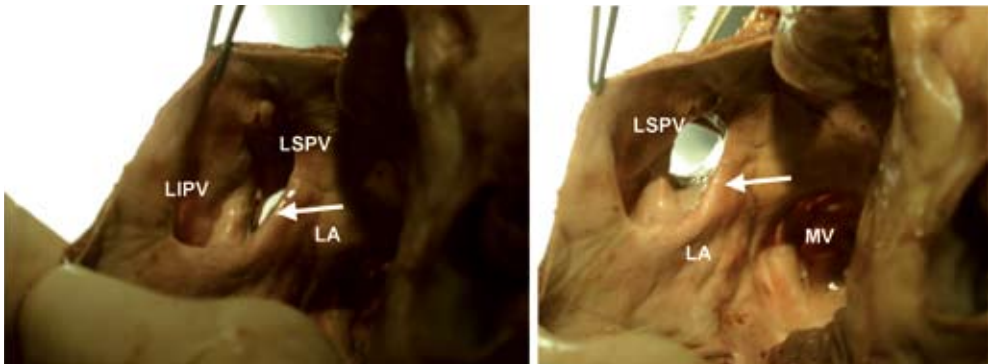


Figure 11

The left pulmonary veins. Both veins are separated from the left atrium by a ridge of tissue (arrow), which forms a large ostium in which both veins drain. LA: left atrium LIPV: left inferior pulmonary vein, LSPV: left superior pulmonary vein, MV: mitral valve.

side^{190 124 191}. The frequency of occurrence in which the different variations are described in several studies using imaging techniques to depict the pulmonary veins, differs largely and ranges from 19% to almost 40%¹⁹²⁻¹⁹⁵. In our experience with human hearts, a ridge of tissue is often present surrounding the ostia of particularly the left pulmonary veins (**Figure 11**). Knowledge about the variations in pulmonary vein anatomy and morphology of the ostia of the pulmonary veins may facilitate radiofrequency catheter ablation at this site.

How to define the atrio-pulmonary venous junction?

The above mentioned different percentages of the occurrence of variations in pulmonary vein anatomy, such as the occurrence of common ostia and additional pulmonary venous branches can mainly be attributed to the fact that to date there is no generally accepted definition of the border between the left atrium and the pulmonary veins. Histologically, there is no clear border between the left atrium and the pulmonary veins. Also, there is no consensus on how to determine the left atrial-pulmonary venous junction using imaging techniques. An anatomical definition of this atrio-pulmonary venous junction is necessary however in procedures where ablation lesions are targeted outside the pulmonary venous ostia, and thus depends on proper recognition of this junction.

Procedure related complications

Risks associated with transseptal puncture

Catheter ablation in the left atrium requires entrance to the left atrium by either a retrograde approach through the aortic valve, or transseptal through an open foramen ovale but more often by transseptal puncture, which is currently preferred by most centres. Although transseptal puncture is usually feasible, adequate targeting of the puncture site, i.e. the *fossa ovalis* in the interatrial septum, is critical as several serious complications can

occur during this procedure. Complications related to this procedure include aortic perforation, perforation with cardiac tamponade and systemic emboli¹⁹⁶. Using fluoroscopy, the target place for puncture, the fossa ovalis can not be visualised. Transseptal puncture can be performed under transoesophageal echocardiographic guidance, but this procedure is uncomfortable for the patient and requires sedation. In recent years, guidance by intracardiac echocardiography has proved a feasible and safe method to guide transseptal puncture (described in **Chapter 6**).

Pulmonary vein stenosis

Pulmonary veins stenosis is a well known complication of ablation at the site of the pulmonary veins, and can be divided in *acute* pulmonary vein stenosis, that occurs directly after ablation, and *late* pulmonary vein stenosis, that may progressively develop after RFCA to become symptomatic in the course of several months¹⁹⁷⁻¹⁹⁹. Acute stenosis is thought to be inflicted by oedema and tissue swelling by the application of radiofrequency current, and does not appear to predict the occurrence of chronic pulmonary vein stenosis^{200 201}. Although mild to moderate pulmonary vein stenosis is often asymptomatic, more severe stenosis, and the presence of more than one stenotic vein, may produce a range of symptoms including chest pain, dyspnoea during exertion or at rest, cough, hemoptysis, recurrent pulmonary infections and pulmonary hypertension^{202 203}.

Percutaneous intervention by balloon dilatation with or without stenting produces a rapid relief of symptoms, but requires repeated intervention in a significant number of patients due to re-stenosis or in-stent restenosis¹⁹⁹.

The risk of this complication is highest when radiofrequency current is applied inside the pulmonary veins^{90 204}. However, also during pulmonary vein isolation with RFCA targeted outside the veins this complication has been reported²⁰⁵.

Imaging techniques, such as intracardiac echocardiography, allowing more accurate visualisation of the left atrial-pulmonary venous junction may diminish the incidence of pulmonary vein stenosis.

Perforation, pericardial effusion, cardiac tamponade

The application of radiofrequency current carries a risk of perforation with subsequent cardiac tamponade of the cardiac or vessel wall, especially when ablation is performed at sites where the myocardium is very thin, and when ablation is performed with high power and temperature settings. Monitoring of catheters and early detection of this complication by on-line imaging techniques improves safety of the procedures.

Systemic thrombo-embolism

As with all left sided procedures, catheter ablation in the left atrium carries a risk of thrombo-embolic complications, such as peripheral or cerebral ischemia and stroke. The risk of this complication can be reduced by continuous heparinisation during these procedures,

and formation of thrombus at the catheter tip can be evaluated by monitoring impedance rise. Direct evaluation of the formation of thrombus by imaging techniques may also contribute to the safety of these procedures.

Phrenic nerve paralysis

The right phrenic nerve runs in close association with the right superior pulmonary vein²⁰⁶. During catheter ablation, irritation to this nerve may present itself as hick-ups, whereas more serious injury may cause diaphragmatic hemiparalysis, a condition that is asymptomatic in most patients, but may give dyspnoea d'effort, especially in patients with underlying lung disease. Partial return of function of the damaged nerve may occur²⁰⁷. Furthermore, damage to the vagal nerve plexus surrounding the oesophagus has may be responsible for the reported cases of pyloric spasm and gastric hypomotility, causing indigestion after ablation²⁰⁸.

Left atrial flutter after ablation. Atypical left atrial flutter may result from a new re-entrant circuit around radiofrequency lesions or left atrial scar tissue. These circuits often involve the left atrial isthmus between the left inferior pulmonary vein and the mitral annulus. To reduce this risk, a left isthmus ablation line can be created during radiofrequency catheter ablation of atrial fibrillation. Also the creation of continuous transmural lines prevents the occurrence of left atrial flutter after ablation²⁰⁹. The coronary sinus musculature can also play a role in the occurrence of atrial flutter after radiofrequency catheter ablation²¹⁰.

Left atrial-oesophageal fistula

The formation of a fistula between the left atrium and the oesophagus is a potentially lethal complication of RFCA for atrial fibrillation. Clinical features may resemble pericarditis. Patients can present with high fever and symptoms of cerebral and cardiac ischemia caused by (air) emboli. The close association of the oesophagus and the left atrial dorsal wall can cause patients with very thin myocardial dorsal walls to be prone to this serious complication, and lower power and temperature settings are recommended during application of radiofrequency energy at this site^{211 212}.

Damage to the cardiac conduction system

Application of radiofrequency current at part of the CCS, e.g. the AV node or His bundle, may result in (transient) bradycardia or asystole. This must be distinguished from bradycardia/asystole due to ablation of the extensive network of autonomic nerve fibers situated at the pulmonary venous ostia, which has been suggested to be a positive predictor of procedural success²¹³.

Anatomical knowledge prior to these procedures and improved monitoring of catheters in relation to the substrate may increase safety and efficacy of these procedures.

Imaging techniques to support RFCA at specific anatomical sites

As described above, there are still several challenges for improvement of safety and efficacy of RFCA procedures. Currently pre-procedural evaluation of cardiac anatomy of target structures for ablation are performed with magnetic resonance imaging (MRI) or computed tomography (CT). During RFCA procedures the use of 3D electro-anatomic mapping systems can be helpful. In addition, intracardiac echocardiography can be used to obtain on-line information on cardiac anatomy, catheter position, hemodynamics and monitoring of complications. Imaging techniques used in the studies of this thesis are described below.

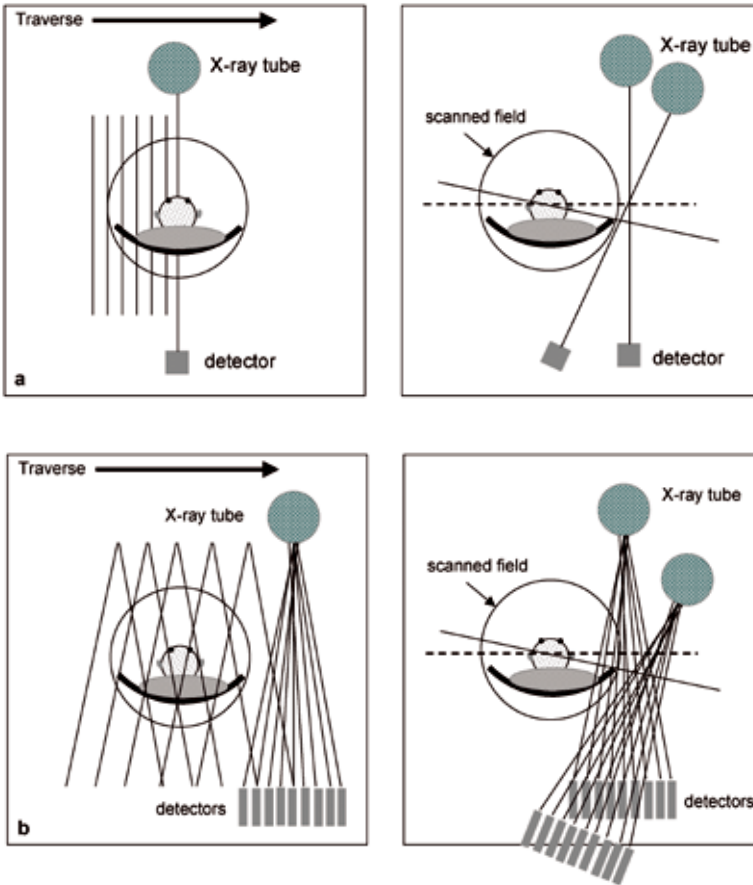
The CARTO system

The name CARTO is derived from *cartography*, the creation of a map. The CARTO system is a non-fluoroscopic, three-dimensional, catheter based electro-anatomic mapping system, that is used to create an anatomical map of a cardiac chamber and other anatomical structures, e.g. the left atrium and the pulmonary veins, on which both local activation times and voltage maps can be superimposed. The CARTO system consists of a miniaturized magnetic field sensor incorporated in a catheter tip, an external ultralow magnetic field emitter (location pad) and a processing unit. The magnetic field emitted by the location pad is received by the sensor in the catheter and sent through the catheter to the processing unit. By moving the catheter containing the sensor in the heart, the system can calculate the location of the catheter in relation to the location pad, and thus depict where in the heart the catheter is located. A second catheter serves as reference catheter, which is usually positioned in right atrium or the coronary sinus. Local activation times are calculated by registration of local unipolar electrograms by the mapping catheter on different sites in the atrium and comparing these with the local activation time measured by the reference catheter. These local activation times are depicted on the anatomical 3-D reconstruction of the cardiac cavity. The catheter is imaged in this 3-dimensional view of the heart, and ablation sites can be annotated ²¹⁴.

Multi-Slice Computed Tomography

History and basics of CT

Computed tomography is a cross-sectional imaging technique that was developed by G.N. Hounsfield and A.M. Cormack in 1972, for which they were granted the Nobel prize in Medicine in 1979. First generation CT scanners consisted of 1 X-ray tube that sent a X-ray beam through the patient, before it hit a single detector opposite the tube (**Figure 12a**). The X-ray tube would thus create 1 recording, where after it would shift to another position to create another recording, after which the tube-detector combination would rotate several degrees and make another series. Second generation CT-scanners had multiple de-



tectors opposite the X-ray tube, thus allowing the acquisition of more data (**Figure 12b**). Currently, with the use of third generation CT scanners the X-ray tube-detector combination rotates around the patient allowing the creation of a slice within 1 breath hold. During spiral CT scanning, the patient table is moving during rotation of the X-ray tube detector combination, creating a spiral, (**Figure 12c**). During multi-slice (multi-detector row) CT (MSCT) scanning, multiple rows of detectors in the Z axis allow multiple axial slices to be obtained during a single rotation of the X-ray tube (4, 16, 32 and 64 for the 4-slice, 16-slice, 32 slice and 64 slice CT scanner respectively). In the scan plane (X,Y plane) the number of detectors is the same as in the conventional third generation scanners, but in the longitudinal plane (Z-plane), the multi-slice detector consists of multiple elements, allowing the creation of multiple slices at the same time (**Figure 12d**). Also, the fast rotation time of the tube adds to a decrease in duration of the scanning period.

For the multi-slice system used in the studies performed in this thesis, this means that with a rotation velocity of 0.5 seconds, 4 slices per rotation can be obtained with the 4-slice scanner (i.e. 8 slices per second) and 16 with the 16-slice scanner (i.e. 32 slices per sec-

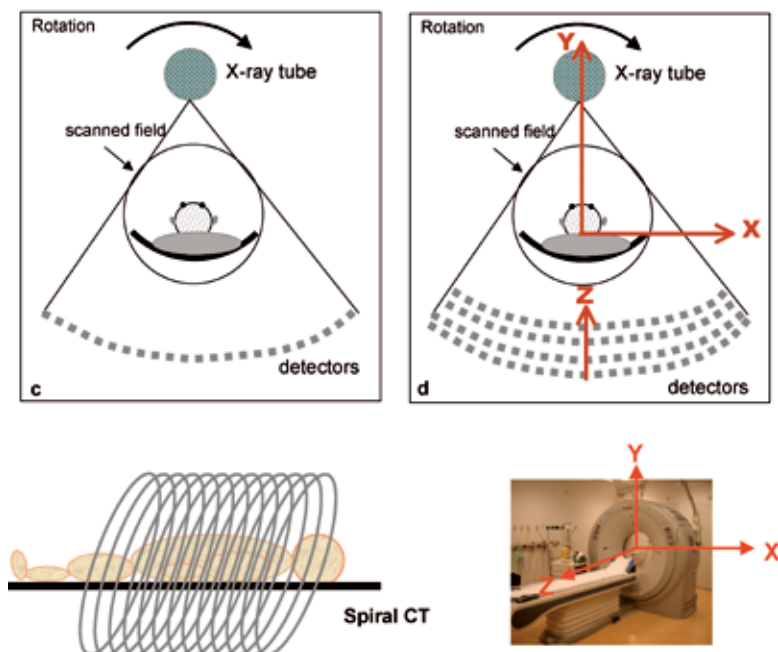


Figure 12

- a. First generation scanner
- b. Second generation scanner
- c. Third generation scanner
- d. Multi-slice (Multi-detector row) scanner

Adapted from: Philips 1990; Computed Tomography, Principles and Practice

ond). Currently, in Leiden a 64-slice scanner is used (i.e. 128 slices per second/160 slices per second, (for rotation velocity of 0.5 seconds and 0.4 seconds respectively). Scanning of the whole heart, which usually can be performed by scanning a traject of 8-12 cm, can be performed during 1 breath hold (that lasts 8-20 seconds, depending on the system used).

Spatial and Temporal Resolution

Spatial resolution is expressed in millimetres and refers to the capacity of the system to separately depict details that highly differ in contrast, in other words the capacity of the system to depict small, high contrast details in relation to the surrounding tissues. The spatial resolution is directly related to the slice thickness and the reconstruction matrix.

Contrast resolution is a measure for distinction between areas with only slight contrast difference, in other words how well the system can depict relatively large details with a small contrast in relation to the surrounding tissues.

Isotropic imaging means that the voxels have the same size in every dimension, which allows data reconstruction in multiple viewing planes (=multiplanar reconstruction).

Temporal resolution is expressed in milliseconds and refers to the time needed to acquire the information (speed of data acquisition), and thus the clarity of imaging of the contracting heart. The temporal resolution determines the degree of motion suppression, and is related to a.o. the pitch factor (i.e. the ratio of the couch increment per rotation to the collimated slice thickness at the axis of rotation), the rotation time of the X-ray tube and detector combination and the heart rate of the patient. The smaller the spatial and temporal resolution, the better the image quality. With the system used in this thesis, temporal resolution can theoretically be as low as approximately 150-250 ms.

Retrospective ECG gated scanning

40 The heart is a continuously moving organ, and the challenge in cardiac CT is to obtain images that are not hindered by cardiac motion artefacts. During ECG gated spiral scanning an attempt is made to synchronise the reconstruction of a continuous spiral CT scan to the cardiac motion, by using a simultaneously recorded ECG trace. The R-peaks of the ECG trace are annotated to the scanned raw data set. A large amount of data is acquired of the *whole cardiac cycle*, and retrospectively different cardiac phases can be reconstructed (which can be useful for selection of optimal image quality by reconstruction of the phase with the least cardiac motion artefacts). Retrospective ECG gating also allows functional analysis, in contrast to prospective scanning, during which the cardiac phase to be reconstructed is pre-selected, and the exposure trigger is determined based on the previous cardiac cycle.

Scanning patients with high heart rates

In the system used in this thesis, segments of cardiac phases from multiple rotations can be used to reconstruct the desired cardiac phase, in other words, views from different rotations are combined to simulate one 180° tube rotation (**Figure 13a**). The more segments that are available for reconstruction, the better the temporal resolution and thus the image quality. This also means that during high heart rates, an increased number of cardiac cycles is available for reconstruction if the scan windows remains the same. (The scan window = rotation time/pitch factor). The system can handle up to 5 segments for reconstruction. Heart frequencies up to 140 beats per minute can be scanned, therefore the use of beta-blocking agents may not be necessary (**Figure 13b**). Also this system has the capacity to adjust to some extent for irregular heart rates using *adaptive temporal resolution*, that is adjusted to the detected heart rate. This means that scanning and processing is not fixed, but that the number of segments to be used for reconstruction is adapted for best temporal resolution by following the fluctuations in the heart rate, while the optimal scan parameters for the patient's heart rate are automatically selected.

CT Viewing modes

Evaluation of cardiac anatomy on MSCT scans can be performed using the 3 standard orthogonal planes, being the transversal plane, the coronal (frontal) plane, and the sagittal

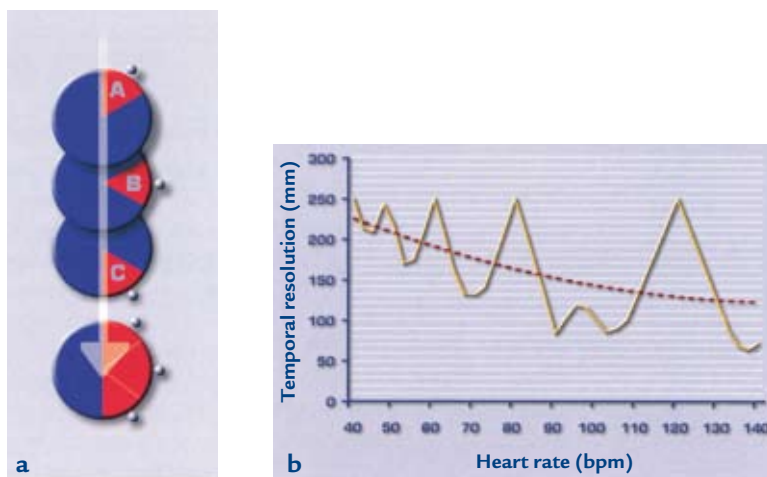


Figure 13

a. Different tube positions allow 3 segments to be reconstructed to a virtual 180° rotation

b. Temporal resolution curve.

From: Toshiba Corporation 2003: *Basics of Cardiac CT Imaging*.

(lateral) plane. Next to the orthogonal planes, sophisticated post processing techniques allow optimal insight into the cardiac venous system by the creation of 3-dimensional reconstructions, virtual endoviews and multiplanar reformats.

Radiation Dosage

The radiation dosage used when scanning using retrospective ECG gated triggering is in the range of 7 to 11 mSv^{215 216}. This is a significant radiation load, when taking into account that a diagnostic coronary angiogram has a radiation load of 2-6 mS. Part of this problem can be solved by using prospective scanning, during which data acquisition is also synchronised with a ECG, but each scan is triggered at a predetermined phase of the RR-interval. Using prospective scanning, radiation exposure is reduced to approximately 4.3 mSv²¹⁷. Prospective scanning does not allow dynamic function analysis and reconstruction in several cardiac phases. Currently, we are applying untriggered scanning for imaging of the pulmonary veins, with satisfactory results, thus allowing significant dose reduction. Alternatively, dose modulation can be used for reduction of the radiation dose: helical scanning is performed with continuous data acquisition; however, a dose reduction can be applied during 0-35% of the cardiac cycle, as these phases are unlikely to be used for further diagnostic evaluation.

Disadvantages and Advantages of MSCT as compared to MRI

The advantage of MRI as compared to MSCT is the lack of ionizing radiation exposure, however MRI cannot be applied to patients with pacemakers, claustrophobia, or in pa-

tients who, due to their clinical condition, cannot tolerate the considerably long scanning times of MRI. Furthermore, better spatial resolution is obtained with CT, making assessment of especially small vascular branches more feasible. Advantages of the multi-slice technique include short scanning times, maximal scan range, and maximal resolution in the Z-plane, allowing high quality post-processing, such as multiplanar reformats and 3-dimensional reconstructions.

Multi-Slice Computed Tomography for Imaging of the Cardiac Veins

CT-imaging of the pulmonary veins

42

As described above, the treatment of atrial fibrillation by radiofrequency catheter ablation is still challenged by several issues, including difficult visualisation and variable anatomy of the pulmonary veins.

Using imaging techniques such as CT and MRI, variations in pulmonary vein anatomy are often noted. Most authors agree that common ostia are observed most frequently on the left side, and additional pulmonary veins and an early branching pattern are observed most frequently on the right side. However as mentioned the frequency in which the different variations are recognised differs largely in between different studies, and ranges from 19% to almost 40 %¹⁹²⁻¹⁹⁵.

Both the occurrence of common ostia and additional pulmonary veins²¹⁸ have been associated with the occurrence of arrhythmias^{193 219}, whereas the frequently observed occurrence of an early branching pattern of the right inferior pulmonary vein has been suggested to be a possible protective anatomic variant, since arrhythmias seem to be initiated less frequently from the right inferior pulmonary vein^{125 220}.

Pulmonary venous ostia can be dilated in patients with atrial fibrillation²²¹. Also, recent data using MRI demonstrated that the shape of the ostia of the pulmonary veins is asymmetric¹⁹⁵. As arrhythmogenicity can arise in all pulmonary veins, the best clinical results are obtained by targeting all pulmonary veins^{222 223}.

A limitation in the evaluation of the occurrence of common ostia on MSCT-images, is the lack of anatomical boundaries demonstrating the exact border between the left atrium and the pulmonary veins. In most imaging studies using MSCT, the left atrial-pulmonary venous border is determined on 3-dimensional reconstructions or single orthogonal planes. The use of a structured method using the 3 different and more accurate orthogonal (transversal, coronal and sagittal) planes may facilitate the recognitions of variations in anatomy.

CT imaging of the coronary venous system

As is the case for the pulmonary veins, variations in anatomy have also been described in anatomical studies for the coronary venous system¹⁰⁶. To date, experience with MSCT for imaging of the coronary venous system is only limited.

The coronary venous system and cardiac resynchronisation therapy

Cardiac resynchronisation therapy offers a good therapeutic option for the treatment of patients with ventricular dyssynchronia and moderate to severe heart failure²²⁴. Right ventricular pacing is achieved by the insertion of a pacemaker lead in the right ventricular apex, whereas the left ventricular pacemaker lead is positioned in one of the tributaries of the coronary sinus. Although success rates for placement of a transvenous cardiac resynchronisation system is relatively high (88-95% in large clinical trials), in 5-12% of patients the procedure does not succeed due to placement failure of the left ventricular (LV) lead using a transvenous approach²²⁴. Reasons for failure of LV lead placement include the lack of suitable side branches^{224 225}, narrowing of the coronary sinus ostium or ostia atresia²²⁶, and the inability to advance catheters through the coronary venous system^{225 227}. This may result in long procedure- and fluoroscopy times and an increased risk of dissection or perforation of the coronary sinus. Also, recent studies have strained the importance of adequate vein selection and several authors have suggested that the pacing site should be individualised for achieving the best results^{228 229}.

Therefore, anatomical knowledge prior to procedures may be helpful to distinguish patients eligible for CRT using a transvenous approach from those who are more likely to benefit from a surgical epicardial approach.

The cardiac venous system and interventional electrophysiology

Next to the interest for the coronary sinus as an anatomical structure for placement of the left ventricular lead, the coronary sinus has also been recognised as an arrhythmogenic structure^{89 178}. Catheter ablation techniques have been successfully applied to eliminate arrhythmogenic foci at the coronary sinus ostium²³⁰. Posteroseptal and left posterior accessory connections have been described at the site of the coronary sinus, which may also be cured by radiofrequency catheter ablation^{231 232 233}. Furthermore, arrhythmogenic capacities have been attributed to the *vein of Marshall* which can be cured by catheter ablation at this site²³⁴. Knowledge of the location of the vein of Marshall may be useful for the guidance of ablation of accessory pathways²³¹. The vein of Marshall can also be used to mark the border between the coronary sinus and the great cardiac vein¹⁰⁶. At this border, the valve of Vieussens is often present, which is an important cause of problems with advancing the catheter into cardiac veins²²⁷.

The close anatomical relationship of the coronary venous system to the coronary arteries and oesophagus warrants careful selection of application sites for radiofrequency current²³⁵.

Intracardiac Echocardiography

Echocardiography is a powerful technique for cardiac imaging, that uses the physical capacities of ultrasound (sound with frequencies that cannot be perceived by the human auditory system) for imaging of the heart and cardiac vessels. The introduction of intra-

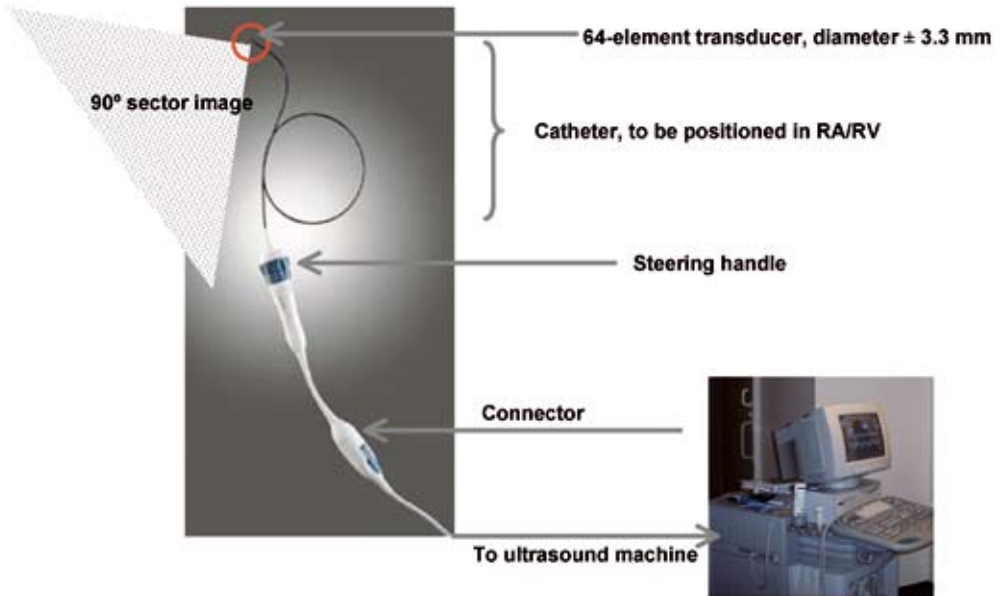


Figure 14

Intracardiac ultrasound catheter. At the tip of the catheter a miniaturized transducer is inserted, that can scan in a 90° monoplane. With gratitude to Siemens.

cardiac ultrasound systems capable of scanning with low frequencies (allowing deep tissue penetration), allows imaging of the whole heart with the ultrasound catheter positioned exclusively in the right atrium or right ventricle. In the studies described in this thesis a phased array intracardiac echocardiography system is used. This system uses a 10 French (± 3.3 mm) ultrasound catheter, positioned in the right atrium or right ventricle for imaging of the entire heart. The ultrasound catheter consists of a miniaturized 64-element, phased array transducer, that is incorporated in a single use catheter (**Figure 14**). The transducer scans in the longitudinal monoplane, providing a 90° sector image with tissue penetration of approximately 15 cm. Two planes of bi-directional steering (anterior-posterior and left-right, each in a direction of 160 degrees) are possible by using a mechanism on the handle of the catheter. The high resolution multiple frequency transducer (5-10 MHz) allows tissue penetration enhancement, thus allowing depth control. Measurements of hemodynamic and physiologic variables can be made using Doppler imaging. The catheter is connected to an ultrasound system (**Figure 14**).

History, technical requirements and clinical applications

An overview of history, technical requirements and clinical applications in interventional procedures of intracardiac echocardiography is provided in **Chapter 6**.

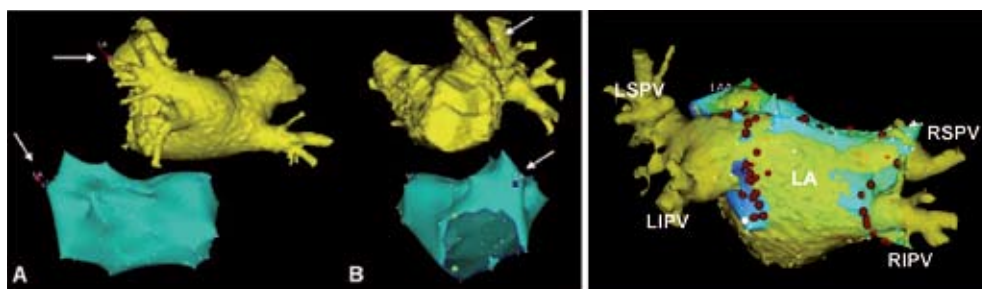


Figure 15

Image integration. Electro-anatomical maps acquired with a non-fluoroscopic mapping system (CARTO) are fused with MSCT images. During the procedure, ablation points can be marked in this fused image, to give the operator optimal insight of patient anatomy in relation to the position of the ablation catheter. LA: left atrium, LIPV: left inferior pulmonary vein, LSPV: left superior pulmonary vein, RIPV: right inferior pulmonary vein, RSPV: right superior pulmonary vein. Modified after Tops et al. *Heart Rhythm*. 2005 Oct;2(10):1076-81.

Imaging planes

To date, there are no standard views for intracardiac echocardiography, such as for trans-thoracic and transesophageal echocardiography. Because the catheter scans in the mono-plane, (as opposed to the rotating transoesophageal transducer), only 2-D imaging can be achieved. However, using a standardized method, accurate views of intracardiac structures can be obtained, which is also described in **Chapter 6**.

Integration of Imaging Techniques for Treatment of Clinical Arrhythmias in the Electrophysiology Cathlab

In the clinical research performed in this thesis, multiple imaging techniques have been used in parallel to facilitate radiofrequency ablation procedures. During these procedures the advantages of the different imaging techniques are integrated: depiction of the substrate prior to treatment by multi-slice spiral CT; during the procedure the substrate can be visualized in relation to catheters and cardiac devices with intracardiac echocardiography and be combined with the information obtained by electroanatomical mapping. However, conventional 3D electroanatomic mapping systems are limited by the use of reconstructed anatomy. New image integration systems allow the use of real cardiac anatomy during catheter ablation procedures²³⁶⁻²³⁸. Using this integrated approach, on line electrical activation maps can be directly correlated to the patient's anatomy as obtained with multi-slice computed tomography (**Figure 15**).

Aim and outline of the thesis

This thesis focuses on cardiac anatomy as a substrate for clinical arrhythmias, as well as the target for treatment strategies. The aim of the first part of this thesis is to correlate results of basic studies of the development of the cardiac conduction system to clinical arrhythmias. The feasibility and evaluation of the treatment of clinical arrhythmias originating in specific anatomical sites guided by imaging techniques is the aim of the second part of this thesis.

In **Chapter 2** the development of the cardiac conduction system was studied in *CCS-lacZ* transgenic mice, and results were correlated to anatomical predilection sites of clinical arrhythmias. Special attention was paid to the development of the primitive pulmonary vein in relation to the developing cardiac conduction system.

Chapter 3 describes the developing cardiac conduction system in *CCS-lacZ* reporter mice in relation to the development of the right ventricular inflow tract and the moderator band, and a morphological substrate for the occurrence of Mahaim re-entrant tachycardias was hypothesized. The morphological results of this study were subsequently tested by functional electrophysiological experiments in murine embryos.

In **Chapter 4** the histological consequences of the incorporation of the primitive pulmonary vein into the left atrium was studied in sequential developmental stages in human fetuses, neonates and adults.

In **Chapter 5**, multi-slice CT was used to create a structured method to identify the left atrial-pulmonary venous border. Furthermore, the feasibility of multi-slice CT for imaging of the left atrium and the pulmonary veins to provide a roadmap for RFCA of atrial fibrillation, is described.

In **Chapter 6** a review of the history, technical requirements and the application of intracardiac echocardiography in interventional electrophysiology, is provided.

Chapter 7 describes a method to identify the atrio-venous border and pulmonary venous anatomy using intracardiac echocardiography during RFCA targeted outside the ostia of the pulmonary veins. Furthermore, pre- and post procedural measurements of pulmonary venous ostia and of flow velocities in the pulmonary veins were performed for evaluation of the occurrence of acute pulmonary vein stenosis and the eventual hemodynamic consequences.

In **Chapter 8**, a head-to-head comparison between multi-slice CT and intracardiac echocardiography for imaging of the pulmonary veins is described.

In **Chapter 9**, variations in the anatomy of the coronary venous system were evaluated using multi-slice CT, and possible clinical implications of the results are described.

Finally, in **Chapter 10** the occurrence and treatment of atrial arrhythmias originating from the mitral annulus-aortic junction is described, and a correlation is made with the developing cardiac conduction system in *CCS-lacZ* transgenic mice.

Reference List

1. Garcia-Martinez V, Schoenwolf GC. Primitive-streak origin of the cardiovascular system in avian embryos. *Dev. Biol.* 1993;**159**:706-19.
2. Schoenwolf GC, Garcia-Martinez V. Primitive-streak origin and state of commitment of cells of the cardiovascular system in avian and mammalian embryos. *Cell Mol. Biol. Res.* 1995;**41**:233-40.
3. Rosenquist GC. Location and movements of cardiogenic cells in the chick embryo: the heart-forming portion of the primitive streak. *Dev. Biol.* 1970;**22**:461-75.
4. DeRuiter MC, Poelmann RE, VanderPlas-de Vries I, Mentink MM, Gittenberger-De Groot AC. The development of the myocardium and endocardium in mouse embryos. Fusion of two heart tubes? *Anat. Embryol. (Berl)* 1992;**185**:461-73.
5. Fishman MC, Chien KR. Fashioning the vertebrate heart: earliest embryonic decisions. *Development* 1997;**124**:2099-117.
6. Kelly RG, Buckingham ME. The anterior heart-forming field: voyage to the arterial pole of the heart. *Trends Genet.* 2002;**18**:210-6.
7. Gittenberger-De Groot AC, DeRuiter MC, Bartelings MM, Poelmann RE. Embryology of congenital heart disease. In: Crawford MH, DiMarco JP, Paulus WJ, eds. *Cardiology*. Richard Furn, 2004:1217-27.
8. Bruneau BG. Transcriptional regulation of vertebrate cardiac morphogenesis. *Circ. Res.* 2002;**90**:509-19.
9. Srivastava D, Olson EN. A genetic blueprint for cardiac development. *Nature* 2000;**407**:221-6.
10. Kirby ML, Gale TF, Stewart DE. Neural crest cells contribute to normal aorticopulmonary septation. *Science* 1983;**220**:1059-61.
11. Poelmann RE, Mikawa T, Gittenberger-De Groot AC. Neural crest cells in outflow tract septation of the embryonic chicken heart: differentiation and apoptosis. *Dev. Dyn.* 1998;**212**:373-84.
12. Kruithof BP, van den Hoff MJ, Wessels A, Moorman AF. Cardiac muscle cell formation after development of the linear heart tube. *Dev. Dyn.* 2003;**227**:1-13.
13. Millino C, Sarinella F, Tiveron C, Villa A, Sartore S, Ausoni S. Cardiac and smooth muscle cell contribution to the formation of the murine pulmonary veins. *Dev. Dyn.* 2000;**218**:414-25.
14. Gorza L, Schiaffino S, Vitadello M. Heart conduction system: a neural crest derivative? *Brain Res.* 1988;**457**:360-6.
15. Gorza L, Vitadello M. Distribution of conduction system fibers in the developing and adult rabbit heart revealed by an antineurofilament antibody. *Circ. Res.* 1989;**65**:360-9.
16. Gourdie RG, Mima T, Thompson RP, Mikawa T. Terminal diversification of the myocyte lineage generates Purkinje fibers of the cardiac conduction system. *Development* 1995;**121**:1423-31.
17. Gourdie RG, Kubalak SW, O'Brien TX, Chien KR, Mikawa T. Development of the pacemaking and cardiac conduction system lineages. In: Chien KR, ed. *Molecular basis of cardiovascular disease*. Saunders, 2004.
18. Cheng S, Litchenberg WH, Cole GJ, Mikawa T, Thompson RP, Gourdie RG. Development of the cardiac conduction system involves recruitment within a multipotent cardiomyogenic lineage. *Development* 1999;**126**:5041-9.
19. Rentschler S, Zander J, Meyers K, France D, Levine R, Porter G *et al.* Neuregulin-1 promotes formation of the murine cardiac conduction system. *Proc. Natl. Acad. Sci. U.S.A* 2002;**99**:10464-9.
20. Patel R, Kos L. Endothelin-1 and Neuregulin-1 convert embryonic cardiomyocytes into cells of the conduction system in the mouse. *Dev. Dyn.* 2005;**233**:20-8.
21. Poelmann RE, Gittenberger-De Groot AC. A subpopulation of apoptosis-prone cardiac neural crest cells targets to the venous pole: multiple functions in heart development? *Dev. Biol.* 1999;**207**:271-86.
22. Poelmann RE, Jongbloed MR, Molin DG, Fekkes ML, Wang Z, Fishman GI *et al.* The neural crest is contiguous with the cardiac conduction system in the mouse embryo: a role in induction? *Anat. Embryol. (Berl)* 2004;**208**:389-93.
23. Viragh S, Challice CE. The development of the conduction system in the mouse embryo heart. I. The first embryonic A-V conduction pathway. *Dev. Biol.* 1977;**56**:382-96.
24. Viragh S, Challice CE. The development of the conduction system in the mouse embryo heart. II. Histogenesis of the atrioventricular node and bundle. *Dev. Biol.* 1977;**56**:397-411.

25. Viragh S, Challice CE. The development of the conduction system in the mouse embryo heart. *Dev.Biol.* 1980;**80**:28-45.
26. Viragh S, Challice CE. The development of the conduction system in the mouse embryo heart. *Dev.Biol.* 1982;**89**:25-40.
27. Wessels A, Markman MW, Vermeulen JL, Anderson RH, Moorman AF, Lamers WH. The development of the atrioventricular junction in the human heart. *Circ.Res.* 1996;**78**:110-7.
28. Wenink AC. Development of the human cardiac conduction system. *J.Anat.* 1976;**121**:617-31.
29. Blom NA, Gittenberger-De Groot AC, DeRuiter MC, Poelmann RE, Mentink MM, Ottenkamp J. Development of the cardiac conduction tissue in human embryos using HNK- 1 antigen expression: possible relevance for understanding of abnormal atrial automaticity. *Circulation* 1999;**99**:800-6.
30. DeRuiter MC, Gittenberger-De Groot AC, Wenink AC, Poelmann RE, Mentink MM. In normal development pulmonary veins are connected to the sinus venosus segment in the left atrium. *Anat.Rec.* 1995;**243**:84-92.
31. Wenink AC, Symersky P, Ikeda T, DeRuiter MC, Poelmann RE, Gittenberger-De Groot AC. HNK-1 expression patterns in the embryonic rat heart distinguish between sinuatrial tissues and atrial myocardium. *Anat.Embryol.(Berl)* 2000;**201**:39-50.
32. Wessels A, Vermeulen JL, Verbeek FJ, Viragh S, Kalman F, Lamers WH *et al.* Spatial distribution of "tissue-specific" antigens in the developing human heart and skeletal muscle. III. An immunohistochemical analysis of the distribution of the neural tissue antigen G1N2 in the embryonic heart; implications for the development of the atrioventricular conduction system. *Anat.Rec.* 1992;**232**:97-111.
33. Chuck ET, Watanabe M. Differential expression of PSA-NCAM and HNK-1 epitopes in the developing cardiac conduction system of the chick. *Dev.Dyn.* 1997;**209**:182-95.
34. Development of the cardiac conduction system. Chichester: John Wiley & Sons Ltd, 2003.
35. Hoogaars WM, Tessari A, Moorman AF, de Boer PA, Hagoort J, Soufan AT *et al.* The transcriptional repressor Tbx3 delineates the developing central conduction system of the heart. *Cardiovasc.Res.* 2004;**62**:489-99.
36. Christoffels VM, Hoogaars WM, Tessari A, Clout DE, Moorman AF, Campione M. T-box transcription factor Tbx2 represses differentiation and formation of the cardiac chambers. *Dev.Dyn.* 2004;**229**:763-70.
37. Davenport TG, Jerome-Majewska LA, Papaioannou VE. Mammary gland, limb and yolk sac defects in mice lacking Tbx3, the gene mutated in human ulnar mammary syndrome. *Development* 2003;**130**:2263-73.
38. Franco D. Unveiling the transcriptional control of the developing cardiac conduction system. *Cardiovasc.Res.* 2004;**62**:444-6.
39. Moskowitz IP, Pizard A, Patel VV, Bruneau BG, Kim JB, Kupersmidt S *et al.* The T-Box transcription factor Tbx5 is required for the patterning and maturation of the murine cardiac conduction system. *Development* 2004;**131**:4107-16.
40. Harris BS, Jay PY, Rackley MS, Izumo S, O'Brien TX, Gourdie RG. Transcriptional regulation of cardiac conduction system development: 2004 FASEB cardiac conduction system minimeeting, Washington, DC. *Anat.Rec.A Discov.Mol.Cell Evol.Biol.* 2004;**280**:1036-45.
41. Thomas PS, Kasahara H, Edmonson AM, Izumo S, Yacoub MH, Barton PJ *et al.* Elevated expression of Nkx-2.5 in developing myocardial conduction cells. *Anat.Rec.* 2001;**263**:307-13.
42. Jay PY, Harris BS, Maguire CT, Buerger A, Wakimoto H, Tanaka M *et al.* Nkx2-5 mutation causes anatomic hypoplasia of the cardiac conduction system. *J Clin.Invest* 2004;**113**:1130-7.
43. Kasahara H, Wakimoto H, Liu M, Maguire CT, Converso KL, Shioi T *et al.* Progressive atrioventricular conduction defects and heart failure in mice expressing a mutant Csx/Nkx2.5 homeoprotein. *J Clin. Invest* 2001;**108**:189-201.
44. Linhares VL, Almeida NA, Menezes DC, Elliott DA, Lai D, Beyer EC *et al.* Transcriptional regulation of the murine Connexin40 promoter by cardiac factors Nkx2-5, GATA4 and Tbx5. *Cardiovasc.Res.* 2004;**64**:402-11.
45. Habets PE, Moorman AF, Clout DE, van Roon MA, Lingbeek M, van Lohuizen M *et al.* Cooperative action of Tbx2 and Nkx2.5 inhibits ANF expression in the atrioventricular canal: implications for cardiac chamber formation. *Genes Dev.* 2002;**16**:1234-46.
46. Jay PY, Maguire CT, Wakimoto H, Izumo S, Berul CI. Absence of Msx2 does not affect cardiac conduction or rescue conduction defects associated with Nkx2-5 mutation. *J Cardiovasc.Electrophysiol.* 2005;**16**:82-5.

47. Satokata I, Ma L, Ohshima H, Bei M, Woo I, Nishizawa K *et al.* Mx2 deficiency in mice causes pleiotropic defects in bone growth and ectodermal organ formation. *Nat.Genet.* 2000;**24**:391-5.
48. Ismat FA, Zhang M, Kook H, Huang B, Zhou R, Ferrari VA *et al.* Homeobox protein Hop functions in the adult cardiac conduction system. *Circ.Res.* 2005;**96**:898-903.
49. Molkenkin JD. The zinc finger-containing transcription factors GATA-4, -5, and -6. Ubiquitously expressed regulators of tissue-specific gene expression. *J Biol.Chem.* 2000;**275**:38949-52.
50. Kuo CT, Morrisey EE, Anandappa R, Sigrist K, Lu MM, Parmacek MS *et al.* GATA4 transcription factor is required for ventral morphogenesis and heart tube formation. *Genes Dev.* 1997;**11**:1048-60.
51. Takebayashi-Suzuki K, Pauliks LB, Eltsefon Y, Mikawa T. Purkinje fibers of the avian heart express a myogenic transcription factor program distinct from cardiac and skeletal muscle. *Dev.Biol.* 2001;**234**:390-401.
52. Davis DL, Edwards AV, Juraszek AL, Phelps A, Wessels A, Burch JB. A GATA-6 gene heart-region-specific enhancer provides a novel means to mark and probe a discrete component of the mouse cardiac conduction system. *Mech.Dev.* 2001;**108**:105-19.
53. Edwards AV, Davis DL, Juraszek AL, Wessels A, Burch JB. Transcriptional regulation in the mouse atrioventricular conduction system. *Novartis.Found.Symp.* 2003;**250**:177-89.
54. Kupersmidt S, Yang T, Anderson ME, Wessels A, Niswender KD, Magnuson MA *et al.* Replacement by homologous recombination of the minK gene with lacZ reveals restriction of minK expression to the mouse cardiac conduction system. *Circ.Res.* 1999;**84**:146-52.
55. Drici MD, Arrighi I, Chouabe C, Mann JR, Lazdunski M, Romey G *et al.* Involvement of Isk-associated K⁺ channel in heart rate control of repolarization in a murine engineered model of Jervell and Lange-Nielsen syndrome. *Circ.Res.* 1998;**83**:95-102.
56. Kondo RP, Anderson RH, Kupersmidt S, Roden DM, Evans SM. Development of the cardiac conduction system as delineated by minK-lacZ. *J.Cardiovasc.Electrophysiol.* 2003;**14**:383-91.
57. Rentschler S, Vaidya DM, Tamaddon H, Degenhardt K, Sassoon D, Morley GE *et al.* Visualization and functional characterization of the developing murine cardiac conduction system. *Development* 2001;**128**:1785-92.
58. Yeager M. Structure of cardiac gap junction intercellular channels. *J Struct.Biol.* 1998;**121**:231-45.
59. Delorme B, Dahl E, Jarry-Guichard T, Marics I, Briand JP, Willecke K *et al.* Developmental regulation of connexin 40 gene expression in mouse heart correlates with the differentiation of the conduction system. *Dev.Dyn.* 1995;**204**:358-71.
60. Miquerol L, Dupays L, Theveniau-Ruissy M, Alcolea S, Jarry-Guichard T, Abran P *et al.* Gap junctional connexins in the developing mouse cardiac conduction system. *Novartis.Found.Symp.* 2003;**250**:80-98.
61. Alcolea S, Theveniau-Ruissy M, Jarry-Guichard T, Marics I, Tzouanacou E, Chauvin JP *et al.* Downregulation of connexin 45 gene products during mouse heart development. *Circ.Res.* 1999;**84**:1365-79.
62. Coppén SR, Severs NJ, Gourdie RG. Connexin45 (alpha 6) expression delineates an extended conduction system in the embryonic and mature rodent heart. *Dev.Genet.* 1999;**24**:82-90.
63. Soufan AT, van den Hoff MJ, Ruijter JM, de Boer PA, Hagoort J, Webb S *et al.* Reconstruction of the patterns of gene expression in the developing mouse heart reveals an architectural arrangement that facilitates the understanding of atrial malformations and arrhythmias. *Circ.Res.* 2004;**95**:1207-15.
64. Coppén SR, Kodama I, Boyett MR, Dobrzynski H, Takagishi Y, Honjo H *et al.* Connexin45, a major connexin of the rabbit sinoatrial node, is co-expressed with connexin43 in a restricted zone at the nodal-crista terminalis border. *J Histochem.Cytochem.* 1999;**47**:907-18.
65. Kwong KF, Schuessler RB, Green KG, Laing JG, Beyer EC, Boineau JP *et al.* Differential expression of gap junction proteins in the canine sinus node. *Circ.Res.* 1998;**82**:604-12.
66. Davis LM, Rodefeld ME, Green K, Beyer EC, Saffitz JE. Gap junction protein phenotypes of the human heart and conduction system. *J Cardiovasc.Electrophysiol.* 1995;**6**:813-22.
67. Dobrzynski H, Nikolski VP, Sambelashvili AT, Greener ID, Yamamoto M, Boyett MR *et al.* Site of origin and molecular substrate of atrioventricular junctional rhythm in the rabbit heart. *Circ.Res.* 2003;**93**:1102-10.
68. Gourdie RG, Severs NJ, Green CR, Rothery S, Germroth P, Thompson RP. The spatial distribution and relative abundance of gap-junctional connexin40 and connexin43 correlate to functional properties of components of the cardiac atrioventricular conduction system. *J Cell Sci.* 1993;**105 (Pt 4)**:985-91.
69. Kirchhoff S, Nelles E, Hagendorff A, Kruger O, Traub O, Willecke K. Reduced cardiac conduction velocity and predisposition to arrhythmias in connexin40-deficient mice. *Curr.Biol.* 1998;**8**:299-302.

70. Bevilacqua LM, Simon AM, Maguire CT, Gehrman J, Wakimoto H, Paul DL *et al.* A targeted disruption in connexin40 leads to distinct atrioventricular conduction defects. *J Interv. Card Electrophysiol.* 2000;**4**:459-67.
71. Simon AM, Goodenough DA, Paul DL. Mice lacking connexin40 have cardiac conduction abnormalities characteristic of atrioventricular block and bundle branch block. *Curr.Biol.* 1998;**8**:295-8.
72. Tamaddon HS, Vaidya D, Simon AM, Paul DL, Jalife J, Morley GE. High-resolution optical mapping of the right bundle branch in connexin40 knockout mice reveals slow conduction in the specialized conduction system. *Circ.Res.* 2000;**87**:929-36.
73. VanderBrink BA, Sellitto C, Saba S, Link MS, Zhu W, Homoud MK *et al.* Connexin40-deficient mice exhibit atrioventricular nodal and infra-Hisian conduction abnormalities. *J Cardiovasc. Electrophysiol.* 2000;**11**:1270-6.
74. Alcolea S, Jarry-Guichard T, de Bakker J, Gonzalez D, Lamers W, Coppens S *et al.* Replacement of connexin40 by connexin45 in the mouse: impact on cardiac electrical conduction. *Circ.Res.* 2004;**94**:100-9.
75. Delorme B, Dahl E, Jarry-Guichard T, Briand JP, Willecke K, Gros D *et al.* Expression pattern of connexin gene products at the early developmental stages of the mouse cardiovascular system. *Circ.Res.* 1997;**81**:423-37.
76. Fromaget C, el Aoumari A, Dupont E, Briand JP, Gros D. Changes in the expression of connexin 43, a cardiac gap junctional protein, during mouse heart development. *J Mol. Cell Cardiol* 1990;**22**:1245-58.
77. Reaume AG, de Sousa PA, Kulkarni S, Langille BL, Zhu D, Davies TC *et al.* Cardiac malformation in neonatal mice lacking connexin43. *Science* 1995;**267**:1831-4.
78. Gutstein DE, Morley GE, Tamaddon H, Vaidya D, Schneider MD, Chen J *et al.* Conduction slowing and sudden arrhythmic death in mice with cardiac-restricted inactivation of connexin43. *Circ.Res.* 2001;**88**:333-9.
79. Nishii K, Kumai M, Egashira K, Miwa T, Hashizume K, Miyano Y *et al.* Mice lacking connexin45 conditionally in cardiac myocytes display embryonic lethality similar to that of germline knockout mice without endocardial cushion defect. *Cell Commun. Adhes.* 2003;**10**:365-9.
80. DEHAAN RL. Migration patterns of the precardiac mesoderm in the early chick embryo. *Exp. Cell Res.* 1963;**29**:544-60.
81. Kamino K, Hirota A, Fujii S. Localization of pacemaking activity in early embryonic heart monitored using voltage-sensitive dye. *Nature* 1981;**290**:595-7.
82. de Jong F, Opthof T, Wilde AA, Janse MJ, Charles R, Lamers WH *et al.* Persisting zones of slow impulse conduction in developing chicken hearts. *Circ.Res.* 1992;**71**:240-50.
83. Anderson RH, Christoffels VM, Moorman AF. Controversies concerning the anatomical definition of the conduction tissues. *Anat. Rec. B New Anat.* 2004;**280**:8-14.
84. Aschoff L. Referat über die Herzstörungen in ihren Beziehungen zu den Spezifischen Muskelsystem des Herzens. *Verh Dtsch Pathol Ges* 1910;**14**:3-35.
85. Monckeberg JG. Beiträge zur normalen und pathologischen Anatomie des Herzens. *Verh Dtsch Pathol Ges* 1910;**14**:64-71.
86. Kalman JM, Olgin JE, Karch MR, Hamdan M, Lee RJ, Lesh MD. "Cristal tachycardias": origin of right atrial tachycardias from the crista terminalis identified by intracardiac echocardiography. *J. Am. Coll. Cardiol.* 1998;**31**:451-9.
87. Olgin JE, Kalman JM, Fitzpatrick AP, Lesh MD. Role of right atrial endocardial structures as barriers to conduction during human type I atrial flutter. Activation and entrainment mapping guided by intracardiac echocardiography. *Circulation* 1995;**92**:1839-48.
88. Tsai CF, Tai CT, Hsieh MH, Lin WS, Yu WC, Ueng KC *et al.* Initiation of atrial fibrillation by ectopic beats originating from the superior vena cava: electrophysiological characteristics and results of radiofrequency ablation. *Circulation* 2000;**102**:67-74.
89. Katritsis D, Ioannidis JP, Giazitzoglou E, Korovesis S, Anagnostopoulos CE, Camm AJ. Conduction delay within the coronary sinus in humans: implications for atrial arrhythmias. *J. Cardiovasc. Electrophysiol.* 2002;**13**:859-62.
90. Haissaguerre M, Jais P, Shah DC, Takahashi A, Hocini M, Quiniou G *et al.* Spontaneous initiation of atrial fibrillation by ectopic beats originating in the pulmonary veins. *N. Engl. J. Med.* 1998;**339**:659-66.
91. Al Khatib SM, Pritchett EL. Clinical features of Wolff-Parkinson-White syndrome. *Am. Heart J.* 1999;**138**:403-13.

92. Kumagai K, Uno K, Khrestian C, Waldo AL. Single site radiofrequency catheter ablation of atrial fibrillation: studies guided by simultaneous multisite mapping in the canine sterile pericarditis model. *J.Am. Coll. Cardiol.* 2000;**36**:917-23.
 93. Kistler PM, Sanders P, Hussin A, Morton JB, Vohra JK, Sparks PB *et al.* Focal atrial tachycardia arising from the mitral annulus: electrocardiographic and electrophysiologic characterization. *J.Am. Coll. Cardiol.* 2003;**41**:2212-9.
 94. Morton JB, Sanders P, Das A, Vohra JK, Sparks PB, Kalman JM. Focal atrial tachycardia arising from the tricuspid annulus: electrophysiologic and electrocardiographic characteristics. *J. Cardiovasc. Electrophysiol.* 2001;**12**:653-9.
 95. James TN. THE CONNECTING PATHWAYS BETWEEN THE SINUS NODE AND A-V NODE AND BETWEEN THE RIGHT AND THE LEFT ATRIUM IN THE HUMAN HEART. *Am. Heart J* 1963;**66**:498-508.
 96. James TN. The internodal pathways of the human heart. *Prog. Cardiovasc. Dis.* 2001;**43**:495-535.
 97. Sherf L, James TN. Fine structure of cells and their histologic organization within internodal pathways of the heart: clinical and electrocardiographic implications. *Am. J. Cardiol.* 1979;**44**:345-69.
 98. Gittenberger-De Groot AC, Wenink ACG. The specialized myocardium in the fetal heart. In: Van Mierop LHS, Oppenheimer-Dekker A, Bruins CLDC, eds. *Embryology and teratology of the heart and the great arteries.* 1978:15-24.
 99. Sakai T, Hirota A, Momose-Sato Y, Sato K, Kamino K. Optical mapping of conduction patterns of normal and tachycardia-like excitations in the rat atrium. *Jpn. J. Physiol* 1997;**47**:179-88.
 100. Spach MS, Kootsey JM. The nature of electrical propagation in cardiac muscle. *Am. J. Physiol* 1983;**244**:H3-22.
 101. Vassalle M, Hoffman BF. The spread of sinus activation during potassium administration. *Circ. Res.* 1965;**17**:285-95.
 102. Wagner ML, Lazzara R, Weiss RM, Hoffman BF. Specialized conducting fibers in the interatrial band. *Circ. Res.* 1966;**18**:502-18.
 103. Racker DK. Sinoventricular transmission in 10 mM K⁺ by canine atrioventricular nodal inputs. Superior atrionodal bundle and proximal atrioventricular bundle. *Circulation* 1991;**83**:1738-53.
 104. Los, J. A. De embryonale ontwikkeling van de venae pulmonales en de sinus coronarius bij de mens. 1958. Leiden University Medical Center.
- Ref Type: Thesis/Dissertation
105. Sadler TW. Langman's medische embryologie. 10 ed. Utrecht/Antwerpen: Bohn, Scheltema & Holkema, 1988.
 106. von Ledinghausen M. The venous drainage of the human myocardium. *Adv. Anat. Embryol. Cell Biol.* 2003;**168**:1-104.
 107. Los JA. Cardiac septation and development of the aorta, pulmonary trunk, and pulmonary veins: previous work in the light of recent observations. *Birth Defects Orig. Artic. Ser.* 1978;**14**:109-38.
 108. Rammos S, Gittenberger-De Groot AC, Oppenheimer-Dekker A. The abnormal pulmonary venous connexion: a developmental approach. *Int. J. Cardiol* 1990;**29**:285-95.
 109. SHANER RF. The development of the bronchial veins, with special reference to anomalies of the pulmonary veins. *Anat. Rec.* 1961;**140**:159-65.
 110. Kutsche LM, Van Mierop LH. Development of the pulmonary vein in the American alligator (*Alligator mississippiensis*). *Anat. Rec.* 1988;**222**:170-6.
 111. Icardo JM, Ojeda JL, Colvee E, Tota B, Wong WP, Ip YK. Heart inflow tract of the African lungfish *Protopterus dolloi*. *J. Morphol.* 2005;**263**:30-8.
 112. Federow V. Über die entwicklung der lungenvene. *Anat. Hefte* 1910;**40**:529-607.
 113. Squier TL. On the development of the pulmonary circulation in the chick. *Anat. Rec.* 1916;**10**:425-38.
 114. Brown AJ. The development of the pulmonary vein in the domestic cat. *Anat. Rec.* 1913;**7**:299-329.
 115. Flint JM. The development of the lungs. *Am. J. Anat.* 1906;**6**:1-137.
 116. Blom NA, Gittenberger-De Groot AC, Jongeneel TH, DeRuiter MC, Poelmann RE, Ottenkamp J. Normal development of the pulmonary veins in human embryos and formulation of a morphogenetic concept for sinus venosus defects. *Am. J. Cardiol.* 2001;**87**:305-9.
 117. Tasaka H, Krug EL, Markwald RR. Origin of the pulmonary venous orifice in the mouse and its relation to the morphogenesis of the sinus venosus, extracardiac mesenchyme (spina vestibuli), and atrium. *Anat. Rec.* 1996;**246**:107-13.
 118. Dor X, Corone P, Jonhson E. [Origin of the common pulmonary vein, septation of the primary sinus venosus atrial situs and theory of the "sinus man"]. *Arch. Mal Coeur Vaiss.* 1987;**80**:483-98.

119. Bliss DF, Hutchins GM. The dorsal mesocardium and development of the pulmonary veins in human embryos. *Am.J.Cardiovasc.Pathol.* 1995;**5**:55-67.
120. Webb S, Brown NA, Wessels A, Anderson RH. Development of the murine pulmonary vein and its relationship to the embryonic venous sinus. *Anat.Rec.* 1998;**250**:325-34.
121. Webb S, Brown NA, Anderson RH, Richardson MK. Relationship in the chick of the developing pulmonary vein to the embryonic systemic venous sinus. *Anat.Rec.* 2000;**259**:67-75.
122. Webb S, Kanani M, Anderson RH, Richardson MK, Brown NA. Development of the human pulmonary vein and its incorporation in the morphologically left atrium. *Cardiol.Young.* 2001;**11**:632-42.
123. Ho SY, Sanchez-Quintana D, Cabrera JA, Anderson RH. Anatomy of the left atrium: implications for radiofrequency ablation of atrial fibrillation. *J.Cardiovasc.Electrophysiol.* 1999;**10**:1525-33.
124. Ho SY, Cabrera JA, Tran VH, Farre J, Anderson RH, Sanchez-Quintana D. Architecture of the pulmonary veins: relevance to radiofrequency ablation. *Heart* 2001;**86**:265-70.
125. Chen SA, Hsieh MH, Tai CT, Tsai CF, Prakash VS, Yu WC *et al.* Initiation of atrial fibrillation by ectopic beats originating from the pulmonary veins: electrophysiological characteristics, pharmacological responses, and effects of radiofrequency ablation. *Circulation* 1999;**100**:1879-86.
126. Brunton TL, Fayer J. Note on independent pulsation of the pulmonary veins and vena cava. *Proc.R.Soc.Lond.* 1874;**25**:174-6.
127. Masani F. Node-like cells in the myocardial layer of the pulmonary vein of rats: an ultrastructural study. *J.Anat.* 1986;**145**:133-42.
128. Perez-Lugones A, McMahon JT, Ratliff NB, Saliba WI, Schweikert RA, Marrouche NF *et al.* Evidence of specialized conduction cells in human pulmonary veins of patients with atrial fibrillation. *J.Cardiovasc.Electrophysiol.* 2003;**14**:803-9.
129. Sealy WC, Bache RJ, Seaber AV, Bhattacharga SK. The atrial pacemaking site after surgical exclusion of the sinoatrial node. *J Thorac.Cardiovasc.Surg.* 1973;**65**:841-50.
130. Rubenstein DS, Fox LM, McNulty JA, Lipsius SL. Electrophysiology and ultrastructure of eustachian ridge from cat right atrium: a comparison with SA node. *J Mol.Cell Cardiol* 1987;**19**:965-76.
131. Ehrlich JR, Cha TJ, Zhang L, Chartier D, Melnyk P, Hohnloser SH *et al.* Cellular electrophysiology of canine pulmonary vein cardiomyocytes: action potential and ionic current properties. *J Physiol* 2003;**551**:801-13.
132. Ehrlich JR, Cha TJ, Zhang L, Chartier D, Villeneuve L, Hebert TE *et al.* Characterization of a hyperpolarization-activated time-dependent potassium current in canine cardiomyocytes from pulmonary vein myocardial sleeves and left atrium. *J Physiol* 2004;**557**:583-97.
133. Chen YJ, Chen SA, Chen YC, Yeh HI, Chang MS, Lin CI. Electrophysiology of single cardiomyocytes isolated from rabbit pulmonary veins: implication in initiation of focal atrial fibrillation. *Basic Res.Cardiol* 2002;**97**:26-34.
134. Tada H, Oral H, Ozaydin M, Greenstein R, Pelosi F, Jr., Knight BP *et al.* Response of pulmonary vein potentials to premature stimulation. *J Cardiovasc.Electrophysiol.* 2002;**13**:33-7.
135. Jais P, Hocini M, Macle L, Choi KJ, Deisenhofer I, Weerasooriya R *et al.* Distinctive electrophysiological properties of pulmonary veins in patients with atrial fibrillation. *Circulation* 2002;**106**:2479-85.
136. Cheung DW. Electrical activity of the pulmonary vein and its interaction with the right atrium in the guinea-pig. *J Physiol* 1981;**314**:445-56.
137. Chen YJ, Chen SA, Chang MS, Lin CI. Arrhythmogenic activity of cardiac muscle in pulmonary veins of the dog: implication for the genesis of atrial fibrillation. *Cardiovasc.Res.* 2000;**48**:265-73.
138. Cheung DW. Pulmonary vein as an ectopic focus in digitalis-induced arrhythmia. *Nature* 1981;**294**:582-4.
139. Honjo H, Boyett MR, Niwa R, Inada S, Yamamoto M, Mitsui K *et al.* Pacing-induced spontaneous activity in myocardial sleeves of pulmonary veins after treatment with ryanodine. *Circulation* 2003;**107**:1937-43.
140. Arora R, Verheule S, Scott L, Navarrete A, Katari V, Wilson E *et al.* Arrhythmogenic substrate of the pulmonary veins assessed by high-resolution optical mapping. *Circulation* 2003;**107**:1816-21.
141. Spach MS, Barr RC, Jewett PH. Spread of excitation from the atrium into thoracic veins in human beings and dogs. *Am.J Cardiol* 1972;**30**:844-54.
142. Chen YC, Chen SA, Chen YJ, Chang MS, Chan P, Lin CI. Effects of thyroid hormone on the arrhythmogenic activity of pulmonary vein cardiomyocytes. *J Am.Coll.Cardiol* 2002;**39**:366-72.
143. Chen YC, Chen SA, Chen YJ, Tai CT, Chan P, Lin CI. T-type calcium current in electrical activity of cardiomyocytes isolated from rabbit pulmonary vein. *J Cardiovasc.Electrophysiol.* 2004;**15**:567-71.

144. Chen YJ, Chen YC, Chan P, Lin CI, Chen SA. Temperature regulates the arrhythmogenic activity of pulmonary vein cardiomyocytes. *J Biomed.Sci.* 2003;**10**:535-43.
145. Dixit S, Gerstenfeld EP, Callans DJ, Marchlinski FE. Mechanisms underlying sustained firing from pulmonary veins: evidence from pacing maneuvers and pharmacological manipulation. *Pacing Clin.Electrophysiol.* 2004;**27**:1120-9.
146. Verheule S, Wilson EE, Arora R, Engle SK, Scott LR, Olgin JE. Tissue structure and connexin expression of canine pulmonary veins. *Cardiovasc.Res.* 2002;**55**:727-38.
147. Hocini M, Ho SY, Kawara T, Linnenbank AC, Potse M, Shah D *et al.* Electrical conduction in canine pulmonary veins: electrophysiological and anatomic correlation. *Circulation* 2002;**105**:2442-8.
148. Nattel S. Basic electrophysiology of the pulmonary veins and their role in atrial fibrillation: precipitators, perpetuators, and perplexers. *J Cardiovasc.Electrophysiol.* 2003;**14**:1372-5.
149. Melnyk P, Ehrlich JR, Pourrier M, Villeneuve L, Cha TJ, Nattel S. Comparison of ion channel distribution and expression in cardiomyocytes of canine pulmonary veins versus left atrium. *Cardiovasc.Res.* 2005;**65**:104-16.
150. Becker AE, Anderson RH. The Wolff-Parkinson-White syndrome and its anatomical substrates. *Anat. Rec.PG.* 1981.
151. McGuire MA, De Bakker JM, Vermeulen JT, Moorman AF, Loh P, Thibault B *et al.* Atrioventricular junctional tissue. Discrepancy between histological and electrophysiological characteristics. *Circulation* 1996;**94**:571-7.
152. Klein GJ, Guiraudon GM, Kerr CR, Sharma AD, Yee R, Szabo T *et al.* "Nodoventricular" accessory pathway: evidence for a distinct accessory atrioventricular pathway with atrioventricular node-like properties. *J.Am.Coll.Cardiol.* 1988;**11**:1035-40.
153. Gollob MH, Green MS, Tang AS, Gollob T, Karibe A, Ali Hassan AS *et al.* Identification of a gene responsible for familial Wolff-Parkinson-White syndrome. *N.Engl.J.Med.* 2001;**344**:1823-31.
154. Sidhu JS, Rajawat YS, Rami TG, Gollob MH, Wang Z, Yuan R *et al.* Transgenic mouse model of ventricular preexcitation and atrioventricular reentrant tachycardia induced by an AMP-activated protein kinase loss-of-function mutation responsible for Wolff-Parkinson-White syndrome. *Circulation* 2005;**111**:21-9.
155. Patel VV, Arad M, Moskowitz IP, Maguire CT, Branco D, Seidman JG *et al.* Electrophysiologic characterization and postnatal development of ventricular pre-excitation in a mouse model of cardiac hypertrophy and Wolff-Parkinson-White syndrome. *J.Am.Coll.Cardiol.* 2003;**42**:942-51.
156. Arad M, Moskowitz IP, Patel VV, Ahmad F, Perez-Atayde AR, Sawyer DB *et al.* Transgenic mice over-expressing mutant PRKAG2 define the cause of Wolff-Parkinson-White syndrome in glycogen storage cardiomyopathy. *Circulation* 2003;**107**:2850-6.
157. Gaussin V. Offbeat mice. *Anat.Rec.A Discov.Mol.Cell Evol.Biol.* 2004;**280**:1022-6.
158. Gaussin V, Morley GE, Cox L, Zwijsen A, Vance KM, Emile L *et al.* Alk3/Bmpr1a Receptor Is Required for Development of the Atrioventricular Canal Into Valves and Annulus Fibrosus. *Circ.Res.* 2005.
159. Go AS, Hylek EM, Phillips KA, Chang Y, Henault LE, Selby JV *et al.* Prevalence of diagnosed atrial fibrillation in adults: national implications for rhythm management and stroke prevention: the AnTicoagulation and Risk Factors in Atrial Fibrillation (ATRIA) Study. *JAMA* 2001;**285**:2370-5.
160. Lloyd-Jones DM, Wang TJ, Leip EP, Larson MG, Levy D, Vasan RS *et al.* Lifetime risk for development of atrial fibrillation: the Framingham Heart Study. *Circulation* 2004;**110**:1042-6.
161. Roden DM. Risks and benefits of antiarrhythmic therapy. *N.Engl.J.Med.* 1994;**331**:785-91.
162. Cox JL, Schuessler RB, D'Agostino HJ, Jr., Stone CM, Chang BC, Cain ME *et al.* The surgical treatment of atrial fibrillation. III. Development of a definitive surgical procedure. *J.Thorac.Cardiovasc.Surg.* 1991;**101**:569-83.
163. Gaynor SL, Diodato MD, Prasad SM, Ishii Y, Schuessler RB, Bailey MS *et al.* A prospective, single-center clinical trial of a modified Cox maze procedure with bipolar radiofrequency ablation. *J Thorac.Cardiovasc. Surg.* 2004;**128**:535-42.
164. Haissaguerre M, Shah DC, Jais P, Hocini M, Yamane T, Deisenhofer I *et al.* Electrophysiological breakthroughs from the left atrium to the pulmonary veins. *Circulation* 2000;**102**:2463-5.
165. Haissaguerre M, Jais P, Shah DC, Garrigue S, Takahashi A, Lavergne T *et al.* Electrophysiological end point for catheter ablation of atrial fibrillation initiated from multiple pulmonary venous foci. *Circulation* 2000;**101**:1409-17.
166. Haissaguerre M, Jais P, Shah DC, Arentz T, Kalusche D, Takahashi A *et al.* Catheter ablation of chronic atrial fibrillation targeting the reinitiating triggers. *J.Cardiovasc.Electrophysiol.* 2000;**11**:2-10.

167. Pappone C, Rosanio S, Oreto G, Tocchi M, Gugliotta F, Vicedomini G *et al.* Circumferential radiofrequency ablation of pulmonary vein ostia: A new anatomic approach for curing atrial fibrillation. *Circulation* 2000;**102**:2619-28.
168. Macle L, Jais P, Scavee C, Weerasooriya R, Shah DC, Hocini M *et al.* Electrophysiologically guided pulmonary vein isolation during sustained atrial fibrillation. *J.Cardiovasc.Electrophysiol.* 2003;**14**:255-60.
169. Cappato R, Negroni S, Pecora D, Bentivegna S, Lupo PP, Carolei A *et al.* Prospective assessment of late conduction recurrence across radiofrequency lesions producing electrical disconnection at the pulmonary vein ostium in patients with atrial fibrillation. *Circulation* 2003;**108**:1599-604.
170. Gerstenfeld EP, Callans DJ, Dixit S, Zado E, Marchlinski FE. Incidence and location of focal atrial fibrillation triggers in patients undergoing repeat pulmonary vein isolation: implications for ablation strategies. *J.Cardiovasc.Electrophysiol.* 2003;**14**:685-90.
171. Nanthakumar K, Plumb VJ, Epstein AE, Veenhuyzen GD, Link D, Kay GN. Resumption of electrical conduction in previously isolated pulmonary veins: rationale for a different strategy? *Circulation* 2004;**109**:1226-9.
172. Verma A, Kilicaslan F, Pisano E, Marrouche NF, Fanelli R, Brachmann J *et al.* Response of atrial fibrillation to pulmonary vein antrum isolation is directly related to resumption and delay of pulmonary vein conduction. *Circulation* 2005;**112**:627-35.
173. Saad EB, Marrouche NF, Saad CP, Ha E, Bash D, White RD *et al.* Pulmonary vein stenosis after catheter ablation of atrial fibrillation: emergence of a new clinical syndrome. *Ann.Intern.Med.* 2003;**138**:634-8.
174. Cappato R, Calkins H, Chen SA, Davies W, Iesaka Y, Kalman J *et al.* Worldwide survey on the methods, efficacy, and safety of catheter ablation for human atrial fibrillation. *Circulation* 2005;**111**:1100-5.
175. Pappone C, Oreto G, Rosanio S, Vicedomini G, Tocchi M, Gugliotta F *et al.* Atrial electroanatomic remodeling after circumferential radiofrequency pulmonary vein ablation: efficacy of an anatomic approach in a large cohort of patients with atrial fibrillation. *Circulation* 2001;**104**:2539-44.
176. Oral H, Scharf C, Chugh A, Hall B, Cheung P, Good E *et al.* Catheter ablation for paroxysmal atrial fibrillation: segmental pulmonary vein ostial ablation versus left atrial ablation. *Circulation* 2003;**108**:2355-60.
177. Karch MR, Zrenner B, Deisenhofer I, Schreieck J, Ndrepepa G, Dong J *et al.* Freedom from atrial tachyarrhythmias after catheter ablation of atrial fibrillation: a randomized comparison between 2 current ablation strategies. *Circulation* 2005;**111**:2875-80.
178. Oral H, Ozaydin M, Chugh A, Scharf C, Tada H, Hall B *et al.* Role of the coronary sinus in maintenance of atrial fibrillation. *J.Cardiovasc.Electrophysiol.* 2003;**14**:1329-36.
179. Shah D, Haissaguerre M, Jais P, Clementy J. High-resolution mapping of tachycardia originating from the superior vena cava: evidence of electrical heterogeneity, slow conduction, and possible circus movement reentry. *J Cardiovasc Electrophysiol* 2002;**13**:388-92.
180. Wit AL, Fenoglio JJ, Jr., Wagner BM, Bassett AL. Electrophysiological properties of cardiac muscle in the anterior mitral valve leaflet and the adjacent atrium in the dog. Possible implications for the genesis of atrial dysrhythmias. *Circ.Res.* 1973;**32**:731-45.
181. Wit AL, Cranefield PF. Triggered activity in cardiac muscle fibers of the simian mitral valve. *Circ.Res.* 1976;**38**:85-98.
182. Wit AL, Fenoglio JJ, Jr., Hordof AJ, Reemtsma K. Ultrastructure and transmembrane potentials of cardiac muscle in the human anterior mitral valve leaflet. *Circulation* 1979;**59**:1284-92.
183. De Bakker JM, Hauer RN, Bakker PF, Becker AE, Janse MJ, Robles de Medina EO. Abnormal automaticity as mechanism of atrial tachycardia in the human heart--electrophysiologic and histologic correlation: a case report. *J.Cardiovasc.Electrophysiol.* 1994;**5**:335-44.
184. Tanner H, Hindricks G, Schirdewahn P, Kobza R, Dorszewski A, Piorkowski C *et al.* Outflow tract tachycardia with R/S transition in lead V3: six different anatomic approaches for successful ablation. *J Am.Coll.Cardiol* 2005;**45**:418-23.
185. van der Burg AE, De Groot NM, van Erven L, Bootsma M, van der Wall EE, Schalij MJ. Long-term follow-up after radiofrequency catheter ablation of ventricular tachycardia: a successful approach? *J.Cardiovasc.Electrophysiol.* 2002;**13**:417-23.
186. Schalij MJ, van Ruggie FP, Siezenga M, van der Velde ET. Endocardial activation mapping of ventricular tachycardia in patients: first application of a 32-site bipolar mapping electrode catheter. *Circulation* 1998;**98**:2168-79.

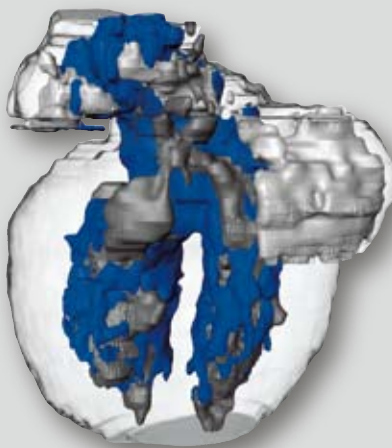
187. Zhou L, Keane D, Reed G, Ruskin J. Thromboembolic complications of cardiac radiofrequency catheter ablation: a review of the reported incidence, pathogenesis and current research directions. *J. Cardiovasc. Electrophysiol.* 1999;**10**:611-20.
188. Jongbloed MR, Bax JJ, van der Burg AE, van der Wall EE, Schalij MJ. Radiofrequency catheter ablation of ventricular tachycardia guided by intracardiac echocardiography. *Eur. J. Echocardiogr.* 2004;**5**:34-40.
189. Nathan H, Eliakim M. The junction between the left atrium and the pulmonary veins. An anatomic study of human hearts. *Circulation* 1966;**34**:412-22.
190. Cabrera JA, Sanchez-Quintana D, Farre J, Navarro F, Rubio JM, Cabestrero F *et al.* Ultrasonic characterization of the pulmonary venous wall: echographic and histological correlation. *Circulation* 2002;**106**:968-73.
191. Moubarak JB, Rozwadowski JV, Strzalka CT, Buck WR, Tan WS, Kish GF *et al.* Pulmonary veins-left atrial junction: anatomic and histological study. *Pacing Clin. Electrophysiol.* 2000;**23**:1836-8.
192. Kato R, Lickfett L, Meininger G, Dickfeld T, Wu R, Juang G *et al.* Pulmonary vein anatomy in patients undergoing catheter ablation of atrial fibrillation: lessons learned by use of magnetic resonance imaging. *Circulation* 2003;**107**:2004-10.
193. Marom EM, Herndon JE, Kim YH, McAdams HP. Variations in pulmonary venous drainage to the left atrium: implications for radiofrequency ablation. *Radiology* 2004;**230**:824-9.
194. Scharf C, Sneider M, Case I, Chugh A, Lai SW, Pelosi F, Jr. *et al.* Anatomy of the pulmonary veins in patients with atrial fibrillation and effects of segmental ostial ablation analyzed by computed tomography. *J. Cardiovasc. Electrophysiol.* 2003;**14**:150-5.
195. Wittkamp FH, Vonken EJ, Derksen R, Loh P, Velthuis B, Wever EF *et al.* Pulmonary vein ostium geometry: analysis by magnetic resonance angiography. *Circulation* 2003;**107**:21-3.
196. Lundqvist C, Olsson SB, Varnauskas E. Transseptal left heart catheterization: a review of 278 studies. *Clin. Cardiol.* 1986;**9**:21-6.
197. Qureshi AM, Prieto LR, Latson LA, Lane GK, Mesia CI, Radvansky P *et al.* Transcatheter angioplasty for acquired pulmonary vein stenosis after radiofrequency ablation. *Circulation* 2003;**108**:1336-42.
198. Dill T, Neumann T, Ekinci O, Breidenbach C, John A, Erdogan A *et al.* Pulmonary vein diameter reduction after radiofrequency catheter ablation for paroxysmal atrial fibrillation evaluated by contrast-enhanced three-dimensional magnetic resonance imaging. *Circulation* 2003;**107**:845-50.
199. Packer DL, Keelan P, Munger TM, Breen JF, Asirvatham S, Peterson LA *et al.* Clinical presentation, investigation, and management of pulmonary vein stenosis complicating ablation for atrial fibrillation. *Circulation* 2005;**111**:546-54.
200. Saad EB, Cole CR, Marrouche NF, Dresing TJ, Perez-Lugones A, Saliba WJ *et al.* Use of intracardiac echocardiography for prediction of chronic pulmonary vein stenosis after ablation of atrial fibrillation. *J. Cardiovasc. Electrophysiol.* 2002;**13**:986-9.
201. Jin Y, Ross DL, Thomas SP. Pulmonary vein stenosis and remodeling after electrical isolation for treatment of atrial fibrillation: short- and medium-term follow-up. *Pacing Clin. Electrophysiol.* 2004;**27**:1362-70.
202. Saad EB, Rossillo A, Saad CP, Martin DO, Bhargava M, Erciyes D *et al.* Pulmonary vein stenosis after radiofrequency ablation of atrial fibrillation: functional characterization, evolution, and influence of the ablation strategy. *Circulation* 2003;**108**:3102-7.
203. Tsao HM, Chen SA. Evaluation of pulmonary vein stenosis after catheter ablation of atrial fibrillation. *Card Electrophysiol. Rev.* 2002;**6**:397-400.
204. Arentz T, Jander N, von Rosenthal J, Blum T, Furmaier R, Gornandt L *et al.* Incidence of pulmonary vein stenosis 2 years after radiofrequency catheter ablation of refractory atrial fibrillation. *Eur. Heart J* 2003;**24**:963-9.
205. Vasamreddy CR, Jayam V, Bluemke DA, Calkins H. Pulmonary vein occlusion: an unanticipated complication of catheter ablation of atrial fibrillation using the anatomic circumferential approach. *Heart Rhythm.* 2004;**1**:78-81.
206. Sanchez-Quintana D, Cabrera JA, Climent V, Farre J, Weiglein A, Ho SY. How close are the phrenic nerves to cardiac structures? Implications for cardiac interventionalists. *J. Cardiovasc. Electrophysiol.* 2005;**16**:309-13.
207. Natale A, Pisano E, Shewchik J, Bash D, Fanelli R, Potenza D *et al.* First human experience with pulmonary vein isolation using a through-the-balloon circumferential ultrasound ablation system for recurrent atrial fibrillation. *Circulation* 2000;**102**:1879-82.

208. Shah D, Dumonceau JM, Burri H, Sunthorn H, Schroft A, Gentil-Baron P *et al.* Acute pyloric spasm and gastric hypomotility: an extracardiac adverse effect of percutaneous radiofrequency ablation for atrial fibrillation. *J.Am.Coll.Cardiol.* 2005;**46**:327-30.
209. Kobza R, Hindricks G, Tanner H, Schirdewahn P, Dorszewski A, Piorkowski C *et al.* Late recurrent arrhythmias after ablation of atrial fibrillation: incidence, mechanisms, and treatment. *Heart Rhythm.* 2004;**1**:676-83.
210. Chugh A, Oral H, Good E, Han J, Tamirisa K, Lemola K *et al.* Catheter ablation of atypical atrial flutter and atrial tachycardia within the coronary sinus after left atrial ablation for atrial fibrillation. *J.Am.Coll.Cardiol.* 2005;**46**:83-91.
211. Pappone C, Oral H, Santinelli V, Vicedomini G, Lang CC, Manguso F *et al.* Atrio-esophageal fistula as a complication of percutaneous transcatheter ablation of atrial fibrillation. *Circulation* 2004;**109**:2724-6.
212. Lemola K, Sneider M, Desjardins B, Case I, Han J, Good E *et al.* Computed tomographic analysis of the anatomy of the left atrium and the esophagus: implications for left atrial catheter ablation. *Circulation* 2004;**110**:3655-60.
213. Pappone C, Santinelli V, Manguso F, Vicedomini G, Gugliotta F, Augello G *et al.* Pulmonary vein denervation enhances long-term benefit after circumferential ablation for paroxysmal atrial fibrillation. *Circulation* 2004;**109**:327-34.
214. Gepstein L, Evans SJ. Electroanatomical mapping of the heart: basic concepts and implications for the treatment of cardiac arrhythmias. *Pacing Clin.Electrophysiol.* 1998;**21**:1268-78.
215. Hunold P, Vogt FM, Schmermund A, Debatin JF, Kerckhoff G, Budde T *et al.* Radiation exposure during cardiac CT: effective doses at multi-detector row CT and electron-beam CT. *Radiology* 2003;**226**:145-52.
216. Morin RL, Gerber TC, McCollough CH. Radiation dose in computed tomography of the heart. *Circulation* 2003;**107**:917-22.
217. Trabold T, Buchgeister M, Kuttner A, Heuschmid M, Kopp AF, Schroder S *et al.* Estimation of radiation exposure in 16-detector row computed tomography of the heart with retrospective ECG-gating. *Rofa* 2003;**175**:1051-5.
218. Tsao HM, Wu MH, Yu WC, Tai CT, Lin YK, Hsieh MH *et al.* Role of right middle pulmonary vein in patients with paroxysmal atrial fibrillation. *J.Cardiovasc.Electrophysiol.* 2001;**12**:1353-7.
219. Schwartzman D, Bazaz R, Nosbisch J. Common left pulmonary vein: a consistent source of arrhythmogenic atrial ectopy. *J Cardiovasc.Electrophysiol.* 2004;**15**:560-6.
220. Perez-Lugones A, Schwartzman PR, Schweikert R, Tchou PJ, Saliba W, Marrouche NF *et al.* Three-dimensional reconstruction of pulmonary veins in patients with atrial fibrillation and controls: morphological characteristics of different veins. *Pacing Clin.Electrophysiol.* 2003;**26**:8-15.
221. Lin WS, Prakash VS, Tai CT, Hsieh MH, Tsai CF, Yu WC *et al.* Pulmonary vein morphology in patients with paroxysmal atrial fibrillation initiated by ectopic beats originating from the pulmonary veins: implications for catheter ablation. *Circulation* 2000;**101**:1274-81.
222. Oral H, Knight BP, Ozaydin M, Chugh A, Lai SW, Scharf C *et al.* Segmental ostial ablation to isolate the pulmonary veins during atrial fibrillation: feasibility and mechanistic insights. *Circulation* 2002;**106**:1256-62.
223. Oral H, Ozaydin M, Tada H, Chugh A, Scharf C, Hassan S *et al.* Mechanistic significance of intermittent pulmonary vein tachycardia in patients with atrial fibrillation. *J Cardiovasc.Electrophysiol.* 2002;**13**:645-50.
224. Abraham WT, Hayes DL. Cardiac resynchronization therapy for heart failure. *Circulation* 2003;**108**:2596-603.
225. Puglisi A, Lunati M, Marullo AG, Bianchi S, Feccia M, Sgreccia F *et al.* Limited thoracotomy as a second choice alternative to transvenous implant for cardiac resynchronisation therapy delivery. *Eur.Heart J.* 2004;**25**:1063-9.
226. Khairy P, Triedman JK, Juraszek A, Cecchin F. Inability to cannulate the coronary sinus in patients with supraventricular arrhythmias: congenital and acquired coronary sinus atresia. *J Interv.Card Electrophysiol.* 2005;**12**:123-7.
227. Corcoran SJ, Lawrence C, McGuire MA. The valve of Vieussens: an important cause of difficulty in advancing catheters into the cardiac veins. *J.Cardiovasc.Electrophysiol.* 1999;**10**:804-8.
228. Butter C, Auricchio A, Stellbrink C, Fleck E, Ding J, Yu Y *et al.* Effect of resynchronization therapy stimulation site on the systolic function of heart failure patients. *Circulation* 2001;**104**:3026-9.

229. Alonso C, Leclercq C, Victor F, Mansour H, de Place C, Pavin D *et al.* Electrocardiographic predictive factors of long-term clinical improvement with multisite biventricular pacing in advanced heart failure. *Am.J.Cardiol.* 1999;**84**:1417-21.
230. Sanders P, Jais P, Hocini M, Haissaguerre M. Electrical disconnection of the coronary sinus by radiofrequency catheter ablation to isolate a trigger of atrial fibrillation. *J.Cardiovasc.Electrophysiol.* 2004;**15**:364-8.
231. Hwang C, Peter CT, Chen PS. Radiofrequency ablation of accessory pathways guided by the location of the ligament of Marshall. *J.Cardiovasc.Electrophysiol.* 2003;**14**:616-20.
232. Chauvin M, Shah DC, Haissaguerre M, Marcellin L, Brechenmacher C. The anatomic basis of connections between the coronary sinus musculature and the left atrium in humans. *Circulation* 2000;**101**:647-52.
233. Sun Y, Arruda M, Otomo K, Beckman K, Nakagawa H, Calame J *et al.* Coronary sinus-ventricular accessory connections producing posteroseptal and left posterior accessory pathways: incidence and electrophysiological identification. *Circulation* 2002;**106**:1362-7.
234. Hwang C, Wu TJ, Doshi RN, Peter CT, Chen PS. Vein of marshall cannulation for the analysis of electrical activity in patients with focal atrial fibrillation. *Circulation* 2000;**101**:1503-5.
235. Lemola K, Mueller G, Desjardins B, Sneider M, Case I, Good E *et al.* Topographic analysis of the coronary sinus and major cardiac veins by computed tomography. *Heart Rhythm.* 2005;**2**:694-9.
236. Packer DL. Evolution of mapping and anatomic imaging of cardiac arrhythmias. *J.Cardiovasc.Electrophysiol.* 2004;**15**:839-54.
237. Solomon SB, Dickfeld T, Calkins H. Real-Time Cardiac Catheter Navigation on Three-Dimensional CT Images. *J.Interv.Card Electrophysiol.* 2003;**8**:27-36.
238. Tops LF, Bax JJ, Zeppenfeld K, Jongbloed MR, Lamb HJ, van der Wall EE *et al.* Fusion of multislice computed tomography imaging with three-dimensional electroanatomic mapping to guide radiofrequency catheter ablation procedures. *Heart Rhythm.* 2005;**2**:1076-81.

Exploration of Cardiac Development and Anatomy
in Relation to the Genesis of Clinical Arrhythmias

Part I



Chapter

2

Monique R.M. Jongbloed^{1 2}

Martin J. Schalij²

Robert E. Poelmann¹

Nico A. Blom²

Madelon L. Fekkes¹

Zhiyong Wang³

Glenn I. Fishman³

Adriana C. Gittenberger-de Groot¹

Departments of ¹Anatomy & Embryology and ²Cardiology and Paediatric Cardiology, Leiden University Medical Center, Leiden, The Netherlands. ³ Division of Cardiology, New York University School of Medicine, New York, U.S.A.

Embryonic Conduction Tissue: A Spatial
Correlation with Adult Arrhythmogenic Areas.
Transgenic CCS-*lacZ* Expression in the
Cardiac Conduction System of Murine Embryos

J Cardiovasc Electrophysiol. 2004 Mar;15(3):349-355

Abstract

Introduction:

The occurrence of arrhythmias in adult patients may arise preferentially in anatomic regions derived from the specialized cardiac conduction system. To examine this hypothesis, we performed a detailed analysis of the developing cardiac conduction system using the recently described CCS-*lacZ* transgenic mouse strain.

62

Methods and Results:

Transgenic embryos (E9.5-15.5) were stained for β -galactosidase activity and co-stained with the myocardial marker HHF35. Results were 3-D-reconstructed. CCS-*lacZ* expression was observed in the sino-atrial node, left and right venous valves and septum spurium, in the right and left atrioventricular ring, His bundle, bundle branches and in the right ventricular moderator band. Furthermore, *lacZ* positive cells could be demonstrated for the first time in the left atrium, in the posterior wall surrounding the pulmonary venous orifice and, in later stages, surrounding the pulmonary venous wall. These cells were continuous with the left venous valve in the right atrium. LacZ positive tissue could also be identified in Bachmann's bundle, running retro-aortically between right atrium and left atrium.

Conclusion:

Known arrhythmogenic areas including Bachmann's bundle, the pulmonary veins and sinus venosus derived internodal structures demonstrate *lacZ* expression. These data support the hypothesis that areas derived from the developing cardiac conduction system may contribute to the arrhythmogenic substrate in adult hearts.

Introduction

In recent years it has been demonstrated that a variety of different arrhythmias may be related to specific anatomical sites and substrates. The Wolf-Parkinson-White syndrome, due to an accessory AV-conduction pathway is the best-known example ¹, but recent studies demonstrate that atrial fibrillation and ectopic atrial tachycardia also may originate from specific anatomical sites. From clinical mapping studies by Haïssaguerre et al. and others, it is clear that the initiation of atrial fibrillation is frequently related to ectopic atrial beats which may originate from the pulmonary veins (PV) ², the ostia of the coronary sinus and of the caval veins ^{3,4}, the terminal crest ^{5,6} and the interatrial bundle referred to as Bachmann's bundle ⁷ may also play an important role in the initiation and perpetuation of atrial fibrillation. Since the presentation of these clinical mapping data, many studies have been performed to unravel the underlying anatomical structures and their relationship with the developing myocardium ⁸⁻¹⁰. Sleeves of myocardium extending for different lengths along the PV may play an important role but the cause of the arrhythmogenicity of these sleeves remains to be clarified.

Since the recognition that anatomical sites in the atria which do not belong to the mature cardiac conduction system (CCS) play an important role in arrhythmogenesis, research has been directed at the development of the CCS. Initially, histological characteristics were used to identify cells with specific conduction properties. This resulted in the ring theory, which proposes that the CCS originates from four rings of specialized tissue ¹¹. During cardiac development, parts of these rings lose their specialized character and the remaining parts are identified as putative components of the mature cardiac conduction system.

The use of immunohistochemical markers, such as GIN2 and HNK1, has facilitated the recognition of the developing CCS, although none of these markers is specific for conduction system only ¹². The developing human CCS has been described based on findings of HNK1 staining ¹³. An embryonic origin of the sino-atrial node and the atrioventricular (AV) conduction system was demonstrated, as well as internodal tracts and a dual origin of the AV-node (overview in ¹⁴). Transient HNK1 staining was also observed in the myocardium surrounding the PV and in the coronary sinus, areas identified by electrical mapping to play an important role in the occurrence of some clinical arrhythmias ^{2,3}. However, in order to link clinical arrhythmias to the development of the specific conduction system, a more specific delineation of the developing and mature CCS is necessary.

Recently the CCS-*lacZ* strain of transgenic mice was described ¹⁵. Using this line of mice, it was possible to accurately delineate the entire developing and mature CCS. Furthermore, optical mapping of areas with β -galactosidase activity demonstrated a correlation of CCS-*lacZ* expression with functional maps of electrical activity ¹⁵. However, until now, no direct relation between arrhythmogenic areas and the developing conduction system, and the possible impact in arrhythmogenesis, was made. Morphological patterning of the developing cardiac conduction system in the CCS-*lacZ* reporter mouse seems to coincide

largely with data in the recently described *MinK-lacZ* reporter mouse¹⁶. There are, however, a number of differences which indicate that only partly common developmental pathways exist. Whereas the *MinK*-model refers to a known gene encoding a protein, the expression of which modulates function of the cardiac delayed rectifier potassium currents¹⁷, the exact locus of the gene responsible for expression in the *CCS-lacZ* construct remains to be clarified. In published data of both models¹⁵⁻¹⁸ there is no remark on expression in the area of the PV. The latter subject is of special interest because of the findings in human embryos in this area¹³. The aim of the current study is to reconstruct the CCS during sequential developmental stages, with attention directed specifically at anatomical sites known to be related to the occurrence of arrhythmias, such as the PV, interatrial and internodal connections.

Methods

The generation and initial characterization of the transgenic line of *CCS-lacZ* reporter mice and staining for β -galactosidase activity has been described¹⁵. Procedures followed were in accordance with institutional and NIH guidelines concerning the use of animals.

Mouse embryos ranging from gestational age E 9,5-E 15,5 days post coitum (d.p.c.) were studied (the morning of the vaginal plug was designated as 0.5 d.p.c.).

Twenty-three embryos were fixed at room temperature in 5% phosphate buffered formalin solution and embedded in paraffin. The embryos were then transected transversely (section thickness 5 μ m) and the sections were washed in phosphate buffered saline. Immunohistochemical staining was performed with the monoclonal anti-muscle actine α antibody HHF 35 (Dako M635; staining protocol described in¹⁹) in order to produce a double staining with the *CCS-lacZ* reporter construct. Slices were counterstained with haematoxylin.

The slices were 3-D reconstructed to obtain optimal insight in the distribution of β -galactosidase activity in the myocardium and their relationship to other intracardiac structures. Reconstruction was done using AMIRATM software (Template Graphics Software, Inc. San Diego, California). AMIRATM is an advanced software system for 3D visualization, data analysis and geometry reconstruction from microscopic images.

Results

Stage E 9,5

At this stage looping of the primitive heart tube has started and the bulboventricular groove can be distinguished. There is no septation between atria and ventricles and septation of the outflow tract has not started yet. β -galactosidase activity is markedly present in the primary fold. *LacZ* positive tissue is observed in the complete AV canal. Already at this stage, the primitive pulmonary vein can be recognized in the dorsal mesocardium, but it lacks *lacZ*-expression at this stage. The lateral wall of the right part of the common atrium however demonstrates marked *lacZ* expression, whereas the posterior wall of the left part of the common atrium shows only minimal *lacZ* expression at this stage.

Stage E 10,5

At this stage, looping of the heart tube has progressed. Ventricular septation has started. The outflow tract is situated above the primitive right ventricle and the AV-canal above the primitive left ventricle (**figure 1 a-f**). Myocardial *lacZ* staining is observed in the proximal part of the outflow tract, but not in the distal outflow tract (**figure 1a,d**). As in the E 9.5 embryo, the transition between the primitive right ventricle (RV) and the future left ventricle is surrounded by a ring of β -galactosidase active cells, the primary fold (**figure 1e,f**). Furthermore, *lacZ* expression is detected along the AV-canal (**figure 1b,e,f**). The AV cushion tissue does not show *lacZ* expression.

In the right part of the common atrium, the right venous valve and left venous valve can be recognized, which show strong *lacZ* expression. The valves encompass the ostia of the right and left cardinal veins. The primitive pulmonary vein can be distinguished in the dorsal mesocardium (**figure 1 c,f**). The dorsal myocardial wall of both the left and right components of the common atrium show *lacZ* expression with more prominent staining in the right component. Three-D reconstructions of findings in this stage with according sections are demonstrated in figure 1a-c.

Stage E 11,5

At this stage, septation of the common atrial chamber has occurred. No β -galactosidase staining is present in the primary atrial septum. As in the previous stage, the right atrial right and left venous valves can clearly be distinguished as two *lacZ* positive structures. The dorsal wall of the left atrium (LA) still demonstrates *lacZ* expression, which extends behind the posterior surface of the primitive pulmonary vein to become continuous with the left venous valve. *LacZ* positive cells can also be observed around the wall of the primitive pulmonary vein at this stage, which was not the case in earlier stages. More cranially, the right and left venous valves fuse to form the septum spurium, which forms a band of *lacZ* positive tissue running anteriorly in the right atrium (RA) to a retro-aortic position. This band continues into the LA and merges with the ring of *lacZ* positive tissue surrounding the AV

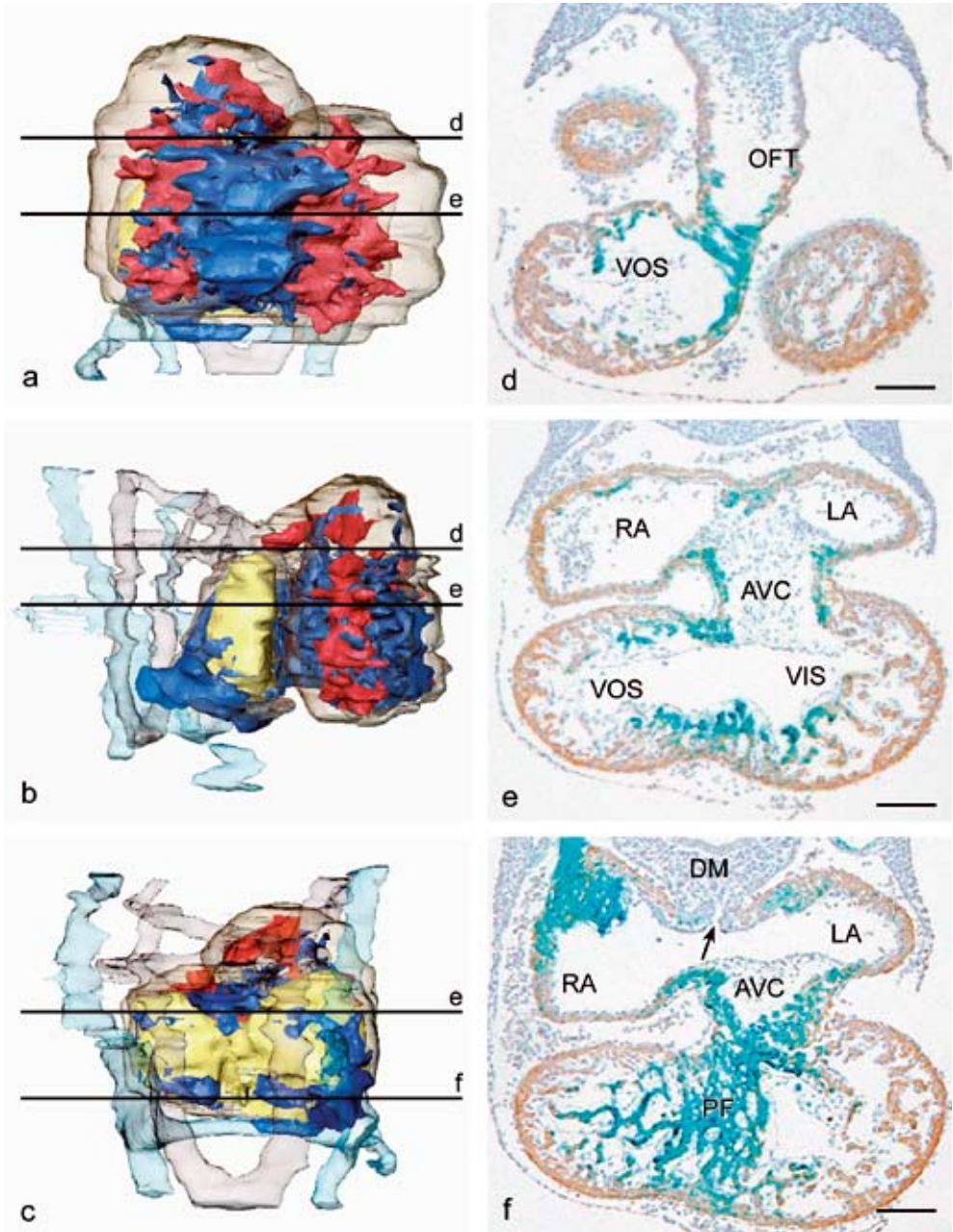


Figure 1

3-D reconstructions (a-c) and transverse slices (d-f) of an E 10,5 embryo. *LacZ* negative myocardium, branchial arch arteries and cardinal veins are transparent. Color-codes: yellow: lumen of the common atrium and the primitive pulmonary vein (PPV); red: lumen of the common ventricle; Blue: *CCS-lacZ* positive myocardium. a. Anterior view. *CCS-lacZ* positive myocardium can be observed in the primary fold and outflow tract. b. Lateral view, demonstrating a ring of *lacZ* expression in the atrioventricular canal. c. Dorsal/oblique view, showing expression in the right and left venous valves in the right part of the atrium. The dorsal wall of the left part of the

canal, the so-called atrioventricular ring bundle (AVRB). This anterior inter-atrial bundle probably is the primordium of Bachmann's bundle. A separate structure is the retro-aortic root bundle, which runs around the aorta towards the right part of the ventricle to become continuous with the *lacZ* positive tissue representing the primary fold. More caudally, connecting to the posterior part of the AVRB (the site of the posterior AV node), *lacZ* expression is detected in the interventricular septum, (His bundle) and spreading in the ventricles (left and right bundle branches and Purkinje fibers).

Stage E 12,5

Progression of outflow tract septum formation leads to a pulmonary trunk that has an anterior position and an aorta that is situated dorsal from this structure. *LacZ* expression is in accordance with previous stages. In the RV *lacZ* positivity can be distinguished in the trabecula septomarginalis, extending across the lumen of the ventricle as the moderator band. The latter is in continuity by way of the lateral RV wall with the right side of the AVRB.

Stage E 13,5

Findings are still in accordance with the previous stage. *LacZ* staining of the left atrial dorsal wall is pronounced at this stage and marked CCS-*lacZ* expression is found in the myocardium surrounding the PV. The latter *lacZ* positive myocardium at this stage can be traced as a sleeve along the pulmonary vein towards the lung tissue (**figure 2a,b**). The top of the interventricular septum is *lacZ* positive and staining extends into the area of both bundle branches. The distal ends of the trabeculae in both ventricles also demonstrate β -galactosidase staining.

Stage E 14,5

At this stage, atrial and ventricular septation has been completed. The primary atrial septum does not show *lacZ* positivity. As in the previous stages, the right and left venous valves are seen in the RA to be strongly *lacZ* positive (**figure 3a,d**). Also, the septum spurium is continuous with the interatrial bundle (Bachmann's bundle). The coronary sinus wall does not show *lacZ* expression, but the myocardium surrounding the orifice is *lacZ* positive. As in the previous stage, the dorsal wall of the LA can be observed as a *lacZ* positive area (**figure 3b,e**) and the *lacZ* positive myocardium extends along the PV. The *lacZ* positive myocardium of the left atrial dorsal wall is connected with the left venous valve in the RA (**figure 2 c-f**).

common atrium surrounding the entrance of the PPV (arrow) also demonstrates *lacZ* expression. d. CCS-*lacZ* expression in the proximal portion of the outflow tract (OFT). e. Expression in the atrioventricular canal (AVC) and the primary fold (PF). f. The PPV (arrow) enters the atrium at the midline. Expression in the dorsal wall of the primitive left part of the atrium (LA) and in the fused venous valves in the primitive right part of the atrium (RA). Levels of sections of d, e and f are indicated by black bars in a, b and c.

VOS: ventricular outlet segment, VIS: ventricular inlet segment, DM: dorsal mesocardium. Bar is 100 μ m.

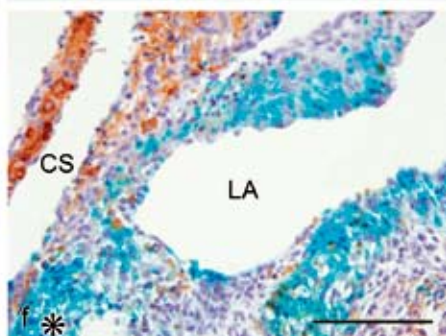
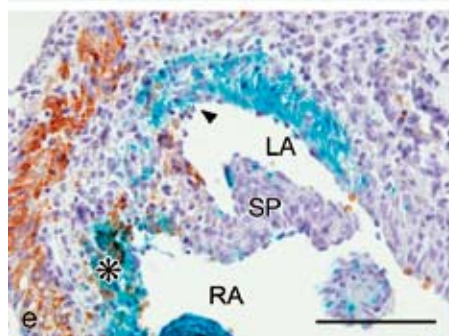
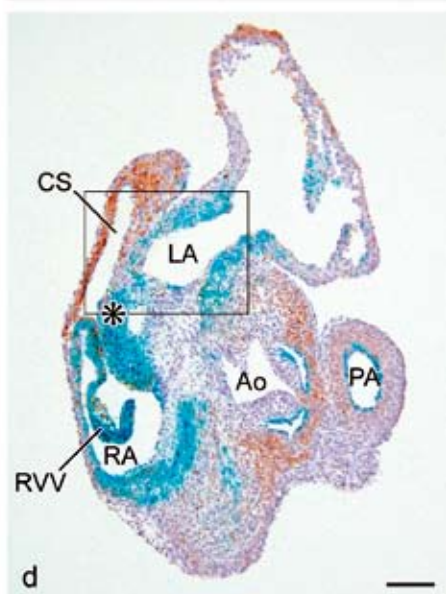
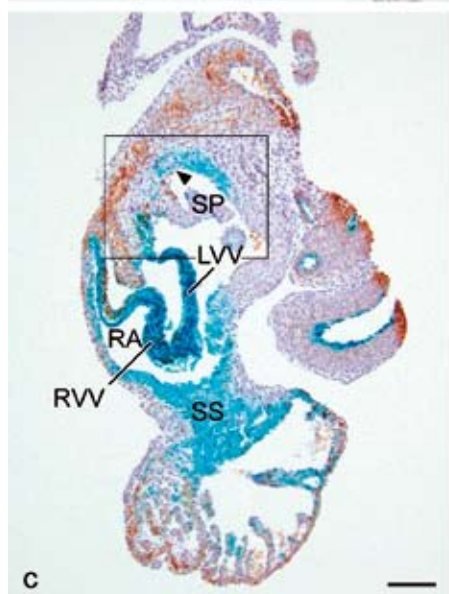
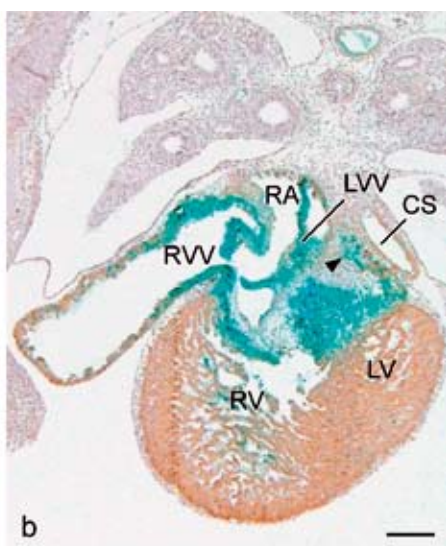
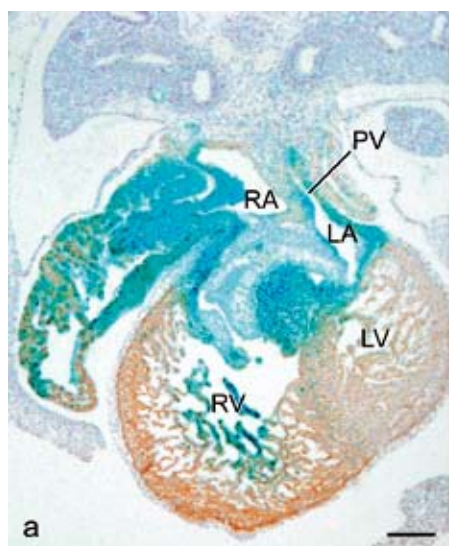


Figure 2

a. Transverse section of an E 13,5 embryo, at the level of the pulmonary vein (PV) which has a cuff of *lacZ* positive myocardial cells around its wall. The left atrial dorsal wall also demonstrates marked *lacZ* expression. b. Section just below the level of the PV in the same embryo. Staining in the left atrial dorsal wall (arrowhead) becomes continuous with the base of the left venous valve (LVV). c. Transverse section through the heart of an E 14,5 embryo, in a slightly different plane as compared to the E13,5 embryo, at the level of the entrance of the PV (arrowhead) in the left atrium. See figure e for detail, in which staining in the left atrial dorsal wall can be followed marginally to the base of the LVV (asterisk). d. Level below section c, coarsing through the coronary sinus (CS) in which the continuity of the CCS-*lacZ* expression between the left atrial dorsal wall and the base of the LVV (asterisk) is now more marked. See figure f for detail.
 RA: right atrium, RV: right ventricle, LV: left ventricle, RVV: right venous valve, SP: septum primum, SS: septum spurium
 Bar is 10 μ m.

There is lack of *lacZ* expression in the newly formed right ventricular inflow tract. The AVRB however can still be distinguished. Staining is also present on top of the interventricular septum, extending towards both ventricles. The moderator band in the RV can be clearly distinguished as a *lacZ* positive band in this stage as well, extending towards the lateral wall of the RV (**figure 3c,f**). Thus a continuous *lacZ* positive connection is present from the right ventricular septum to the right AVRB. No *lacZ* expression is present in the distal outflow tract. Figure 3 a-c demonstrates 3-D reconstructions and corresponding histological sections of findings in this stage.

Stage E 15

Findings in this stage are in accordance with those in previous stages, although staining becomes less marked, indicating regression of staining in older embryos. Staining of the left atrial dorsal wall and the myocardium surrounding the PV has markedly reduced at this stage.

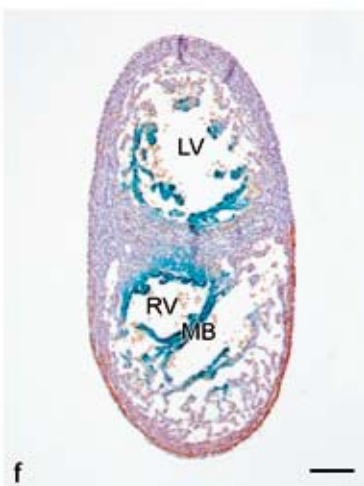
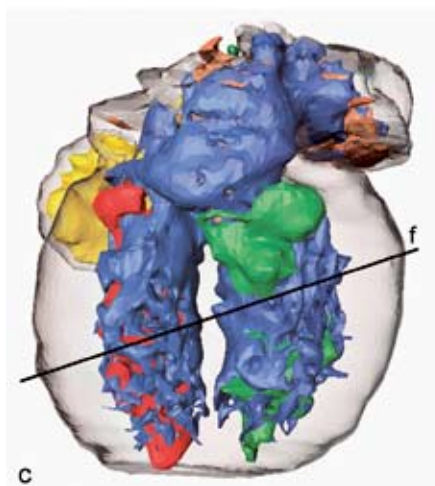
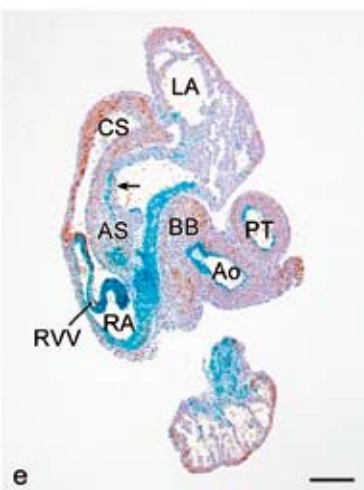
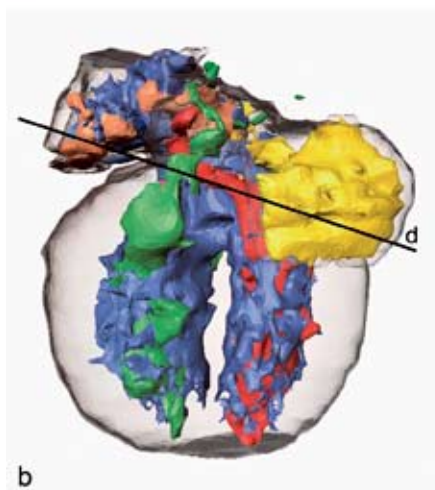
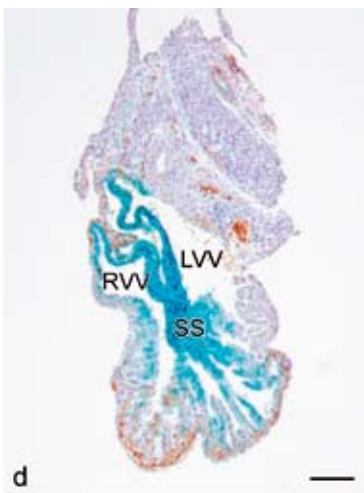
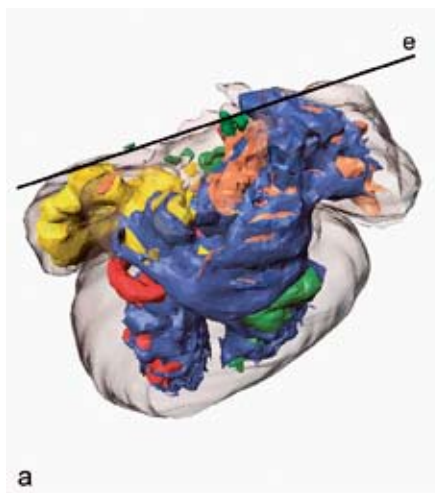


Figure 3

3-D reconstructions (a-c) and transverse sections (d-f) of an E 14,5 embryo. *LacZ* negative myocardium has been made transparent. Color-codes: orange: lumen of the right atrium; yellow: lumen of the left atrium; green: lumen of the right ventricle and the pulmonary trunk; red: lumen of the left ventricle and aorta; blue: CCS-*lacZ* positive myocardium. a. Dorso-lateral view. b. Anterior view. c. Posterior view. d. CCS-*lacZ* expression in right atrial internodal structures: The right venous valve (RVV) and the left venous valve (LVV) fuse anteriorly to form the septum spurium (SS). e. Section at the level of the pulmonary veins. The left atrial dorsal wall is *lacZ* positive (arrow). Bachmann's bundle (BB) can be observed as an anterior atrial band of *lacZ* positive tissue, which runs retro-aortically between the right atrium (RA) and the left atrium (LA). f. Section at the level of the ventricles. The right ventricular (RV) moderator band (MB) shows marked *lacZ* expression. Levels of sections of d, e and f are indicated by black bars in a, b and c. CS: coronary sinus, AS: atrial septum, Ao: aorta, PT: pulmonary trunk, LV: left ventricle. Bar is 10 μm .

Discussion

Atrial arrhythmias often originate from sinus venosus related tissue, like the terminal crest or the ostia of the veins in the RA^{4,5} and in the pulmonary veins in the LA². Recently, several studies have taken advantage of genetically engineered mouse models to visualize the formation of the specialized CCS, including the CCS-*lacZ* mouse described by Fishman and colleagues^{15,18}, as well as the *minK-lacZ* knockin mouse generated by Roden et al.¹⁷ and analyzed during development by Evans et al.¹⁶

However the extent of reporter gene expression in the area of the pulmonary veins and surrounding the pulmonary venous wall, a pivotal area in later life for the origin of atrial arrhythmias, remains unclear.

Debate continues concerning the exact origin of the PV and the corresponding entry area in the LA. Previous studies report a connection of the area of entrance of the PV with the sinus venosus area^{13,20,21} though other investigators disputed this relation²². In the current study, we concentrated on the area of the primitive PV, that was found to be delineated in the dorsal mesocardium. This primitive PV entered the common atrium at the midline and in later stages the entrance shifted towards the left atrium. At this venous entrance CCS-*lacZ* positive myocardial cells were present in the left atrial dorsal wall. These *lacZ* positive cells were continuous with the left venous valve. Thus the entrance of the primitive pulmonary vein in the LA was surrounded by a CCS-*lacZ* positive area, which was continuous with the sinus venosus area of the RA. These findings are consistent with findings in earlier studies in chicken²¹, rat²³ and human¹³ embryos, using the HNK1 epitope to delineate the CCS (overview in (14)), but are distinct from the *MinK-lacZ* model that does not show expression in the pulmonary venous area¹⁶. At later stages, *lacZ* positive cells were observed forming a sleeve around the PV. The first signs of these cells were observed in stage E 11,5 and the most pronounced staining of the pulmonary venous myocardial wall appeared to occur in stage E 13,5. These findings correspond to the process of secondary myocardialization of the heart tube²⁴. The presence of a myocardial sleeve of *lacZ* positive tissue at

this site may be linked to the occurrence of atrial ectopic tachycardia or atrial fibrillation originating from sites within the PV². Distinctive electrophysiological properties from the atrial myocardium have been observed in the pulmonary veins^{25,26} and recently the presence of specialized conduction cells was demonstrated morphologically in human PV of patients with atrial fibrillation²⁷.

As in the HNK1 study in human embryos¹³, in the murine *CCS-lacZ* model, evidence was found that embryonic internodal structures connect the sino-atrial node with the AV-node. Furthermore, besides the well-known right AV-ring, we found a left AV-ring. Abundant *lacZ* expression was also observed in the primary fold. In contrast, the myocardial primary atrial septum does not express β -galactosidase activity, indicating that the septum is probably a secondary atrial myocardial structure and does not share the expression of the *CCS-lacZ* gene as found so markedly in the sinus venosus.

Another interesting finding in the *CCS-lacZ* model is that the coronary sinus wall per se does not show β -galactosidase staining, although the myocardium surrounding the ostium of this vein in the RA was *lacZ* positive. This result corresponds to the HNK-1 expression pattern in human embryos¹³.

An interesting structure with respect to the induction of atrial fibrillation is Bachmann's bundle, a bundle of fibers connecting both atria^{28,29}. Positioned in the anterior atrial wall, this bundle passes retro-aortically crossing the interatrial septum from the RA to the LA. In our study we demonstrated that this bundle corresponds to a *lacZ* positive bundle, which connects to the septum spurium in the RA, and when traced caudally, to the AVRB. These findings may explain the importance of this structure in the genesis and/or perpetuation of arrhythmias²⁹. Distinctive electrophysiological properties in Bachmann's bundle have been demonstrated in patients with atrial fibrillation³⁰. Node-like cells have been observed at this site in dogs³¹. Besides the bundle of fibers running towards the LA, another retro-aortic bundle (referred to as retro-aortic root bundle) was observed, which lies at the basis of the outflow tract and connects to the primary fold.

Data obtained in the *CCS-lacZ* reporter mouse match largely with data based on histological examination of human embryos¹¹. In the latter study four myocardial rings with histologic characteristics of primitive conduction tissue were observed, namely a sino-atrial, atrioventricular, bulboventricular and truncobulbar ring. *LacZ* positivity could be demonstrated in corresponding areas in the *CCS-lacZ* model (**Figure 4**). These data match largely with the *MinK-lacZ* model¹⁶. However, only the proximal and not the distal outflow tract shows *lacZ* expression in the *CCS-lacZ* mouse, which may be linked to the current finding of expansion of the anterior heart field³². This poses a difference with the *MinK-lacZ* model, in which expression is observed more extensive throughout the outflow tract¹⁶.

The trigger for differentiation of primary cardiomyocytes into cells of the cardiac conduction system remains to be identified. Retroviral lineage studies in the chick have supported the theory that recruitment, rather than specification, of cardiomyocytes plays a major role in this process³³. It is unclear if this process of continual recruitment is also active in

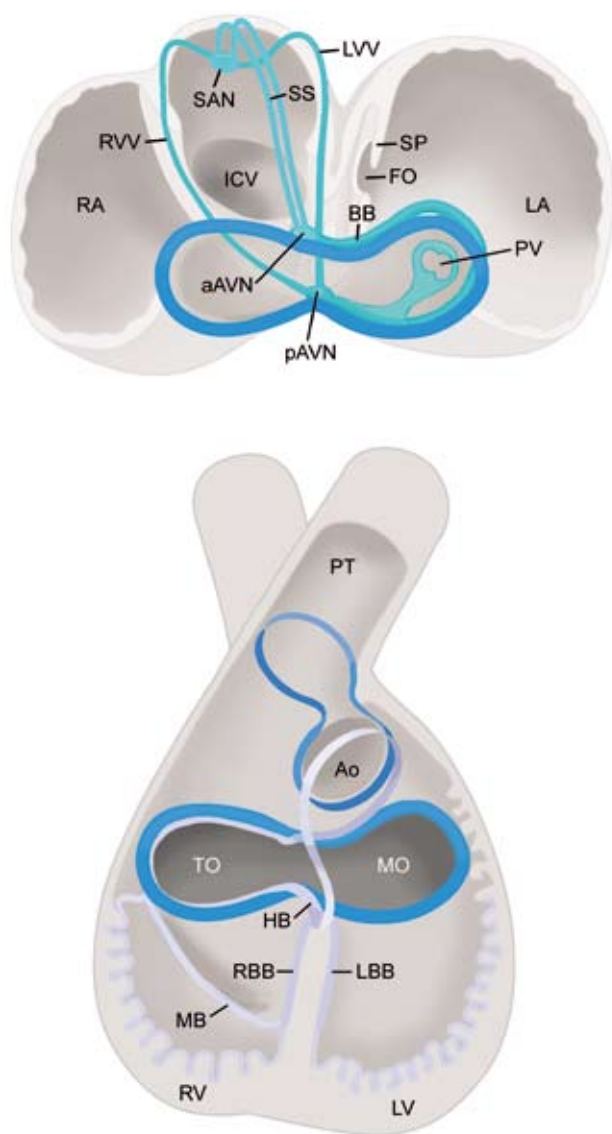


Figure 4

Schematic representation of CCS-*lacZ* expression in the E 14,5 embryo. Upper panel: atrial level. Depicted in turquoise are the right venous valve (RVV) and left venous valve (LWV), which fuse anteriorly to form the septum spurium (SS). The latter connects to Bachmann's bundle (BB), which runs in between the right atrium (RA) and the left atrium (LA) in a retro-aortic position. Bachmann's bundle merges with the left atrioventricular ring bundle, which continues into the dorsal wall of the LA and pulmonary veins (PV). The LWV is continuous with the *lacZ* positive area surrounding the PV. The atrioventricular ring bundle is depicted in blue. Lower panel: ventricular level, demonstrating the ventriculo-arterial ring (upper dark blue ring), the primary fold (bulboventricular ring, grey-blue) and the atrioventricular ring bundle (blue, as in upper panel).

SAN: sino-atrial node, ICV: inferior caval vein, SP: septum primum, aAVN: anterior atrioventricular node, pAVN: posterior atrioventricular node, FO: fossa ovalis, PT: pulmonary trunk, Ao: aorta, TO: tricuspid orifice, MO: mitral orifice, HB: His bundle, RBB: right bundle branch, LBB: left bundle branch, MB: moderator band, RV: right ventricle, LV: left ventricle

mammalian CCS development. In this study we observed relatively late addition of *CCS-lacZ* expressing cardiomyocytes to the pulmonary venous wall, but whether this represents additional recruitment or migration of cells into this region was not determined in our study.

Study limitations

74

A murine model was used to delineate the developing cardiac conduction system. Although findings in murine embryos are not necessarily valid for the human heart, several mouse models are now generally accepted for study of the cardiac conduction system, being discussed in recent literature³⁴. Results of our study largely coincide with previously published data in human embryos¹³, that guided our research in the mouse model. Electrophysiological study in order to confirm the hypothesis that arrhythmogenesis at these sites is related to embryonic remnants/re-expression of embryonic phenotype, was not performed in these embryos. However, optical mapping has demonstrated a correlation of *lacZ* expression with functional maps of electrical activity¹⁵. Although our hypothesis was not confirmed by electrophysiological mapping, recently emerging data of both electrophysiological^{26 25 35} and morphological²⁷ studies point at the occurrence of specialized cells at several specific anatomical sites, such as the pulmonary veins. Further study is warranted to link electrophysiological mapping data with specific anatomical embryological sites.

Conclusion

Using the *CCS-lacZ* murine model, we demonstrated that sites related to the occurrence of clinically relevant cardiac arrhythmias correlate with cells positive for *CCS-lacZ*, indicative of the developing specialized CCS. This supports the hypothesis that a developmental pathway utilized in the embryonic conduction system myocardium may correlate with areas of myocardium that are disturbed in adult atrial arrhythmias. To examine whether embryonic genes are re-expressed in pathological states would require the development of specific animal models.

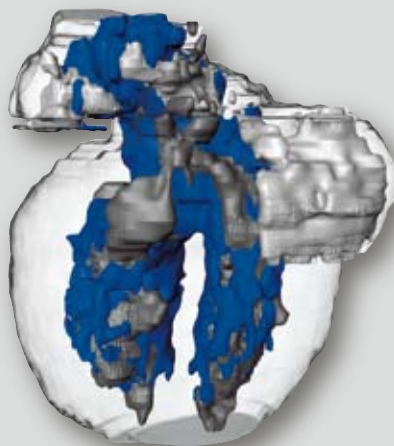
Acknowledgements

This work was supported by HL64757 (G.I.F.) from the National Institutes of Health and a Burroughs Wellcome Fund Clinical Scientist Award in Translational Research (G.I.F.).

Reference List

1. Al Khatib SM, Pritchett EL. Clinical features of Wolff-Parkinson-White syndrome. *Am.Heart.J.* 1999;**138**:403-13.
2. Haissaguerre M, Jais P, Shah DC, Takahashi A, Hocini M, Quiniou G *et al.* Spontaneous initiation of atrial fibrillation by ectopic beats originating in the pulmonary veins. *N.Engl.J.Med.* 1998;**339**:659-66.
3. Katritsis D, Ioannidis JP, Giazitzoglou E, Korovesis S, Anagnostopoulos CE, Camm AJ. Conduction delay within the coronary sinus in humans: implications for atrial arrhythmias. *J.Cardiovasc.Electrophysiol.* 2002;**13**:859-62.
4. Tsai CF, Tai CT, Hsieh MH, Lin WS, Yu WC, Ueng KC *et al.* Initiation of atrial fibrillation by ectopic beats originating from the superior vena cava: electrophysiological characteristics and results of radiofrequency ablation. *Circulation* 2000;**102**:67-74.
5. Kalman JM, Olgin JE, Karch MR, Hamdan M, Lee RJ, Lesh MD. "Cristal tachycardias": origin of right atrial tachycardias from the crista terminalis identified by intracardiac echocardiography. *J.Am.Coll. Cardiol.* 1998;**31**:451-9.
6. Olgin JE, Kalman JM, Fitzpatrick AP, Lesh MD. Role of right atrial endocardial structures as barriers to conduction during human type I atrial flutter. Activation and entrainment mapping guided by intracardiac echocardiography. *Circulation* 1995;**92**:1839-48.
7. Kumagai K, Uno K, Khrestian C, Waldo AL. Single site radiofrequency catheter ablation of atrial fibrillation: studies guided by simultaneous multisite mapping in the canine sterile pericarditis model. *J.Am. Coll. Cardiol.* 2000;**36**:917-23.
8. Anderson RH, Ho SY. Anatomy of the atrioventricular junctions with regard to ventricular preexcitation. *Pacing Clin. Electrophysiol.* 1997;**20**:2072-6.
9. Ho SY, Sanchez-Quintana D, Cabrera JA, Anderson RH. Anatomy of the left atrium: implications for radiofrequency ablation of atrial fibrillation. *J.Cardiovasc. Electrophysiol.* 1999;**10**:1525-33.
10. Ho SY, Cabrera JA, Tran VH, Farre J, Anderson RH, Sanchez-Quintana D. Architecture of the pulmonary veins: relevance to radiofrequency ablation. *Heart* 2001;**86**:265-70.
11. Wenink AC. Development of the human cardiac conduction system. *J.Anat.* 1976;**121**:617-31.
12. Moorman AF, de Jong F, Denyn MM, Lamers WH. Development of the cardiac conduction system. *Circ. Res.* 1998;**82**:629-44.
13. Blom NA, Gittenberger-De Groot AC, DeRuiter MC, Poelmann RE, Mentink MM, Ottenkamp J. Development of the cardiac conduction tissue in human embryos using HNK-1 antigen expression: possible relevance for understanding of abnormal atrial automaticity. *Circulation* 1999;**99**:800-6.
14. Gittenberger-De Groot AC, DeRuiter MC, Bartelings MM, Poelmann RE. Embryology of congenital heart disease. In: Crawford MH, DiMarco JP, Paulus WJ, eds. *Cardiology*. Richard Furn, 2004:1217-27.
15. Rentschler S, Vaidya DM, Tamaddon H, Degenhardt K, Sassoon D, Morley GE *et al.* Visualization and functional characterization of the developing murine cardiac conduction system. *Development* 2001;**128**:1785-92.
16. Kondo RP, Anderson RH, Kupersmidt S, Roden DM, Evans SM. Development of the cardiac conduction system as delineated by minK-lacZ. *J.Cardiovasc. Electrophysiol.* 2003;**14**:383-91.
17. Kupersmidt S, Yang T, Anderson ME, Wessels A, Niswender KD, Magnuson MA *et al.* Replacement by homologous recombination of the minK gene with lacZ reveals restriction of minK expression to the mouse cardiac conduction system. *Circ. Res.* 1999;**84**:146-52.
18. Rentschler S, Zander J, Meyers K, France D, Levine R, Porter G *et al.* Neuregulin-1 promotes formation of the murine cardiac conduction system. *Proc.Natl.Acad.Sci.U.S.A* 2002;**99**:10464-9.
19. Bartram U, Molin DG, Wisse LJ, Mohamad A, Sanford LP, Doetschman T *et al.* Double-outlet right ventricle and overriding tricuspid valve reflect disturbances of looping, myocardialization, endocardial cushion differentiation, and apoptosis in TGF-beta(2)-knockout mice. *Circulation* 2001;**103**:2745-52.
20. Blom NA, Gittenberger-De Groot AC, Jongeneel TH, DeRuiter MC, Poelmann RE, Ottenkamp J. Normal development of the pulmonary veins in human embryos and formulation of a morphogenetic concept for sinus venosus defects. *Am.J. Cardiol.* 2001;**87**:305-9.
21. DeRuiter MC, Gittenberger-De Groot AC, Wenink AC, Poelmann RE, Mentink MM. In normal development pulmonary veins are connected to the sinus venosus segment in the left atrium. *Anat. Rec.* 1995;**243**:84-92.

22. Webb S, Brown NA, Anderson RH, Richardson MK. Relationship in the chick of the developing pulmonary vein to the embryonic systemic venous sinus. *Anat.Rec.* 2000;**259**:67-75.
23. Wenink AC, Symersky P, Ikeda T, DeRuiter MC, Poelmann RE, Gittenberger-De Groot AC. HNK-1 expression patterns in the embryonic rat heart distinguish between sinuatrial tissues and atrial myocardium. *Anat.Embryol.(Berl)* 2000;**201**:39-50.
24. Kruihof BP, van den Hoff MJ, Tesink-Taekema S, Moorman AF. Recruitment of intra- and extracardiac cells into the myocardial lineage during mouse development. *Anat.Rec.* 2003;**271A**:303-14.
25. Jais P, Hocini M, Macle L, Choi KJ, Deisenhofer I, Weerasooriya R *et al.* Distinctive electrophysiological properties of pulmonary veins in patients with atrial fibrillation. *Circulation* 2002;**106**:2479-85.
26. Hocini M, Ho SY, Kawara T, Linnenbank AC, Potse M, Shah D *et al.* Electrical conduction in canine pulmonary veins: electrophysiological and anatomic correlation. *Circulation* 2002;**105**:2442-8.
27. Perez-Lugones A, McMahon JT, Ratliff NB, Saliba WI, Schweikert RA, Marrouche NF *et al.* Evidence of specialized conduction cells in human pulmonary veins of patients with atrial fibrillation. *J.Cardiovasc. Electrophysiol.* 2003;**14**:803-9.
28. Ho SY, Anderson RH, Sanchez-Quintana D. Atrial structure and fibres: morphologic bases of atrial conduction. *Cardiovasc.Res.* 2002;**54**:325-36.
29. Platonov PG, Mitrofanova LB, Chireikin LV, Olsson SB. Morphology of inter-atrial conduction routes in patients with atrial fibrillation. *Europace.* 2002;**4**:183-92.
30. O'Donnell D, Bourke JP, Furniss SS. Interatrial transseptal electrical conduction: comparison of patients with atrial fibrillation and normal controls. *J.Cardiovasc.Electrophysiol.* 2002;**13**:1111-7.
31. Sherf L, James TN. Fine structure of cells and their histologic organization within internodal pathways of the heart: clinical and electrocardiographic implications. *Am.J.Cardiol.* 1979;**44**:345-69.
32. Kelly RG, Buckingham ME. The anterior heart-forming field: voyage to the arterial pole of the heart. *Trends Genet.* 2002;**18**:210-6.
33. Cheng G, Litchenberg WH, Cole GJ, Mikawa T, Thompson RP, Gourdie RG. Development of the cardiac conduction system involves recruitment within a multipotent cardiomyogenic lineage. *Development* 1999;**126**:5041-9.
34. Wessels A, Phelps A, Trusk T.C., Davis D.L., Edwards A.V., Burch J.B.E. *et al.* Mouse Models for Cardiac Conduction Development. In: Chadwick D.J., Good J, eds. *Development of the Cardiac Conduction System*. Chichester: Wiley J & Sons Ltd, 2003:44-59.
35. Honjo H, Boyett MR, Niwa R, Inada S, Yamamoto M, Mitsui K *et al.* Pacing-induced spontaneous activity in myocardial sleeves of pulmonary veins after treatment with ryanodine. *Circulation* 2003;**107**:1937-43.



Chapter

3

Monique R.M. Jongbloed^{1 2}
Maurits C.E.F. Wijffels²
Martin J. Schalij²
Nico. A. Blom³
Robert E. Poelmann¹,
Arnoud van der Laarse²
Monica M.T. Mentink¹
Zhiyong Wang⁴
Glenn I. Fishman⁴
Adriana C. Gittenberger-de Groot¹

¹ Dept. of Anatomy & Embryology, Leiden University Medical Center, Leiden, The Netherlands

² Dept. of Cardiology, Leiden University Medical Center, Leiden, The Netherlands

³ Dept. of Paediatric Cardiology, Leiden University Medical Center, Leiden, The Netherlands

⁴ Leon H. Charney Division of Cardiology, New York University School of Medicine, New York, USA.

Development of the Right Ventricular Inflow Tract
and Moderator Band;
A Possible Morphological and Functional
Explanation for Mahaim Tachycardia



Circulation Research 2005 Apr;96(7):776-83

Abstract

80

Atriofascicular accessory bundles with AV-node like conduction properties can sustain atrioventricular (AV) re-entrant tachycardia (Mahaim tachycardia). During early embryogenesis, the AV canal is situated above the primitive left ventricle (LV), and a right AV connection has not been achieved yet. We studied the formation of the right ventricular (RV) inflow tract in relation to the developing cardiac conduction system and hypothesized a morphological explanation for functional atriofascicular bypass tracts. Analysis of *lacZ*-expression during sequential stages of cardiogenesis was performed in *CCS-lacZ* transgenic mice (E 9,5-15,5). Embryos were stained for β -galactosidase activity and the myocardial marker HHF35. At early stages *CCS-lacZ* expression was observed in a ring surrounding the AV canal, which connected at the inner curvature to the primary fold. The first sign of formation of the (*CCS-lacZ* negative) RV inlet component was a groove in the *CCS-lacZ* positive tissue of the primary fold. Outgrowth of the RV inlet tract resulted in division of the primary fold in a septal part, the trabecula septomarginalis and a lateral part, the moderator band, which extended laterally up to the right AV ring. Electrophysiological measurements in embryonic hearts (E 15,5) in which the right atrium (RA) and RV were isolated from the left atrium (LA) and LV supported the functionality of this AV-connection via the moderator band, by demonstrating sequential atrial and ventricular activation in both RA/RV and LA/LV preparations. In conclusion, our observations may provide a possible morphological and functional explanation for atriofascicular accessory pathways via the moderator band, underlying Mahaim tachycardia.

Introduction

Atrioventricular (AV) re-entrant tachycardias are based on the presence of accessory myocardial bundles connecting atrial and ventricular tissue, thus bypassing the insulating function of the AV-groove. A unique arrhythmia based on re-entry, is the so-called Mahaim tachycardia. In Mahaim tachycardia the accessory AV-pathway is formed by atriofascicular accessory fibers, which can sustain exclusively antidromic AV re-entrant tachycardias¹. During Mahaim tachycardia, antegrade conduction occurs over an accessory pathway with AV-node like conduction properties. The proximal insertion of these fibers is localized to the lateral, anterolateral or posterolateral part of the tricuspid annulus; distally the fibers connect to the right ventricular free wall or the right bundle branch^{1,2}. The origin of Mahaim fibers and their functional characteristics (such as AV-node like conduction properties and, as recently reported, spontaneous automaticity³) have not yet been explained. The precursors of the cardiac conduction system have been described as junctional rings of specialized myocardium based on histological criteria⁴. It has been hypothesized that right-sided AV accessory bundles originate from embryologic remnants of the primitive ring of specialized tissue surrounding the orifice of the tricuspid valve during the early stages of the development of the conduction system⁵. This hypothesis was supported by observations in human embryos using the HNK1 marker, which was found in the right, but not in the left, AV-ring⁶. However, these findings cannot explain the occurrence of Mahaim re-entrant tachycardias.

Several transgenic mouse models have been used to study the developing cardiac conduction system^{7,8}. Results of these studies showed that the area stained by the markers used to delineate the embryonic cardiac conduction system is more extensive than the mature cardiac conduction system. In 2001, Rentschler et al. demonstrated the ability of the *CCS-lacZ* transgenic mouse model to delineate the embryonic and mature cardiac conduction system⁹. In this model not only the atrial, but also the ventricular components of the cardiac conduction system, showed β -galactoside staining. Interestingly, during further study, we found that anatomic regions derived from the developing specialized conduction system correlated with areas prone to arrhythmias later in life¹⁰.

During early embryogenesis, the AV canal is situated entirely above the primitive left ventricle, and a right AV connection has not been achieved yet. We hypothesized that the outcome of the process of outgrowth of the right ventricular inflow tract and the remodeling of the primary fold tissue may provide a developmental basis for the occurrence of functional Mahaim fibers. The development of the right ventricular inflow tract in relation to the developing cardiac conduction system in the *CCS-lacZ* strain of transgenic embryos, was therefore examined. Our analysis of this murine model suggests that Mahaim tachycardias may be explained from a developmental morphological origin

Methods

Morphological Analysis

82 A transgenic strain of *CCS-lacZ* mice was used to investigate the formation of the right ventricular inflow tract in relation to the developing cardiac conduction system. The generation of a stable transgenic line of *CCS-lacZ* reporter mice and staining for β -galactosidase activity has been described⁹. Twenty-three murine embryos ranging from gestational age E 9,5-E 15,5 days post coitum (d.p.c.) were studied (the morning of the vaginal plug was designated as 0.5 d.p.c.). Embryos were fixed at room temperature in 5% phosphate buffered formalin solution and embedded in paraffin. The embryos were then transected transversely (5 μ m) and the sections were washed in phosphate buffered saline. Alternate sections were co-stained with the monoclonal anti-muscle actin α antibody HHF 35 (Dako M635; staining protocol described in¹¹) in order to produce a double staining with the *CCS-lacZ* reporter construct. Slices were counterstained with haematoxylin and examined using light microscopy. Procedures followed were in accordance with institutional guidelines.

The slices were 3-D reconstructed to obtain optimal insight in the distribution of β -galactosidase activity in the myocardium and their relationship to other intracardiac structures. Reconstruction was done using AMIRA™ software (Template Graphics Software, Inc. San Diego, California). AMIRA™ is an advanced software system for 3D visualization, data analysis and geometry reconstruction from microscopic images.

Electrophysiological Measurements

A total of 8 embryo's with a gestational age of 15.5 d.p.c. were used for electrophysiological measurements. Two wild type-Swiss pregnant mice were sacrificed by cervical dislocation, the uterus was removed and placed in a heated 0.9% NaCl solution (37°C). Hearts were dissected from the embryos and a cut was made to isolate the RA to RV continuity over the lateral right atrioventricular junction. The RV section included the apical part of the ventricle with the insertion of the crossing moderator band. This specimen did not contain any parts of the atrioventricular node/bundle tissue, ensuring that possible conduction could only take place by way of a myocardial connection over the right atrioventricular junction. The left specimen contained the complete LA and LV but also the atrial septum and the main part of the ventricular septum as well as both great arteries. The atrioventricular node, bundle of His and right and left bundle branches were also part of this specimen. Both preparations were simultaneously placed in the same tissue bath containing heated (± 30 -32°C) oxygenated (95% O₂ and 5% CO₂) Tyrode's solution containing Na⁺ 150, K⁺ 5.6, Ca²⁺ 1.5, Mg²⁺ 0.6, H₂PO₄⁻ 1.2, Cl⁻ 132,4, SO₄²⁻ 0.6, HCO₃⁻ 25, glucose 5 and pyruvate 5 mmol/l. A fixed reference electrode was placed in the tissue bath and simultaneous electrogram recordings from the right and left atrial and ventricular surfaces were performed by metal unipolar microelectrodes (TM33BKT 1-2M Ω , World Precision

Instruments, Inc. Sarasota, FL, U.S.A.). Electrodes were positioned at the free wall of each cardiac chamber assuring no contact with the AV-ring. Signals were fed into an amplifier (ISO-DAM8A, World Precision Instruments, Inc, Sarasota, FL, U.S.A.), filtered (typically between 1 and 500Hz) and written on paper with a speed of 25-100mm/s (Graphtec MARK 12 DMS 1000, Western Graphtec, Irvine, CA, USA). If no spontaneous activity was present, preparations were stimulated in the atrium and/or ventricle using a monophasic stimulus, with a width of 2ms and a strength of 2 times the diastolic threshold. The experiments were performed under a microscope allowing visual confirmation between electrical and mechanical activity (contraction) of atria and ventricles.

Results

Morphological data

E 9,5 and E 10,5

In the earliest stages studied, cardiac septation has not yet commenced. The atrial myocardium is continuous with the myocardium of the ventricles via the atrioventricular canal. At these early unseptated stages, the AV-canal is still situated above the primitive left ventricle and the outflow tract is situated above the primitive right ventricle. A ring of *CCS-lacZ* positive myocardium surrounding the entire AV-canal is present. In the inner curvature of

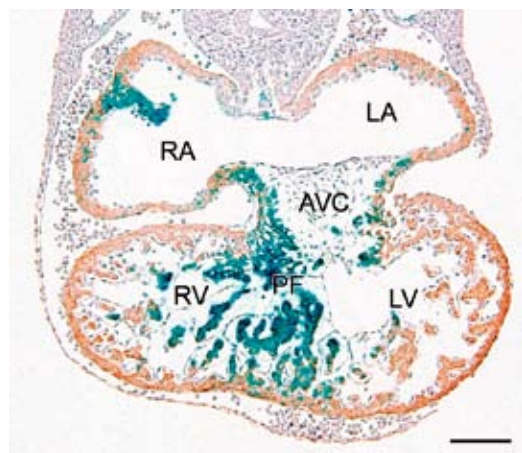


Figure 1

Transverse section of an embryo at embryological day 10.5. At this early unseptated stage there is myocardial continuity at the AV canal (AVC). The AV canal is still situated above the left part of the primitive ventricle. The *CCS-lacZ* positive myocardium lining the AV canal is continuous with the primary fold (PF) at the inner curvature of the heart. HNF35 staining. Bar is 100 μ m. LA: primitive left atrium, LV: primitive left ventricle, RA: primitive right atrium, RV: primitive right ventricle.

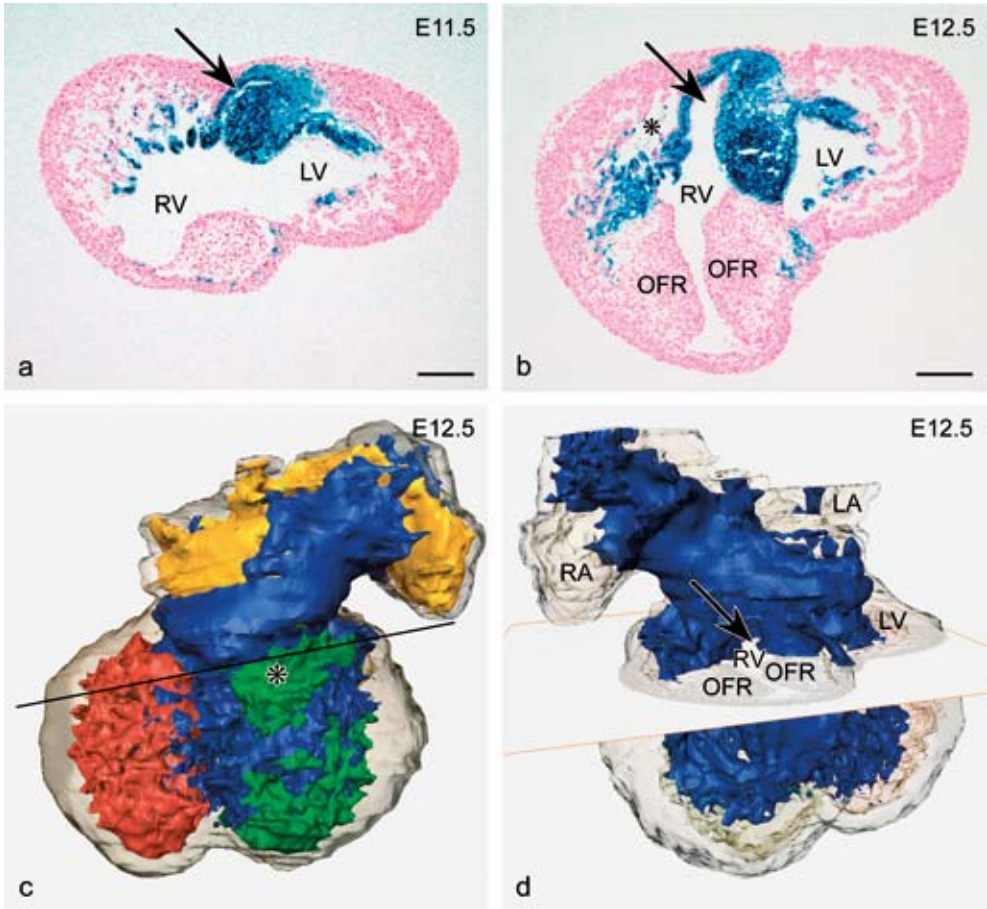
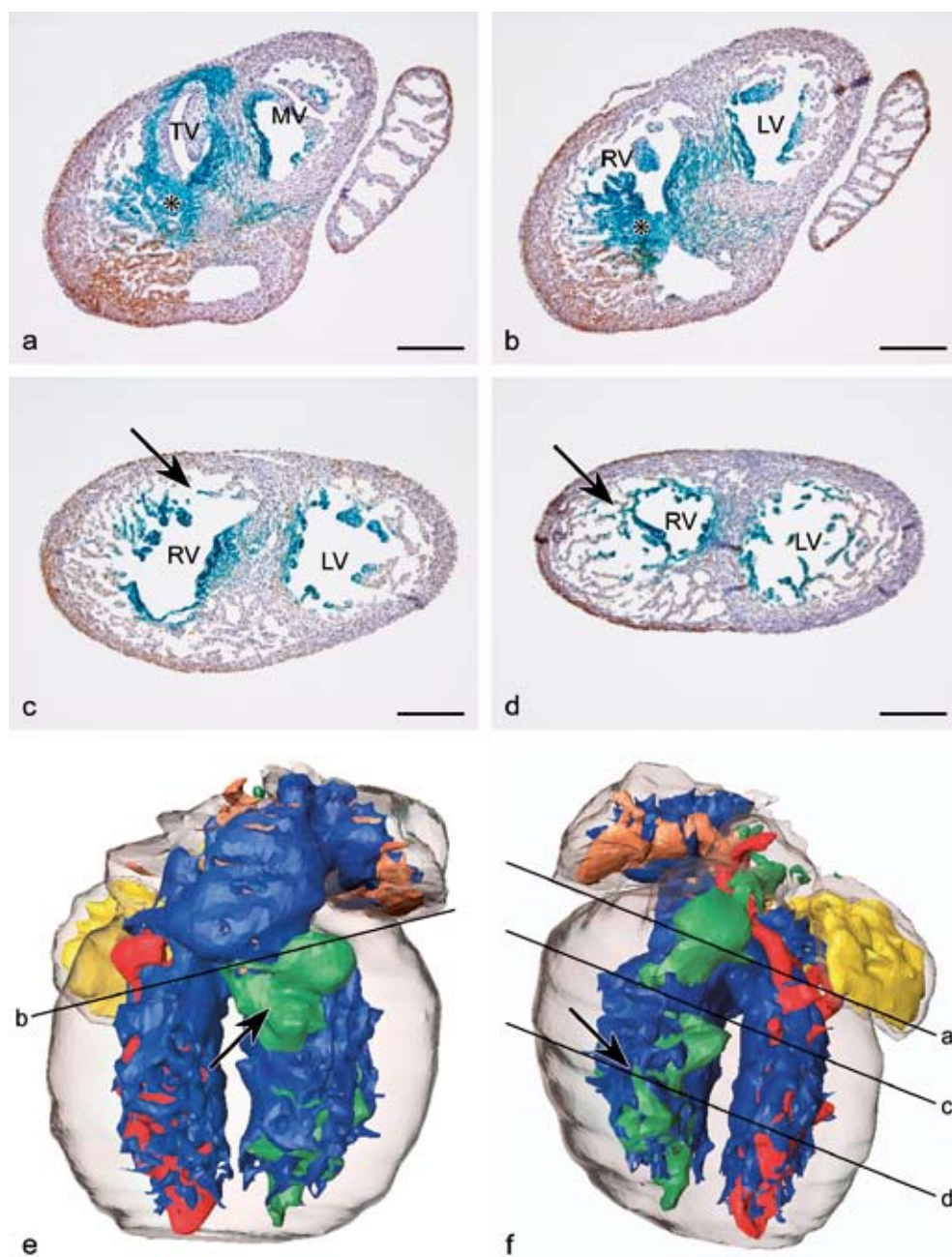


Figure 2

Transverse sections from an E 11.5 embryo (a) and an E 12.5 embryo (b-d). (a) A myocardial groove precedes the formation of the right ventricular inflow tract. This groove is embedded in the tissue of the primary fold (arrow). (b) At stage E 12.5 the groove has widened (arrow). Haematoxylin staining. Bar is 100 μ m. (c) 3-D reconstruction of sections of the E12.5 embryo, dorsal view. The different cardiac compartments are color-encoded. The lumina of the right and left atrium are represented by orange and yellow respectively, the lumina of the right and left ventricle are depicted in green and red respectively. Blue depicts the areas positive for β -galactosidase staining. The level of section b is indicated by the black bar. The asterisk corresponds to the asterisk in the dorsal wall of the section demonstrated in b. (d) Level of the section demonstrated in figure 3b, frontal view, demonstrating the myocardial groove (arrow). The myocardium and lumina have been made transparent, thus demonstrating only *CCS-lacZ* expression. LA: left atrium, LV: left ventricle, OFR: outflow tract ridges, RA: right atrium, RV: right ventricle.

Figure 3

Transverse sections and 3-D reconstructions of an E14.5 embryo. (a and b (20 μ m lower than a)) *CCS-lacZ* expression is present surrounding both the tricuspid valve (TV) and mitral valve (MV). On the right side, expression becomes continuous with *lacZ* staining in the right ventricle (asterisks). (c) Due to outgrowth of the right ventricular inflow tract, a *CCS-lacZ* negative area of compact myocardium can be observed at the posterior wall of the right ventricle (arrow). (d) Division of the primary fold tissue has resulted in formation of the moderator band (arrow), that crosses the right ventricle (arrow) and becomes continuous with the right AV ring. HHF35



and haematoxylin staining. Bar is 200 μm . (e) 3-D reconstruction of sections of the same embryo, dorsal view. The posterior area, caudal of the tricuspid valve consists of compact CCS-*lacZ* negative myocardium, as is indicated by the lack of blue staining at this side (arrow). The different cardiac compartments are color-coded as described in the legend of Figure 3. (f) 3-D reconstruction of sections of the same embryo, frontal view. The moderator band is indicated by the arrow. Levels of sections of a-d are indicated by black bars in e and f. Color-codes as described in the legend of Figure 3. LV: left ventricle, RV: right ventricle.

the heart, this ring of tissue connects to another *lacZ* positive ring, the primary fold, as is demonstrated in **Figure 1**. The primary fold demarcates the border between the ventricular inlet segment of the heart, the primitive left ventricle and the ventricular outlet segment of the heart, the primitive right ventricle.

E 11.5 and 12.5

At stage E 11.5, atrial and ventricular septation have been initiated, but not completed. The ventricles connect through the primary interventricular foramen. As in the previous stages, the myocardium surrounding the AV-canal stains positive for *CCS-lacZ* and there is continuity of the atrial myocardium with the ventricular myocardium via the AV-canal. The AV canal is still situated mainly above the primitive left ventricle and connects at the inner curvature to the *CCS-lacZ* positive tissue of the primary fold. However, at stage 11.5 a myocardial groove towards the right ventricle is formed. This groove, which precedes the formation of the tricuspid valve, is embedded in the *CCS-lacZ* positive tissue of the primary fold, as demonstrated in **Figure 2a** (arrow). At stage E 12.5 the groove has widened, leading into the primitive right ventricle, as demonstrated in **Figure 2b** (arrow). **Figure 2c** shows a dorsal view of a 3-D reconstruction of the same E 12.5 embryo. **Figure 2d** demonstrates the level of section of **Figure 2b** on a ventral view of the 3-D reconstruction, in which the *CCS-lacZ* negative structures have been rendered transparent, demonstrating the myocardial groove in the *CCS-lacZ* positive myocardium.

E 13.5 and 14.5

Septation has progressed and at stage 14.5 ventricular septation has been completed. At these stages atrioventricular valves can be distinguished. The *CCS-lacZ* positive atrioventricular ring bundle remains visible in these stages and surrounds both the tricuspid and mitral valves (**Figure 3a**). On the right side, *CCS-lacZ* positive tissue of the AV ring becomes continuous with *lacZ* staining in the right ventricle (**Figure 3b**). The atrioventricular sulcus tissue has not fused with the atrioventricular cushion tissue yet and therefore no fibrous tissue is present in the primitive AV-canal. Consequently, the atrial myocardium is still continuous with the ventricular myocardium at this stage.

The right ventricular inflow tract has further expanded at these stages, as is demonstrated by the outgrowth of myocardium in the right ventricular dorsal wall. This has resulted in a shift of the right side of the AV canal, to become positioned above the primitive right ventricle. The newly formed myocardium of the right ventricular inflow tract, which is wedged in between the tissue of the primary fold, does not express *CCS-lacZ* (**Figure 3c** and **3e**, arrows). This outgrowth of the right ventricular inflow tract results in a division of the primary fold tissue into two branches. Thus the primary fold is now divided into a septal part, the trabecula septomarginalis, and a lateral part, the moderator band, that transverses the lumen of the right ventricle, as is demonstrated in **Figure 3d** and **3f** and **Figure 4** for stage E 14.5 and E 13.5, respectively. The trabecula septomarginalis, which

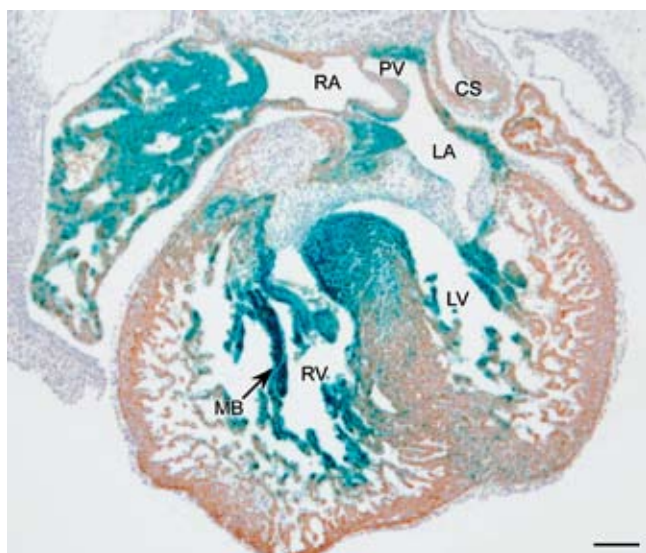


Figure 4

E 13.5. At stage 13.5 the right ventricular inlet tract has further developed by expansion of the myocardium in the posterior part of the inner curvature. This addition of myocardium has resulted in a division of primary fold tissue. The lateral part of the primary fold tissue is formed by the moderator band (MB, arrow). HHF-35 staining. Bar is 200 μ m. CS: coronary sinus, LA: left atrium, LV: left ventricle, PV: pulmonary vein, RA: right atrium, RV: right ventricle.

contains the right bundle branch, represents the border between the inlet septum and the trabeculated septum of the muscular ventricular septum. The trabecula septomarginalis is connected to the moderator band, which runs via the apex of the right ventricle up to the right ventricular lateral wall and, more cranially, to the right side of the AVRB (**Figure 3b, d, f, 4**: see arrows).

E 15.5

At stage E15.5, CCS-*lacZ* positive myocardium, although less marked than in previous stages, can still be distinguished at the AV junction. Strands of fibrous tissue are now observed at the AV junction, but myocardial continuity between atria and ventricles is still present, as demonstrated by the presence of CCS-*lacZ* positive myocardium at the AV junction (data not shown).

As in the previous stages, the right ventricular moderator band can be distinguished as a *lacZ* positive structure connecting via the apex of the right ventricle to the right part of the AV junction. The right ventricular inflow tract is still recognizable as *lacZ* negative myocardium in the right ventricular dorsal wall. Thus at this stage, a *lacZ* positive connection between atrial and ventricular tissue, other than the AV node connection, is still present.

Electrophysiological Measurements

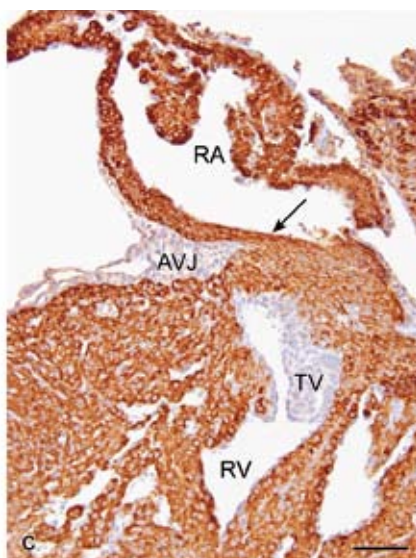
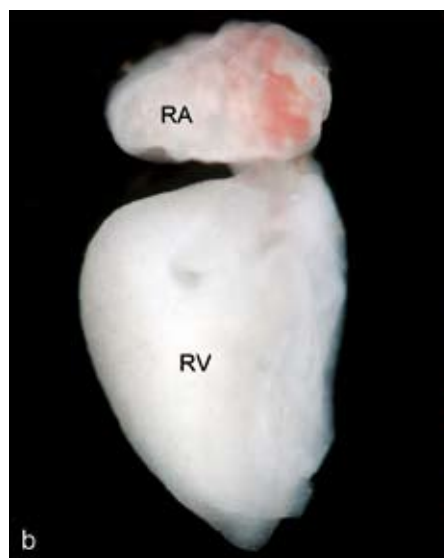
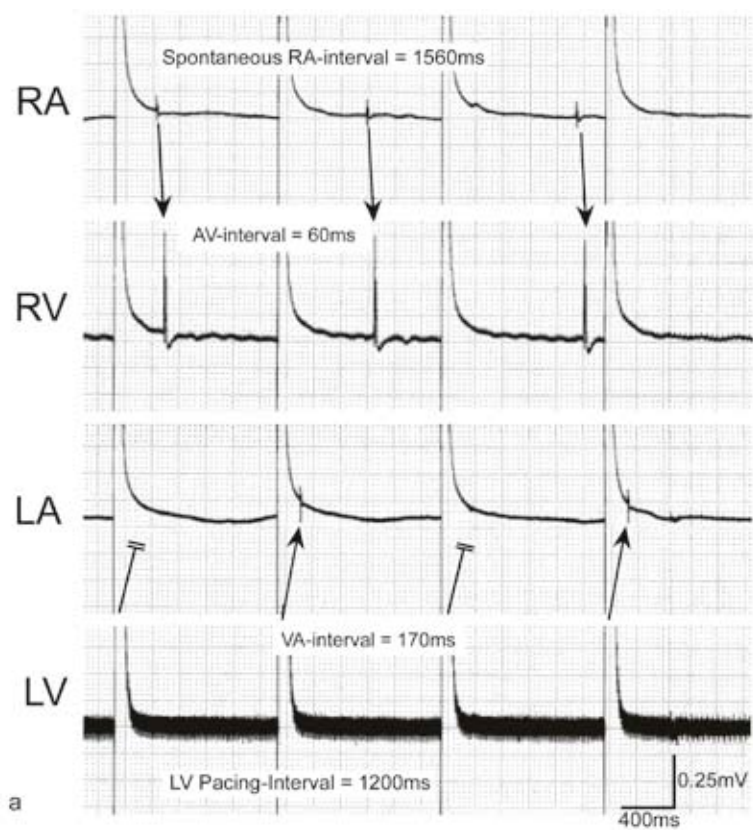
88

As mentioned, by cutting the heart we aimed to include the AV-node in the LA/LV preparation and the apical part of the ventricular septum (containing the insertion of the moderator band) in the RA/RV preparation. In the first 5 preparations only an electrical connection between the LA/LV was present. By including increasingly more of the apical septum in the RA/RV preparation, the preparation from the 6th embryo showed only an electrical connection between the RA and RV chambers and not between the LA and LV. However, in preparations from the 7th and 8th embryo's a sequential electrical and mechanical activation of atria and ventricles was observed in both RA/RV and LA/LV preparations. As can be seen from **Figure 5** (embryo #8) slow but spontaneous and sequential activity was present in the RA and RV (**Figure 5a**). Although no spontaneous activity was present in the LA/LV preparation, pacing the LV clearly resulted in retrograde 2:1 conduction (1:1 LV capture was visually confirmed by contraction of the LV). **Figure 5b** and **5c** show the whole mount (b) and the section (c) of the same embryo #8 as in **Figure 5a**. The specimen was cut as described in the Methods section, demonstrating that the isolated RA and RV were only myocardially connected at the lateral AV-junction. Study of sections of both the LA/LV specimen and the RA/RV specimen showed that fibrous tissue was starting to dissociate the atria from the ventricles (not shown). In the RA/RV specimen depicted, the myocardial connection was only clearly discernable over a distance of 9 sections (45 μm). This implicates that conduction of the electrical impulse could only have travelled over this connection, along the free wall of the RA to the RV.

Figure 5

Four tracings showing simultaneously recorded electrograms from the isolated RA/ RV and the LA/LV preparations (embryo #8) (a). As can be seen in the upper two panels spontaneous and slow activity (cycle length 1560ms) was present in the RA 60ms later followed by RV activation. Although no spontaneous activity was present in the LA/LV preparation (lower two tracings), pacing the LV at a rate of 50 beats per minute (interval 1200 ms) resulted in 2:1 retrograde conduction and activation of the LA (1:1 ventricular capture was visually confirmed by contraction of the LV).

(b) The RA-RV preparation (same embryo as in panel a) showing that the isolated RA and RV were only myocardially connected at the free wall. c. Longitudinal section of the specimen depicted in (b) stained with anti-muscle actin (HHF35) showing myocardial connection of the RA to the RV (arrow). This implicates that AV conduction as illustrated in panel (a) can only have occurred across the free wall of the RA to the RV. Bar is 100 μm . AVJ: atrioventricular junction, LA: left atrium, LV: left ventricle, RA: right atrium, RV: right ventricle, TV tricuspid valve.



Discussion

90

It is well established that AV-accessory pathways can be composed of abnormal fibers, which bypass the insulating AV groove. Furthermore, histological studies have demonstrated that atrioventricular connections can be composed of specialised myocardium¹². Electrophysiological studies demonstrated that atriofascicular fibers as present in patients with Mahaim tachycardias display properties very similar to that of the AV node¹³ and the presence of AV-node like cells in Mahaim pathways has been reported¹⁴. **Figure 6a** demonstrates a schematic drawing of the cardiac conduction system with a Mahaim fiber. **Figures 6b-c** show surface ECG and intracardiac recordings in a patient with Mahaim tachycardia. The potential presence of AV-nodal-like cells in these pathways is supported by the occurrence of spontaneous automaticity in Mahaim fibers, as reported recently³. However, the mechanism whereby nodal cells, possibly underlying the frequency dependent propagation of these tracts, may be present at this site, remains unclear. In the current study, we examined the developing cardiac conduction system in the *CCS-lacZ* mouse, in order to provide a possible explanation for the occurrence of functional atriofascicular bypass tracts causing Mahaim AV-re-entrant tachycardias. Mahaim-fibers, mostly atriofascicular fibers, connect proximally to the lateral right atrium or right AV junction and insert distally in the right bundle branch or right ventricular free wall¹¹⁵. As mentioned above, the conduction properties of these fibers have been attributed to AV-node-like specific conduction tissue in the proximal part of these fibers, while the distal part inserts in the right bundle branch⁵¹⁵. Thus far, no developmental model of the cardiac conduction system has been able to demonstrate the presence of a connection of the right bundle branch with the right AV ring. The explanation of the presence of a *lacZ* positive moderator band as a primary fold derived structure requires understanding of formation of the right ventricular inflow tract. In early embryological stages the primary fold delineates the border between the primitive left and right ventricle. During outgrowth of the right ventricle the primary fold follows a process of division and growth (summarized in¹⁶). Newly formed, *CCS-lacZ* negative, myocardium will form the dorsal inflow portion of the right ventricle, laterally demarcated by the moderator band. Medially, the inflow septum and the crista supraventricularis of the muscular ventricular septum are derived from the primary fold, with the trabecula septomarginalis (which contains the right bundle branch) as a border structure between the inlet septum and the trabeculated part of the muscular septum. In the current study, the *CCS-lacZ* positive right ventricular moderator band could be traced from the trabecula septomarginalis via the apex of the right ventricle all the way up to the lateral wall of the right ventricle. This band connected with the right atrioventricular ring, thus providing a direct connection with the right ventricular apex, supplying a potential pathway for re-entry, as seen in Mahaim tachycardia. These data are supported by observations in the *MinK-lacZ* knockout murine embryo⁷. The formation of the right ventricular

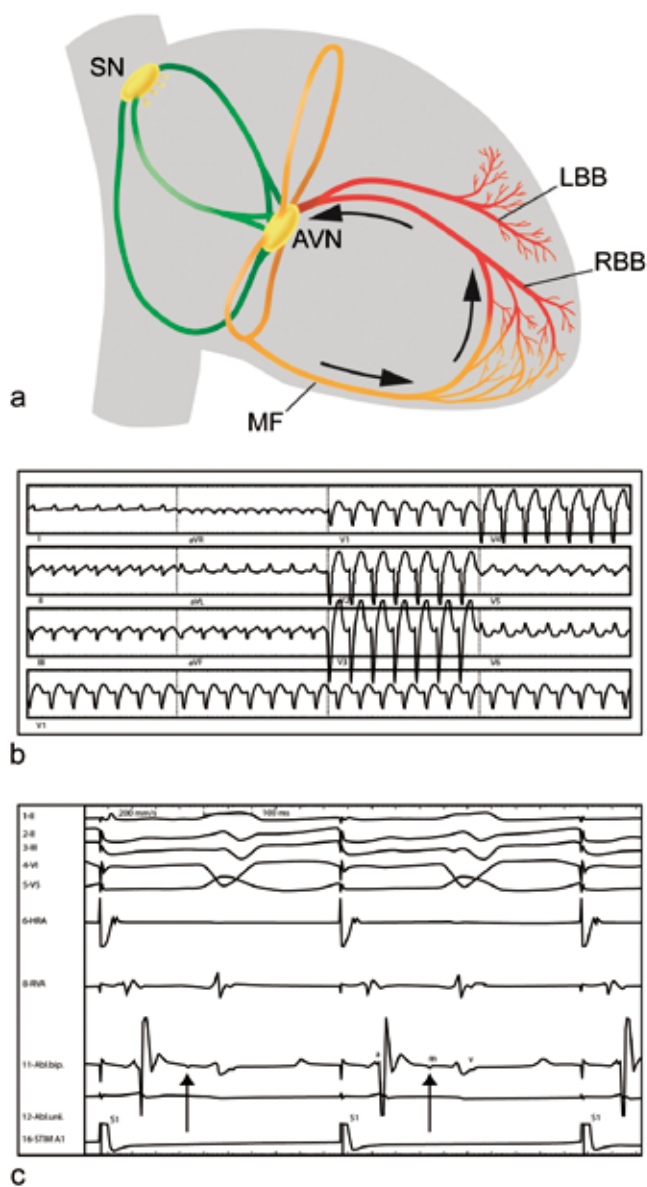


Figure 6
 (a) Mahaim fibers (MF) consist of atriofascicular fibers, which can possess AV-node like conduction properties. The proximal insertion of these fibers is localized to the lateral, anterolateral or posterolateral part of the tricuspid annulus; distal insertion is to the right ventricular free wall or the right bundle branch (RBB). The arrows indicate the direction of conduction over the Mahaim fiber.
 (b) Surface ECG during Mahaim tachycardia, showing an antidromic tachycardia.
 (c) Intracardiac recordings during rapid atrial pacing. Arrows point at the Mahaim-potential. a: atrial signal, m; Mahaim potential, v; ventricular signal.
 AVN: atrioventricular node, LBB, left bundle branch, SN: sinus node.

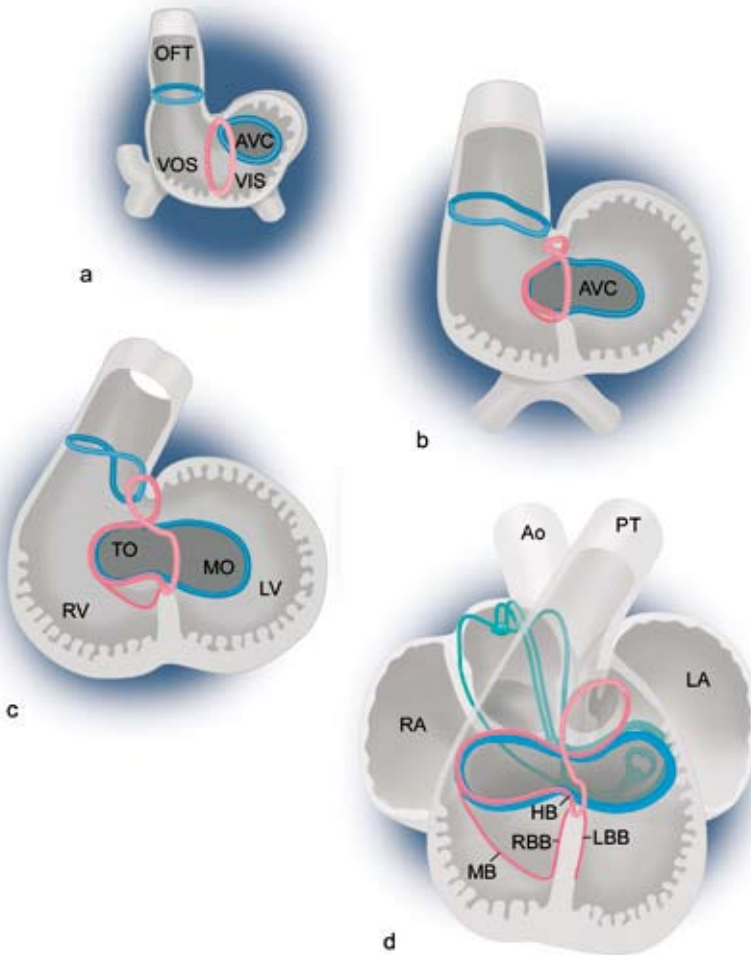


Figure 7

Schematic summary of the process of formation of the right ventricular inflow tract and remodeling of the primary ring in sequential stages of development. (a) Unseptated heart. The primary fold is depicted by the pink ring of tissue at the border between ventricular inlet segment (VIS) and the ventricular outlet segment (VOS) of the heart. The CCS-*lacZ* positive myocardium of the AV canal (AVC) is depicted by the blue ring. Both rings connect at the inner curvature of the heart. (b) The first sign of the formation of a right AV connection is observed as the formation of a slit-like myocardial groove in the CCS-*lacZ* positive tissue of the primary fold. (c) During further outgrowth of the right ventricular inflow tract, the tissue of the primary fold is pulled towards the AV junction and surrounds the right part of the AV canal. The rapid outgrowth of the right ventricular inflow tract results in a division of the primary fold tissue. (d) The addition of newly formed, CCS-*lacZ* negative myocardium to the right ventricular inflow tract, which is wedged in between the CCS-*lacZ* positive tissue of the primary fold, results in further division of the primary fold tissue. The primary fold now consists of a medial part, the trabecula septomarginalis, and a lateral part, the moderator band (MB). The outgrowth of the right ventricular inflow tracts further pulls the primary fold tissue around the right side of the AV canal. The moderator band connects medially to the trabecula septomarginalis, which contains the right bundle branch (RBB). Laterally, the moderator band runs via the apex and then the lateral wall of the right ventricle (RV) up to connect to the right side of the AVRB.

Ao: aorta, HB: His bundle, LA: left atrium, LBB: left bundle branch, LV: left ventricle, MO: mitral orifice, OFT: outflow tract, PT: pulmonary trunk, RA: right atrium, TO: tricuspid orifice.

moderator band in relation to the development of the right ventricular inflow tract and the cardiac conduction system is summarized schematically in **Figure 7**.

In order to electrically insulate the atria from the ventricles, continuity of the annulus fibrosus is important. In the stages we examined, the development of the fibrous skeleton of the atrioventricular junction had not been completed. However, a mature electrical activation pattern, with a delay between the atrial and ventricular signal on the ECG, is already present around the time that ventricular septation is completed. This suggests that there is already a functional insulation between atria and ventricles¹⁷, which was confirmed in 6 out of 8 embryo's showing AV-conduction in only one of the RA/RV or LA/LV preparations. However, in the other 2 embryo's conduction from the atrium to the ventricle and/or vice versa could be demonstrated in both RA/RV and LA/LV preparations indicating that next to conduction over the AV-node a second functional AV-connection was present. Although we did not perform high resolution mapping to show that conduction indeed occurred over the lateral AV ring and the moderator band to the right bundle branch, the data presented in **Figure 5** indicate that, at this developmental stage, a functional accessory connection running from the right atrial free wall to the right ventricle was present. Interestingly, the location of this accessory connection is similar to the most common location of a so called Mahaim fiber in patients. The existence of accessory AV-bundles with conductive capacities bypassing the insulating annulus, may produce re-entrant tachycardias, as is the case in the WPW-syndrome. It has been suggested that remnants of embryonic atrial conduction tissue may serve as AV- bypass tracts⁵. Using the epitope HNK1, the presence of a right, but not a left, AV ring was demonstrated in human embryos^{6;18}. In the CCS-*lacZ* reporter mouse, both the right and the left AV ring demonstrate β -galactosidase staining. It has been reported that AV junctional cells surrounding both the tricuspid and mitral annuli resemble nodal cells in their cellular electrophysiology¹⁹. Interestingly, recent reports also describe the occurrence of atrial tachycardia originating from the mitral and tricuspid annulus^{20 21}.

The exact mechanism of why Mahaim tracts may become or remain functional is not clear. Several mechanisms can be hypothesized to be responsible for the occurrence of functional accessory pathways, such as failure of regression of embryonic conduction tissue, failure of apoptosis or re-expression of the embryonic phenotype. Indeed, several studies have reported the occurrence of specialized tissue in bypass tracts and demonstrated the presence of myocardial cells running through the fibrous insulating AV tissue^{12 22}. The frequent occurrence of Mahaim tachycardia and WPW-syndrome in patients with Ebstein's anomaly¹, may relate to the persistence of embryological functional bypass tracts during an abnormal development of the right AV junction, or renewed differentiation of cardiomyocytes at these sites, as described in the WPW-model of Patel et al.²³. Apoptosis, which under normal circumstances occurs postnatally in the right ventricle, may play a crucial role in peri/postnatal morphogenesis²⁴. Apoptosis can also involve the human cardiac conduction system and failure of apoptotic morphogenesis may result in the persistence

of embryonic conduction tissue^{25,26}. The role of genetic re-expression (a well known-mechanism in the genesis of hypertrophic cardiomyopathy²⁷), or activation of the embryonic gene program in the persistence of expression of these functional bypass tracts warrants further investigation.

Acknowledgements

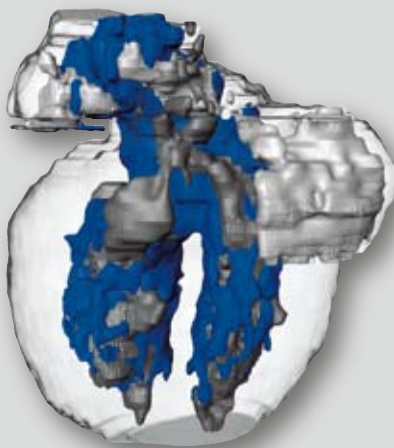
This work was supported by HL64757 (G.I.F.) from the National Institutes of Health and a Burroughs Wellcome Fund Clinical Scientist Award in Translational Research (G.I.F.)¹.

94

Reference List

1. Aliot E, de Chillou C, Revault dG, Mabo P, Sadoul N. Mahaim tachycardias. *Eur.Heart J.* 1998;**19** Suppl E:E25-3.
2. Pinski SL. The right ventricular tachycardias. *J.Electrocardiol.* 2000;**33** Suppl:103-14.
3. Sternick EB, Sosa EA, Timmermans C, Filho FE, Rodriguez LM, Gerken LM *et al.* Automaticity in Mahaim Fibers. *J.Cardiovasc.Electrophysiol.* 2004;**15**:738-44.
4. Wenink AC. Development of the human cardiac conduction system. *J.Anat.* 1976;**121**:617-31.
5. Anderson RH, Ho SY. Anatomy of the atrioventricular junctions with regard to ventricular preexcitation. *Pacing Clin.Electrophysiol.* 1997;**20**:2072-6.
6. Blom NA, Gittenberger-De Groot AC, DeRuiter MC, Poelmann RE, Mentink MM, Ottenkamp J. Development of the cardiac conduction tissue in human embryos using HNK- 1 antigen expression: possible relevance for understanding of abnormal atrial automaticity. *Circulation* 1999;**99**:800-6.
7. Kondo RP, Anderson RH, Kupershmidt S, Roden DM, Evans SM. Development of the cardiac conduction system as delineated by minK-lacZ. *J.Cardiovasc.Electrophysiol.* 2003;**14**:383-91.
8. Wessels A, Phelps A, Trusk T.C., Davis D.L., Edwards A.V., Burch J.B.E. *et al.* Mouse Models for Cardiac Conduction Development. In: Chadwick D.J., Good J, eds. *Development of the Cardiac Conduction System.* Chichester: Wiley J & Sons Ltd, 2003:**44**-59.
9. Rentschler S, Vaidya DM, Tamaddon H, Degenhardt K, Sassoon D, Morley GE *et al.* Visualization and functional characterization of the developing murine cardiac conduction system. *Development* 2001;**128**:1785-92.
10. Jongbloed MR, Schalij MJ, Poelmann RE, Blom NA, Fekkes ML, Wang Z *et al.* Embryonic Conduction Tissue. *J.Cardiovasc.Electrophysiol.* 2004;**15**:349-55.
11. Bartram U, Molin DG, Wisse LJ, Mohamad A, Sanford LP, Doetschman T *et al.* Double-outlet right ventricle and overriding tricuspid valve reflect disturbances of looping, myocardialization, endocardial cushion differentiation, and apoptosis in TGF-beta(2)-knockout mice. *Circulation* 2001;**103**:2745-52.
12. Becker AE, Anderson RH, Durrer D, Wellens HJ. The anatomical substrates of wolff-parkinson-white syndrome. A clinicopathologic correlation in seven patients. *Circulation* 1978;**57**:870-9.
13. Lee PC, Kanter R, Gomez-Marin O, Wolff GS, Young ML. Quantitative assessment of the recovery property of atriofascicular/atrioventricular-type Mahaim fiber. *J.Cardiovasc.Electrophysiol.* 2002;**13**:535-41.
14. Guiraudon CM, Guiraudon GM, Klein GJ. "Nodal Ventricular" Mahaim Pathway: Histologic Evidence for an Accessory Atrioventricular Pathway With AV Node-Like Morphology (abstract). *Circulation* 1988;**78**, supplement II:40.
15. Sternick EB, Gerken LM, Vrandecic M. Appraisal of "Mahaim" automatic tachycardia. *J.Cardiovasc. Electrophysiol.* 2002;**13**:244-9.
16. Gittenberger-De Groot AC, DeRuiter MC, Bartelings MM, Poelmann RE. Embryology of congenital heart disease. In: Crawford MH, DiMarco JP, Paulus WJ, eds. *Cardiology.* Richard Furn, 2004:1217-27.

17. Pennisi DJ, Rentschler S, Gourdie RG, Fishman GI, Mikawa T. Induction and patterning of the cardiac conduction system. *Int.J.Dev.Biol.* 2002;**46**:765-75.
18. Wessels A, Vermeulen JL, Verbeek FJ, Viragh S, Kalman F, Lamers WH *et al.* Spatial distribution of “tissue-specific” antigens in the developing human heart and skeletal muscle. III. An immunohistochemical analysis of the distribution of the neural tissue antigen G1N2 in the embryonic heart; implications for the development of the atrioventricular conduction system. *Anat.Rec.* 1992;**232**:97-111.
19. McGuire MA, De Bakker JM, Vermeulen JT, Moorman AF, Loh P, Thibault B *et al.* Atrioventricular junctional tissue. Discrepancy between histological and electrophysiological characteristics. *Circulation* 1996;**94**:571-7.
20. Kistler PM, Sanders P, Hussin A, Morton JB, Vohra JK, Sparks PB *et al.* Focal atrial tachycardia arising from the mitral annulus: electrocardiographic and electrophysiologic characterization. *J.Am.Coll.Cardiol.* 2003;**41**:2212-9.
21. Morton JB, Sanders P, Das A, Vohra JK, Sparks PB, Kalman JM. Focal atrial tachycardia arising from the tricuspid annulus: electrophysiologic and electrocardiographic characteristics. *J.Cardiovasc.Electrophysiol.* 2001;**12**:653-9.
22. Peters NS, Rowland E, Bennett JG, Green CR, Anderson RH, Severs NJ. The Wolff-Parkinson-White syndrome: the cellular substrate for conduction in the accessory atrioventricular pathway. *Eur.Heart J.* 1994;**15**:981-7.
23. Patel VV, Arad M, Moskowitz IP, Maguire CT, Branco D, Seidman JG *et al.* Electrophysiologic characterization and postnatal development of ventricular pre-excitation in a mouse model of cardiac hypertrophy and Wolff-Parkinson-White syndrome. *J.Am.Coll.Cardiol.* 2003;**42**:942-51.
24. James TN. Apoptosis in cardiac disease. *Am.J.Med.* 1999;**107**:606-20.
25. James TN. Normal and abnormal consequences of apoptosis in the human heart. From postnatal morphogenesis to paroxysmal arrhythmias. *Circulation* 1994;**90**:556-73.
26. Brechenmacher C, Fauchier JP, James TN. Persistent fetal dispersion of the atrioventricular node. Association with the Wolff-Parkinson-White syndrome. *Arch.Intern.Med.* 1980;**140**:377-82.
27. Durand JB. Genetic basis of cardiomyopathy. *Curr.Opin.Cardiol.* 1999;**14**:225-9.



Chapter

4

Yvonne L. Douglas^{1,3*}

Monique R.M. Jongbloed^{2,3*}

Adriana C. Gittenberger-de Groot³

Dorothea Evers³

Robert A.E. Dion⁴

Pieter Voigt⁴

Margot M. Bartelings³

Martin J. Schalij²

Tjark Ebels¹

Marco C. DeRuiter³

** Both authors contributed equally*

Depts of ¹Cardio-thoracic Surgery, University Medical Center Groningen, University of Groningen, ²Cardiology, ³Anatomy and Embryology, ⁴Cardio-thoracic Surgery, Leiden University Medical Center, Leiden, The Netherlands.

Histology of Vascular-Myocardial Wall of Left Atrial Body after Pulmonary Venous Incorporation

Modified after
Am J Cardiol. 2006 Mar 1;97(5):662-70

Abstract

98

During embryonic development the common pulmonary vein (PV) becomes incorporated into the left atrium giving rise to separate PV ostia. We describe the consequences of this incorporation process for the histology of the left atrium and the possible clinical implications. The histology of the left atrial (LA) wall in relation to PV incorporation was studied immunohistochemically in 16 human embryos and fetuses, one neonate and 5 adults. The PV wall, surrounded by extrapericardially differentiated myocardial cells, incorporated into the LA body. After incorporation, the composition of PVs and smooth-walled LA body wall was histologically identical. The LA appendage however, consisted of an endocardial and myocardial layer without a vessel wall component. In 2 adults the myocardium in the LA posterior wall was absent. At the transition of the LA body and the LA appendage, a smooth-walled myocardial zone lacking the venous wall was observed. This zone was histologically identical to the sinus venarum of the right atrium. In conclusion, the LA body arises by incorporation and growth of the PVs, presenting with a histologically identical structure of vessel wall covered by extrapericardially differentiated myocardium of the PVs. Discontinuity of myocardium may be the substrate for arrhythmias, whereas absence of myocardium in some individuals makes this area potentially vulnerable to damage inflicted by ablation strategies. A borderzone between the LA body and the LA appendage is hypothesized to be the left part of the embryonic sinus venosus.

Introduction

During development, the common PV becomes myocardialised whereafter it is incorporated into the posterior LA wall giving rise to separate PV orifices¹. The degree of incorporation is variable between individuals and only about 75% to 80% of individuals possess 4 discrete PV orifices^{2,3}. Though the development and incorporation of the PVs has been studied and several histological studies of the left atrium and the PVs have been performed, until now, there are no extensive reports that emphasize the histological result of PV incorporation in the left atrium in subsequent stages in the human. It seems logical to expect characteristic venous wall tissue, consisting of an intima, media with elastin and smooth muscle cells (SMCs) in the LA after the incorporation process, but no histological veno-atrial border has been described in the literature. In the cardiology cathlab this atriovenous border and the structure of the LA and the PV have gained interest in recent years, in relation to the treatment of atrial fibrillation originating from the PV⁴. Ablation strategies, aimed at electrical isolation of the PV from the LA are often targeted at the left atrial tissue just outside the atriovenous junction to avoid the occurrence of PV stenosis by damaging the vulnerable PV vessel wall⁵. The present study investigates the histological outcome of the incorporation process of the PVs in the LA during subsequent stages of development.

Methods

Normal hearts of 16 human embryos and fetuses, 1 neonate and 5 adults were studied. The embryos and fetuses, obtained by legal or spontaneous abortion, ranged from 7 to 22 weeks (crown-rump lengths from 19 to 170 mm). The studies were approved by the local medical-ethical committee. The neonate had died during delivery as a result of asphyxia. Adult hearts were obtained from human bodies used in anatomy teaching lessons. The cause of death was unknown due to privacy regulations. Preservation of the bodies was performed by injection of embalming fluid in the femoral artery, consisting of 36% formaldehyde with a mixture of ethanol, glycerine, phenol, K_2SO_4 , Na_2SO_4 , $NaHCO_3$ and Na_2SO_3 . The fetal and neonatal specimens were fixed in a 4% paraformaldehyde in 0.1M phosphate buffer (pH 7.2).

Samples/sectioning of material. Embryonic hearts were embedded in paraffin and serially sectioned transversely (5-10 μ m). From the neonatal and adult hearts, cross-sectional samples were taken from all PVs, the posterior and anterior LA wall, and the LA appendage. Samples taken from the posterior and anterior right atrial wall and the right atrial appendage served as reference. Samples were embedded in paraffin and sectioned (5 μ m) using a Leica microtome. Sections were mounted onto slides using chicken albumine dissolved in glycerine (1:1) and dried at 37° C for at least 24 hours.

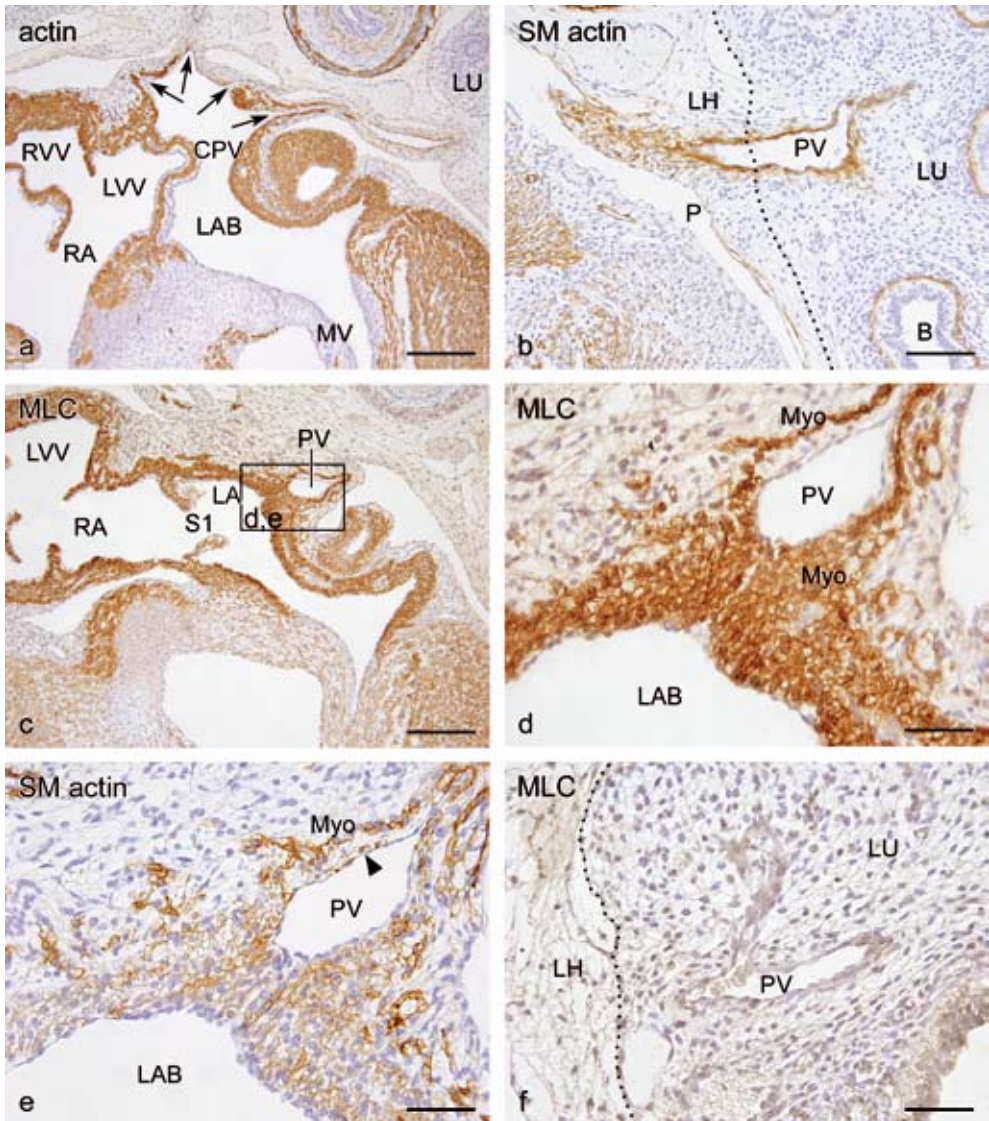


Figure 1

Sections of a 54 days old human embryo stained with HHF35 for muscle actins (**a**; **actin**), alpha-smooth muscle actin (**b,e**; **SM actin**), atrial myosin light chain (**c,d,f**; **MLC**), showing the differentiation of the PVs and their entrance in the left atrial body (**LAB**). **a**. Four pulmonary veins (**arrows**) drain via one common pulmonary vein (**CPV**) into the LAB. The wall of both intra- and extrapulmonary PVs consists of 1-3 layers of SMC (**b**), while an additional layer of actin and MLC positive myocardium (**Myo**) only encircles the extrapulmonary part of the vessel wall (**c-f**). Consecutive sections in **c**, **d** and **e** demonstrate that part of the MLC-positive myocardial cells surrounding the SMC of the PVs (**Myo**) are also 1A4-positive, which is related to early differentiating myocardial cells²¹. Beneath these myocardial cells a real SMC layer develops (**e**; **arrow head**). Bronchus (**B**), Intra/extrapulmonary borderline (.....), lung (**Lu**), left venous valve (**LVV**), lung hilum (**LH**), mitral valve (**MV**), pericardial cavity (**P**), right atrium (**RA**), right venous valve (**RVV**), septum primum (**S1**). Scale bar = 200 μ M in a,c; 100 μ M in b,d-f.

Staining. Standard histological stainings were performed with Haematoxylin-Eosin (HE), Elastic Von Gieson (EvG) or elastic Resorcin-Fuchsin (RF) to detect elastic filaments, and Sirius Red to demonstrate collagen fibers⁶. Furthermore, sections were stained immunohistochemically with the pan-muscle actin antibody HHF35 (1:500, Dako, M0635), to study myocardial structure, 1A4 (1:3000, Sigma Aldrich, Product No. A2547) against alpha-smooth muscle (SM) actin, and an antibody against atrial myosin light chain (MLC2a, 1:2000, a generous gift of Steve Kubalak), specific for atrial myocardium. Staining procedures were performed as described previously^{7,8}.

Results

Embryonic stage: *Seven to 7.5 weeks of gestation, crown-rump length 19 to 24 mm:* Proximal to the heart, 4 PVs drained via a common PV into the smooth-walled segment of the LA (**figure 1a**), also called the LA body, that could already be distinguished from the trabeculated LA appendage. The wall of both the intra- and extrapulmonary parts of the veins consisted of 1-3 layers of alpha-SM actin expressing SMCs around the endothelium (**figure 1b,e**). The extrapulmonary part of the PVs being continuous with the dorsal wall of the LA were encircled by an additional layer of MLC-positive myocardial cells (**figure 1c,d**). In the wall of the intrapulmonary part of the veins myocardial cells were absent (**figure 1f**). The left atrial wall does not express smooth muscle cell actin at this stage.

Fetal stages: *Ten to 22 weeks' gestation, crown-rump length 42 to 170 mm:* As incorporation of the common PV had progressed, in all but 2 fetuses there were 2 separate right pulmonary venous orifices, while 2 left PVs drained via one common left PV into the LA. At 16 weeks, in 2 fetuses (out of 5) four separate PV ostia were observed. From the lung hilum to the heart, the PVs were completely covered by myocardium. Subendothelially, the wall of the PVs consisted of 1-3 layers of SMCs embedded within a collagenous matrix (**figure 2a-c**). This layer extended from the intrapulmonary veins to the smooth-walled LA body (**figure 2d,e**). A thin layer of collagen was also found in the LA appendage, atrial septum and in the complete right atrium, but no SMCs were observed (**figure 2f-k**). The myocardial layer around the PVs had thickened as well as the subendothelial collagenous vessel wall with SMCs in the PVs and the LA body. The presence of vascular SMCs in the heart was restricted to the LA body. At 21 weeks, the first indication of elastic fiber formation was observed within this layer (**figure 2l**).

Neonatal stage: *Pulmonary veins and left atrial body:* As in previous stages there were 2 separate right PV ostia and one common left PV ostium. At the transition of the PV ostia and LA body no histological veno-atrial demarcation was found (**figure 3a,b**). In both the PVs and the LA body the following layers could be distinguished: an inner venous vessel wall with an

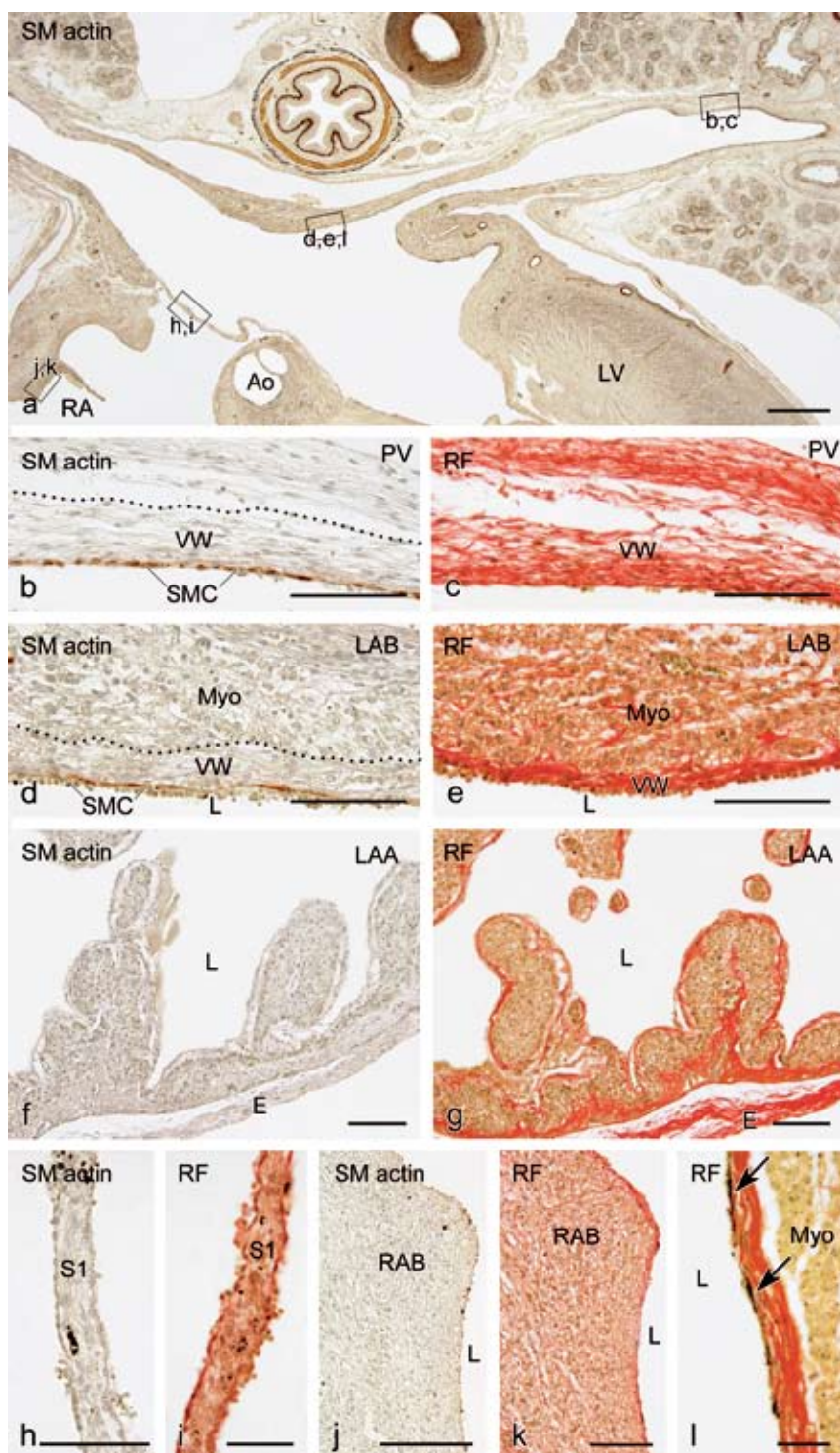


Figure 2

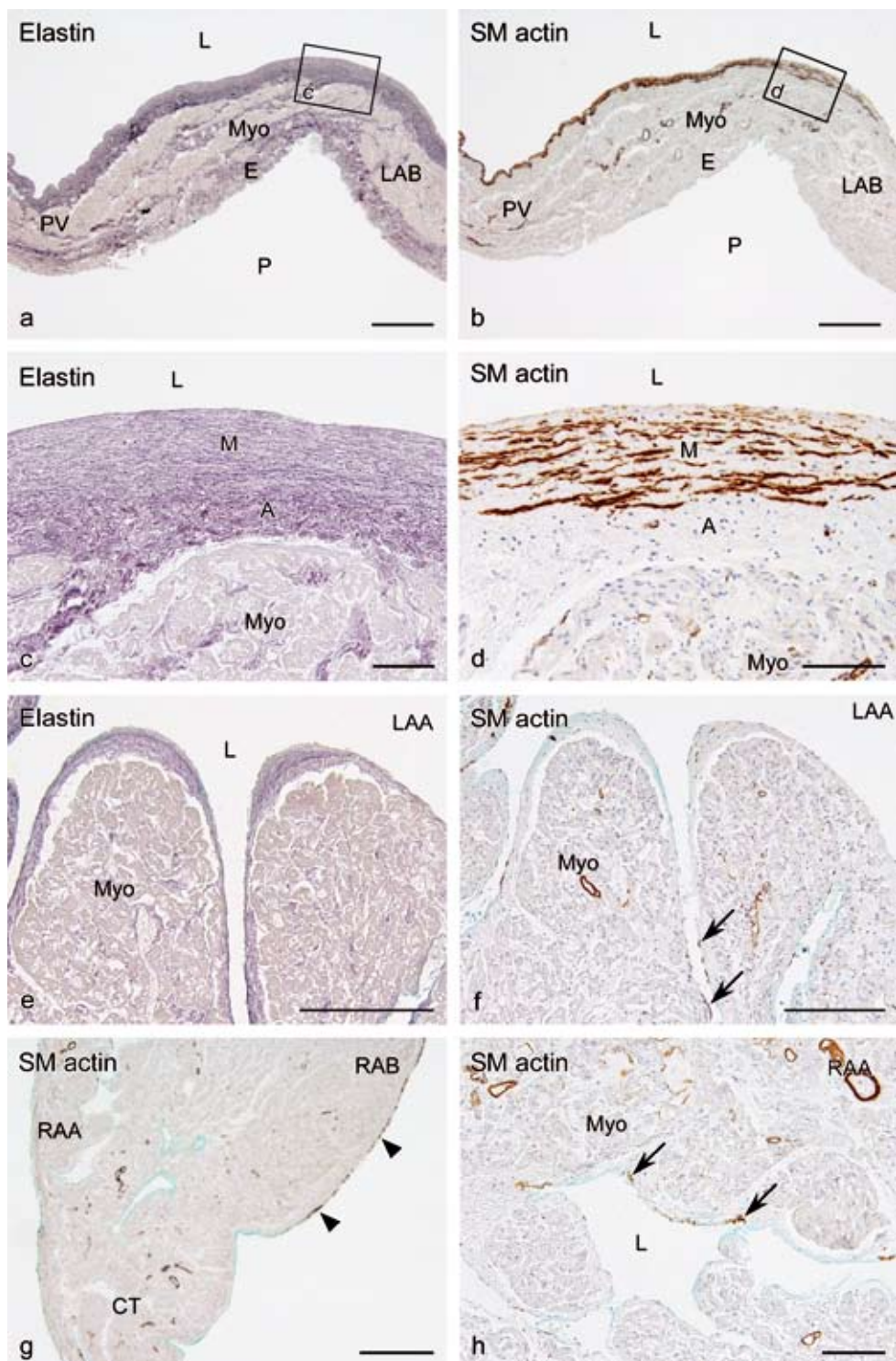
Sections of a 15.5 week old human embryo. Boxes in figure **a** indicate the position of the enlargements in **b-k**. RF-sirius red stained sections in **c, e, g, i, k and l** are adjacent sections of fig **a, b, d, f, h and j**, that are stained for alpha-SM actin. Collagen fibers are red and elastic fibers are black in the RF stained sections. **a-c**. SMC have differentiated within the subendothelial collagenous matrix of the pulmonary vessel wall (**VW**). **d,e**. This differentiating vessel wall extends into the smooth-walled left atrial body (**LAB**). Although the left atrial appendage (**LAA**), the septum primum (**S1**), and the right atrial body (**RAB**) have a thin subendothelial collagen matrix (**g, i, k**) no SMCs are found (**f, h, j**). **l**. At 21 weeks elastin is deposited (**arrows**) in the differentiating venous vessel wall in the LAB. Aorta (**Ao**), epicardium (**E**), external borderline (.....) of the VW, left ventricle (**LV**), lumen (**L**), myocardium (**Myo**). Scale bar = 500 μ M in **a**; 100 μ M in **b-h,k,l**; 50 μ M in **i**; 200 μ M in **j**.

endothelium, several medial layers of SMCs with longitudinally oriented elastic fibers, and an adventitial layer with randomly distributed elastic fibers with fibroblasts and vasa vasorum. These vessel wall structures were covered by a myocardial layer and an epicardium on the outside (**figure 3a-d**).

Left atrial appendage: In the trabeculated LA appendage the inner surface consisted of an endocardium with a thin subendocardial sheet consisting of well-organized collagen and elastic fibers, but without well-organized layers of alpha-SM actin positive cells. Only a few scattered actin positive cells were found. Characteristic vessel wall layers as seen in the body of the atrium, were lacking (**figure 3e,f**). At the outer side, a thick layer of myocardium covered by an epicardium was present.

Right atrium: The right atrial body or sinus venarum consisted of smooth-walled myocardium. The inner side of the wall near the systemic veins consisted of one layer of SMCs. This layer did not represent a proper tunica media as seen in the systemic veins which had a well organised vessel wall with five layers of SMCs. At the junction of the terminal crest with the right atrial body, this smooth muscle layer disappeared (**figure 3g**). Within the trabeculated right atrial appendage, only scattered subendocardial SMCs were observed (**figure 3h**).

Adult stage: Pulmonary veins and left atrial body: The PVs of 4 adult hearts had discrete PV orifices. In one heart a common left PV orifice was still present. In 2 hearts, an early branching pattern of the right inferior PV was observed. The outer side of the wall of the LA body consisted of a non-trabeculated myocardial layer. Around the outside of the PVs this myocardium formed a circular or spirally arranged muscular sleeve. The sleeves tended to be thicker and more complete near the junction with the posterior LA body, but tapered more distally. In the PVs, a characteristic vessel wall was found consisting of an intimal layer and a medial layer with SMCs (**figure 4a**). In the wall of the entire LA body, in addition to the outer myocardial layer, a prominent vessel wall layer being continuous with the PV vessel wall was present (**figure 4b**). In between the media and myocardium an adventitial layer with fibroblasts (not expressing SM actin) was found (**figure 4a,b**). In contrast to the neonatal stage, intimal thickening was observed in the PVs and the LA body, which was most profound in the PVs (**figure 4a,b**). At the entry of the PVs into the LA, no histological



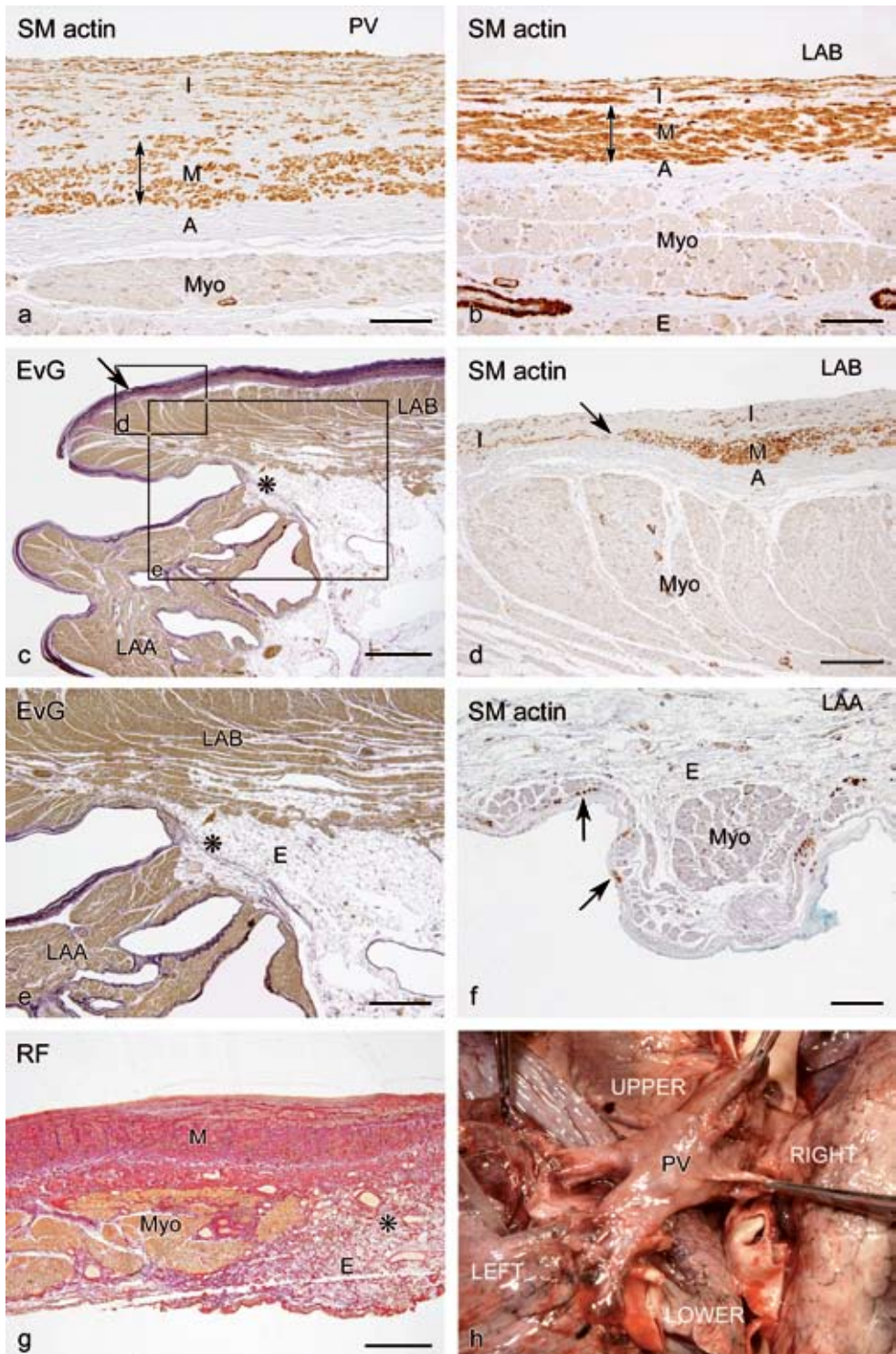
demarcation was found. Interestingly, at the junction of the LA body with the LA appendage, a borderzone with distinctive tissue was identified (**figure 4c-e**). The inner surface of this area lacked trabeculation. In contrast to the remaining part of the LA body and the PVs, the characteristic tunica media was lacking in this borderzone (**figure 4d,e**). Another finding was that the myocardium at the transition of the LA body and the trabeculated LA appendage was either very thin or absent (**figure 4c,e**). Moreover, in 2 of the adult hearts examined, the myocardium covering the LA body in between the confluence of the 4 PVs was discontinuous thus allowing the epicardium to line the vessel wall of the PVs (**figure 4g,h**). These areas of discontinuous myocardium were only several millimeters wide. It should, however, be noted that in these areas (partly) isolated bundles of myocytes were observed.

Atrial appendages: The wall of the trabeculated LA appendage differed from the PVs and LA body in that it did not contain a vessel wall component. The inner surface consisted of a thin subendocardial collagenous layer with some elastic fibers and an occasional SMC (**figure 4f**). The histology of the LA appendage was similar to that of the right atrial appendage (**figure 5a,b**).

Right atrial body: The non-trabeculated sinus venarum of the right atrium consisted at the inside of a thin subendocardial collagenous layer covered by myocardium. No characteristics of vessel wall structures were present at this site (**figure 5c,d**).

Figure 3

Sections of various segments of a human neonatal heart. **a-d** At the transition of the PV and LA body no histological veno-atrial demarcation was found. The wall consisted of an endothelium/endocardium, a medial layer (**M**) with SMCs and elastic fibers, an adventitial layer (**A**) with fibroblasts and elastic fibers, a sheet of myocardium (**Myo**) and an outer epicardium (**E**). **e,f** In the left atrial appendage (**LAA**) no organised vessel wall was present. Only a subendothelial layer of elastin (**e**) and isolated SMCs (**arrows** in **f**) was present. In the right atrium only one layer of SMCs, not characteristic for a tunica media, could be detected in the right atrial body (**arrow heads** in **g**) near the entrance of the caval veins. The histology of the right atrial appendage (**RAA**) is comparable with the LAA with only isolated SMCs (**arrows; h**). Terminal crest (**CT**), Lumen (**L**), pericardial cavity (**P**). Scale bar = 500 μ M in a,b,g; 100 μ M in c-f; 200 μ M in h.

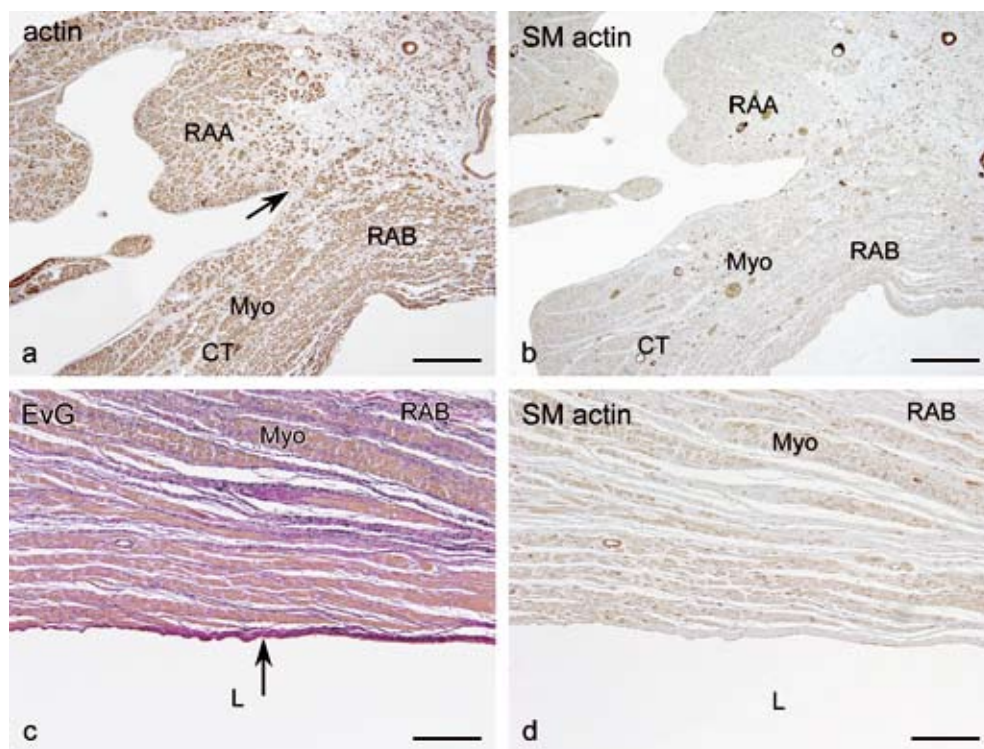


◀ Figure 4

Adult stage sections stained for alpha-SM actin (**a,b,d,f; SM actin**), Elastic Von Gieson (**c,e; EvG**) and Resorcin-Fuchsin (**g; RF**). Figure **h** is a macroscopical picture of the area in between the confluence of the PVs where discontinuous myocardium is found as shown in figure **g**. Boxes in figure **c** indicate the position of the enlargements in figure **d,e**. In EvG stained sections collagen fibers are purple and elastic fibers are black, in RF stained sections collagen fibers are red and elastic fibers are black.

a,b. In the pulmonary veins (**PV**) as well as in the left atrial body (**LAB**) an identical and characteristic vessel wall is found consisting of an intimal layer (**I**), a medial layer (**M; double arrow**) with SMCs and elastic lamellae, and an adventitial layer (**A**) in between the media and myocardium (**Myo**). In contrast to the neonatal stage, a profound intimal thickening is observed, most profound in the PVs. At the junction of the LAB with the left atrial appendage (**LAA**) a borderzone with distinctive tissue is identified (**c,d; arrow**). The inner surface of this area lacks trabeculation and vessel wall tissue (**d**). The myocardium at the transition between LAB and LAA is very thin or absent, facing the epicardium (**c,e; asterisk**). **f.** On the inner surface of the LAA occasional SMCs are found (**arrows**) but a vessel wall component is lacking.

g,h. In between the confluence of the four PVs, in two adults, the myocardium (**Myo**) is discontinuous or absent (**asterisk in g**). Epicardium (**E**). Scale bar = 100 μM in a,b,f; 1 mm in c; 200 μM in d; 500 μM in e,g.



▲ Figure 5

Adult stage sections stained with HHF35 for muscle actins (**a; actin**), alpha-smooth muscle actin (**b,d-f; SM actin**) and Elastic Von Gieson (**c; EvG**). Figure **b** and **d** are adjacent sections of fig **a** and **c**.

a,b. At the transition of the smooth-walled right atrial body (**RAB**) to the trabeculated right atrial appendage (**RAA**), the myocardial layer (**Myo**) is very thin (**a; arrow**) comparable to the left side. In the RAA, vessel wall tissue is absent (**b**) which is comparable to the left atrial appendage. **c,d.** The right atrial body (**RAB**) consists at the inner side of a thin subendocardial layer (**c; arrow**), covered by myocardium (**Myo**). No characteristics of vessel wall tissue were present at this site (**d**). Terminal crest (**CT**), lumen (**L**). Scale bar = 500 μM in a,b; 200 μM in c-d.

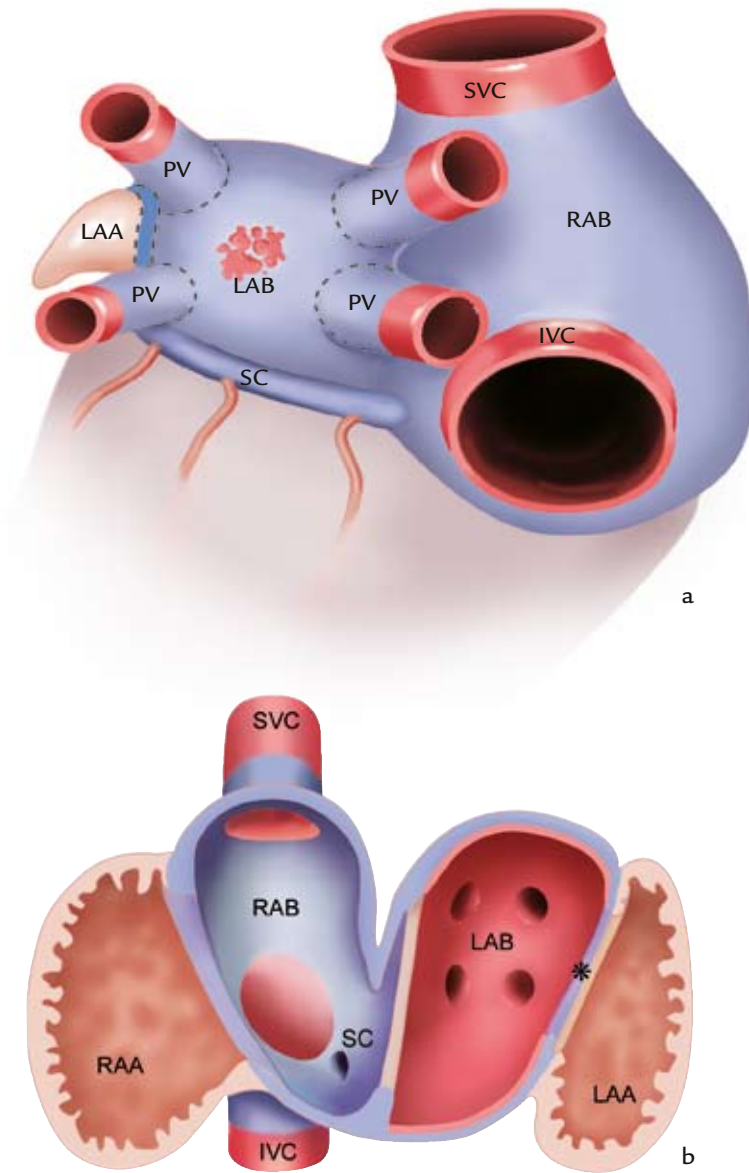


Figure 6

Schematic depiction of the outer side of the atrial chambers with the pulmonary veins (PV) and systemic veins. The left atrial body (LAB) and right atrial body (RAB) are covered by myocardium with a smooth-walled inner aspect (blue), which stretches out over the extracardiac segments of the PV and over a small peripheral part of the systemic veins (blue area above and below dotted line). The left atrial appendage (LAA) and right atrial appendage (RAA) consist of trabeculated myocardium (brown). A zone of smooth-walled myocardium that lacks characteristics of vessel wall tissue is found at the junction of the LAB to the LAA (blue between dotted lines). **b.** Schematic depiction of the tissue types found in the left and right atria seen from the inside of the atria. Vessel wall tissue (red), myocardial tissue with a smooth-walled inner aspect (blue), primary atrial segment tissue (brown), transitional zone (asterisk) which is smooth-walled, lacking vessel wall tissue. Coronary sinus (SC), inferior caval vein (IVC), superior caval vein (SVC).

Discussion

In this study, the histological outcome of the incorporation of the PVs into the LA was described in subsequent developmental stages. Our study demonstrates that, based on histological criteria, 3 different compartments can be distinguished in the LA (schematically demonstrated in **figure 6**): the smooth-walled LA body with vessel wall tissue (i.e. incorporated PV tissue); the trabeculated LA appendage, without vessel wall tissue; and a transitional zone in between the LA appendage and the LA body, which is smooth-walled and lacks vessel wall tissue. The right atrial appendage, the body of the right atrium and the atrial septum are not lined by vessel wall tissue. The borderzone between the LA appendage and the LA body histologically resembles the smooth-walled sinus venarum (body) of the right atrium.

The origin of the pulmonary veins is an issue of controversy. Based on findings using the marker HNK1, several authors have described that the myocardium surrounding the primitive PV in the LA is continuous with the sinus venosus in the right atrium⁹⁻¹¹. However, other authors have disputed this relation¹². These discrepancies depend largely on different application of definitions (especially how to define the sinu-atrial transition and the sinus venosus), and on different interpretation of possibly similar observations. Regardless of these differences, most authors seem to agree that the myocardium surrounding the primitive pulmonary vein possess different characteristics and can be differentiated from the working myocardium of the left atrial appendages. The aim of the current study was not to provide the answer for the origin of the primitive pulmonary vein. However, based on the observation of a zone of myocardium at the transition of the left atrial appendage with the left atrial body that histologically resembles the sinus venosus in the right atrium, we hypothesize that during incorporation of the PV and surrounding myocardium into the LA, the contribution of vessel wall to the body of the LA increases, which may reduce the area of sinus venosus myocardium to a small zone encircling the entrance to the LA appendage. An interesting finding was the very thin or even absent myocardium at this junction zone between the LA body and the LA appendage; within this zone slow conduction or conduction block may occur that are prerequisites for the induction of reentry¹³.

At early stages, the wall of the PVs consisted of a mixture of extrapericardially differentiated myocardial cells and SMCs. These SMCs proliferated and differentiated into an inner venous vessel wall. In the neonate and the adult, due to the incorporation process of the PVs, vessel wall tissue and extrapericardially differentiated myocardium were not only present in the PVs, but also in the LA body. It is currently unclear whether the outer circular or spirally arranged myocardial sleeves are formed due to extracardial mesenchymal triggers as is strongly supported by studies of Kruithof et al.^{14,15}, or are a direct continuation of the LA myocardium as supposed by Millino in the mouse¹⁶. Our study demonstrates that the myocardium and venous wall differentiate simultaneously, but does not support either a cardiac or an extracardiac origin.

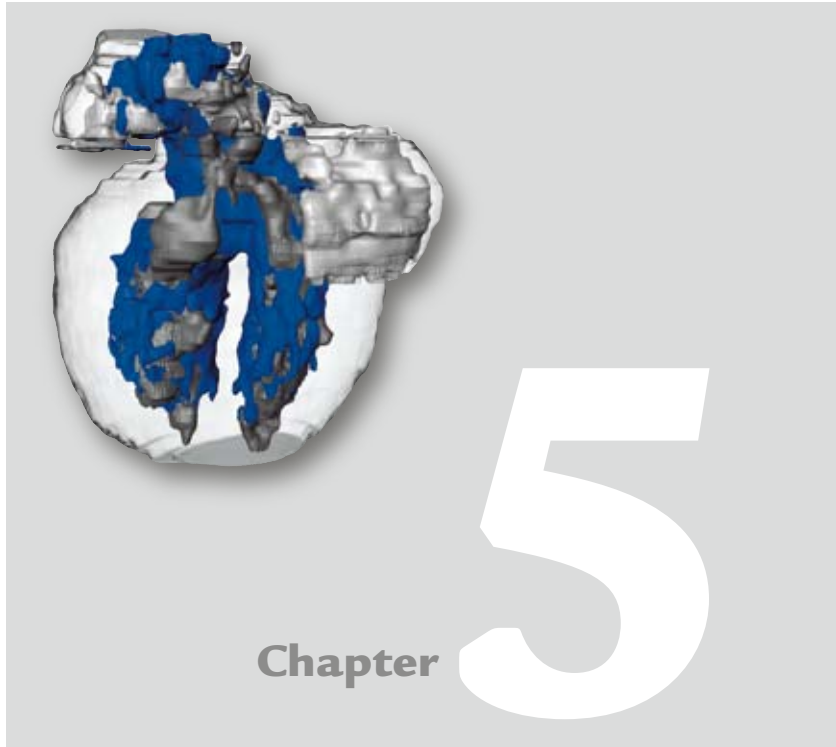
In the adult PVs and the LA body, beneath the endothelium/endocardium a prominent fibroelastic subendothelial layer was observed, which extended to a lesser extent in the right and left appendages and the atrial septum. Interestingly, in the neonatal stage, only a very thin subendothelial layer was observed, raising the possibility of an aging reaction to different stimuli e.g. continuous shear stress. In congenital heart diseases causing persistent and increased wall tension on the ventricles e.g. aortic stenosis or atresia and hypoplastic left heart, a comparable intimal thickening, so-called fibro-elastosis, can be found¹⁷. However, as all our adult hearts showed this intimal thickening, it is debatable whether these findings represent a true form of fibro-elastosis or are part of normal aging. Reactive intimal thickening in the PVs, leading to PV stenosis, can be seen after ablative therapy for arrhythmias, which suggests that the intimal layer is not only susceptible to internal but also to external stimuli¹⁸. Especially in this context, the results of this study can be of importance since it demonstrates that the LA body contains areas of discontinuous myocardium and areas without myocardium, e.g. in between the PV orifices, that might be the electrophysiological substrate of arrhythmias¹³. An increased susceptibility for arrhythmias may be explained by a difference in the composition of the extracellular matrix, the cellular junctions or the phenotype of these extrapericardially differentiated myocardial cells with regard to the intrapericardially differentiated myocardial cells of the sinus venosus and the atrial segment. These arrhythmias are amenable to catheter ablation but one must be alert that the vessel wall can be easily damaged due to a lack of myocardium. These considerations are specifically important when performing ablation at the LA dorsal wall, that is in close contact to the oesophagus. Recent studies have emphasized the risk of atrio-oesophageal fistula due to the application of radiofrequency current at this site^{19,20}. Lower dosage of radiofrequency current is therefore recommended when ablating in this area.

Reference List

1. Bliss DF, Hutchins GM. The dorsal mesocardium and development of the pulmonary veins in human embryos. *Am.J.Cardiovasc.Pathol.* 1995;**5**:55-67.
2. Ho SY, Sanchez-Quintana D, Cabrera JA, Anderson RH. Anatomy of the left atrium: implications for radiofrequency ablation of atrial fibrillation. *J.Cardiovasc.Electrophysiol.* 1999;**10**:1525-33.
3. Ho SY, Cabrera JA, Tran VH, Farre J, Anderson RH, Sanchez-Quintana D. Architecture of the pulmonary veins: relevance to radiofrequency ablation. *Heart* 2001;**86**:265-70.
4. Haissaguerre M, Jais P, Shah DC, Takahashi A, Hocini M, Quiniou G *et al.* Spontaneous initiation of atrial fibrillation by ectopic beats originating in the pulmonary veins. *N.Engl.J.Med.* 1998;**339**:659-66.
5. Pappone C, Rosanio S, Oreto G, Tocchi M, Gugliotta F, Vicedomini G *et al.* Circumferential radiofrequency ablation of pulmonary vein ostia: A new anatomic approach for curing atrial fibrillation. *Circulation* 2000;**102**:2619-28.
6. Romeis B. *Mikroskopische Technik.* 16 ed. Munchen: R. Oldenbourg Verlag, 1968.
7. Bergwerff M, DeRuiter MC, Hall S, Poelmann RE, Gittenberger-De Groot AC. Unique vascular morphology of the fourth aortic arches: possible implications for pathogenesis of type-B aortic arch interruption and anomalous right subclavian artery. *Cardiovasc.Res.* 1999;**44**:185-96.
8. Blom NA, Gittenberger-De Groot AC, Jongeneel TH, DeRuiter MC, Poelmann RE, Ottenkamp J. Normal development of the pulmonary veins in human embryos and formulation of a morphogenetic concept for sinus venosus defects. *Am.J.Cardiol.* 2001;**87**:305-9.
9. Blom NA, Gittenberger-De Groot AC, DeRuiter MC, Poelmann RE, Mentink MM, Ottenkamp J. Development of the cardiac conduction tissue in human embryos using HNK-1 antigen expression: possible relevance for understanding of abnormal atrial automaticity. *Circulation* 1999;**99**:800-6.
10. DeRuiter MC, Gittenberger-De Groot AC, Wenink AC, Poelmann RE, Mentink MM. In normal development pulmonary veins are connected to the sinus venosus segment in the left atrium. *Anat.Rec.* 1995;**243**:84-92.
11. Wenink AC, Symersky P, Ikeda T, DeRuiter MC, Poelmann RE, Gittenberger-De Groot AC. HNK-1 expression patterns in the embryonic rat heart distinguish between sinuatrial tissues and atrial myocardium. *Anat.Embryol.(Berl)* 2000;**201**:39-50.
12. Webb S, Brown NA, Wessels A, Anderson RH. Development of the murine pulmonary vein and its relationship to the embryonic venous sinus. *Anat.Rec.* 1998;**250**:325-34.
13. Jais P, Hocini M, Weerasoryia R, Macle L, Scavee C, Raybaud F *et al.* Atypical left atrial flutters. *Card Electrophysiol.Rev.* 2002;**6**:371-7.
14. Kruithof BP, van den Hoff MJ, Wessels A, Moorman AF. Cardiac muscle cell formation after development of the linear heart tube. *Dev.Dyn.* 2003;**227**:1-13.
15. Kruithof BP, van den Hoff MJ, Tesink-Taekema S, Moorman AF. Recruitment of intra- and extracardiac cells into the myocardial lineage during mouse development. *Anat.Rec.* 2003;**271A**:303-14.
16. Millino C, Sarinella F, Tiveron C, Villa A, Sartore S, Ausoni S. Cardiac and smooth muscle cell contribution to the formation of the murine pulmonary veins. *Dev.Dyn.* 2000;**218**:414-25.
17. Bryan CS, Oppenheimer EH. Ventricular endocardial fibroelastosis. Basis for its presence or absence in cases of pulmonic and aortic atresia. *Arch.Pathol.* 1969;**87**:82-6.
18. Weiss C, Gocht A, Willems S, Hoffmann M, Risius T, Meinertz T. Impact of the distribution and structure of myocardium in the pulmonary veins for radiofrequency ablation of atrial fibrillation. *Pacing Clin. Electrophysiol.* 2002;**25**:1352-6.
19. Pappone C, Santinelli V. The who, what, why, and how-to guide for circumferential pulmonary vein ablation. *J.Cardiovasc.Electrophysiol.* 2004;**15**:1226-30.
20. Pappone C, Oral H, Santinelli V, Vicedomini G, Lang CC, Manguso F *et al.* Atrio-esophageal fistula as a complication of percutaneous transcatheter ablation of atrial fibrillation. *Circulation* 2004;**109**:2724-6.
21. DeRuiter MC, Rensen SS, Coolen GP, Hierck BP, Bergwerff M, Debie WM *et al.* Smoothelin expression during chicken embryogenesis: detection of an embryonic isoform. *Dev.Dyn.* 2001;**221**:460-3.

Exploration of Cardiac Anatomy
Using Different Imaging Techniques
to Guide the Treatment of Arrhythmias

Part II



Monique R.M. Jongbloed¹

Martijn S. Dirksen²

Jeroen J. Bax¹

Eric Boersma³

Koos Geleijns²

Hildo J. Lamb²

Ernst E. van der Wall¹

PhD; Albert de Roos²

Martin J. Schalij¹

¹ Dept. of Cardiology, Leiden University Medical Center, Albinusdreef 2, Leiden, The Netherlands

² Dept. of Radiology, Leiden University Medical Center, Albinusdreef 2, Leiden, The Netherlands

³ Dept. of Epidemiology and Statistics, Erasmus Medisch Centrum, Dr. Molewaterplein 40/50, Rotterdam, The Netherlands

Multi-Slice Computed Tomography
to Evaluate Pulmonary Vein Anatomy
Prior to Radiofrequency Catheter Ablation
of Atrial Fibrillation-Initial Experience

Radiology. 2005 Mar;234(3):702-9

Abstract

Purpose: To evaluate multi-slice computed tomography (MSCT) depiction of the pulmonary veins (PV) to provide a roadmap for subsequent radiofrequency catheter ablation (RFCA).

Materials and Methods: In 23 patients (17 men, 6 women mean age 48 ± 11 years) with atrial fibrillation admitted for RFCA-isolation of PV, MSCT was performed. PV anatomy was evaluated and diameters of PV ostia were measured. To determine the shape of the ostia, a venous ostium index was calculated for all veins, by dividing measurements performed in the anterior-posterior direction by measurements performed in the superior-inferior direction. Results were compared with a control group of 11 patients (8 men, 3 women; mean age 56 ± 11) without atrial fibrillation. Images were evaluated in consensus by two observers.

Results: Additional PV to the 4 main PV were found in 7/23(30%) of patients. Common ostia of left and right PV were detected in 19/23(83%) and 9/23(39%) patients respectively. Early branching occurred more often in right vs. left PV (19/23(83%) vs. 3/23(13%), $P < 0.05$) in both patients and controls. Mean anterior-posterior diameter of PV ostia was 12.8 ± 3.3 mm for left PV, 16.2 ± 3.8 mm for right PV and 18.8 ± 7.7 mm and 28.7 ± 5.1 mm for left and right common ostia respectively. Ostia of right PV were more round-shaped than ostia of left PV (Venous ostium indexes 0.91 ± 0.21 vs. 0.75 ± 0.17 respectively, $P < 0.05$ and in controls 0.93 ± 0.12 vs. 0.82 ± 0.17 , $P < 0.05$). MSCT data were used to determine the ablation strategy and to guide catheters during RFCA.

Conclusion: MSCT is a valuable technique as a roadmap for PV anatomy prior to RFCA. Variations in number/insertion of PV were observed in a considerable number of patients and controls.

Introduction

Ectopic foci located within the pulmonary veins may trigger the induction of atrial fibrillation and/or tachycardia¹. This recognition has provided the basis for therapies directed at eliminating these foci by radiofrequency catheter ablation (RFCA). Different ablation strategies have been developed to either eliminate the foci or to encircle and electrically isolate the pulmonary veins²⁻⁵. The acute success rate of these procedures is acceptable, but procedure/fluoroscopy times are significant, partly due to the laborious visualization of the pulmonary veins.

Arrhythmogenicity of the pulmonary veins has been attributed to sleeves of atrial myocardium extending in the pulmonary veins^{6,7}. Anomalies in number and insertion of the pulmonary veins have been described, and some authors have indicated a possible role of the right middle pulmonary vein in initiating atrial fibrillation⁸. It is not possible to adequately detect these anomalies using fluoroscopy alone.

Magnetic resonance imaging (MRI) has been applied to detect anomalous insertion of pulmonary veins, and to evaluate pulmonary vein stenosis after RFCA⁹⁻¹¹. The advantage of MRI is the lack of ionizing radiation exposure, but MRI cannot be applied to patients with pacemakers, claustrophobia, or in patients who, due to their clinical condition, cannot tolerate the considerable long scanning times of MRI.

Accordingly, The purpose of our study was to evaluate multi-slice computed tomography (MSCT) depiction of the pulmonary veins to provide a roadmap for subsequent RFCA.

Materials and Methods

Study population:

Treatment of drug refractory atrial fibrillation by radiofrequency catheter ablation is standard practise in our hospital. The study population consisted of 23 consecutive patients with drug-refractory atrial fibrillation admitted for RFCA of the pulmonary vein ostia. Mean age was 48 ± 11 years, range 24-68 years (17 men, 48 ± 9 years, range 31-62 years; 6 female, 49 ± 17 , range 24-68 years). Furthermore a control group of 11 consecutive patients (mean age 56 ± 11 , range 31-73 years, 8 men, 56 ± 5 years, range 46-62 years; 3 female, 55 ± 22 years, range 31-73 years) without atrial fibrillation, admitted for evaluation of coronary artery disease, was studied. There were no statistically significant differences in age and sex between the study group and the control group (determined with the Independent Student's t-test and the Fisher's Exact Test respectively, using SPSS 11.0 software), although in both groups more male subjects were present. For both groups, we did not include patients with clinically important valvular disease, patients who had undergone coronary artery bypass grafting and patients with severe left ventricular dysfunction. Three of 23 (13%) patients and none of the control patients had a permanent pacemaker. Our Institu-

tional Review Board does not require its approval or written informed consent for a retrospective review, as was performed for the 23 patients having standard practice treatment in our hospital. However, all 23 patients were extensively informed about the treatment and they all gave informed consent prior to MSCT scanning. The 11 control patients are part of a research protocol for non-invasive evaluation of coronary artery disease that was approved by the Institutional Review Board of our institution. These 11 control patients gave informed consent to participate in that study and the use of the data for scientific research. We retrospectively analyzed the data obtained in these 11 control patients, and our Institutional Review Board did not require its approval or additional informed consent for that retrospective analysis.

Multi-Slice Computed Tomography

MSCT was performed two days prior to RFCA (by MSD, AdR, MRMJ) using a Toshiba Multi-slice Aquilion 0.5-T system (Toshiba Medical Systems, Otawara, Japan). Non-ionic contrast material (Xenetix 300, Guerbet, Aulnay S. Bois, France) was injected in the ante-brachial vein (160 ml, flow rate 4.0 ml/sec.).

The first 19 examinations were performed on a 4-slice CT scanner; in 4 patients, a 16-slice CT scanner was used. In the control group MSCT was performed on a 4-slice CT scanner in 3 patients, the other 8 patients were scanned with a 16-slice CT-scanner. Cranio-caudal scanning (coverage length 80-120 mm) was performed at the level of the atria using simultaneous acquisition of 4 sections with a collimated slice thickness of 2 mm (when using the 4-slice system), and 16 sections with a collimated slice thickness of 0.5 mm (when using the 16-slice system). Helical pitch was 1 mm/-0.5 sec. for the 4-slice scanner and 4 mm/-0.5 sec. for the 16-slice scanner, rotation time was 500 ms and tube voltage was 120 kV at 250 mA.

Scanning was performed during breath-holding. A segmental reconstruction algorithm was used to allow for the inclusion of patients with a range of heart rates without the need for pre-oxygenation or beta-blocker therapy. Retrospective ECG-gating was performed to eliminate cardiac motion artefacts. Data acquisition was completed in 20 seconds.

Data reconstruction was performed on a Vitrea post-processing workstation (Vital images, Plymouth, Mn, USA) with use of 2-D viewing modes and 3-D reconstructions.

Analysis of MSCT

Evaluation of pulmonary vein anatomy was first performed by examining anatomy of the pulmonary veins and their insertion in the left atrium on 3-D epicardial reconstructions. Thereafter, reconstructions were evaluated in three different orthogonal planes (transversal, sagittal and coronal) or with angulated multiplanar reformat. The number of pulmonary veins, number of ostia and the branching pattern of the pulmonary veins were assessed. Two experienced observers (MSD & AdR, experience in chest CT interpretation 6 and 25 years respectively) assessed the MSCT images in consensus.

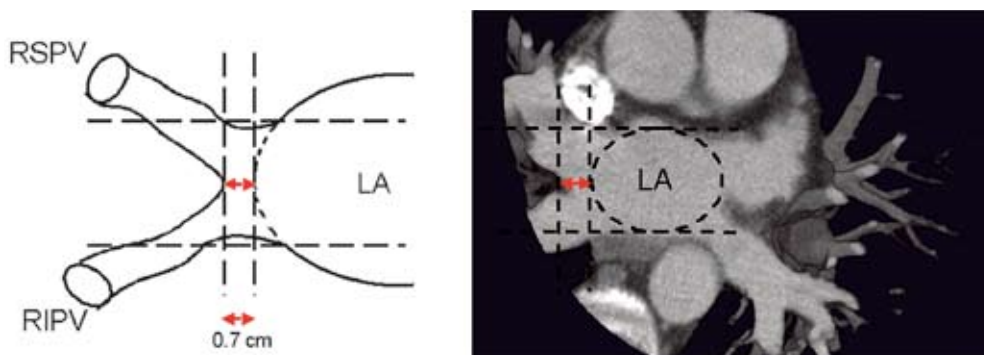


Figure 1

Schematic drawing (left panel) and maximum intensity projection after injection of intravenous contrast (right panel) of the left atrium (LA) and the right pulmonary veins in the transversal plane, to demonstrate the application of definitions. The dotted line represents the extrapolated border of the left atrium. If the distance between this virtual border and the bifurcation of both pulmonary veins (double arrow) is ≥ 0.5 cm, as is the case in this example, the ostium of both pulmonary veins is defined as a ‘common ostium’, because both veins enter the virtual border of the left atrium through a common trunk. RSPV: right superior pulmonary vein, RIPV: right inferior pulmonary vein.

The ostial insertion of the pulmonary veins was defined as either separate insertion or as common ostium. In order to analyze insertion of the pulmonary veins in the left atrium, definitions were constructed (MSD, AdR, MRMJ, JJB, MJS). Application of definitions was as follows. To determine the site of the veno-atrial junction, extrapolation of the outer left atrial contour was performed in three orthogonal directions. A line following the outer left atrial contour was drawn (**Figure 1**), indicating the border between the left atrium and the pulmonary veins. Pulmonary veins which either enter this “virtual” left atrial contour separately or which bifurcate within a distance < 0.5 cm from the line were defined as having ‘separate ostia’. If the distance between the border of the left atrium and the bifurcation of the pulmonary veins was ≥ 0.5 cm on the transversal and coronal plane, the ostium was defined as a ‘common ostium’. Also, the sagittal plane was used to confirm that both veins either enter the left atrial contour separately or unite before entering the left atrium in case of separate and common ostia respectively. Multiplanar reformatting was used to obtain optimal insight of the ostial insertion in the three orthogonal planes. ‘Additional pulmonary veins’ enter the left atrium in a separate ostium, which is located < 0.5 cm from the virtual line representing the left atrial contour. ‘Early branching’ was defined as bifurcation of the pulmonary vein in 2 or more separate branches within 1 cm of their origin of the left atrium.

Next, measurements of pulmonary vein diameters were made at the level of the ostium (MSD, MRMJ in consensus). Pulmonary veins have been reported to be more oval-shaped than round-shaped¹². Accordingly, the diameter of the ostia of all pulmonary veins was measured in 2 directions. Multiplanar reformat was used to obtain imaging planes that

were perpendicular to the course of the veins, to allow measurements in 2 orthogonal directions. The venous ostium index (measurements performed in anterior-posterior direction divided by measurements performed in superior-inferior direction) was calculated to determine whether these data provided evidence for asymmetry of pulmonary vein ostia. Particular attention was paid to the presence of macroscopic pre-existent stenosis of pulmonary veins. The ablation strategy was planned according to MSCT data.

Radiofrequency catheter ablation:

The aim of RFCA was to electrically isolate all pulmonary veins from the left atrium by applying radiofrequency-current circumferentially around the ostia of all pulmonary veins, according to the method described by Pappone et al.⁴ Ablation points were to be targeted at ± 5 mm outside the ostium of the pulmonary veins, in order to prevent pulmonary vein stenosis. Radiofrequency current was applied via a Stockert-Cordis (Stockert-Cordis, Freiburg, Germany) generator at each ablation point for 30 seconds, with maximum temperature setting at 60° C and maximum radiofrequency energy 50 W. Prior to RFCA, the ablation strategy was planned using data obtained with MSCT.

If a separate pulmonary venous insertion was observed on the MSCT scan, radiofrequency current was targeted to form separate circles surrounding the pulmonary venous ostia. If the distance between the border of the left atrium and the bifurcation of the pulmonary veins was >0.5 cm, the ostium was defined as a common ostium because the ablation of these veins would be performed by encircling the common ostium rather than approaching each vein independently. If a common ostium was observed, ablation points were targeted in a large circle surrounding the common ostium. All additional pulmonary veins observed were targeted, in order to electrically isolate these veins from the left atrium as well. During the procedure, the MSCT scan was placed on a light panel opposite to the operator, and served as a roadmap for ablation during the procedure. Results of measurements of the pulmonary vein ostia and indexes were available during the procedure to guide the operator in targeting the pulmonary veins. A 3-D non-fluoroscopic mapping system (CARTO, Biosense Webster, Diamond Bar, CA, USA) was used to tag pulmonary veins, to acquire electrophysiological information and to mark ablation points. Tagging of the pulmonary veins was guided by the information of the MSCT scan, concerning number and insertion of pulmonary veins. All patients received heparin (activated clotting time 2-3 times baseline value, checked hourly) to reduce the risk of thrombo-embolic complications. Electrical isolation of the pulmonary veins was confirmed by pacing from the left atrium and the pulmonary veins. The procedure was designated successful when there was no capture after pacing in the left atrium or pulmonary veins and when the patient was in sinus rhythm after the procedure. RFCA was performed by MJS, assisted by MRMJ.

Statistical analysis (EB)

Continuous data are expressed as mean values and corresponding standard deviation (SD), and dichotomous data are expressed as numbers and percentages. Differences in baseline demographic and clinical characteristics between patient subgroups are analysed by unpaired student's t-tests or Fisher's exact tests, as appropriate. The paired student's test t- test was applied to evaluate differences in the venous ostium indexes between right sided and left sided veins. Finally, the McNemar test was used to evaluate the occurrence of common ostia and early branching between left sided and right-sided veins. All tests were two-tailed, and the threshold for statistical significance was stated at the classical 0.05 probability level. Analyses were performed using SPSS 11.0 software.

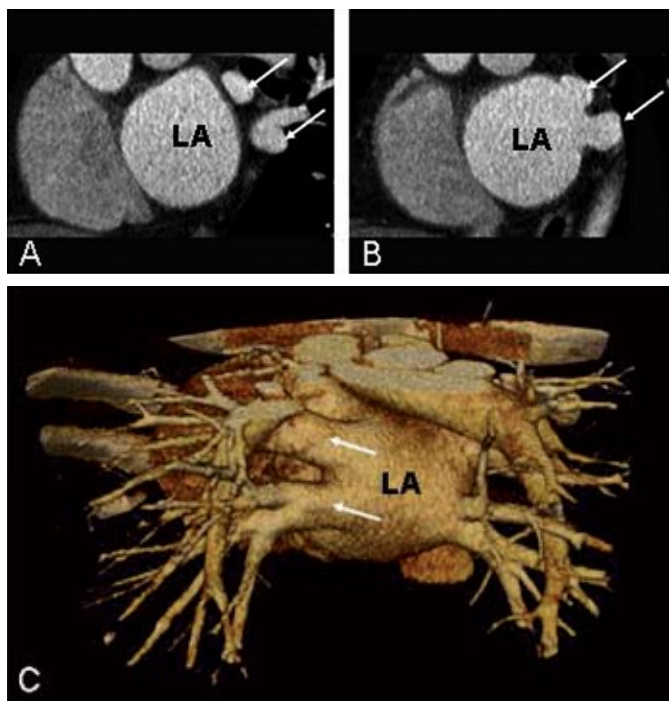


Figure 2

A/B. Sagittal view illustrating separate insertion of the left pulmonary veins. Both veins (arrows) enter the left atrium separately.

C. 3-D reconstruction, posterior view. The descending aorta and spine are removed by segmentation to increase visualization. The left pulmonary veins insert in the left atrium via separate ostia (arrows).

LA: left atrium

Results

Mean heart rate during scanning was 80 ± 17 beats per minute (range 47-104). Reconstruction of data was performed in several cardiac phases and the cardiac phase showing minimal cardiac motion artefacts was evaluated.

122

Pulmonary vein anatomy. In 23 patients, a total of 100 pulmonary veins were detected (4.4 ± 0.6 per patient), whereas in the 11 control subjects a total of 47 pulmonary veins were observed (4.3 ± 0.5 per patient). Additional right pulmonary veins to the 4 main pulmonary veins were observed in 6/23 (26%) patients and in 3/11 (27%) control subjects. One patient (of the 6 patients in whom additional veins were observed) had 2 additional right pulmonary veins. Thus, 7 additional right pulmonary veins were observed in the patients group. Five were situated between the 2 native right pulmonary veins and referred to as right middle pulmonary veins. One additional right pulmonary vein was situated below the native lower right pulmonary vein. In the patient with 2 additional pulmonary veins, there was a large common ostium on the right side, from which 2 native and 2 additional veins originated. In 1 (4%) patient an additional left pulmonary vein was observed. Additional left pulmonary veins were not observed in the control group. **Figure 2** demonstrates MRCT images obtained from a patient with normal insertion of the pulmonary veins. MRCT images of a patient with an additional right pulmonary vein are shown in **Figure 3**.

Common ostia were observed more frequently in left as compared to right pulmonary veins in both groups (83% vs. 39%, $P < 0.05$ in patients and 55% vs. 9% in controls, $P < 0.05$). Examples are shown in **Figure 4 and 5**.

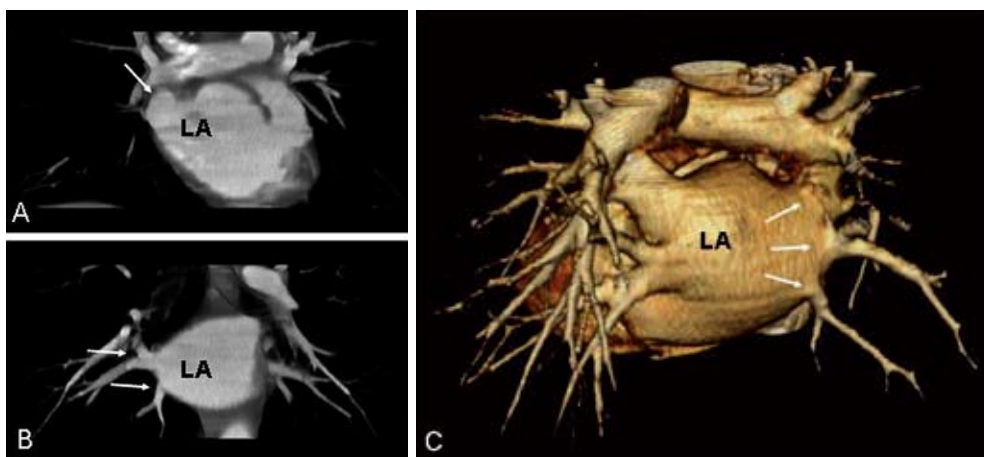


Figure 3

A/B. Maximum intensity projections (coronal views) showing three right pulmonary veins (arrows).

C. 3-D reconstruction, posterior view. Arrows point at the three right pulmonary veins.

LA: left atrium

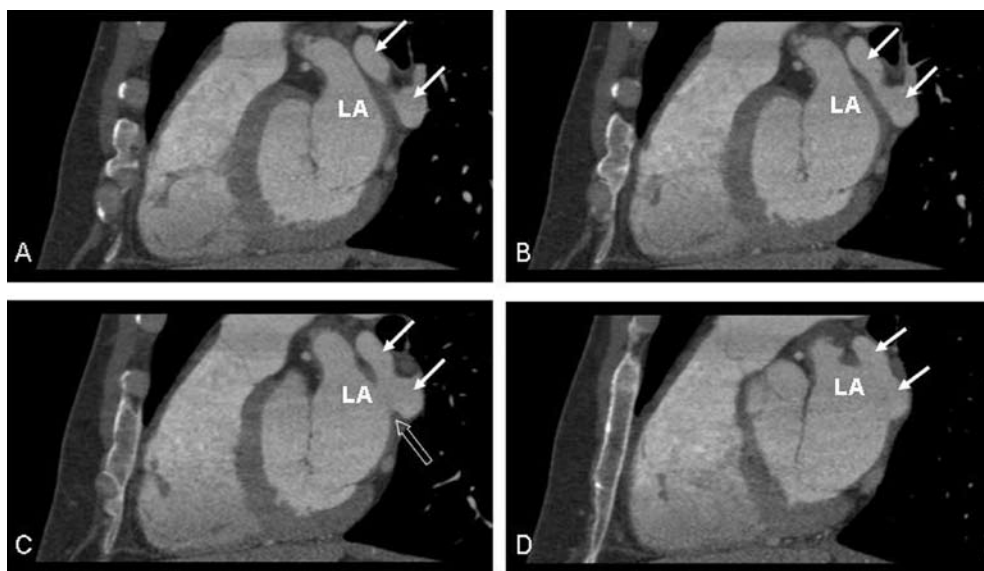


Figure 4

Sagittal views, demonstrating a common ostium of the left pulmonary veins. Upper and lower arrows point at the left superior and left inferior pulmonary veins, respectively

A. The left superior and left inferior pulmonary veins approach the LA separately.

B. The left superior and inferior veins unite before entering the left atrium.

C/D. Both veins enter the left atrium via the same ostium (open arrow).

LA: left atrium

Early branching occurred more often in right as compared to left pulmonary veins (83% vs. 13%, $P < 0.05$ in patients and 82% vs. 0% in controls $P < 0.05$). All anatomic findings are summarized in **Table 1**.

Table 1 Anatomical Results MSCT

	Patients (n=23)	Controls (n=11)
Mean number of PV/pt	4.4±0.6	4.3±0.5
Mean number ostia/pt	3.1±0.9	3.4±0.7
Pts with additional RPV	6 (26%)	3 (27%)
Pts with additional LPV	1 (4%)	0
Pts with common ostium RPV	9 (39%)	1 (9%)
Pts with common ostium LPV	19 (83%)	6 (55%)
Pts with early branching RPV	19 (83%)	9 (82%)
Pts with early branching LPV	3 (13%)	0

PV: pulmonary veins, LPV: left pulmonary veins, RPV: right pulmonary veins, pts: patients

* $P < 0.05$ vs. patients with common ostia RPV

† $P < 0.05$ vs. patients with early branching RPV

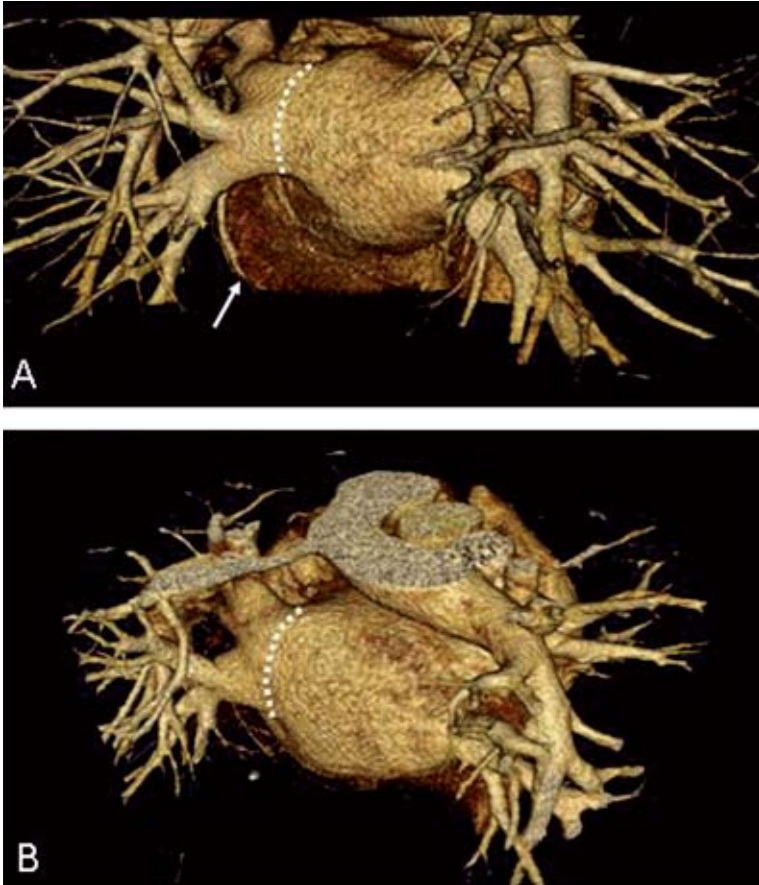


Figure 5

A/B. 3-D reconstructions, posterior views. Examples of common ostia of the left pulmonary veins. To facilitate interpretation, the extrapolated border of the LA is depicted by the dotted line. In figure B the ostium is funnel-shaped. The arrow points at the left ventricular apex.

Quantitative measurements of pulmonary vein ostia. Measurements at the level of the pulmonary vein ostium were performed in two perpendicular directions (**Table 2**). Mean anterior-posterior diameters were larger for the right pulmonary veins as compared to the left pulmonary veins in both groups. Mean diameters measured in the superior-inferior direction were comparable for the left and right pulmonary veins in both groups, and are summarized in **Table 2**. Although there was a trend towards larger diameters of pulmonary venous ostia in the patients group as compared to the control group, these differences were not statistically significant.

The venous ostium indexes (fraction of anterior-posterior and superior-inferior diameters) were calculated to determine ovality of the ostia and are shown in **Table 2**. As this ratio approaches 1, the ostium of the pulmonary vein is more round shaped, whereas differences in

diameter result in an outcome of the venous ostium index, which deviates from 1, indicating the presence of a more asymmetric or oval-shaped ostium. Ostia of right-sided pulmonary veins were significantly more round-shaped as compared to the left pulmonary veins (0.91 ± 0.21 vs. 0.75 ± 0.17 respectively in the patients group and 0.93 ± 0.12 vs. 0.82 ± 0.17 for the control group, $P < 0.05$).

Radiofrequency catheter ablation. Eventually 21 patients were treated with RFCA for pulmonary vein isolation. Two patients were excluded for the presence of intracardiac thrombus detected with echocardiography prior to RFCA. Targeting of RF-ablation points was performed according to the information obtained with MSCT. In patients with common ostia, the RFCA-lesions were targeted around the common ostium of the pulmonary veins, in order to achieve a circumferential line of block around the veins. In patients with additional pulmonary veins, RFCA was aimed at isolation of these veins as well. Procedural success was achieved in 20/21 (95%) of patients. Mean procedure time was 309 ± 83 minutes and mean fluoroscopy time 56 ± 16 minutes. No complications were observed during the first 48 hours after the procedure. After 14.3 ± 3.8 months of follow up, 14/21 (67%) patients were in sinus rhythm.

Table 2 Measurements of Pulmonary Venous Ostia

Vein	N	Patients Diameter AP (mm)	Patients Diameter SI (mm)	Patients Venous ostium index	Controls Diameter AP (mm)**	Controls Diameter SI (mm)**	Controls Venous ostium index
LSPV	23	13.8±3.1	18.7±4.4	0.76±0.17	12.7±1.7	15.9±2.4	0.81±0.15
LIPV	23	11.8±3.3	16.1±3.1	0.74±0.16	12.7±2.2	15.8±2.6	0.82±0.19
Both LPV		12.8±3.3	17.4±4.0	0.75±0.17	12.7±1.9	15.9±2.4	0.82±0.17
RSPV	23	16.9±2.9	19.5±3.0	0.88±0.14	15.0±1.7	16.7±2.6	0.91±0.10
RIPV	23	15.9±4.3	17.7±4.4	0.94±0.27	13.7±1.7	14.5±2.4	0.95±0.13
Both RPV		16.2±3.8*	18.6±3.8	0.91±0.21*	14.3±1.8*†	15.6±2.7†	0.93±0.12*
LCO	19	18.8±7.7	26.2±8.0	0.82±0.57	16.3±2.1	23.4±4.1	0.71±0.13
RCO	9	28.7±5.1	31.2±7.3	0.98±0.34	21.4	25.0	0.86
Add LPV	1	11.0	10.1	1.09	-	-	-
Add RPV	7	6.7±0.9	7.2±2.3	1.00±0.3	7.9±1.1	6.9±1.1	1.15±0.07

LSPV: left superior pulmonary vein, LIPV: left inferior pulmonary vein, RSPV: right superior pulmonary vein, RIPV: right inferior pulmonary vein, LCO: left common ostium, RCO: right common ostium, LPV: left pulmonary veins, RPV: right pulmonary veins, Add LPV: additional left pulmonary vein, Add RPV: additional right pulmonary veins, AP: anterior-posterior, SI: superior-inferior

* $P < 0.05$ vs. both left pulmonary veins in the same group

** no statistically significant difference as compared to the patients group

† $P < 0.05$ vs. diameters ostia RPV in the patients group

Discussion

Key findings of this study are the presence of additional pulmonary veins and the common insertion of pulmonary veins in a substantial number of patients. Since the recognition that atrial fibrillation may originate from triggers within the pulmonary veins and RFCA can eliminate these triggers, interest for pulmonary vein anatomy has increased^{6 7 13 14}. Knowledge of pulmonary vein anatomy prior to RFCA is therefore mandatory to facilitate an anatomical based ablation procedure. In the current study, we used MSCT to evaluate pulmonary vein anatomy prior to RFCA procedures.

126

Pulmonary vein anatomy. Information on the prevalence of variations in pulmonary vein anatomy is scarce. In the present study, interindividual variations in anatomy of pulmonary veins were demonstrated in both the study population and the control group. A recent study provides a useful classification system of pulmonary venous drainage patterns¹⁵. However, lack of definitions concerning the border between the left atrium and the pulmonary veins, complicates the description of pulmonary vein anatomy and their entrance in the left atrium. We have used extrapolation of the left atrial contour on the orthogonal 2-D planes as the boundary of the left atrium. The presence of a common ostium was determined according to the distance between this virtual border of the left atrium and the bifurcation of the two pulmonary veins on the transversal and coronal plane. In case of a common ostium, both veins could also be observed to unite before entering the left atrium on the sagittal plane. According to this definition, the pulmonary veins could be demonstrated to unite and enter the left atrium via the same ostium in 83% of patients. In 39% a common ostium of the right pulmonary veins was observed. On 3-D reconstructions, often a large funnel-shaped entrance could be observed.

A total of 7 additional right pulmonary veins were observed, with 5 positioned between the two native veins, and they were thus considered as right middle pulmonary veins. In one patient an additional left pulmonary vein was observed.

The exact prevalence of pulmonary vein anomalies has not been thoroughly investigated. Nathan et al.¹⁶ have reported variations in number of pulmonary veins and the insertion in the left atrium, although exact details were not provided. Ho et al.⁷ and Cabrera et al.¹⁷, based on observations in human autopsy hearts, observed common ostia in 25%⁷ and in an additional 40% the veins were only separated by muscle tissue <3 mm wide⁷. In another study, an anomalous number of veins was present in 23% of examined hearts⁶. Moubarak et al. describe confluent superior and inferior veins in 25% of examined hearts, most common on the left side¹⁸.

High spatial resolution imaging, such as MSCT and MRI, may allow more precise visualization of anatomy, and may therefore detect more anomalies. This is precisely the information needed prior to RFCA, in order to completely isolate all veins.

In particular, the right middle pulmonary vein has been associated with the occurrence of atrial fibrillation⁸. This anatomical variant can be adequately delineated with MSCT, as was observed in 5 (22%) patients in our study.

In addition, the diameter and shape of the ostia is important information for RFCA. For this purpose, 3-D imaging is needed, since the diameter of the pulmonary venous wall is often oval-shaped and 2-D assessment using angiography will not be sufficient. In the present study, the diameter of the pulmonary veins was measured at the ostia and the venous ostium index was calculated from measurements performed in two perpendicular planes. Results indicated a more asymmetric or oval shape of the left pulmonary veins, whereas venous ostium indexes in right pulmonary veins suggested a more round shape of these veins. These findings are in line with recent observations by Wittkampf et al. using 3-D visualization of pulmonary veins with MRI¹². As also demonstrated by Wittkampf et al., 3-D evaluation of ostia is very important prior to RFCA since ostia can be very narrow (due to the oval shape), and this information cannot be derived from 2-D fluoroscopy.

MSCT for 3-D visualization of pulmonary veins. Cardiac MSCT has mostly been performed for evaluation of coronary artery stenoses^{19,20}. MSCT for evaluation of pulmonary anatomy has recently been applied^{21,15,22}. Data acquisition of MSCT is only 20 seconds, and all patients (including those with pacemakers, or metallic objects (intracranial clips) and claustrophobia) can potentially undergo MSCT. This imaging technique allows thin slices to be obtained within reasonable breath-hold duration. Because of the thin slice-thickness, advanced post-processing techniques such as multiplanar reformatting, 3-D volume rendering and maximum intensity projection can be applied for diagnostic evaluation. With the recent introduction of 16-slice systems, the z-axis resolution can be cut down to 0.5 mm, allowing true isotropic imaging in any anatomical plane with preservation of in-plane resolution. This may result in improved diagnosis of small pulmonary vein branches, which may facilitate RFCA procedures. Finally, real-time catheter navigation in the heart using of three-dimensional CT images has been described recently²³.

A limitation of the use of MSCT is the radiation dosage. In the current study, radiation exposure of MSCT was approximately 8 mSv. New acquisition techniques, e.g. ECG-dependent dose modulation or acquisition protocols that employ prospective cardiac triggering, will allow substantial dose-reduction. A disadvantage of prospective triggering is that only one cardiac phase can be constructed, which may cause inaccuracy of measurements of pulmonary veins in patients with irregular heart rhythms, such as in atrial fibrillation.

Study limitations

128

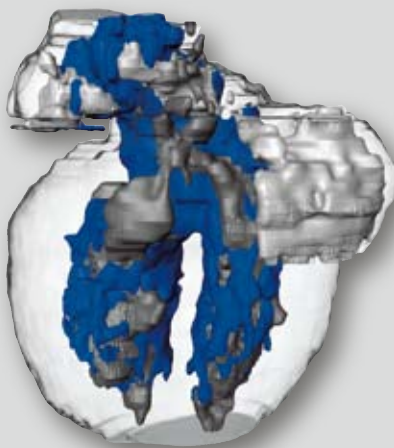
This study is a descriptive study, with the emphasis on the methodology to determine the atrio-venous junction, in order to describe variations in pulmonary venous anatomy prior to radiofrequency catheter ablation. To describe the size and shape of the ostia, measurements of the diameters of the pulmonary veins were performed. The current study is a pilot study to evaluate the occurrence of different anatomical variations in a group of patients with, and without atrial fibrillation. Inferential statistics were performed, with the marginal note that samples sizes may not be sufficient to draw positive conclusions. Although our results demonstrate a trend towards larger ostial diameters in the atrial fibrillation group, the small size of the studied group does not allow a valid comparison between the groups. Likewise, to determine whether our findings reflect anomalies or mere variations of normal anatomy, examination of larger patient groups both with and without atrial fibrillation is mandatory.

ECG triggering may not be feasible in patients who are in atrial fibrillation during scanning. However, the MSCT system we used allows adaptive segmentation/adaptive temporal resolution, which corrects irregularities in cardiac rhythm to a certain extent by adjusting the segmentation for every heartbeat. Furthermore, retrospective ECG gating has the advantage that reconstructions during different phases of the cardiac cycle can be obtained, which allows reconstruction of the cardiac phase showing the minimum amount of motion artefacts.

In conclusion, MSCT allows visualization of pulmonary vein anatomy, providing a road-map prior to RFCA, which may be used to guide the application of radiofrequency current around pulmonary vein ostia in patients with atrial fibrillation.

Reference List

1. Haissaguerre M, Jais P, Shah DC, Takahashi A, Hocini M, Quiniou G *et al.* Spontaneous initiation of atrial fibrillation by ectopic beats originating in the pulmonary veins. *N.Engl.J.Med.* 1998;**339**:659-66.
2. Haissaguerre M, Shah DC, Jais P, Hocini M, Yamane T, Deisenhofer I *et al.* Electrophysiological breakthroughs from the left atrium to the pulmonary veins. *Circulation* 2000;**102**:2463-5.
3. Haissaguerre M, Jais P, Shah DC, Garrigue S, Takahashi A, Lavergne T *et al.* Electrophysiological end point for catheter ablation of atrial fibrillation initiated from multiple pulmonary venous foci. *Circulation* 2000;**101**:1409-17.
4. Pappone C, Rosanio S, Oreto G, Tocchi M, Gugliotta F, Vicedomini G *et al.* Circumferential radiofrequency ablation of pulmonary vein ostia: A new anatomic approach for curing atrial fibrillation. *Circulation* 2000;**102**:2619-28.
5. Pappone C, Oreto G, Rosanio S, Vicedomini G, Tocchi M, Gugliotta F *et al.* Atrial electroanatomic remodeling after circumferential radiofrequency pulmonary vein ablation: efficacy of an anatomic approach in a large cohort of patients with atrial fibrillation. *Circulation* 2001;**104**:2539-44.
6. Ho SY, Sanchez-Quintana D, Cabrera JA, Anderson RH. Anatomy of the left atrium: implications for radiofrequency ablation of atrial fibrillation. *J.Cardiovasc.Electrophysiol.* 1999;**10**:1525-33.
7. Ho SY, Cabrera JA, Tran VH, Farre J, Anderson RH, Sanchez-Quintana D. Architecture of the pulmonary veins: relevance to radiofrequency ablation. *Heart* 2001;**86**:265-70.
8. Tsao HM, Wu MH, Yu WC, Tai CT, Lin YK, Hsieh MH *et al.* Role of right middle pulmonary vein in patients with paroxysmal atrial fibrillation. *J.Cardiovasc.Electrophysiol.* 2001;**12**:1353-7.
9. Godart F, Willoteaux S, Rey C, Cochetoux B, Francart C, Beregi JP. Contrast enhanced magnetic resonance angiography and pulmonary venous anomalies. *Heart* 2001;**86**:705.
10. Greil GF, Powell AJ, Gildein HP, Geva T. Gadolinium-enhanced three-dimensional magnetic resonance angiography of pulmonary and systemic venous anomalies. *J.Am.Coll.Cardiol.* 2002;**39**:335-41.
11. Yang M, Akbari H, Reddy GP, Higgins CB. Identification of pulmonary vein stenosis after radiofrequency ablation for atrial fibrillation using MRI. *J.Comput.Assist.Tomogr.* 2001;**25**:34-5.
12. Wittkampff FH, Vonken EJ, Derksen R, Loh P, Velthuis B, Wever EF *et al.* Pulmonary vein ostium geometry: analysis by magnetic resonance angiography. *Circulation* 2003;**107**:21-3.
13. Hocini M, Ho SY, Kawara T, Linnenbank AC, Potse M, Shah D *et al.* Electrical conduction in canine pulmonary veins: electrophysiological and anatomic correlation. *Circulation* 2002;**105**:2442-8.
14. Lin WS, Prakash VS, Tai CT, Hsieh MH, Tsai CF, Yu WC *et al.* Pulmonary vein morphology in patients with paroxysmal atrial fibrillation initiated by ectopic beats originating from the pulmonary veins: implications for catheter ablation. *Circulation* 2000;**101**:1274-81.
15. Marom EM, Herndon JE, Kim YH, McAdams HP. Variations in pulmonary venous drainage to the left atrium: implications for radiofrequency ablation. *Radiology* 2004;**230**:824-9.
16. Nathan H, Eliakim M. The junction between the left atrium and the pulmonary veins. An anatomic study of human hearts. *Circulation* 1966;**34**:412-22.
17. Cabrera JA, Sanchez-Quintana D, Farre J, Navarro F, Rubio JM, Cabestrero F *et al.* Ultrasonic characterization of the pulmonary venous wall: echographic and histological correlation. *Circulation* 2002;**106**:968-73.
18. Moubarak JB, Rozwadowski JV, Strzalka CT, Buck WR, Tan WS, Kish GF *et al.* Pulmonary veins-left atrial junction: anatomic and histological study. *Pacing Clin.Electrophysiol.* 2000;**23**:1836-8.
19. Achenbach S, Giesler S, Ropers D, Ulzheimer S, Derlien H, Schulte C *et al.* Detection of coronary artery stenoses by contrast-enhanced, retrospectively electrocardiographically-gated, multislice spiral computed tomography. *Circulation* 2001;**103**:2535-8.
20. Nieman K, Rensing BJ, van Geuns RJ, Vos J, Pattynama PM, Krestin GP *et al.* Non-invasive coronary angiography with multislice spiral computed tomography: impact of heart rate. *Heart* 2002;**88**:470-4.
21. Schwartzman D, Lacomis J, Wigginton WG. Characterization of left atrium and distal pulmonary vein morphology using multidimensional computed tomography. *J.Am.Coll.Cardiol.* 2003;**41**:1349-57.
22. Perez-Lugones A, Schwartzman PR, Schweikert R, Tchou PJ, Saliba W, Marrouche NF *et al.* Three-dimensional reconstruction of pulmonary veins in patients with atrial fibrillation and controls: morphological characteristics of different veins. *Pacing Clin.Electrophysiol.* 2003;**26**:8-15.
23. Solomon SB, Dickfeld T, Calkins H. Real-Time Cardiac Catheter Navigation on Three-Dimensional CT Images. *J.Interv.Card Electrophysiol.* 2003;**8**:27-36.



Chapter

6

Monique R.M. Jongbloed

Martin J. Schalij

Katja Zeppenfeld

Pranobe V. Oemrawsingh

Ernst E. van der Wall

Jeroen J. Bax

Dept. of Cardiology, Leiden University Medical Center, Leiden, The Netherlands

Clinical Applications
of Intracardiac Echocardiography in
Interventional Procedures

Heart. 2005 Jul;91(7):981-90

Abstract

Accurate knowledge of the anatomy of intracardiac structures is essential for the efficiency and safety of performing interventional procedures. Although fluoroscopy is an important aid while advancing catheters in the heart, it is not sufficient to supply accurate anatomical information on the position of veins, ridges and septa in the heart. Furthermore radiation exposure forms a risk to both the patient and the operator.

Intracardiac echocardiography (ICE) is a promising technique for imaging of intracardiac structures, and may serve as an alternative for the transesophageal approach, which is semi-invasive and requires anaesthesiology. The introduction of ICE catheters with low frequencies, allows accurate visualisation of intracardiac anatomical structures with an ultrasound catheter placed exclusively in the right side of the heart. This report focuses on the use of ICE in guiding percutaneous interventional procedures.

Introduction

Accurate knowledge of the anatomy of intracardiac structures is essential for the efficiency and safety of performing interventional procedures. Although fluoroscopy is an important aid while advancing catheters in the heart, it is not sufficient to supply accurate anatomical information on the position of veins, ridges and septa in the heart. Furthermore radiation exposure forms a risk to both the patient and the operator.

Intracardiac echocardiography (ICE) is a promising technique for imaging of intracardiac structures, and may serve as an alternative for the transesophageal approach¹, which is semi-invasive and requires anaesthesiology. The introduction of ICE catheters with low frequencies, allows accurate visualisation of intracardiac anatomical structures with an ultrasound catheter placed exclusively in the right side of the heart. This report focuses on the use of ICE in guiding percutaneous interventional procedures.

Basics of ICE

2-D intracardiac ultrasound systems – History

The first application of ICE was done using *mechanical ultrasound systems*, which were introduced in the 1980s. These systems provided high resolution imaging, but due to the high frequency of the transducers (20-40 MHz), tissue penetration was only limited and anatomic intracardiac overviews could not be obtained. The subsequent development of lower-frequency transducers allowed imaging of intracardiac structures, but these systems were still limited by the low steerability and over-the-wire design of the catheters². The clinical use was improved by the development of flexible lower-frequency transducers (9MHz), but depth control of these catheters still was not sufficient to allow visualisation of the whole heart from the right side of the heart. In the 1990s, systems modified after transesophageal echocardiographic probes were introduced. In these systems depth was improved by the use of lower frequencies (5MHz). However, the large size of these transducers limited the clinical use. In recent years the development of steerable *phased array ultrasound catheter systems* with low frequency and Doppler qualities has expanded the clinical use of ICE.

What are the technical requirements?

– Mechanical ultrasound tipped catheter

The mechanical ultrasound transducer tipped catheter (Clearview, Cardiovascular Imaging Systems Inc, Fremont, CA, USA) can be used for both intravascular and intracardiac imaging. For intracardiac use, a 9 MHz single element transducer is incorporated in an 8 French catheter. A piezoelectric crystal is rotated at 1800 rpm in the radial dimension perpendicular to the catheter shaft, thus providing cross sectional images in a 360° radial

plane. A sheath surrounding the imaging transducer is necessary to prevent contact of the imaging transducer with the cardiac wall. The ICE catheter needs to be filled with 3-5 cc sterile water before it is connected to the ultrasound machine (Boston Scientific Corp., San Jose, CA, USA). 3-D reconstruction of the acquired data can be created.

– *Phased array ultrasound tipped catheter*

This system uses a 10 French ultrasound catheter (Acunav Diagnostic Ultrasound Catheter, Acuson Corporation, Mountain View, CA, USA), which is positioned in the RA or RV via a femoral approach, through a 10 French introducer. The ultrasound catheter consists of a miniaturized 64-element, phased array transducer, which is incorporated in a single use catheter. The transducer scans in the longitudinal monoplane, providing a 90° sector image with tissue penetration of approximately 15 cm. Two planes of bi-directional steering (anterior-posterior and left-right, each in a direction of 160 degrees) are possible by using a mechanism on the handle of the catheter. The high resolution multiple frequency transducer (5MHz-10 MHz) allows tissue penetration enhancement, thus allowing depth control. Measurements of hemodynamic and physiologic variables can be made using Doppler imaging. The catheter is connected to an ultrasound system (Acunav/Sequoia, Acuson corp, Mountain view, CA, USA).

– *Mechanical versus phased array ultrasound tipped catheter*

Although the mechanical ultrasound systems can be used at a considerably lower cost compared to the phased array systems, there are several disadvantages as compared to the phased array transducers. Currently, no functional analysis can be performed with mechanical systems, due to the lack of colour and pulsed Doppler features. Since these systems use a single ultrasound frequency of 9 MHz and provide a limited radial depth of view (5 cm), imaging of left sided structures is not feasible with the ultrasound catheter placed in the right heart. This could increase the risk of thrombo-embolic complications when using the device for imaging of left sided structures. Furthermore, the design of the mechanical rotating catheter shaft and the lack of an articulation mechanism at the handle, limits steering of the transducer and thus a dynamic view on intracardiac structures. In the remainder of the current report we mainly focus on the use of phased array ICE in guiding percutaneous interventional procedures.

Advantages and limitations of ICE during interventional procedures

In the past, if percutaneous interventions needed guiding, fluoroscopy, transthoracic echocardiography (TTE) or transesophageal echocardiography (TEE) were used. The use of ICE has several advantages over these other techniques. No radiation is needed. In comparison to TEE, patient discomfort is less, general anaesthesia is not needed, allowing communication with the patient during the procedure. As compared to TTE, the transvenous access has the advantage that it is not necessary to position a transducer in a sterile field.

General advantages of ICE are the availability of direct on-line information on the position of catheters and devices and the possibility of direct monitoring of acute procedure-related complications (such as thrombus formation, pericardial effusion etc).

Several limitations of ICE currently exist. First the considerable shaft size (10 Fr) and the lack of additional catheter features, such as ports for guidewires, therapeutic devices and pressure, form a limitation. Second, the phased array catheters are expensive and single use only. Third, phased array ICE provides only monoplane image sections. Although this can partly be overcome by the steerability of the catheter, operators who are used to multi-plane TEE transducers may have difficulty obtaining the same views. Moreover, no standard views for ICE are currently defined, as are available for TTE and TEE.

Which views can be obtained with intracardiac echocardiography?

Using phased array ICE, views of all anatomic landmarks can be obtained with the ultrasound catheter positioned in either the RA or the RV. Although images quite similar to TEE can be obtained, the relatively “loose” position of the ultrasound probe in the heart, may give the inexperienced operator a feeling of disorientation. To overcome this, structured introduction and steering/manipulation of the ultrasound tipped catheter can ultimately provide orientation, supported by recognition of the anatomical landmarks. The catheter is advanced via the femoral vein, into the middle part of the RA via the inferior caval vein, thus visualising the RA, tricuspid valve and RV (**Figure 1A**). This view with the catheter positioned in the middle of the RA, can be used a “basic point of orientation”, from which other views can be derived. Counterclockwise rotation with the catheter positioned in the superior part of the RA provides imaging of the terminal crest, whereas clockwise rotation of the catheter from the inferior RA provides a view of Eustachian ridge with the tricuspid-caval isthmus (**Figure 1B**); these are important target structures in atrial flutter ablation. By turning the catheter around its axis (clockwise fashion as seen from the operator), imaging of the aortic valve, the right ventricular outflow tract and the pulmonary artery is feasible (**Figure 1C**). Long-axis views of both aorta and pulmonary trunks can be imaged in the same plane, which is not feasible with TEE. By rotating the catheter clockwise from the low right atrium, a short axis view of the coronary sinus can be obtained, while left-to-right movements of the ICE catheter provide a long-axis view of this structure (**Figure 1D and E**). When the catheter is further rotated, the next anatomical structure important in interventional cardiology to be recognised is the atrial septum (important for septal puncture, see below). By counterclockwise movement of the catheter from this position, imaging of the left atrium (LA), mitral valve and left ventricle (LV) is performed (**Figure 1F**). By increasing the depth setting of the catheter with the transducer directed at the left atrial posterior wall, imaging of the left and right pulmonary veins (PVs) and the left atrial appendage (LAA) is performed from the position of the atrial septum (important for pulmonary vein (PV) ablation, see below). As is it sometimes difficult to distinguish between the LAA and the left superior PV, Doppler capacities can be used to differentiate. Finally, by advancing

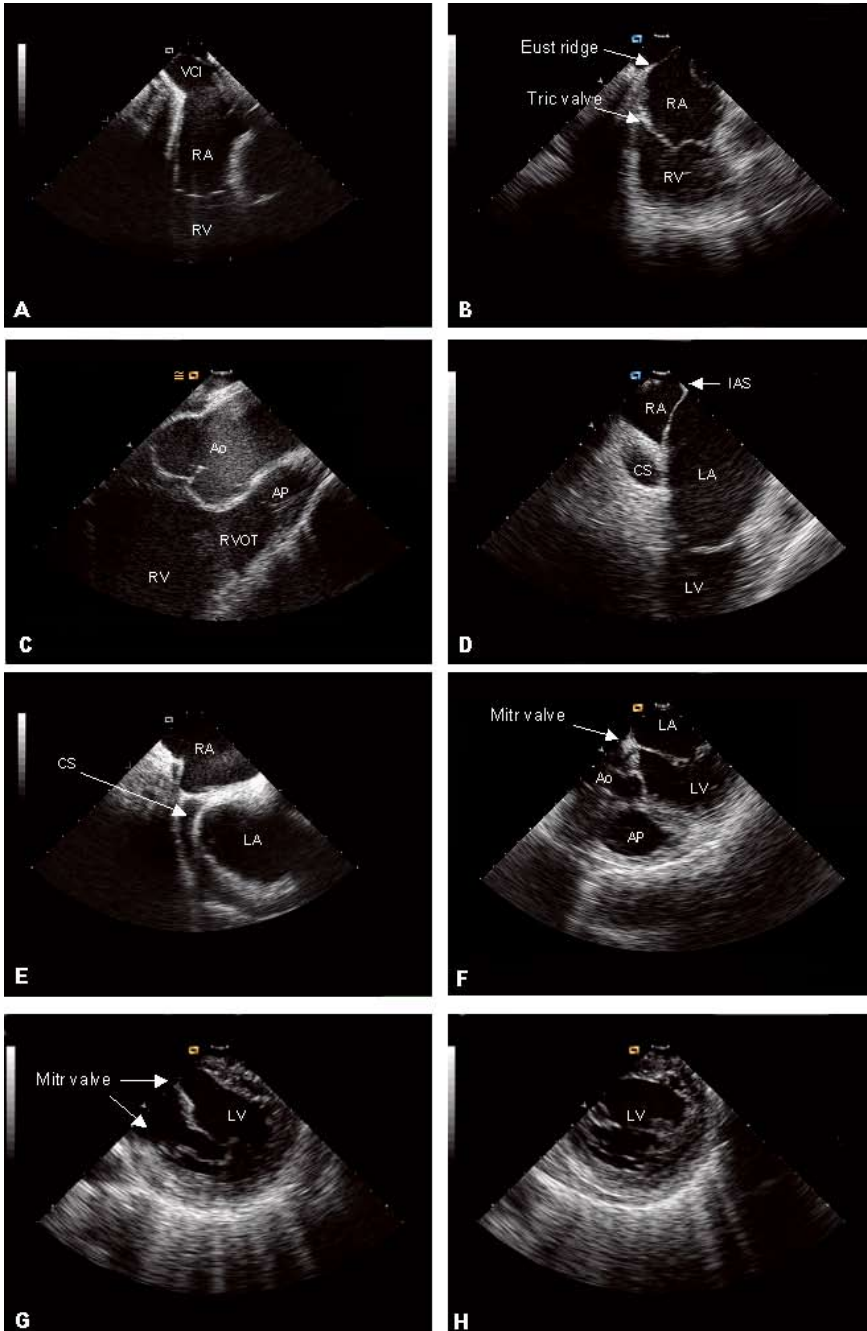


Figure 1

Different views obtained with the ICE transducer in either the RA or the RV. Explanation see text.

Ao: aorta, AP: pulmonary artery, CS: coronary sinus, Eust ridge: Eustachian ridge, IAS: interatrial septum, LA: left atrium, LV: left ventricle, Mitr valve: mitral valve, RA: right atrium, RV: right ventricle, RVOT: right ventricular outflow tract, Tric valve: tricuspid valve, VCI: inferior caval vein

the catheter into the RV, detailed imaging of the LV can be obtained. Both long- and short-axis views of the LV can be obtained (**Figure 1G and H**).

Table 1 Applications of ICE in Interventional Procedures

- Evaluation intracardiac thrombus
- Transseptal puncture
- ASD/PFO closure
- Interventional electrophysiological procedures
 - PV ablation in patients with atrial fibrillation
 - Atrial flutter ablation
 - VT ablation
- Other applications
 - Diagnosis/biopsy intracardiac masses
 - Balloon mitral valvuloplasty
 - Atrial appendage occlusion
 - Visualisation coronary sinus

Detection of intracardiac thrombus

Due to the risk of systemic embolism, evaluation of the presence of intracardiac thrombus prior to left-sided procedures is mandatory. The risk of thrombo-embolic events is related to the presence of LA spontaneous contrast and a LAA peak emptying velocity ≤ 20 cm/sec³. ICE can serve as an alternative for TEE assessment of LA and LAA function⁴. (**Figure 2A, B**). Prior to left sided interventions, the LAA can be evaluated for the presence of thrombus (**Figure 2C**).

The reported incidence of thrombo-embolic complications during left sided interventional procedures is approximately 2%⁵, possibly as high as 5% in patients with a history of transient ischemic attacks⁶. Detection of intracardiac thrombus with ICE during left-sided interventional procedures is discussed below (see PV ablation).

Transseptal puncture

Potential life-threatening complications of transseptal puncture include aortic puncture, pericardial puncture or tamponade, systemic arterial embolism and perforation of the inferior caval vein⁷. Accurate visualization of the fossa ovalis reduces the risk of complications. Especially less experienced operators may find ICE a better imaging modality than fluoroscopy, by its ability to accurately visualise the target for transseptal puncture, the fossa ovalis⁸. The Valsalva manoeuvre during injection of saline/contrast can be performed to reveal the presence of a patent foramen (PFO) (**Figure 2D**). In 10%-20% a PFO is present, omitting the need for transseptal puncture (**Figure 2E**). Positioning of the ultrasound catheter in the RA provides a clear vision of the interatrial septum, which consist of a thicker part, the limbus and the remains of the primary atrial septum, the fossa ovalis, which is the safest target for the transseptal puncture. During the puncture a Brockenbrough needle (DAIG Corp) is inserted via a transseptal sheath and dilator system and directed towards

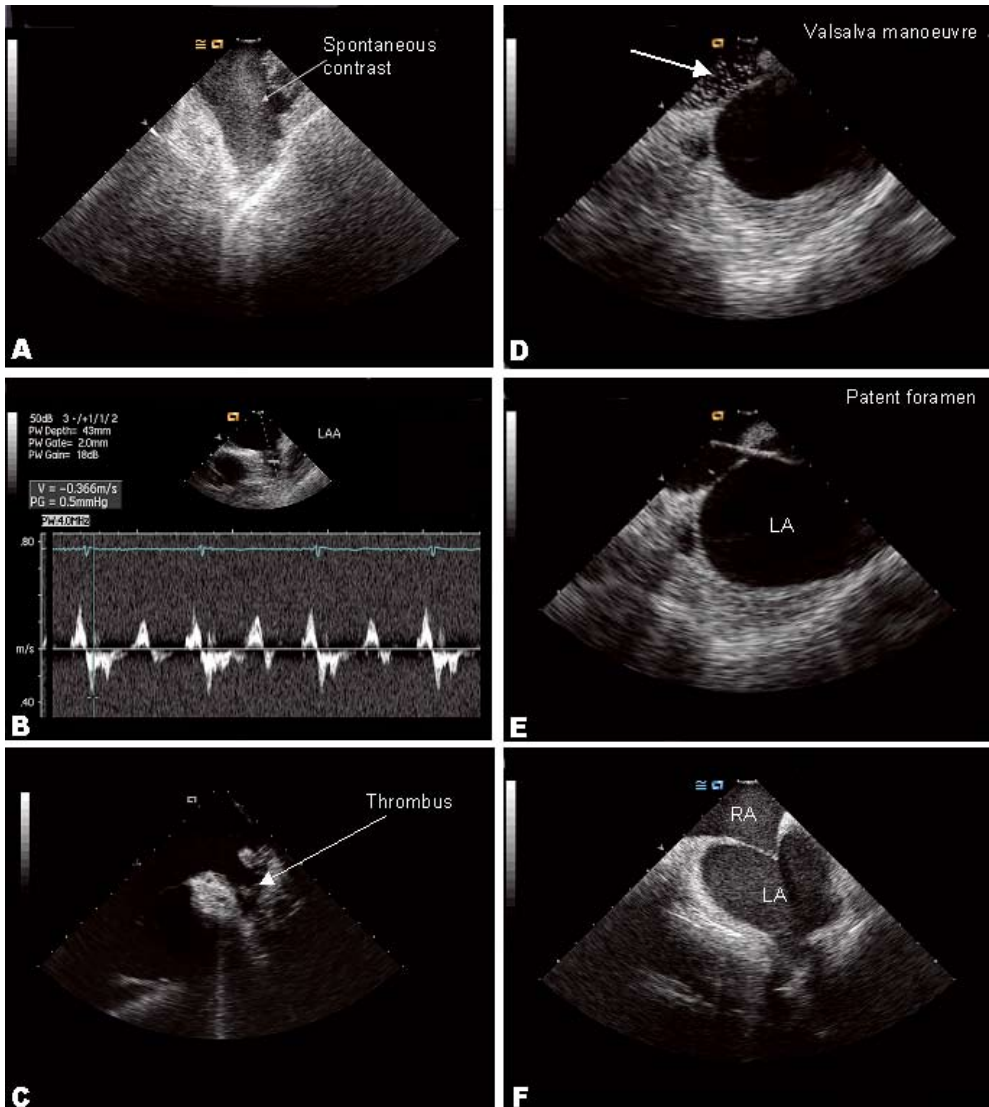


Figure 2

- A. Spontaneous contrast in the LAA, a risk factor for thrombus formation.
 - B. Function of the LAA can be determined with phased array ICE, using pulsed wave Doppler.
 - C. Thrombus in the LAA.
 - D. The Valsalva Manoeuvre is performed prior to transseptal puncture to determine the presence of patent foramen ovale. Contrast bubbles can be observed in the RA (arrow). The lack of bubbles in the LA confirms the presence of a closed foramen.
 - E. The catheter is shifted through the septum through a PFO.
 - F. Tenting of the septum caused by stable contact of the transseptal dilator/needle.
- LA: left atrium, LAA: left atrial appendage, RA: right atrium

the fossa ovalis. The first sign of a stable contact of the transeptal dilator at the oval fossa, is “tenting” of the septum at this site (**Figure 2F**). Successful puncture can be confirmed by the appearance of contrast in the LA after contrast injection. After withdrawal of the needle a mapping/ ablation catheter can be positioned in the LA.

Guidance of closure of atrial septal defect (ASD) and PFO

Percutaneous transcatheter device closure of ASD and PFO has become a safe and efficient alternative to open-heart surgery. Guidance of these procedures by TEE is standard practise and in recent years several studies have reported the feasibility and safety of ICE for guiding these procedures^{9,10}. The closure of atrial septal defects guided by transesophageal echocardiography, *without* use of fluoroscopy has been described. However, although the procedure could be satisfactorily performed in most cases without prolongation of procedure times, patients needed to undergo extensive TEE, and significantly higher doses of sedation were used¹¹. Especially for this application, when long and continuous echocardiography imaging is required, ICE reduces procedure and fluoroscopy times, does not require general anaesthesia and is less discomforting than TEE⁹. During these procedures, ICE is used to determine the size and location of the defect in relation to cardiac anatomy and the presence of rims and septal remnants. Clear visualization of the ASD/PFO, RA, LA, sizing balloon and closure device is feasible with a phased array catheter positioned in the RA (**Figure 3**). Deployment of the device can be evaluated using ICE. Particularly when the remaining part of the septum is floppy, accurate evaluation of the stability of the closure device using Doppler dynamics is necessary before releasing the device.

Guidance of Interventional Electrophysiology Procedures

A. PV isolation procedures

The observation that ectopic foci originating in the PVs can initiate atrial fibrillation¹², has led to the development of percutaneous catheter ablation strategies aimed at ablation at the site of the PVs. Although results are promising, long procedure times and procedure-related complications, such as PV stenosis, are still challenges for improvement. These issues are (in part) related to the fact that the ablation targets, the veno-atrial junctions and the PVs or their ostia, are not easily visualized using fluoroscopy. Furthermore, inter-individual variations in PV anatomy occur, which may require adjustment of the ablation strategy. During PV ablation procedures, ICE can provide information on the individual PV anatomy, such as the number of PVs, the presence of common ostia and of additional PVs, which may influence the ablation strategy in anatomical based isolation procedures¹³ (**Figure 4 A,B**) Furthermore, ICE can be used to guide ablation catheters. In order to deliver optimal radiofrequency energy to the tissue, with a minimum amount of heat loss, a firm contact of the catheter tip with the myocardium must be established. It has been demonstrated that ICE can assure adequate catheter-tip tissue contact in order to achieve transmural ablative lesions¹⁴ and that the use of ICE improves the outcome¹⁵.

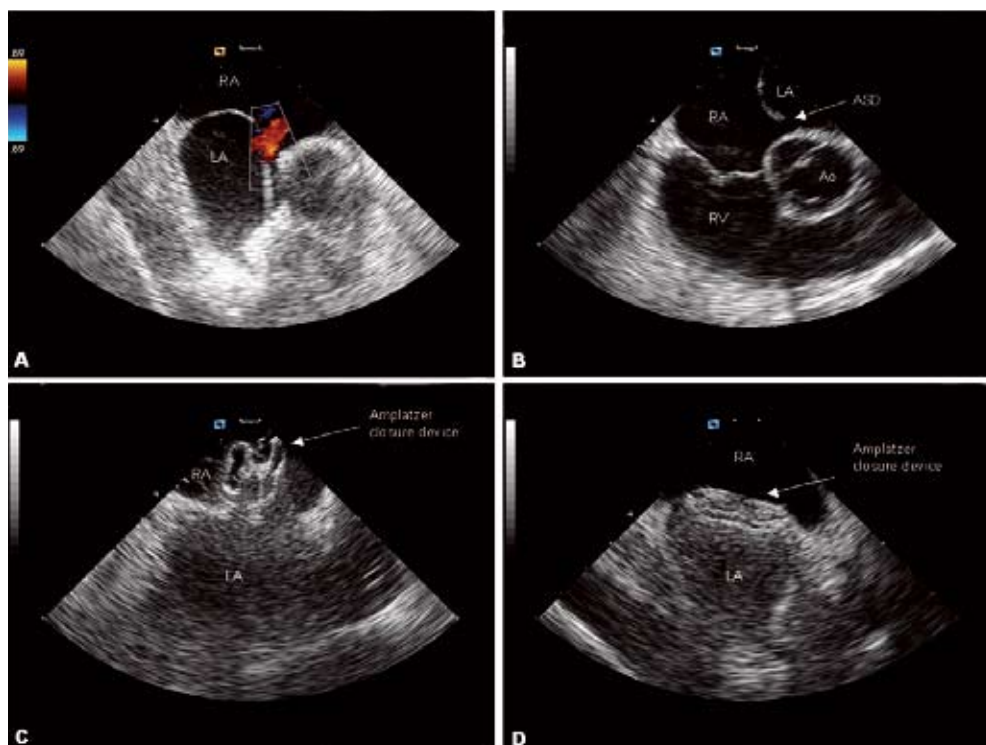


Figure 3

Closure of a atrial septal defect (ASD) under ICE guidance.

A. Colour Doppler demonstrating an ASD located in the inferior part of the atrial septum

B. Relation of the ASD (arrow) to intracardiac structures

C. Positioning of the Amplatzer closure device

D. After several minutes, flattening of the closure device occurs. The device is positioned stable in between the RA and LA.

Ao: aorta, LA: left atrium, RA: right atrium, RV: right ventricle

Another advantage of the use of ICE during these procedures, is the ability to monitor the occurrence of acute complications. Potential complications of ablation at the site of the PVs are: PV stenosis, thrombo-embolic complications, and perforation with pericardial tamponade. Visualisation of *micro-bubble formation* is an important characteristic according to which power-settings of the radiofrequency energy delivery can be adjusted¹⁵, to ensure maximal energy delivery at the lowest risk of PV stenosis (**Figure 4C**). The occurrence of PV stenosis can be monitored by ICE by measuring the ostia of the PV and the systolic and diastolic flow velocities prior to and after catheter ablation. Both colour and pulse Doppler qualities can be used to demonstrate flow in the PV (**Figure 4D**). Although usually increases in PV flow velocities do not give significant symptoms and most patients seem to return to baseline flow characteristics within 3 months, cases have been reported of significant late PV stenosis/occlusion requiring PV stenting¹⁶. In general however, mild to moderate acute changes in ostial diameters and hemodynamic parameters caused by

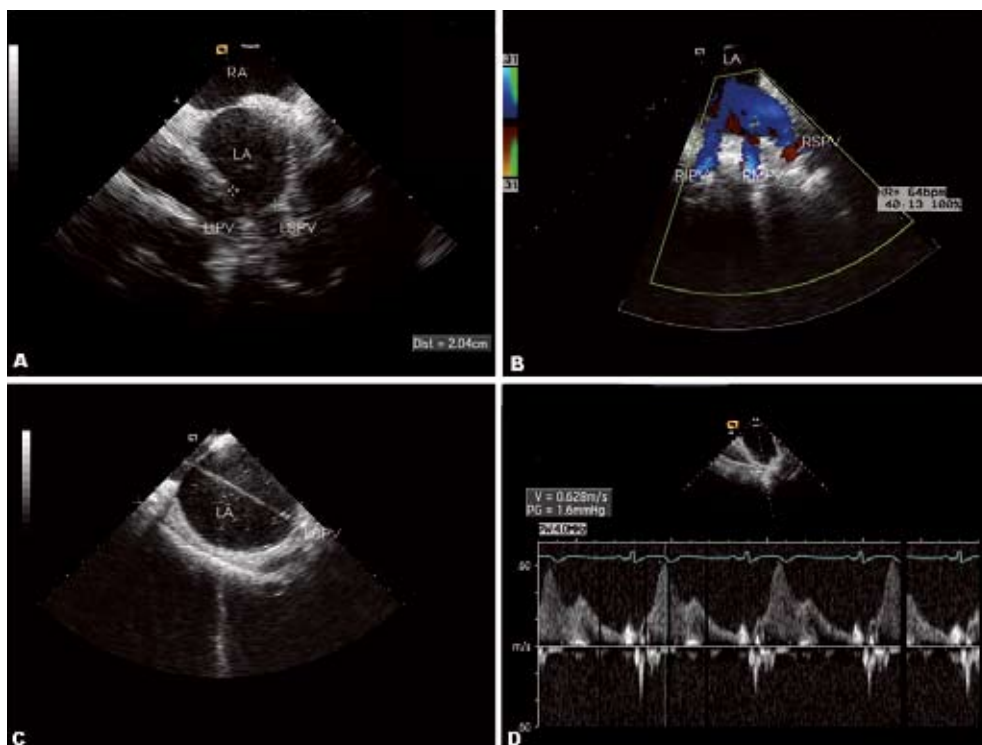


Figure 4

A. Left PVs. There is a common ostium of the left PVs (diameter 2.04 cm).

B. Colour Doppler in the right PVs. Three right PVs are visible.

C. Ablation catheter at ostium of the left superior PV. Note the presence of micro-bubbles, indicating heat loss during ablation.

D. Pulsed wave Doppler measurements of flow in the PVs

LA: left atrium, LIPV: left inferior pulmonary vein, LSPV: left superior pulmonary vein, RA: right atrium,

RSPV: right superior pulmonary vein, RMPV: right middle pulmonary vein, RIPV: right inferior pulmonary vein

acute oedema, do not seem to have significant implications for the occurrence of late PV stenosis¹⁷. A recent report demonstrated the utility of intracardiac Doppler assessment of LA contractile function and reservoir function to predict the outcome of PV isolation¹⁸. Finally, another important reason to consider the use of ICE during ablation procedures in the LA, is that despite anti-coagulation, left atrial thrombus may occur *during* left atrial interventional procedures, usually by attachment of thrombus material to the stable positioned transseptal sheath and/or mapping catheter¹⁹.

B. Complex atrial flutter ablation

Electrophysiological mapping under guidance of ICE has been able to identify the cavo-tricuspid isthmus, Eustachian ridge and the terminal crest as anatomical barriers in atrial flutter, which cannot be visualized using fluoroscopy²⁰. Treatment of atrial flutter is performed by linear ablation at the site of the cavo-tricuspid isthmus, thus creating a line of

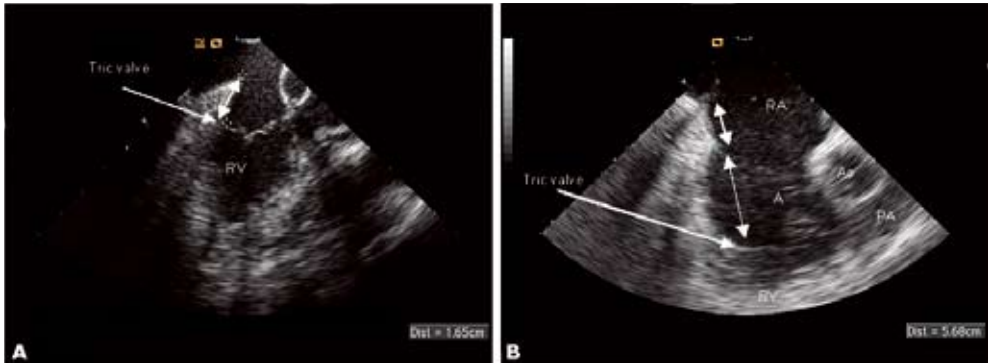


Figure 5

- A. The cavo-tricuspid isthmus (double arrow) demonstrated with ICE as the area in between the inferior caval vein and the tricuspid annulus.
- B. Imaging of the cavo-tricuspid isthmus area in a patient with atrial flutter and Ebstein anomaly. Due to the low insertion of the tricuspid valve leaflet, part of the right ventricle is incorporated in the right atrium (A indicates “atrialized” right ventricle).

Ao: aorta, PA: pulmonary artery, Tric valve: tricuspid valve, RA: right atrium, RV: right ventricle

lesions from the inferior caval vein towards the tricuspid valve annulus (**Figure 5A**). Stable endocardial catheter contact can be confirmed by ICE ²¹. Next to the presence of an atrial flutter circuit based on re-entry around right sided anatomical structures, atrial flutter based on a macro-re-entrant circuit surrounding scar tissue can occur, e.g. in patients treated for congenital heart disease. In these patients, anomalous cardiac anatomy often complicates the treatment of atrial flutter. Particularly in these patients, identification of intracardiac structures using ICE, is useful. **Figure 5B** demonstrates the cavo-tricuspid isthmus area in a patient with Ebstein’s anomaly. Due to the low insertion of the tricuspid valve leaflet, part of the right ventricle is incorporated in the right atrium (length of the “atrialized” ventricle 5.68 cm).

C. Ablation of ventricular tachycardia (VT)

Morphologically altered myocardium, for instance the presence of scar tissue or aneurysms after myocardial infarction, and multiple aneurysms as present in arrhythmogenic right ventricular dysplasia/cardiomyopathy (ARVD/C), is prone to the formation of re-entrant circuits.

The majority of VT’s however is secondary to ischemic heart disease; arrhythmias originate either from extensive scars or ischemic border zones after infarction. The regions with scar formation are frequently akinetic or dyskinetic (aneurysmatic), which can easily be visualized on ICE (**Figure 6**).

Potential complications of VT ablations include thrombo-embolic events, valvular damage, perforation and pericardial tamponade. ICE can be used to guide catheters and for continuous monitoring of complications during VT ablation procedures ^{22 23}. The ability of

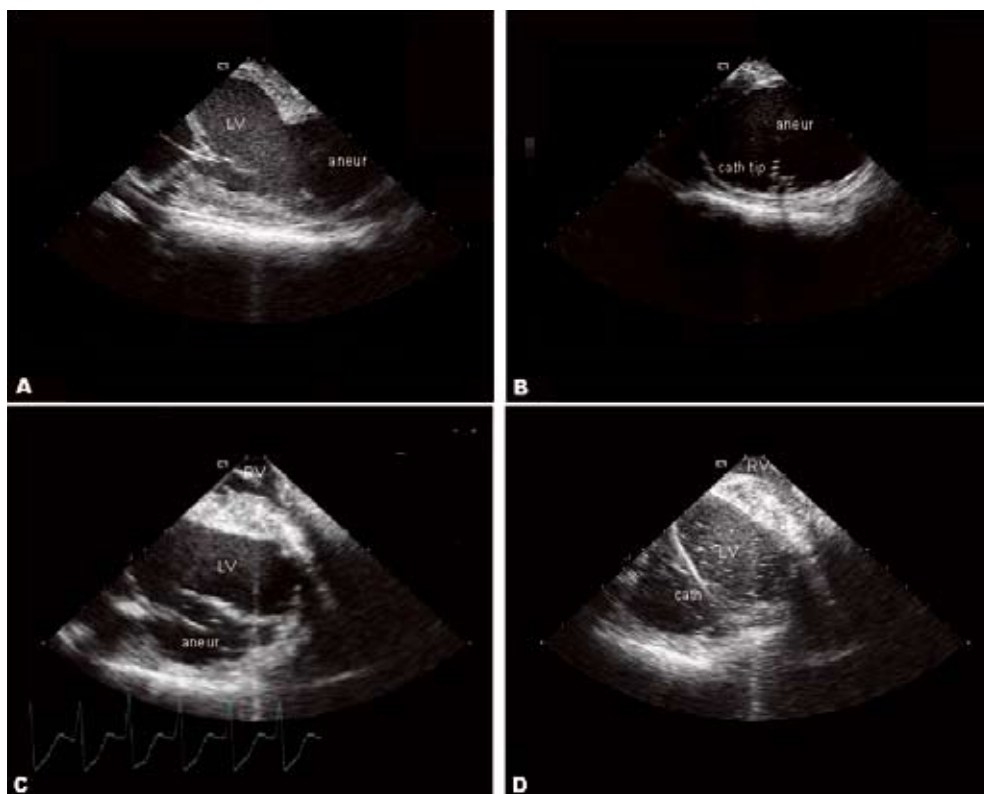


Figure 6

- A. Long axis view of the left ventricle (LV) and an apical LV aneurysm (aneur) in a patient with ventricular tachycardia.
 - B. Ablation catheter at the site of the LV aneurysm (short axis view), demonstrating perpendicular catheter tip-tissue contact
 - C. Postero-basal LV aneurysm
 - D. Microbubble formation during ablation, indicating heat-loss.
- cath tip: catheter tip

phased array ICE catheters to image left sided cardiac structures with the imaging catheter exclusively in the right heart is especially advantageous in patients with dilated ventricles, in order to evaluate the presence of intracardiac thrombus, without the need of arterial or transeptal puncture. Lamberti et al. have reported the use of ICE as an aid in establishing the position and stability of the ablation electrode in relation to the anatomic localization of the VT in the LV outflow tract, thus avoiding the application of RF current to valvular leaflets and coronary arteries ²⁴. **Figure 7A-C** demonstrates ablation of VT originating from the RV outflow tract. Furthermore, ICE can provide additional information to currently used imaging techniques with regard to tissue characterisation in the diagnosis of ARVD/C ²⁵ (**Figure 7D**). Thus the main value of ICE for guiding VT ablation procedures is three-fold: 1) Identification of the substrate, 2) Monitoring of the position of catheters in

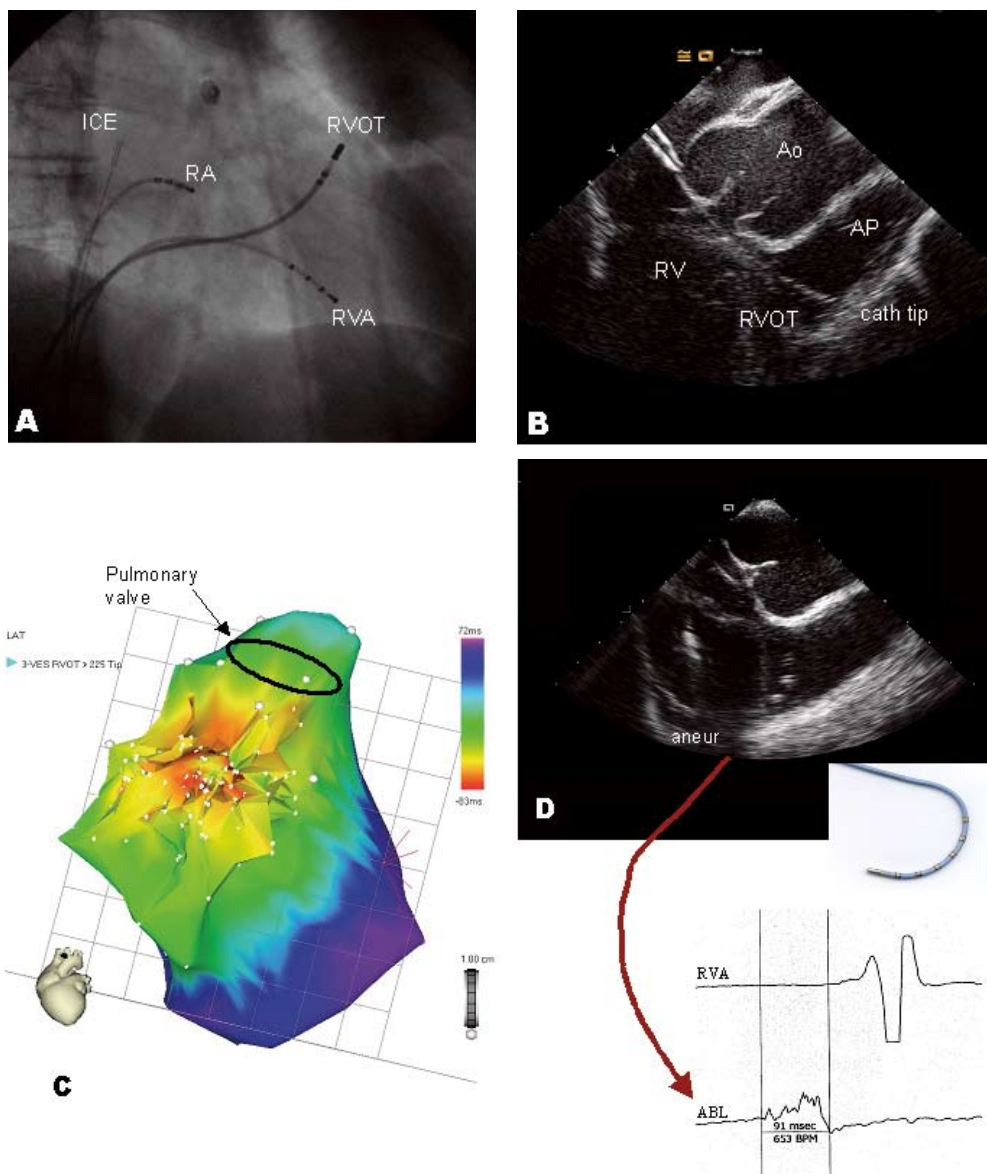


Figure 7

- A. Position of catheters as seen on fluoroscopy in a patient with VT originating from the right ventricular outflow tract (RVOT).
- B. ICE image of the same patient, demonstrating the position of the ablation catheter in the RVOT.
- C. Electro-anatomical map of the right ventricle (RV) (CARTO). The activation of the RV is colour encoded. Red indicates the area of earliest activation in the RVOT.
- D. Imaging in a patient with ventricular tachycardia secondary to ARVD/C. An aneurysmatic area was observed at the inferior part of the RV. Early fragmented signals were recorded at this site during tachycardia and subsequent radiofrequency catheter ablation was initiated at this site.
- aneur: aneurysm, Ao: aorta, AP: pulmonary artery, cath tip: catheter tip, ICE: intracardiac ultrasound catheter, RA: right atrium, RVA: right ventricular apex

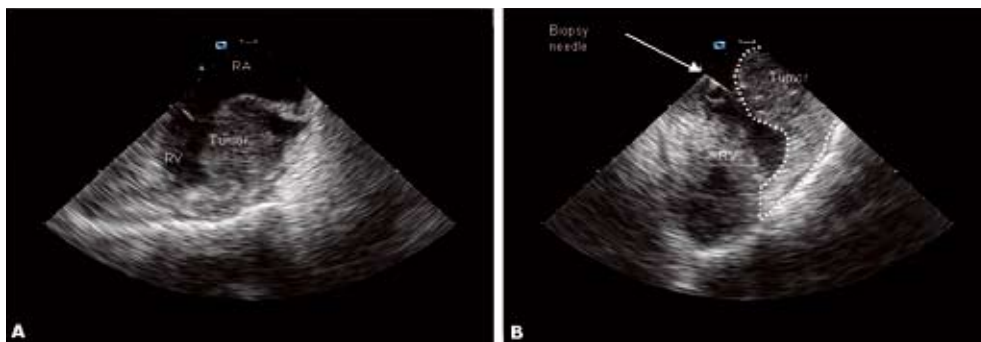


Figure 8

- A. Evaluation of an intracardiac mass by ICE. An extensive mass is present in the RA, which extends over the tricuspid annulus to the wall of the RV.
 B. Biopsies were taken under ICE guidance. The final diagnosis was B-cell Non-Hodgkin lymphoma.
 RA: right atrium, RV: right ventricle

relation to cardiac structures, such as valves and coronary arteries and 3) Direct monitoring of procedure-related complications.

Other Applications

ICE can also be used as a tool to guide diagnostic evaluation of cardiac masses. Using ICE, the extent of the process, its surface and relation to other cardiac structures can be determined. Furthermore, ICE can guide the biopsy needle and monitor acute complications of the biopsy, such as perforation or bleeding²⁶. **Figure 8** demonstrates an example of an extensive intracardiac mass. In this patient, several biopsies were obtained guided by ICE. Furthermore, initial results on the use of ICE in balloon mitral valvuloplasty²⁷, LAA exclusion²⁸ and visualisation of valves in the coronary sinus²⁹ have been reported. It is in the line of expectations that the applications of ICE will expand in accordance with the expanding experience with percutaneous transcatheter procedures.

Summary and Conclusions

With the expanding development of percutaneous interventional procedures in the cathlab, accurate on-line identification of intracardiac structures, catheters and devices is mandatory. At present, the image modality most commonly used in the cathlab is fluoroscopy, which does not allow accurate evaluation of intracardiac structures. Besides TEE, ICE is at present the only imaging modality that can provide this information, combined with hemodynamic information during the procedures. ICE has several clear advantages over the use of TEE, including less patient discomfort, no anaesthesia, allowing communication with the patient during the procedure. Recently ICE has been implemented in a growing

number of interventional procedures. Advantages of the clinical use of ICE are summarized in **Table 2**.

Table 2 Advantages of the clinical use of ICE

- Accurate visualisation of intracardiac anatomy that cannot be visualised using fluoroscopy
- Real-time visualisation of catheters and intracardiac devices
- Direct monitoring of procedure-related complications
- Assessment of hemodynamic function on-line using Doppler capacities
- Reduction of radiation exposure for patient and operators
- No need for anaesthesia

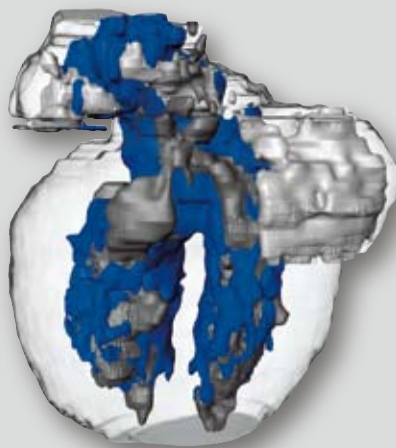
146

In conclusion, ICE is a valuable tool for guiding percutaneous interventional procedures, such as transseptal puncture and placement of closure devices. Efficiency is improved in electrophysiological interventional procedures by the ability to identify anatomical structures and integrate this information with electrophysiological information. Furthermore, ICE can be used as a diagnostic tool. Direct detection of intra-procedural complications, such as pericardial effusion and cardiac tamponade, is possible with ICE, allowing immediate intervention. Integration of ICE in procedures is likely to result in reduction of fluoroscopy and procedure times and improved outcome.

Reference List

1. Dairywala IT, Li P, Liu Z, Bowie D, Stewart SR, Bayoumy AA *et al*. Catheter-based interventions guided solely by a new phased-array intracardiac imaging catheter: in vivo experimental studies. *J.Am.Soc.Echo-cardiogr.* 2002;**15**:150-8.
2. Chu E, Fitzpatrick AP, Chin MC, Sudhir K, Yock PG, Lesh MD. Radiofrequency catheter ablation guided by intracardiac echocardiography. *Circulation* 1994;**89**:1301-5.
3. Antonielli E, Pizzuti A, Palinkas A, Tanga M, Gruber N, Michelassi C *et al*. Clinical value of left atrial appendage flow for prediction of long- term sinus rhythm maintenance in patients with nonvalvular atrial fibrillation. *J.Am.Coll.Cardiol.* 2002;1443-9.
4. Morton JB, Sanders P, Sparks PB, Morgan J, Kalman JM. Usefulness of phased-array intracardiac echocardiography for the assessment of left atrial mechanical “stunning” in atrial flutter and comparison with multiplane transesophageal echocardiography(*). *Am.J.Cardiol.* 2002;**90**:741-6.
5. Thakur RK, Klein GJ, Yee R, Zardini M. Embolic complications after radiofrequency catheter ablation. *Am.J.Cardiol.* 1994;**74**:278-9.
6. Kok LC, Mangrum JM, Haines DE, Mounsey JP. Cerebrovascular complication associated with pulmonary vein ablation. *J.Cardiovasc.Electrophysiol.* 2002;**13**:764-7.
7. Lundqvist C, Olsson SB, Varnauskas E. Transseptal left heart catheterization: a review of 278 studies. *Clin.Cardiol.* 1986;**9**:21-6.
8. Epstein LM, Smith T, TenHoff H. Nonfluoroscopic transseptal catheterization: safety and efficacy of intracardiac echocardiographic guidance. *J.Cardiovasc.Electrophysiol.* 1998;**9**:625-30.
9. Bartel T, Konorza T, Arjumand J, Ebradlidze T, Eggebrecht H, Caspari G *et al*. Intracardiac echocardiography is superior to conventional monitoring for guiding device closure of interatrial communications. *Circulation* 2003;**107**:795-7.

10. Earing MG, Cabalka AK, Seward JB, Bruce CJ, Reeder GS, Hagler DJ. Intracardiac echocardiographic guidance during transcatheter device closure of atrial septal defect and patent foramen ovale. *Mayo Clin.Proc.* 2004;**79**:24-34.
11. Ewert P, Berger F, Daehner I, van Wees J, Gittermann M, Abdul-Khaliq H *et al.* Transcatheter closure of atrial septal defects without fluoroscopy: feasibility of a new method. *Circulation* 2000;**101**:847-9.
12. Haissaguerre M, Jais P, Shah DC, Takahashi A, Hocini M, Quiniou G *et al.* Spontaneous initiation of atrial fibrillation by ectopic beats originating in the pulmonary veins. *N.Engl.J.Med.* 1998;**339**:659-66.
13. Jongbloed MR, Bax JJ, Zeppenfeld K, van der Wall EE, Schalij MJ. Anatomical observations of the pulmonary veins with intracardiac echocardiography and hemodynamic consequences of narrowing of pulmonary vein ostial diameters after radiofrequency catheter ablation of atrial fibrillation. *Am.J.Cardiol.* 2004;**93**:1298-302.
14. Olgin JE, Kalman JM, Chin M, Stillson C, Maguire M, Ursel P *et al.* Electrophysiological effects of long, linear atrial lesions placed under intracardiac ultrasound guidance. *Circulation* 1997;**96**:2715-21.
15. Marrouche NF, Martin DO, Wazni O, Gillinov AM, Klein A, Bhargava M *et al.* Phased-array intracardiac echocardiography monitoring during pulmonary vein isolation in patients with atrial fibrillation: impact on outcome and complications. *Circulation* 2003;**107**:2710-6.
16. Ernst S, Ouyang F, Goya M, Lober F, Schneider C, Hoffmann-Riem M *et al.* Total pulmonary vein occlusion as a consequence of catheter ablation for atrial fibrillation mimicking primary lung disease. *J.Cardiovasc.Electrophysiol.* 2003;**14**:366-70.
17. Saad EB, Cole CR, Marrouche NF, Dresing TJ, Perez-Lugones A, Saliba WI *et al.* Use of intracardiac echocardiography for prediction of chronic pulmonary vein stenosis after ablation of atrial fibrillation. *J.Cardiovasc.Electrophysiol.* 2002;**13**:986-9.
18. Verma A, Marrouche NF, Yamada H, Grimm RA, Cummings J, Burkhardt JD *et al.* Usefulness of intracardiac Doppler assessment of left atrial function immediately post-pulmonary vein antrum isolation to predict short-term recurrence of atrial fibrillation. *Am.J.Cardiol.* 2004;**94**:951-4.
19. Ren JF, Marchlinski FE, Callans DJ. Left atrial thrombus associated with ablation for atrial fibrillation: identification with intracardiac echocardiography. *J.Am.Coll.Cardiol.* 2004;**43**:1861-7.
20. Olgin JE, Kalman JM, Fitzpatrick AP, Lesh MD. Role of right atrial endocardial structures as barriers to conduction during human type I atrial flutter. Activation and entrainment mapping guided by intracardiac echocardiography. *Circulation* 1995;**92**:1839-48.
21. Chu E, Kalman JM, Kwasmann MA, Jue JC, Fitzgerald PJ, Epstein LM *et al.* Intracardiac echocardiography during radiofrequency catheter ablation of cardiac arrhythmias in humans. *J.Am.Coll.Cardiol.* 1994;**24**:1351-7.
22. Callans DJ, Ren JF, Narula N, Michele J, Marchlinski FE, Dillon SM. Effects of linear, irrigated-tip radiofrequency ablation in porcine healed anterior infarction. *J.Cardiovasc.Electrophysiol.* 2001;**12**:1037-42.
23. Jongbloed MR, Bax JJ, van der Burg AE, van der Wall EE, Schalij MJ. Radiofrequency catheter ablation of ventricular tachycardia guided by intracardiac echocardiography. *Eur.J.Echocardiogr.* 2004;**5**:34-40.
24. Lamberti F, Calo' L, Pandozi C, Castro A, Loricchio ML, Boggi A *et al.* Radiofrequency catheter ablation of idiopathic left ventricular outflow tract tachycardia: utility of intracardiac echocardiography. *J.Cardiovasc.Electrophysiol.* 2001;**12**:529-35.
25. Peters S, Brattstrom A, Gotting B, Trummel M. Value of intracardiac ultrasound in the diagnosis of arrhythmogenic right ventricular dysplasia-cardiomyopathy. *Int.J.Cardiol.* 2002;**83**:111-7.
26. Segar DS, Bourdillon PD, Elsner G, Kesler K, Feigenbaum H. Intracardiac echocardiography-guided biopsy of intracardiac masses. *J.Am.Soc.Echocardiogr.* 1995;**8**:927-9.
27. Salem MI, Makaryus AN, Kort S, Chung E, Marchant D, Ong L *et al.* Intracardiac echocardiography using the AcuNav ultrasound catheter during percutaneous balloon mitral valvuloplasty. *J.Am.Soc.Echocardiogr.* 2002;**15**:1533-7.
28. Nakai T, Lesh MD, Gerstenfeld EP, Virmani R, Jones R, Lee RJ. Percutaneous left atrial appendage occlusion (PLAATO) for preventing cardioembolism: first experience in canine model. *Circulation* 2002;**105**:2217-22.
29. Cohen TJ, Juang G. Utility of intracardiac echocardiography to facilitate transvenous coronary sinus lead placement for biventricular cardioverter-defibrillator implantation. *J.Invasive.Cardiol.* 2003;**15**:685-6.



Chapter

7

Monique R.M. Jongbloed

Jeroen J. Bax

Katja Zeppenfeld

Ernst E. van der Wall

Martin J. Schalij

Dept. of Cardiology, Leiden University Medical Center, Leiden, The Netherlands

Anatomical observations of the Pulmonary Veins
with Intracardiac Echocardiography and
Hemodynamic Consequences of Narrowing of
Pulmonary Vein Ostial Diameters
after Radiofrequency Catheter Ablation of
Atrial Fibrillation

Modified after
Am J Cardiol. 2004 May;93(10):1298-302

Abstract

Radiofrequency catheter ablation (RFCA) at the ostia of the pulmonary veins (PV) may cure atrial fibrillation. Variations in PV anatomy may complicate RFCA and the procedure carries a risk of pulmonary vein stenosis. Intracardiac echocardiography (ICE) was used to explore PV anatomy and to monitor PV stenosis in 31 patients (age 51 ± 9 yrs) referred for RFCA at PV ostia. Prior to RFCA PV anatomy was evaluated by ICE. PV ostia and flow velocities were measured pre and post RFCA. A common ostium of the left and right PV was observed in 22(71%) and 10(32%) patients respectively. Additional right PV were observed in 6(19%) patients. Two patients were not treated with RFCA because of suspicion of intracardiac thrombus and in one patient transseptal puncture could not be performed because of an aneurysmatic septum. In the 28 patients treated, mean ostial diameters of right superior PV and common ostia of left PV were significantly smaller after RFCA (14.5 ± 3.1 vs. 13.4 ± 2.9 , $p < 0.01$ and 23.4 ± 4.7 vs. 21.3 ± 3.1 , $p < 0.05$ respectively). For the other veins, ostial diameters were slightly but not significantly smaller. Mean systolic peak flow velocities in PV after RFCA were not significantly higher in any of the veins, although there was a positive trend. In conclusion, ICE can be used to observe interindividual variations in number and insertion of pulmonary veins, which may be of relevance for determination of the ablation strategy. Although oedema inflicted by radiofrequency-current may cause diameter reduction of pulmonary vein ostia, this may not have significant hemodynamic consequences.

Introduction

Atrial fibrillation is the most common arrhythmia and its prevalence increases with age. Since the recognition that atrial fibrillation may originate from the pulmonary veins in the majority of cases, several treatment strategies have been developed such as radiofrequency catheter ablation (RFCA) at the site of the pulmonary veins¹. During these procedures, radiofrequency current may be used to either eliminate pulmonary venous ectopic foci inside pulmonary veins², or to create circular lesions surrounding pulmonary venous ostia³. Although acute success rates are reasonable, recurrence of atrial fibrillation may necessitate multiple ablation sessions¹. Furthermore, RFCA inside the pulmonary veins or at their ostia may cause pulmonary vein or ostial stenosis, which is asymptomatic in a large number of patients, but may evolve into serious symptoms requiring pulmonary venous stenting⁴.

In order to prevent pulmonary vein stenosis, accurate visualization of the catheter tip in relation to the pulmonary venous ostium is mandatory, which cannot be performed by fluoroscopy alone. Intracardiac echocardiography (ICE) has been used to successfully guide catheters during RFCA of the pulmonary veins or their ostia⁵, and to monitor the occurrence of acute pulmonary vein stenosis after RFCA at the site of the pulmonary veins^{6,7}. In the current study, we have examined the feasibility of ICE to evaluate left atrial and pulmonary vein anatomy prior to RFCA, to guide RFCA surrounding pulmonary venous ostia, and to evaluate the hemodynamic consequences of RFCA at the site of the pulmonary veins.

Methods

Patients: The study population consisted of 31 consecutive patients (age 51±9 years, 25 men) with symptomatic drugrefractory atrial fibrillation who were referred for RFCA encircling the pulmonary vein ostia, in order to isolate the pulmonary veins electrically from the left atrium. Patient characteristics are described in **Table 1**.

ICE: ICE was performed with an Acunav™ Diagnostic Ultrasound Catheter, connected to a Sequoia® ultrasound system (Acuson Corporation, Mountain View, California). The ultrasound catheter consists of a miniaturized 64-element, phased array transducer, which is incorporated in a 10 French single use catheter. The transducer scans in the longitudinal monoplane, providing a 90° two-dimensional sector. Two planes of bi-directional steering (anterior-posterior and left-right, each in a direction of 160 degrees) are possible by using a mechanism on the handle of the catheter. Measurements of hemodynamic and physiologic variables can be performed using Doppler imaging. A high resolution multiple frequency transducer (5-10 MHz) allows tissue penetration enhancement, thus allowing

Table 1 Patient characteristics

Number of patients	31
Sex	25 male, 6 female
Age (years)	51±9 (range 31-68)
Atrial fibrillation	
<i>Paroxysmal</i>	17
<i>Persistent</i>	10
<i>Permanent</i>	4
Duration of atrial fibrillation (years)	5±4 (range 1-25 years)
NYHA class 1/2	31
NYHA class 3/4	-
Mean number of anti-arrhythmic drugs used	3.8±1.6
Amiodarone (number of patients)	23

NYHA: New York Heart Association

152

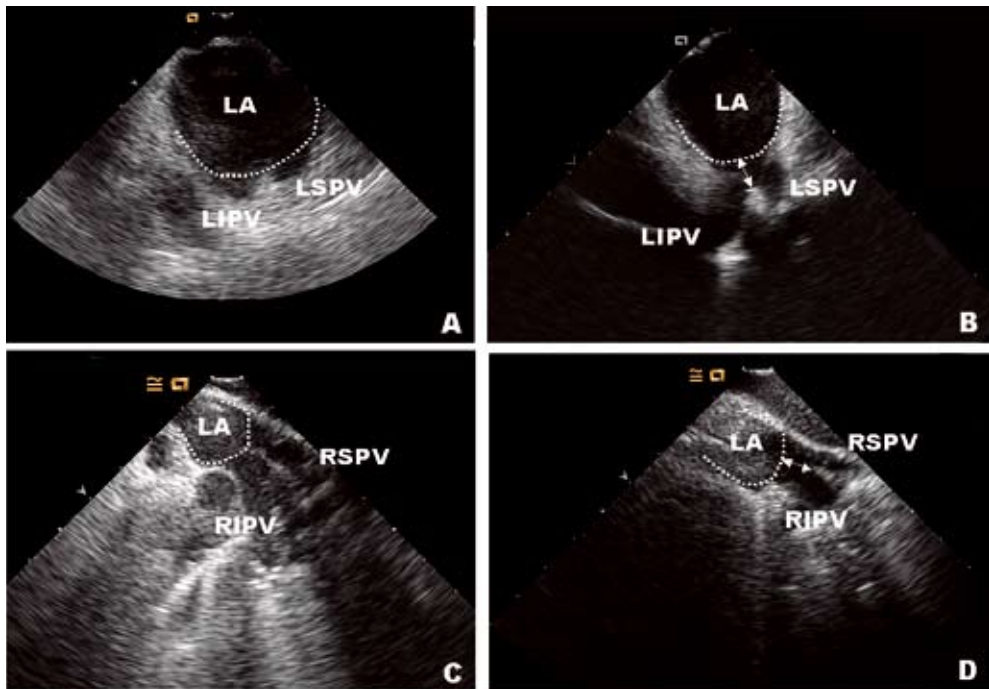


Figure 1

Evaluation of the insertion of the left and right pulmonary veins. A virtual line following the left atrial contour was drawn to indicate the border between the left atrium and the pulmonary veins, indicated by the dotted line.

- A. Separate ostial insertion of the left pulmonary veins. Atrial tissue can be distinguished between the upper and lower pulmonary veins.
- B. Common ostium of the left pulmonary veins. A common truncal part, indicated by the double arrow, can be distinguished between the left atrial border, indicated by the dotted line, and the bifurcation of both pulmonary veins.
- C. Separate ostium of the right pulmonary veins.
- D. Common truncal part (double arrow) of the right pulmonary veins.

LA: left atrium, LSPV: left superior pulmonary vein, LIPV: left inferior pulmonary vein, RSPV: right superior pulmonary vein, RIPV: right inferior pulmonary vein

depth control. Imaging of the left atrium and pulmonary veins can thus be performed with the ultrasound catheter positioned in the right atrium. The ultrasound catheter was inserted through the left femoral vein, using a 10 French introducer, and positioned in the right atrium. Fluoroscopy was used to guide the catheter into the right atrium. At initiation of all RFCA procedures, left atrial and pulmonary vein anatomy were explored with ICE. Ostial insertion was described as either “separate ostia” or, when a common truncal part of the upper and lower pulmonary veins was observed, the insertion was described as “common ostium”. The border between the left atrium and the pulmonary veins was determined by extrapolating the left atrial contour and drawing a line at the atriovenous junction (**Figure 1**). Attention was further paid to the presence of additional pulmonary veins. Measurements of pulmonary venous ostia and flow velocities at the ostia were performed before and after RFCA to evaluate diameter reduction and hemodynamic consequences of RFCA.

Transseptal puncture: Before transseptal puncture, the presence of intracardiac thrombus was examined by ICE. After excluding intracardiac thrombi, the ICE transducer was directed towards the interatrial septum in order to visualize the fossa ovalis. The presence of a patent foramen was investigated by the injection of saline during the Valsalva manoeuvre after which the passage of bubbles to the left atrium was evaluated. In the absence of a patent foramen, a standard transseptal puncture was performed by directing a transseptal needle towards the fossa ovalis guided by ICE. An 8 French mapping/ablation catheter (Biosense Navistar, Diamond Bar, CA, U.S.A.) was subsequently positioned in the left atrium. A 6 French diagnostic catheter was positioned in the right atrium and served as reference catheter.

Radiofrequency catheter ablation: RFCA was aimed at electrical isolation of the pulmonary veins from the left atrium by creating circumferential lesions at approximately 5 mm from the pulmonary vein ostia. Data obtained by ICE were used to determine the ablation strategy. When a common ostium was present, these lesions were targeted to form a circular lesion around the common ostium. Additional veins observed by ICE were targeted for RFCA as well. Furthermore, a linear ablation lesion was created in between the left and right superior pulmonary veins and at the left isthmus between the mitral valve and the left inferior pulmonary vein. Temperature controlled (maximum temperature setting 60°C) radiofrequency current was applied via a Stockert generator at each ablation point for 30 seconds. A 3-D non-fluoroscopic mapping system (CARTO, Biosense Webster, Diamond Bar, CA, USA) was used to tag pulmonary veins, to acquire electrophysiological information and to mark ablation points. All patients received heparin (activated clotting time > 300 seconds, checked hourly) to reduce the risk of thrombo-embolic complications. Electrical isolation of the pulmonary veins was confirmed by pacing from the coronary sinus and the pulmonary veins. The procedure was considered successful when there was

no capture after pacing in the coronary sinus in the pulmonary veins and when the patient was in sinus rhythm after the procedure. During the RFCA-procedure the monitors of ICE, fluoroscopy and the CARTO system were situated side-by-side opposite the operator, to allow comparison and integration of these techniques.

Statistical analysis: Data are expressed as mean \pm SD. Continuous variables were compared using the paired independent Student's t-test. A P-value <0.05 was considered significant.

154

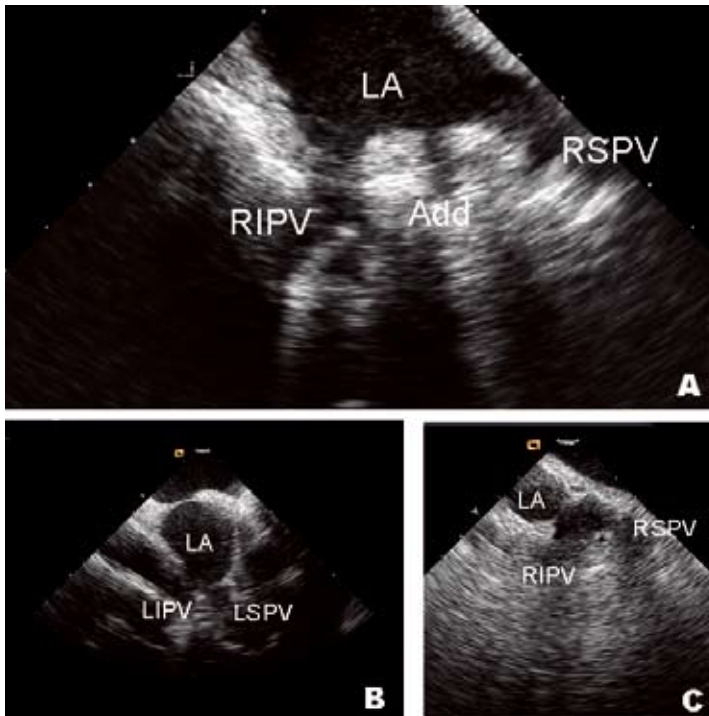


Figure 2

A. Additional right pulmonary vein (diameter 0.47 cm) situated in between the right superior (diameter 1.05 cm) and inferior (diameter 1.10 cm) pulmonary veins.

B. A common ostium of the left pulmonary veins.

C. Common ostium of the right pulmonary veins.

Add: additional right pulmonary vein, LA: left atrium, LSPV: left superior pulmonary vein, LIPV: left inferior pulmonary vein, RSPV: right superior pulmonary vein, RIPV: right inferior pulmonary vein

Results

Anatomical observations: In 31 patients a total of 130 pulmonary veins were observed. Additional right pulmonary veins were observed only on the right side (**Figure 2A**). ICE provided a longitudinal view of the left pulmonary veins in all patients, whereas either a sagittal or longitudinal view could be obtained of the right pulmonary veins. When only a sagittal view was obtained, insertion of right pulmonary veins in the left atrium was more difficult to evaluate. A common truncal part of the left or right pulmonary veins of varying distance could be observed in the majority of patients. An example of a patient with a common truncal part of the left pulmonary veins and an example of a common ostium of the right pulmonary veins is demonstrated in **Figure 2B and 2C**. Results of anatomical observations are summarized in **Table 2**.

Measurements of pulmonary venous ostia and systolic peak flow velocities prior to RFCA: Ostial diameters of right pulmonary veins were comparable with those of left pulmonary veins. Mean diameters for common ostia were larger than ostia of separate veins. Results of measurements of pulmonary vein ostia are listed in **Table 3**.

RFCA: Eventually 28 of 31 patients were treated with left-sided RFCA. In 2 patients there was an enlarged left atrium with spontaneous echo contrast and strong suspicion of the presence of a thrombus in the left atrial appendage as observed by ICE. In these patients transseptal puncture was not performed and alternative treatment for atrial fibrillation was considered. In one patient there was a thin, aneurysmatic atrial septum, which made transseptal puncture not feasible and RFCA was not performed. A patent foramen ovale was observed in 3 patients and transseptal puncture was performed in 25 patients in order to gain access to the left atrium. RFCA was targeted at the ostia of all pulmonary veins, including the additional veins identified with ICE. When a common ostium was identified with ICE, the ablation points were targeted surrounding the common truncal area of both veins (**Figure 3**). Mean number of ablation points was 73 ± 26 per patient.

Table 2 Anatomical results

Total number of observed pulmonary veins	130
Mean number of pulmonary veins per patient	4
Total number of observed ostia	95
Pts with additional right pulmonary veins	6(19%)
Pts with additional left pulmonary veins	0
Pts with common ostium right pulmonary veins	10(32%)
Pts with common ostium left pulmonary veins	22(71%)

Table 3 *Diameters ostia pulmonary veins and systolic flow velocities measured with intracardiac echocardiography pre-and post radiofrequency catheter ablation*

Variable	Diameter ostia pre-ablation (mm)	Diameter ostia post-ablation (mm)	P	Systolic peak flow velocity pre-ablation (cm/s)	Systolic peak flow velocity post-ablation (cm/s)
Left superior pulmonary vein	15±4	13±3	NS	44±11	49±13
Left inferior pulmonary vein	15±3	13±3	0.054	45±13	50±10
Right superior pulmonary vein	15±5	14±3	0.001	47±17	50±14
Right inferior pulmonary vein	15±5	15±4	NS	39±9	43±12
Common ostium left pulmonary veins	23±5	21±3	0.04	38±13	53±28
Common ostium right pulmonary veins	19±5	19±5	NS	42±13	42±11

RFCA: radiofrequency catheter ablation
NS: not significant

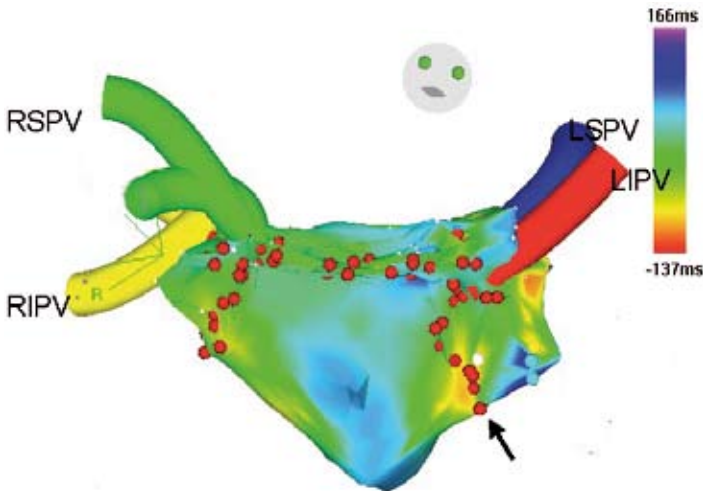


Figure 3

CARTO image after RFCA. The left and right right pulmonary veins are depicted, as well early branches of the right pulmonary veins. Ablation points are depicted by red dots. Ablation points have been placed in a wide circle around the left and right pulmonary veins. There is a common ostium of the left pulmonary veins. Furthermore, a line of ablation lesions is present at the roof of the atrium between the right and left superior pulmonary veins and towards the mitral annulus (arrow). RSPV: right superior pulmonary vein, RIPV: right inferior pulmonary vein, LSPV: left superior pulmonary vein, LIPV: left inferior pulmonary vein.

Measurements of pulmonary venous ostia and systolic peak flow velocities after RFCA: After the ablation procedure, overall measurements of ostial diameters were smaller when compared to diameters obtained prior to RFCA (Table 3, Figure 4 – upper panel). The ostia of the right superior pulmonary veins and the common ostia of the left pulmonary veins were statistically significant smaller after RFCA ($p < 0.001$, $p < 0.05$ respectively). The ostium of the left inferior pulmonary vein after RFCA tended to be smaller then before RFCA ($p = 0.05$).

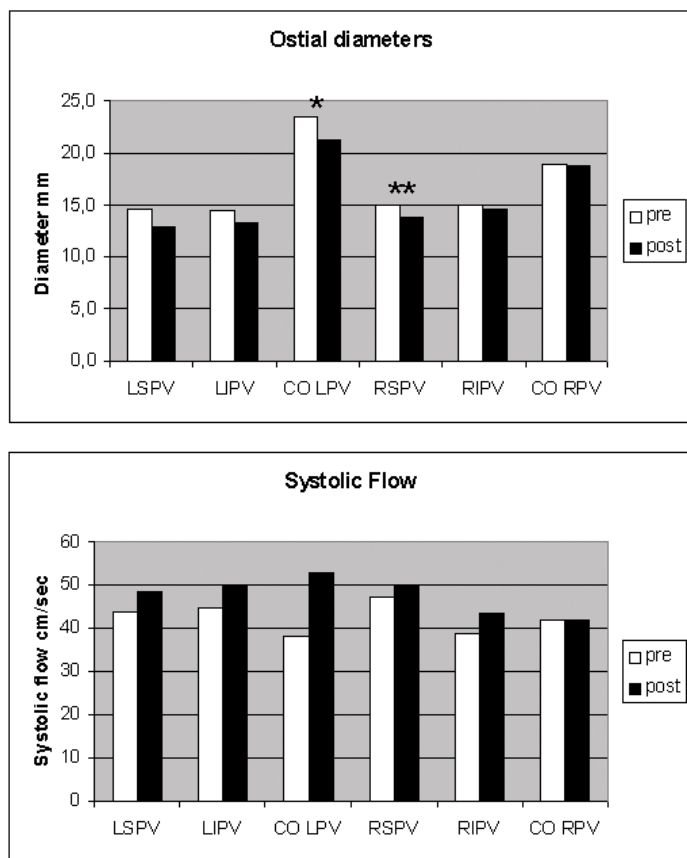


Figure 4

Pulmonary venous ostial diameters and systolic peak flow velocities pre-and post RFCA. Common ostia of left pulmonary veins and the ostia of right superior pulmonary veins after ablation were statistically significant smaller.

Peak systolic flow velocities tended to be higher after RFCA, although not significant.

LSPV: left superior pulmonary vein, LIPV: left inferior pulmonary vein, CO LPV: common ostium left pulmonary veins, RSPV: right superior pulmonary vein, RIPV: right inferior pulmonary vein, CO RPV: common ostium right pulmonary veins.

* $p < 0.05$, ** $p < 0.001$

Similarly, mean overall flow velocity measured at the ostia of the pulmonary veins was slightly higher after RFCA compared with values prior to RFCA. However, these differences were not statistically significant (**Table 2, Figure 4 – lower panel**). Examples of measurements of pulmonary vein ostia and systolic peak flow velocities prior to and after RFCA, are demonstrated in **Figure 5**.

After the procedure no signs of pericardial effusion were detected with ICE. Mean procedure time was 268 ± 79 minutes and fluoroscopy time 51 ± 15 minutes. After the RFCA procedure 26/28 (93%) patients were in sinus rhythm and 20/28 (71 %) after 9.2 ± 5.4 months (range 4-20 months) of follow up. During outpatient visits no patients reported symptoms suggestive of pulmonary vein stenosis.

158

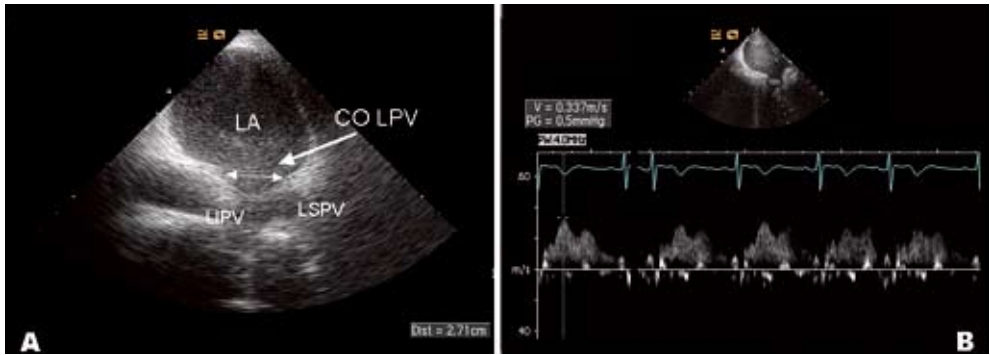


Figure 5
Measurements at the level of the common ostium of the left pulmonary veins (A) and systolic peak flow velocity (B)
LA: left atrium, LSPV: left superior pulmonary vein, LIPV: left inferior pulmonary vein, CO LPV: common ostium left pulmonary veins

Discussion

In the current study we evaluated pulmonary vein and left atrial anatomy and the occurrence of pulmonary vein stenosis in a patient population treated by RFCA using an ostial approach. Main observations in this study were: 1) the occurrence of interindividual anatomical variations in pulmonary venous anatomy and insertion in the left atrium, 2) the occurrence of pulmonary venous ostial narrowing after RFCA and 3) the lack of significant hemodynamic changes in systolic peak flow velocity in pulmonary veins after RFCA compared to velocities prior to RFCA.

The use of ICE for guiding left atrial interventional electrophysiological procedures, has been described previously^{5,8}. During these procedures, ICE can be used to explore the left atrium and pulmonary vein anatomy and to evaluate the presence of left atrial thrombi prior to the procedure. In our population, two patients were excluded from left atrial ablation because of strong suspicion of intracardiac thrombus, which had not been observed with transthoracic echocardiography prior to RFCA. Furthermore, ICE can be used to guide transseptal puncture in order to gain access to the left atrium^{9,10}. The application of radiofrequency current targeted outside the pulmonary venous ostium is not feasible using fluoroscopy alone, unless repeated contrast injection is supplied¹¹. Using ICE, the pulmonary venous insertion in the left atrium can be visualised continuously, thus reducing the need for fluoroscopy and administration of intravenous contrast.

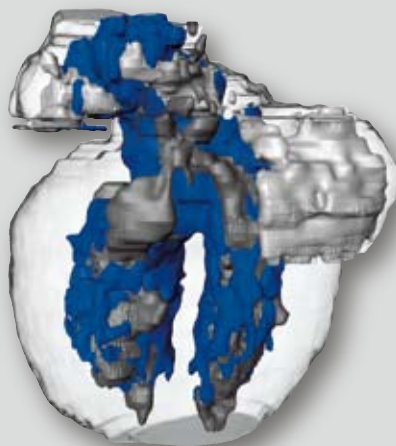
Variations in number and insertion of pulmonary veins have been described in anatomical studies^{12,13} as well as in clinical studies using ICE^{8,11,14}. A limitation of the evaluation of pulmonary venous insertion is the lack of anatomical boundaries identifying the exact border between the left atrium and the pulmonary veins. In our study, we used the extrapolated border of the left atrium as boundary between the LA and the pulmonary veins (Figure 1). In our study, a common truncal part of left pulmonary veins was visualized in 71% and of right pulmonary veins in 31% of patients. Additional right pulmonary veins were observed in 19%. The occurrence of right-sided additional veins can probably be linked to drainage of the right middle lung lobe. The recognition of variations in pulmonary vein anatomy may have implications for the RFCA-strategy. The pulmonary venous wall consists of a thin endothelium, a media of smooth muscle and fibrous tissue and a thick adventitia. Muscular sleeves of different lengths may extend distally in the veins¹³. The pulmonary venous wall is more sensitive to damage inflicted by the application of RF current than the atrial myocardium. Consequently, pulmonary vein stenosis is a major complication of RFCA in the pulmonary veins¹⁵, and pericardial effusion with cardiac tamponade due to perforation has been described¹⁶. Therefore, an increasing number of operators choose for an approach that aims at applying RF current outside the pulmonary venous ostia. In patients with a common truncal part of the pulmonary veins, the application of RF lesions in a large circle surrounding the common ostium, may be a more safe procedure than targeting both veins separately, which carries a risk of damaging the vessel wall. Furthermore, the pres-

ence of electrical connections between pulmonary veins has been described, in which case isolation of contiguous separate veins or additional veins is required to achieve successful disconnection¹⁷. The application of RF current may cause the formation of oedema of the myocardium or the vessel wall¹⁸, which may lead to several degrees of acute stenosis^{7,19}. However, this stenosis caused by the formation of acute oedema does not seem to be a predictor of the occurrence of chronic stenosis^{6,7}, and swelling usually resolves within 4 weeks¹⁸. Furthermore, as was demonstrated in the current study, even the occurrence of statistically significant acute stenosis (as evidenced by significant diameter reduction of the PV ostium) may not have significant hemodynamic consequences, since a statistically significant increase in pulmonary venous systolic peak flow velocities measured at the ostia after RFCA was not observed. In our study, late follow-up imaging after RFCA was not performed. However, at mean late follow-up, none of the patients expressed symptoms suggestive for pulmonary vein stenosis.

In conclusion, ICE is a safe and feasible method to guide RFCA outside pulmonary venous ostia. ICE can be used to explore left atrial and pulmonary vein anatomy, guide trans-septal puncture, to guide catheters at the pulmonary venous ostia and to continuously monitor the occurrence of acute complications. Interindividual variations in number of pulmonary veins and the insertion in the left atrium occur, which may be of relevance for determination of the ablation strategy. Although oedema inflicted by the application of radiofrequency-current at pulmonary venous ostia may cause acute significant anatomical diameter reduction of pulmonary vein ostia, this may not have significant hemodynamic consequences.

Reference List

1. Haissaguerre M, Jais P, Shah DC, Takahashi A, Hocini M, Quiniou G *et al.* Spontaneous initiation of atrial fibrillation by ectopic beats originating in the pulmonary veins. *N.Engl.J.Med.* 1998;**339**:659-66.
2. Haissaguerre M, Jais P, Shah DC, Garrigue S, Takahashi A, Lavergne T *et al.* Electrophysiological end point for catheter ablation of atrial fibrillation initiated from multiple pulmonary venous foci. *Circulation* 2000;**101**:1409-17.
3. Pappone C, Rosanio S, Oreto G, Tocchi M, Gugliotta F, Vicedomini G *et al.* Circumferential radiofrequency ablation of pulmonary vein ostia: A new anatomic approach for curing atrial fibrillation. *Circulation* 2000;**102**:2619-28.
4. Ernst S, Ouyang F, Goya M, Lober F, Schneider C, Hoffmann-Riem M *et al.* Total pulmonary vein occlusion as a consequence of catheter ablation for atrial fibrillation mimicking primary lung disease. *J.Cardiovasc.Electrophysiol.* 2003;**14**:366-70.
5. Marrouche NF, Martin DO, Wazni O, Gillinov AM, Klein A, Bhargava M *et al.* Phased-array intracardiac echocardiography monitoring during pulmonary vein isolation in patients with atrial fibrillation: impact on outcome and complications. *Circulation* 2003;**107**:2710-6.
6. Saad EB, Cole CR, Marrouche NF, Dresing TJ, Perez-Lugones A, Saliba WJ *et al.* Use of intracardiac echocardiography for prediction of chronic pulmonary vein stenosis after ablation of atrial fibrillation. *J.Cardiovasc.Electrophysiol.* 2002;**13**:986-9.
7. Ren JF, Marchlinski FE, Callans DJ, Zado ES. Intracardiac Doppler echocardiographic quantification of pulmonary vein flow velocity: an effective technique for monitoring pulmonary vein ostia narrowing during focal atrial fibrillation ablation. *J.Cardiovasc.Electrophysiol.* 2002;**13**:1076-81.
8. Mangrum JM, Mounsey JP, Kok LC, DiMarco JP, Haines DE. Intracardiac echocardiography-guided, anatomically based radiofrequency ablation of focal atrial fibrillation originating from pulmonary veins. *J.Am.Coll.Cardiol.* 2002;**39**:1964-72.
9. Johnson SB, Seward JB, Packer DL. Phased-array intracardiac echocardiography for guiding transseptal catheter placement: utility and learning curve. *Pacing Clin.Electrophysiol.* 2002;**25**:402-7.
10. Epstein LM, Smith T, TenHoff H. Nonfluoroscopic transseptal catheterization: safety and efficacy of intracardiac echocardiographic guidance. *J.Cardiovasc.Electrophysiol.* 1998;**9**:625-30.
11. Martin RE, Ellenbogen KA, Lau YR, Hall JA, Kay GN, Shepard RK *et al.* Phased-array intracardiac echocardiography during pulmonary vein isolation and linear ablation for atrial fibrillation. *J.Cardiovasc.Electrophysiol.* 2002;**13**:873-9.
12. Ho SY, Sanchez-Quintana D, Cabrera JA, Anderson RH. Anatomy of the left atrium: implications for radiofrequency ablation of atrial fibrillation. *J.Cardiovasc.Electrophysiol.* 1999;**10**:1525-33.
13. Ho SY, Cabrera JA, Tran VH, Farre J, Anderson RH, Sanchez-Quintana D. Architecture of the pulmonary veins: relevance to radiofrequency ablation. *Heart* 2001;**86**:265-70.
14. Marrouche NF, Dresing T, Cole C, Bash D, Saad E, Balaban K *et al.* Circular mapping and ablation of the pulmonary vein for treatment of atrial fibrillation. Impact of different catheter technologies. *J.Am.Coll.Cardiol.* 2002;**40**:464-74.
15. Tsao HM, Chen SA. Evaluation of pulmonary vein stenosis after catheter ablation of atrial fibrillation. *Card Electrophysiol.Rev.* 2002;**6**:397-400.
16. Stabile G, Bertaglia E, Senatore G, de Simone A, Zerbo F, Carreras G *et al.* Feasibility of pulmonary vein ostia radiofrequency ablation in patients with atrial fibrillation: a multicenter study (CACAF pilot study). *Pacing Clin.Electrophysiol.* 2003;**26**:284-7.
17. Takahashi A, Iesaka Y, Takahashi Y, Takahashi R, Kobayashi K, Takagi K *et al.* Electrical connections between pulmonary veins: implication for ostial ablation of pulmonary veins in patients with paroxysmal atrial fibrillation. *Circulation* 2002;**105**:2998-3003.
18. Schwartzman D, Ren JF, Devine WA, Callans DJ. Cardiac swelling associated with linear radiofrequency ablation in the atrium. *J.Interv.Card Electrophysiol.* 2001;**5**:159-66.
19. Saad EB, Marrouche NF, Saad CP, Ha E, Bash D, White RD *et al.* Pulmonary vein stenosis after catheter ablation of atrial fibrillation: emergence of a new clinical syndrome. *Ann.Intern.Med.* 2003;**138**:634-8.



Chapter

8

Monique R.M. Jongbloed¹

Jeroen J. Bax¹

Hildo J. Lamb²

Martijn S. Dirksen²

K. Zeppenfeld¹

Ernst E. van der Wall¹

Albert de Roos²

Martin J. Schalij¹

¹ Dept. of Cardiology, Leiden University Medical Center, Albinusdreef 2, Leiden, The Netherlands

² Dept. of Radiology, Leiden University Medical Center, Albinusdreef 2, Leiden, The Netherlands

Multi-Slice Computed Tomography
versus Intracardiac Echocardiography to Evaluate
the Pulmonary Veins Prior to Radiofrequency
Catheter Ablation of Atrial Fibrillation:
A Head-to-Head Comparison

J Am Coll Cardiol. 2005 Feb;45(3):343-50

Abstract

Objectives: To perform a head-to-head comparison between multi-slice computed tomography (MSCT) and intracardiac echocardiography (ICE).

Background: Different imaging techniques have been used to visualize the pulmonary veins (PV) prior to radiofrequency ablation of atrial fibrillation.

Methods: The PV and their atrial insertion were evaluated in 42 patients (35 men, 49 ± 9 years) admitted for ablation of PV ostia. Ostia were measured in 2 directions (anterior-posterior (AP) and superior-inferior (SI)) with MSCT. 2-D measurements of PV ostia were performed with ICE. Results were compared, considering MSCT as the gold standard. Venous ostium indexes were calculated by dividing MSCT-measurements in AP-direction and SI-direction.

Results: Common ostia of left PV were observed in 33(79%) patients with MSCT and 31(74%) patients with ICE. Common ostia of right PV were observed in 13(31%) and 16(38%) patients, respectively. Additional PV were observed in 13(31%) patients with MSCT and in 7(17%) patients with ICE. Ostial diameters by MSCT in AP-direction were similar to 2-D measurements by ICE. By contrast, diameters by MSCT in SI-direction were significantly larger than 2-D diameters measured with ICE. Venous ostium indexes were 0.77 ± 0.18 and 0.90 ± 0.15 ($p < 0.01$) for left and right PV respectively, indicating an oval shape of particularly left PV ostia.

Conclusions: Variation in PV anatomy is frequently observed with both techniques. The sensitivity for detection of additional branches is higher for MSCT. Results of measurements of PV ostia suggest an underestimation of ostial size by ICE. 3-D imaging techniques, such as MSCT, are required to demonstrate an oval shape of PV ostia.

Introduction

Radiofrequency catheter ablation (RFCA) is a potentially curative treatment modality for atrial fibrillation originating in the pulmonary veins¹. RFCA for atrial fibrillation can be aimed at either eliminating ectopic pulmonary venous foci^{2,3} or at electrical isolation of pulmonary veins⁴. For proper targeting of radiofrequency lesions, accurate visualisation and knowledge about pulmonary vein anatomy is necessary. Fluoroscopy alone cannot provide sufficient information on intracardiac anatomical structures such as the pulmonary venous ostia.

In recent years, the value of different imaging techniques to guide RFCA procedures has been recognized. For the acquisition of anatomical information of pulmonary vein anatomy prior to RFCA, 3-D imaging techniques, such as multi-slice computed tomography (MSCT), have been applied⁵. MSCT has proved to be able to provide accurate and detailed information of pulmonary vein anatomy⁶.

On-line acquisition of anatomical information regarding left atrial and pulmonary vein anatomy can also be obtained by intracardiac echocardiography (ICE)^{7,8}. Advantages of this imaging technique include the possibility to obtain on-line information of left atrial anatomy and pulmonary veins in relation to ablation catheters, the potential to assess hemodynamic function and the monitoring of acute complications, such as pericardial effusion and acute pulmonary vein stenosis.

Thus, both MSCT and ICE can be used for imaging of the pulmonary veins and their ostia prior to RFCA, and to obtain quantitative information. To date, there is limited information on the comparison between MSCT and ICE. In the current study, considering MSCT as the gold standard, we have compared the ability of both techniques to: 1) provide anatomical information regarding pulmonary vein anatomy in patients admitted for pulmonary vein isolation for atrial fibrillation, and 2) compare measurements of the ostia of the pulmonary veins in 2 directions obtained with MSCT with 2-D measurements obtained with ICE.

Patients and Methods

Study population. The study population consisted of 42 consecutive patients (35 men, age 49 ± 9 years, range 24-68) with symptomatic drug-refractory atrial fibrillation, admitted for RFCA aimed at electrical isolation of the pulmonary veins by the application of radiofrequency current at the pulmonary venous ostia. Mean duration of atrial fibrillation was 5 ± 4 years (range 1-25). Atrial fibrillation was paroxysmal in 28 patients, persistent in 10 and permanent in 4 patients. Mean left atrial size was 4.4 ± 0.8 cm. Mean number of anti-arrhythmic drugs used was 3.8 ± 1.6 per patient. Mean left ventricular ejection fraction was $62.8 \pm 9.6\%$. Thirteen patients had a history of heart failure (NYHA class 1-2); heart failure

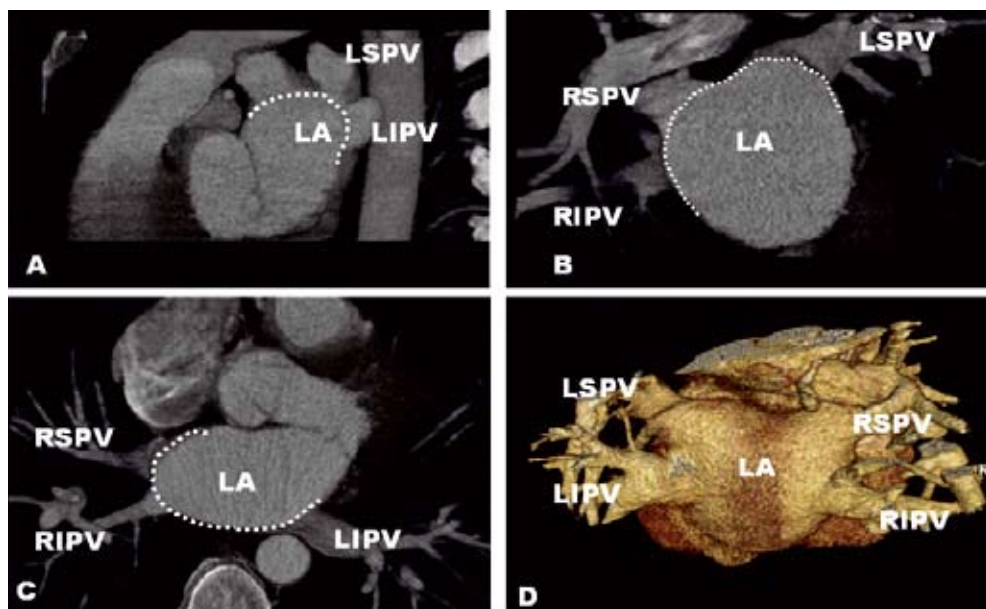


Figure 1

Evaluation of pulmonary venous ostial insertion in 3 different orthogonal planes in a patient with separate insertion of both left and right pulmonary veins in the left atrium. The dotted line depicts the extrapolated outer left atrial border. A. Sagittal plane. Both left pulmonary veins enter the left atrium separately. B. Coronal plane and C. Transversal plane. D. 3-D reconstruction. No common truncal part is observed in any plane before the veins enter the left atrium. Left atrial insertion of these veins was therefore designated as separate.

LA: left atrium, LIPV: left inferior pulmonary vein, LSPV: left superior pulmonary vein, RIPV: right inferior pulmonary vein, RSPV: right superior pulmonary vein

was due to tachycardia induced cardiomyopathy in 5 of these patients. One patients had a history of coronary artery disease, in 14 patients mild valvular disease was present (mitral regurgitation grade 1-2). Four patients had a pacemaker.

Multi-slice Computed Tomography. MSCT was performed using a Toshiba Multi-slice Aquilion system (Toshiba Medical Systems, Otawara, Japan), with either a 4-slice (16 patients) or a 16-slice (26 patients) system two days prior to RFCA. Non-ionic contrast material (Xenetix 300, Guerbet, Aulnay S. Bois, France) was injected in the antebrachial vein (160 ml, flow rate 4.0 ml/sec.). Cranio-caudal scanning (coverage length 80-120 mm) was performed at the level of the atria using simultaneous acquisition of 4 sections with a collimated slice thickness of 2 mm or 16 sections with a collimated slice thickness of 0.5 mm respectively. Helical pitch was 1 mm/0.5 sec for the 4-slice scanner and 4 mm/0.5 sec. for the 16-slice scanner. Rotation time was 400 to 600 ms (dependant on the patient's heart rate) and tube voltage was 120 kV at 250 mA. Scanning was performed during breath-holding. A segmental reconstruction algorithm was used to allow for the inclusion of patients

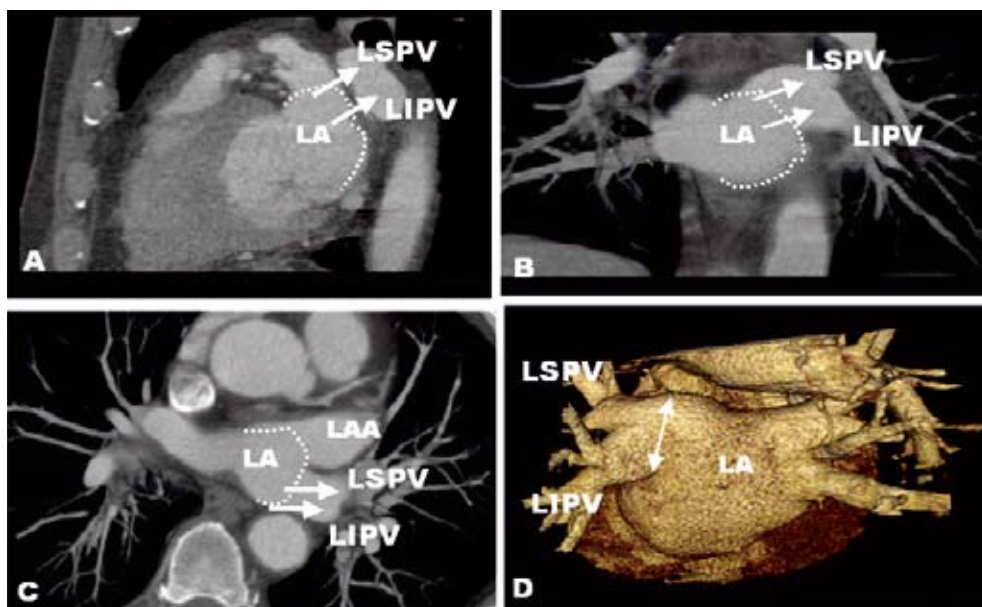


Figure 2

Common ostium of the left pulmonary veins, as evaluated in 3 different orthogonal planes and a 3-D reconstruction using MSCT. A. sagittal plane. The superior and inferior pulmonary veins have united to form a common truncus before entering the left atrial body. B. Coronal plane, C. Transversal plane, D. 3-D reconstruction. A common truncus of the left pulmonary veins can be observed in all orthogonal planes and on the 3-D reconstruction.

LA: left atrium, LAA: left atrial appendage, LIPV: left inferior pulmonary vein, LSPV: left superior pulmonary vein, RIPV: right inferior pulmonary vein, RSPV: right superior pulmonary vein

with a range of heart rates. Retrospective ECG-gating was performed to eliminate cardiac motion artefacts. Data acquisition was completed in 20 seconds. Data reconstruction was performed on a Vitrea post-processing workstation (Vital images, Plymouth, Mn, USA) with use of 2-D viewing modes and 3-D reconstructions.

Reconstructions were evaluated in three different orthogonal planes (transversal, sagittal and coronal) or with angulated multiplanar reformat. In addition, pulmonary vein anatomy was evaluated using 3-D reconstructions.

Intracardiac Echocardiography. Intracardiac echocardiography was performed with an Acunav™ Diagnostic Ultrasound Catheter, connected to a Sequoia® ultrasound system (Acuson Corporation, Mountain View, California). The ultrasound catheter consists of a miniaturized 64-element, monoplane phased array transducer, which is incorporated in a 10 French single use catheter. This catheter was positioned in the right atrium through the left femoral vein. On initiation of each RFCA-procedure, pulmonary vein anatomy was explored with ICE and measurements of pulmonary vein ostia were performed.

Definitions. For the evaluation of the pulmonary venous ostia, the following definitions were used.

MSCT: A line following the outer contour of the LA was drawn in different orthogonal planes in order to determine whether there was a separate or common insertion of the pulmonary veins in the left atrium. If the pulmonary venous ostia entered the left atrium separately outside this line, the ostia were defined as being “separate ostia” (**Figure 1**). When the pulmonary veins united before entering the drawn outer left atrial contour in the transversal, coronal and sagittal orthogonal plane, the ostium was defined as a “common ostium” (**Figure 2**). “Additional PV” were defined as entering the LA in separate ostia. “Early branching” was defined as branching of the pulmonary vein within 1 cm of the bifurcation of the pulmonary veins.

ICE: Similar to MSCT, the site of the atriovenous border was determined by extrapolation of the outer border of the left atrium, and a line was drawn at the junction of the pulmonary veins with the left atrium. If atrial tissue could be distinguished between the ostia of both

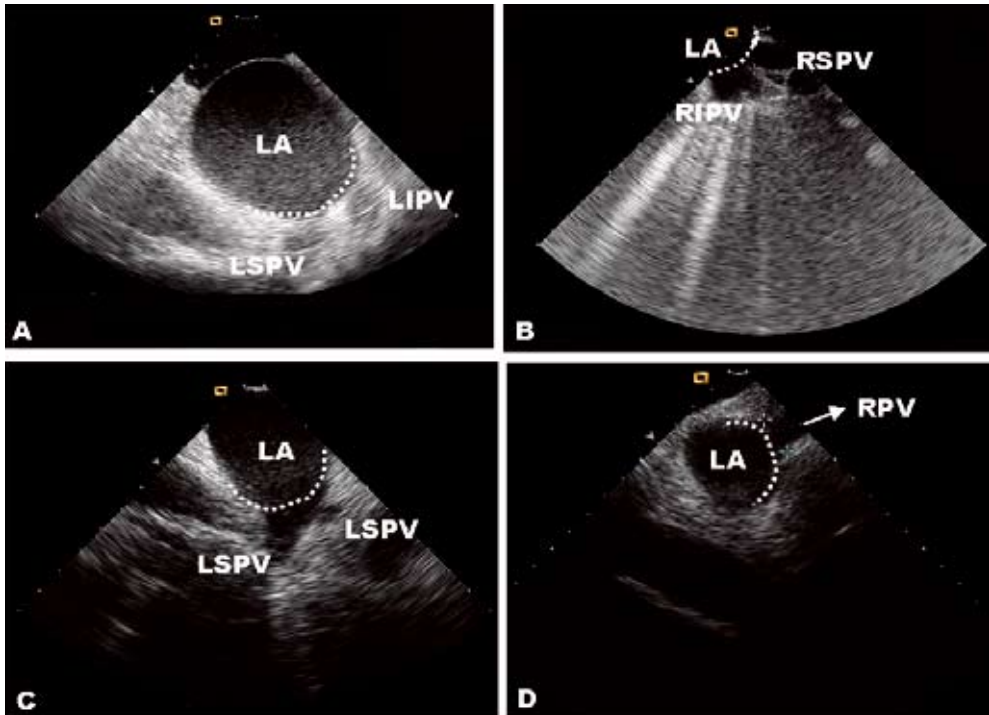


Figure 3

Method used to determine pulmonary vein ostial insertion in the left atrium, using ICE. The dotted line depicts the extrapolated outer left atrial border. Figures A and B represent separate insertion of left and right pulmonary veins respectively, whereas C and D demonstrate a common ostium of the left and right pulmonary veins respectively.

LA: left atrium, LIPV: left inferior pulmonary vein, LSPV: left superior pulmonary vein, RIPV: right inferior pulmonary vein, RPV: right pulmonary veins, RSPV: right superior pulmonary vein

pulmonary veins, the ostia were defined as “separate ostia”. When a common truncal part was present before entering this line, the ostia were defined as “common ostia” (**Figure 3**). For right pulmonary veins, evaluation of ostia was not always possible in this way, as the right PV are situated in close proximity with the interatrial septum and often make a sharp angle with this structure. Therefore, it is not always possible to obtain longitudinal views, as is possible for the left PV. When the ICE-transducer was positioned at the bifurcation of both right PV and a common trunk could be visualized, then the ostia of the right PV were defined as “common ostia”. Similar to MSCT, “additional pulmonary veins” enter the LA in separate ostia and “early branching” was defined as branching of the pulmonary vein within 1 cm of the bifurcation of the pulmonary veins.

Quantative Measurements. For MSCT, measurements of the PV ostia in two directions were obtained, being (1) the *anterior-posterior*-direction and (2) the *superior-inferior* direction. Multiplanar reformatting was used to obtain these measurements in 2 perpendicular directions (**Figure 4**). Furthermore, the ratio between these measurements, the *venous ostium index*, was calculated in order to obtain information on the shape of the ostium. The more the venous ostium index deviates from the value 1, the more asymmetrical the shape of the ostium.

ICE: On the 2-D images obtained by ICE, the largest possible diameter of the PV ostium was measured (**Figure 3 and 4**). Measurements of pulmonary vein ostia by ICE were compared with both anterior-posterior diameters and superior-inferior diameters obtained with MSCT.

All measurements were performed in consensus by two observers. The observers responsible for evaluation of the ICE data were blinded for the MSCT data and vice versa.

RFCA. RFCA was aimed at electrical isolation of all pulmonary veins from the left atrium by the circumferential application of ablation points aimed ± 5 mm outside the ostium of the pulmonary veins. Radiofrequency current was applied via a Stockert-Cordis (Freiburg, Germany) generator at each ablation point for 30 seconds, with maximum temperature setting at 60° C and maximum radiofrequency energy 50 W. ICE was used to exclude the presence of intracardiac thrombus, to guide transeptal puncture and to evaluate the anatomy of the pulmonary veins prior to RFCA. After the evaluation of the pulmonary venous anatomy and measurements of the ostia by ICE, the ablation strategy was planned using data obtained with both MSCT and ICE. If a separate pulmonary venous insertion was observed with both techniques, radiofrequency current was targeted to form separate circles surrounding the pulmonary venous ostia. If a common ostium was observed with one or both techniques, ablation points were targeted in a large circle surrounding the common ostium. All additional pulmonary veins observed were targeted as well. During the procedure, the MSCT scan was placed on a light panel opposite to the operator. On-line information obtained by ICE was used to monitor catheter navigation in the left

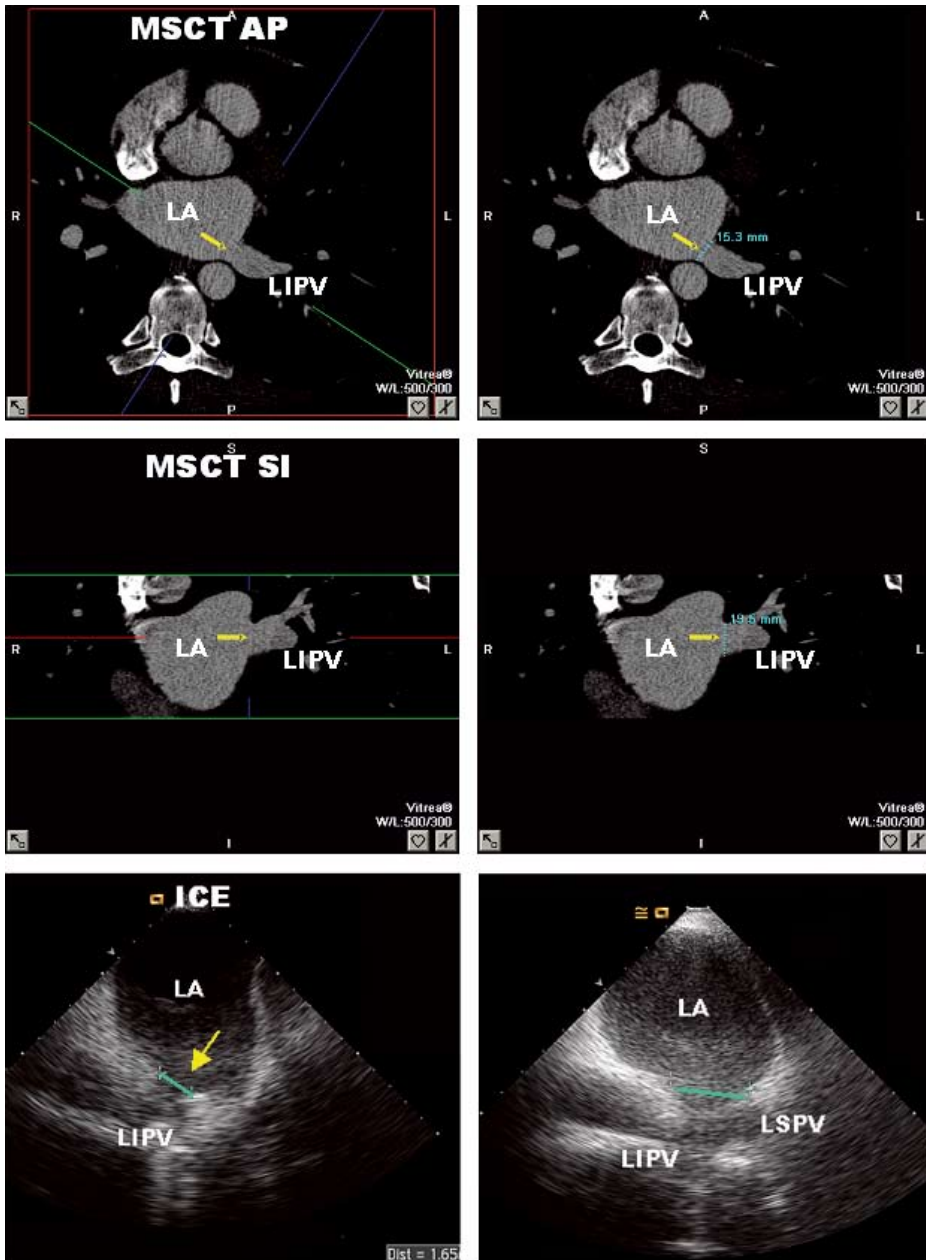


Figure 4

Measurements of the left inferior pulmonary vein (LIPV) with MSCT in 2 directions (upper and middle panel) using multiplanar reformatting, and with ICE (lower panel).

Upper panel: Measurements in anterior-posterior direction in the transversal orthogonal plane. The green line is placed parallel to the left inferior pulmonary vein, and depicts the coronal plane, which is used to measure the ostium in the superior-inferior direction (*middle panel*). *Lower panel:* Measurement of the LIPV (left panel) and of a common ostium of the left pulmonary veins (right panel) using ICE.

AP: anterior-posterior, ICE: intracardiac echocardiography, LA: left atrium, LSPV: left superior pulmonary vein, MSCT: multi-slice computed tomography, SI: superior-inferior

atrium and to evaluate the position of the ablation catheter in relation to the ostia of the pulmonary veins. When micro-bubbles were observed, the application of radiofrequency current was stopped and the catheter was repositioned in an attempt to provide better catheter-tip tissue contact. Furthermore, ICE was used to monitor the occurrence of acute complications during the procedure. A 3-D non-fluoroscopic mapping system (CARTO, Biosense Webster, Diamond Bar, CA, USA) was used to tag pulmonary veins, to acquire electrophysiological information and to mark ablation points. Tagging of the pulmonary veins was guided by the information of MSCT and ICE imaging, concerning number and insertion of pulmonary veins. The procedure was designated successful when there was no capture in the pulmonary veins and left atrium after pacing in the left atrium or pulmonary veins, respectively and when the patient was in sinus rhythm after the procedure. All patients received heparin (activated clotting time 2-3 times baseline value, checked hourly).

Statistical analysis. Statistical analysis was performed using Microsoft Excel spreadsheets and SPSS 11.0 software for Windows. Data are expressed as mean \pm SD. Diameters of pulmonary vein ostia measured on line with ICE prior to ablation were compared with measurements in anterior-posterior direction performed with MSCT, and with measurements performed in superior-inferior direction with MSCT, using the paired Student's T-test. This test was also used for comparisons between the measurements in two directions performed with MSCT. Bland Altman analysis was used to quantify the level of agreement between measurements with ICE and measurements with MSCT in both anterior-posterior and superior inferior direction. All tests were two-tailed and a P-value <0.05 was considered significant.

Results

Pulmonary vein anatomy: In 42 patients, a total number of 181 pulmonary veins was observed with MSCT and 175 pulmonary veins with ICE.

In all patients, at least 4 veins could be identified with both techniques (**Table 1**).

Additional veins: Additional veins were observed more frequently on the right side with both ICE and MSCT. However, additional right veins were observed in 12(29%) patients with MSCT as compared to 7(17%) with ICE. Considering MSCT as the gold standard, the sensitivity of ICE to demonstrate additional right pulmonary veins was 7/12(58%). In one patient, an additional left pulmonary vein was observed with MSCT, which was not recognized by ICE. **Figure 5 (upper panel)** demonstrates a MSCT image of a patient with an additional right pulmonary vein and the visualization of the right pulmonary veins with ICE.

Early branching: An early branching pattern of the right pulmonary veins was observed in the majority (83%) of patients with MSCT, but was only recognized in 19(45%) patients with ICE (sensitivity 19/35(54%)). An early branching pattern of the left pulmonary veins was observed in 5(12%) with both MSCT and ICE.

Table 1 Anatomical results MSCT versus ICE

	MSCT	ICE
Total number of observed PV	181	175
Mean number of PV/pt	4.3±0.6	4.2±0.4
Pts with additional RPV	12(29%)	7(17%)
Pts with additional LPV	1(3%)	0
Pts with early branching RPV	5(12%)	5(12%)
Pts with early branching LPV	35(84%)	19(45%)
Pts with common ostium RPV	13(31%)	16(38%)
Pts with common ostium LPV	33(79%)	31(74%)

LPV: left pulmonary veins, pts: patients, PV: pulmonary veins, RPV: right pulmonary veins

172

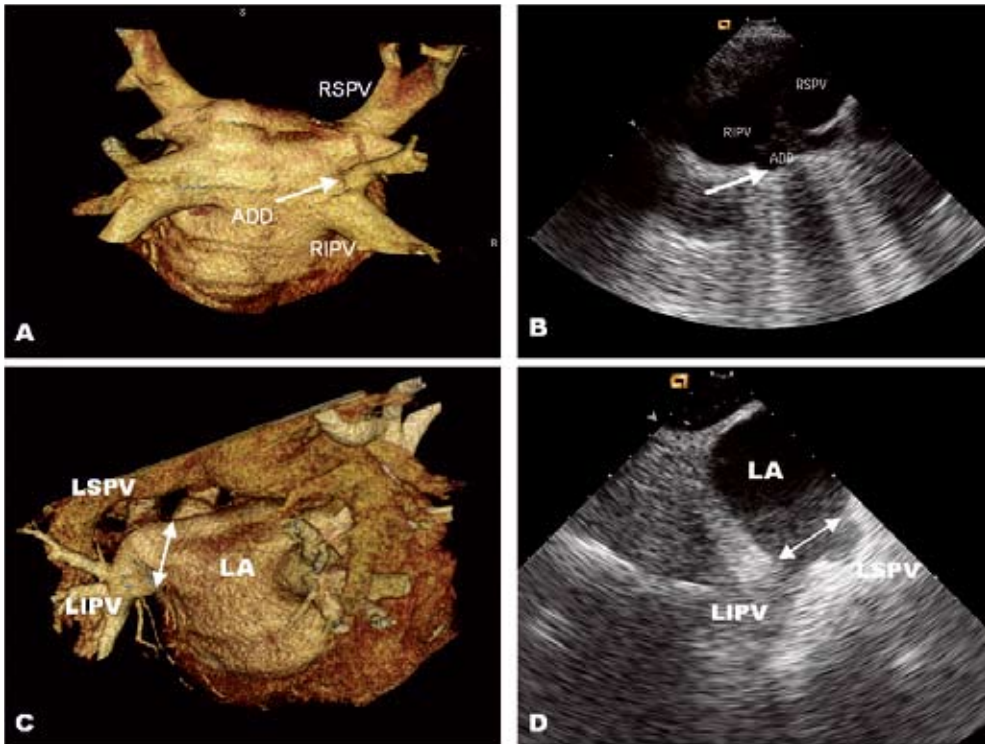


Figure 5

Upper panel: Additional right pulmonary vein (arrow), as observed with MSCT (A) and with ICE (B).

Lower panel: Common ostium (double arrow) of the left pulmonary veins, as observed with MSCT (C) and with ICE (D).

LA: left atrium, LIPV: left inferior pulmonary vein, LSPV: left superior pulmonary vein, RIPV: right inferior pulmonary vein, RSPV: right superior pulmonary vein

Common ostia: Before entering the left atrium, often both left and right-sided veins united in a short or long common trunk. Such a common ostium of the upper and lower pulmonary veins was observed more often in the left pulmonary veins with both techniques. Common ostia of left pulmonary veins were observed in 33(79%) patients with MSCT and in 31(74%) patients with ICE. Common ostia of right pulmonary veins were seen in 13(31%) of patients with MSCT and in 16(38%) of patients with ICE. In 3 cases, visualisation of right-sided pulmonary veins was laborious, and ostia appeared confluent. These patients were scored by the observers as common ostia, whereas separate ostia were identified using MSCT. **Figure 5 (lower panel)** demonstrates images obtained with MSCT and ICE in a patient with a common ostium of the left pulmonary veins and of the right pulmonary veins.

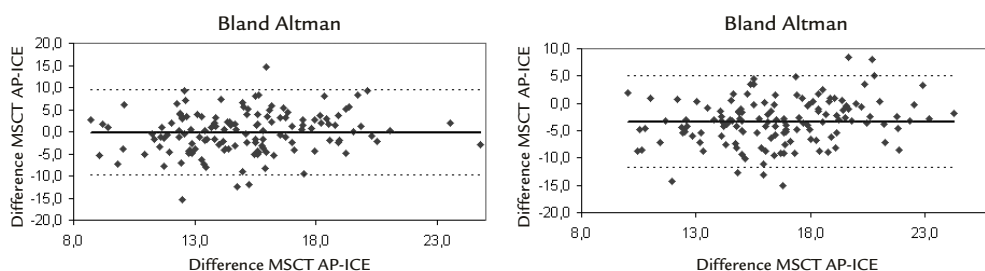


Figure 6 Bland Altman analysis of measurements performed with MSCT and ICE in AP-direction (left panel) and in SI-direction (right panel). The difference between all measurements performed with MSCT and with ICE was within 2 standard deviations from the average difference for the majority of measurements.

Quantitative measurements: Average measurements of pulmonary venous ostia in anterior-posterior direction performed with MSCT were similar to measurements in the largest directions performed with ICE, except for measurements in the left inferior PV. When both left veins were compared with measurements performed with MSCT in anterior-posterior direction, this difference was no longer significant. On the contrary, measurements performed with MSCT in superior-inferior directions were significantly larger than measurements performed with ICE in the largest direction (**Table 2**). The difference between all measurements performed with MSCT and with ICE was within 2 standard deviations from the average difference for most measurements, as was demonstrated with Bland Altman analysis (**Figure 6**).

Calculations of the venous ostium indexes (ratios of measurements of pulmonary vein ostia in anterior-posterior and in superior-inferior direction) as measured with MSCT, demonstrated that the venous ostium indexes of the left PV were significantly smaller than the venous ostium indexes of the right pulmonary veins, indicating a more oval shape of left pulmonary vein ostia (**Table 3**). The diameters in the superior-inferior direction were sig-

Table 2 Measurements Ostia Pulmonary Veins: MSCT versus ICE

	MSCT AP-diameters (mm)	MSCT SI-diameters (mm)	ICE diameters (mm)	AP diameter MSCT vs. ICE P-value	SI-diameter MSCT vs. ICE P-value
LSPV	14.6±3.0	19.0±3.8*	14.3±3.9	NS	<0.01
LIPV	12.8±3.0	17.1±2.9*	14.3±3.0	<0.01	<0.01
Both LPV	13.7±3.1	18.0±3.5*	14.3±3.5	NS	<0.01
RSPV	16.5±3.2	19.2±2.8*	15.9±4.7	NS	<0.01
RIPV	16.6±3.9	18.2±3.7*	15.4±4.3	NS	<0.01
Both RPV	16.6±3.6	18.7±3.3*	15.7±4.5	NS	<0.01
LCO	20.4±7.5	26.8±6.8*	24.3±3.9	NS	NS
RCO	25.9±7.5	33.5±7.6*	21.6±7.3	NS	<0.05
Add RPV	7.4±1.6	7.6±2.0	8.5±1.8	NS	<0.05
Add LPV	11.0	10.1	–	–	–
All PV	15.1±3.6	18.4±3.4*	14.9±4.0	NS	<0.01

* Significantly larger compared to AP-diameters.

Add RPV = additional right pulmonary veins, Add LPV = additional left pulmonary veins, AP: anterior-posterior, LCO: left common ostium, LIPV: left inferior pulmonary vein, LPV:left pulmonary veins, LSPV: left superior pulmonary vein, NS: not significant, PV = pulmonary veins, RCO: right common ostium, RIPV: right inferior pulmonary vein, RPV: right pulmonary veins, RSPV: right superior pulmonary vein, SI: superior-inferior

Table 3 Indexes of diameters measured in anterior-posterior and superior-inferior direction of pulmonary venous ostia, as measured with MSCT

Vein	Index AP/SI diameters
LSPV	0.79±0.20*
LIPV	0.75±0.16**
Both LPV	0.77±0.18†
RSPV	0.88±0.13
RIPV	0.92±0.16
both RPV	0.90±0.15
CO LPV	0.89±0.63
CO RPV	0.82±0.30
Add LPV	1.09
Add RPV	1.02±0.27

Add PV: additional pulmonary veins, AP: anterior-posterior, LCO: left common ostium, LIPV: left inferior pulmonary vein, LPV: left pulmonary veins, LSPV: left superior pulmonary vein, RCO: right common ostium, RIPV: right inferior pulmonary vein, RPV: right pulmonary veins, RSPV: right superior pulmonary vein, SI: superior-inferior,

* p<0.05 vs. RSPV

** p<0.01 vs. RIPV

† p<0.01 vs. both RPV

nificantly larger than the diameters in the anterior-posterior direction, indicating the long axis of the ostia to be in the superior-inferior direction (**Table 2**). Right-sided additional veins were significantly smaller as the “native” veins, and venous ostium indexes indicated a round shape of these ostia (1.02 ± 0.27). As the monoplane ICE transducer provides only 2-D images, multidimensional information cannot be obtained by ICE.

RFCA: Eventually 36 patients were treated with RFCA for pulmonary vein isolation. In 5 patients left-sided RFCA was not performed because of the presence of left atrial thrombus detected by ICE (2 patients), the inability to perform transeptal puncture (1 patient) and the induction of only atrial flutter (1 patient) or atrial tachycardia (1 patient), for which right atrial isthmus ablation and focal ablation of atrial tachycardia were performed, respectively. In 1 patient the procedure was terminated because of recurrent strong vagal response with hypotension and severe bradycardia during the application of radiofrequency current. Procedural success was achieved in 34/36(94%) of patients. Mean procedure time was 252 ± 76 minutes and mean fluoroscopy time 49 ± 14 minutes. In 3 patients, mild pericardial effusion (<1.5 cm) was observed at the end of the procedure, without hemodynamic consequences. This effusion resolved on follow-up transthoracic echocardiography. No complications were observed during the first 48 hours after the procedure. At 6 months follow-up, 23/36 (64%) patients were in sinus rhythm.

Discussion

In this study, we have compared the ability of MSCT and ICE to obtain both anatomical and quantitative information on the pulmonary veins prior to radiofrequency catheter ablation. Considering MSCT as the gold standard, main findings of this study are: 1) a higher sensitivity of MSCT to detect additional veins and right-sided early pulmonary venous branches and 2) an underestimation of pulmonary venous ostial size using ICE.

176

Anatomical information: At present, there is no generally accepted definition which defines the exact border between the left atrial body and the pulmonary veins. Also, data on the exact prevalence of pulmonary vein variability is scarce. In general common ostia are observed more frequently on the left side, while the presence of additional veins and early branching is described more often for right sided veins^{5,6,9-11}, which agrees with data in the current study. Although variations in pulmonary vein anatomy were observed with both MSCT and ICE, additional pulmonary veins were observed more frequently with MSCT. Furthermore, an early branching pattern of right sided pulmonary veins was more often observed by MSCT. These data are in line with recent observations¹². In our experience, evaluation of the left sided pulmonary veins with ICE is more easily performed than evaluation of the right-sided veins. This may be attributed to the fact that the right-sided veins often make a sharp angle with the interatrial septum, thus limiting a longitudinal evaluation using the monoplane ICE transducer.

Knowledge of the existence of additional pulmonary veins may have implications for the RFCA strategy. Since arrhythmogenic capacities have been demonstrated in additional right pulmonary veins¹³, targeting of these veins during RFCA procedures may improve procedural success rates.

Quantitative information: Main observations regarding quantitative data comparing both techniques demonstrated that the average measurements in anterior-posterior direction performed with MSCT were similar to measurements performed in the largest direction with ICE. Furthermore, average ostial diameters in superior-inferior direction as measured by MSCT were larger as compared to the monoplane measurements in the largest direction performed with ICE, indicating that ICE may underestimate the true ostial size in the largest direction. This hypothesis is supported by the fact that the venous ostium indexes (ratios of the measurements in two directions obtained by MSCT) were indicative of an oval shape of especially the left, and to a lesser extent the right, pulmonary venous ostia, with the long axis in the superior-inferior direction. These data agree with data reported by Witkampf et al.¹¹. Consequently, using a monoplane intracardiac ultrasound transducer, pulmonary veins may appear smaller than their true dimensions. Intracardiac 3-D echocardiography may be a solution for this problem¹⁴.

RFCA: An advantage from 3-D imaging with MSCT is the ability to accurately evaluate the pulmonary venous ostial dimensions prior to the ablation procedure, since the ostia can be observed in different orthogonal planes. Three-dimensional reconstructions of these images may provide a roadmap for targeting ablation points during RFCA, whereas information on ostial shape and size may also be useful to determine the size of Lasso catheters. Detailed knowledge of individual 3-D morphology of the pulmonary veins may also contribute to improved clinical success rate of pulmonary vein isolation¹⁵. Additionally, ICE can be useful to exclude thrombus in the left atrial appendage, guide transseptal puncture, provide on-line information on the position of catheters and pulmonary vein hemodynamics pre-and post RFCA. Some authors recommend the adjustment of radiofrequency power settings according to the appearance of microbubbles detected by ICE⁷. Besides MSCT and ICE, electro-anatomical mapping using 3-D non-fluoroscopic mapping systems have become important tools for guiding electrophysiological ablation procedures. These systems have the advantage that catheter navigation can be traced on-line and correlated to local electrograms^{16,17}. New technology is able to use CT-information on-line¹⁸ and a future application is the integration of activation maps on 3-D CT images and the fusion of real-time ICE images with images obtained by CT/MRI¹⁹.

Conclusions: Variation in pulmonary vein anatomy is frequently observed with both MSCT and ICE. The sensitivity for detection of additional branches and right-sided early branching is higher for MSCT. Measurements performed in the anterior-posterior direction using MSCT agree with measurements performed with ICE in the largest direction, whereas average measurements in superior-inferior direction performed with MSCT are significantly larger than average measurements performed with ICE, suggesting underestimation of true ostial size by ICE. 3-D imaging techniques, such as MSCT, are required to demonstrate an asymmetrical shape of pulmonary vein ostia. The integration of MSCT data with on-line information obtained by ICE may optimize the treatment of atrial fibrillation by RFCA at pulmonary vein ostia.

Reference List

1. Haissaguerre M, Jais P, Shah DC, Takahashi A, Hocini M, Quiniou G *et al.* Spontaneous initiation of atrial fibrillation by ectopic beats originating in the pulmonary veins. *N.Engl.J.Med.* 1998;**339**:659-66.
2. Haissaguerre M, Shah DC, Jais P, Hocini M, Yamane T, Deisenhofer I *et al.* Electrophysiological breakthroughs from the left atrium to the pulmonary veins. *Circulation* 2000;**102**:2463-5.
3. Haissaguerre M, Jais P, Shah DC, Garrigue S, Takahashi A, Lavergne T *et al.* Electrophysiological end point for catheter ablation of atrial fibrillation initiated from multiple pulmonary venous foci. *Circulation* 2000;**101**:1409-17.
4. Pappone C, Rosanio S, Oreto G, Tocchi M, Gugliotta F, Vicedomini G *et al.* Circumferential radiofrequency ablation of pulmonary vein ostia: A new anatomic approach for curing atrial fibrillation. *Circulation* 2000;**102**:2619-28.
5. Perez-Lugones A, Schwartzman PR, Schweikert R, Tchou PJ, Saliba W, Marrouche NF *et al.* Three-dimensional reconstruction of pulmonary veins in patients with atrial fibrillation and controls: morphological characteristics of different veins. *Pacing Clin.Electrophysiol.* 2003;**26**:8-15.
6. Schwartzman D, Lacomis J, Wigginton WG. Characterization of left atrium and distal pulmonary vein morphology using multidimensional computed tomography. *J.Am.Coll.Cardiol.* 2003;**41**:1349-57.
7. Marrouche NF, Martin DO, Wazni O, Gillinov AM, Klein A, Bhargava M *et al.* Phased-array intracardiac echocardiography monitoring during pulmonary vein isolation in patients with atrial fibrillation: impact on outcome and complications. *Circulation* 2003;**107**:2710-6.
8. Mangrum JM, Mounsey JP, Kok LC, DiMarco JP, Haines DE. Intracardiac echocardiography-guided, anatomically based radiofrequency ablation of focal atrial fibrillation originating from pulmonary veins. *J.Am.Coll.Cardiol.* 2002;**39**:1964-72.
9. Kato R, Lickfett L, Meininger G, Dickfeld T, Wu R, Juang G *et al.* Pulmonary vein anatomy in patients undergoing catheter ablation of atrial fibrillation: lessons learned by use of magnetic resonance imaging. *Circulation* 2003;**107**:2004-10.
10. Scharf C, Sneider M, Case I, Chugh A, Lai SW, Pelosi F, Jr. *et al.* Anatomy of the pulmonary veins in patients with atrial fibrillation and effects of segmental ostial ablation analyzed by computed tomography. *J.Cardiovasc.Electrophysiol.* 2003;**14**:150-5.
11. Wittkamp FH, Vonken EJ, Derksen R, Loh P, Velthuis B, Wever EF *et al.* Pulmonary vein ostium geometry: analysis by magnetic resonance angiography. *Circulation* 2003;**107**:21-3.
12. Wood MA, Wittkamp M, Henry D, Martin R, Nixon JV, Shepard RK *et al.* A comparison of pulmonary vein ostial anatomy by computerized tomography, echocardiography, and venography in patients with atrial fibrillation having radiofrequency catheter ablation. *Am.J.Cardiol.* 2004;**93**:49-53.
13. Tsao HM, Wu MH, Yu WC, Tai CT, Lin YK, Hsieh MH *et al.* Role of right middle pulmonary vein in patients with paroxysmal atrial fibrillation. *J.Cardiovasc.Electrophysiol.* 2001;**12**:1353-7.
14. Smith SW, Light ED, Idriss SF, Wolf PD. Feasibility study of real-time three-dimensional intracardiac echocardiography for guidance of interventional electrophysiology. *Pacing Clin.Electrophysiol.* 2002;**25**:351-7.
15. Ernst S, Antz M, Ouyang F, Vogtmann T, Goya M, Bansch D *et al.* Ostial PV isolation: is there a role for three-dimensional mapping? *Pacing Clin.Electrophysiol.* 2003;**26**:1624-30.
16. Macle L, Jais P, Scavee C, Weerasooriya R, Hocini M, Shah DC *et al.* Pulmonary vein disconnection using the Localisa three-dimensional nonfluoroscopic catheter imaging system. *J.Cardiovasc.Electrophysiol.* 2003;**14**:693-7.
17. Nademanee K, McKenzie J, Kosar E, Schwab M, Sunsaneewitayakul B, Vasavakul T *et al.* A new approach for catheter ablation of atrial fibrillation: mapping of the electrophysiologic substrate. *J.Am.Coll.Cardiol.* 2004;**43**:2044-53.
18. Solomon SB, Dickfeld T, Calkins H. Real-Time Cardiac Catheter Navigation on Three-Dimensional CT Images. *J.Interv.Card Electrophysiol.* 2003;**8**:27-36.
19. Packer DL. Evolution of mapping and anatomic imaging of cardiac arrhythmias. *J.Cardiovasc.Electrophysiol.* 2004;**15**:839-54.



Monique R.M. Jongbloed¹

Hildo J. Lamb²

Jeroen J. Bax¹

Joanne D. Schuijf¹

Albert de Roos²

Ernst E. van der Wall¹

Martin J. Schalij¹

*Departments of ¹Cardiology and ²Radiology, Leiden University Medical Center, Leiden,
The Netherlands*

Non-invasive Visualization of the Cardiac Venous System Using Multi-Slice Computed Tomography



J Am Coll Cardiol. 2005 Mar;45(5):749-53

Abstract

Objectives: To evaluate the value of multi-slice computed tomography (MSCT) to depict the cardiac venous anatomy.

Background: During cardiac resynchronisation therapy (CRT), left ventricular (LV) pacing is established by a pacemaker lead in a tributary of the coronary sinus (CS). Knowledge about the CS anatomy and variations may facilitate the implantation of LV leads.

Methods: MSCT-scans of 38 patients (34 men, age 60 ± 12 years) were studied. Anatomical variants were divided in 3 groups, dependent on the continuity of the cardiac venous system at the crux cordis. The CS-ostium and distances between the main tributaries were measured.

Results: The most frequently observed variant had a separate insertion of the CS and the small cardiac vein in the right atrium (24(63%) patients). In 11(29%) patients, there was continuity of the anterior and posterior venous system at the crux cordis. In 3(8%) patients, the posterior interventricular vein (PIV) did not connect to the CS. The mean distance from the PIV to the posterior vein of the left ventricle (PVLV) was 42.4 ± 18.1 mm, from the PVLV to the left marginal vein (LMV) 39.9 ± 15.6 mm, and from the LMV to the anterior interventricular vein 45.4 ± 15.3 mm. The diameter of the CS ostium was 12.6 ± 3.6 mm in anterior-posterior and 15.5 ± 4.5 mm in superior-inferior direction ($p < 0.01$).

Conclusions: The anatomy of the CS and its tributaries can be evaluated using MSCT. As substantial variation in anatomy was observed, pre-implantation knowledge of the venous anatomy may help to decide whether transvenous LV lead placement for CRT is feasible.

Introduction

In cardiac resynchronisation therapy (CRT), left ventricular (LV) pacing is achieved by positioning the LV lead in one of the tributaries of the coronary sinus. Although the success rate for transvenous LV lead placement is relatively high (88-95% in large clinical trials), in 5-12% of patients the procedure does not succeed¹, and these numbers may be higher in inexperienced centers. Failure of LV lead placement has been attributed to the inability to insert catheters in the coronary sinus and the lack of suitable side branches^{1,2}. Knowledge of the cardiac venous anatomy prior to these procedures may facilitate LV lead positioning. In addition, it has been demonstrated that the success of CRT is related to the ability to improve ventricular function by lowering the degree of dyssynchrony¹. However, the optimal pacing site with respect to dyssynchrony improvement (site of latest activation within the LV) may not always have a suitable vein. In this case, a surgical approach may be preferred^{2,3}.

MSCT has become an important tool for non-invasive evaluation of cardiovascular structures⁴. However, no data are currently available on the use of MSCT to visualize the coronary venous anatomy. The aim of this study was to evaluate the feasibility of MSCT to depict the venous drainage system of the heart: the coronary sinus and its tributaries.

Methods

Study population: The anatomy of the cardiac venous system was studied in 38 patients (34 men, age 60±12 years) in whom MSCT-scanning was performed for non-invasive evaluation of coronary artery disease (n=18), evaluation of the pulmonary veins prior to radiofrequency catheter ablation of atrial fibrillation (n=10) and in 10 patients with severe heart failure (mean LV ejection fraction 29±5%) and who are considered for CRT. Three patients had a pacemaker.

Multi-slice computed tomography: MSCT was performed with a 16-slice Toshiba Multi-slice Aquilion 0.5 system (Toshiba Medical Systems, Otawara, Japan). Non-ionic contrast material (Xenetix 300, Guerbet, Aulnay S. Bois, France) was used. Scanning was performed using simultaneous acquisition of 16 sections with a collimated slice thickness of 0.5 mm. Helical pitch was 4 mm/0.5 sec, rotation time was 400 to 600 ms and tube voltage was 120 kV at 250 mA. A segmental reconstruction algorithm allowed inclusion of patients with a range of heart rates without the need for pre-oxygenation or beta-blocking agents. Retrospective ECG-gating was performed to eliminate cardiac motion artefacts. Data reconstruction was performed on a Vitrea post-processing workstation (Vital images, Plymouth, Minnesota, USA). The scans were evaluated in consensus by two observers.

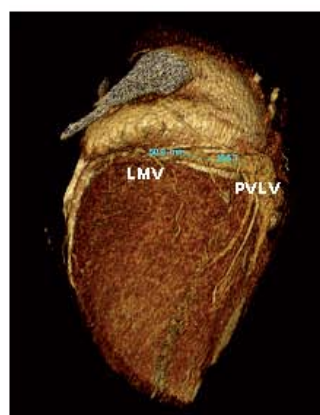
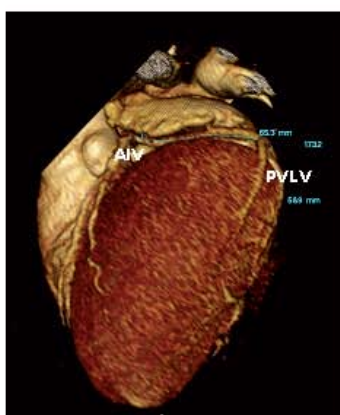
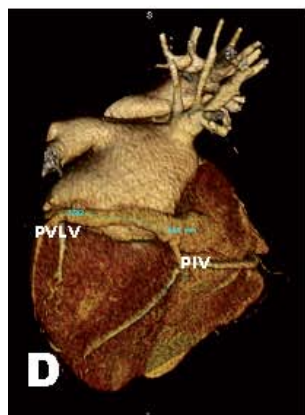
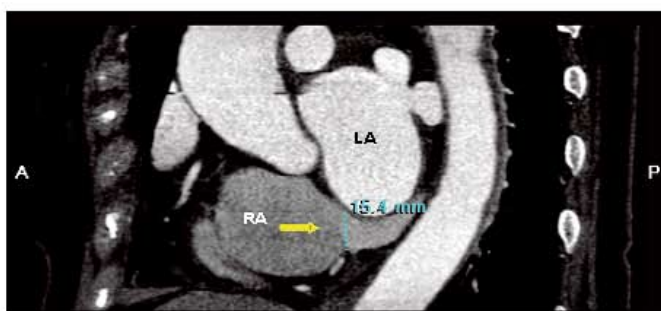
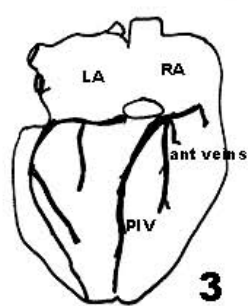
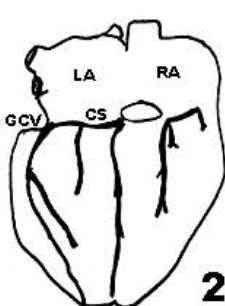
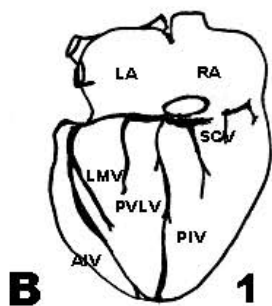
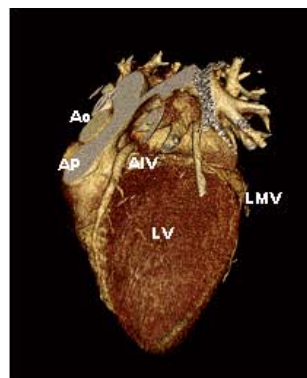
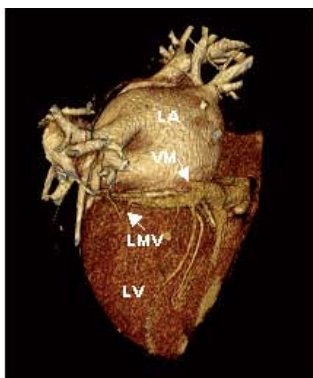
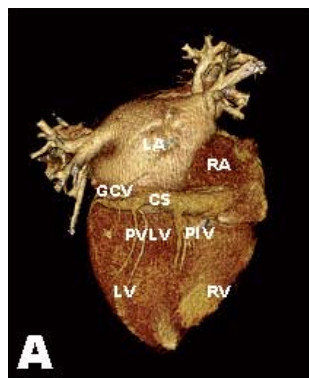


Figure 1

The cardiac venous system.

A. The border of the coronary sinus (CS) is marked by the vein of Marshall (VM). The CS continues in the great cardiac vein (GCV), which continues anteriorly in the anterior interventricular vein (AIV). As seen from the RA, the first tributary of the coronary sinus is the posterior interventricular vein (PIV). The next tributaries are the posterior vein of the left ventricle (PVLV) and the left marginal vein (LMV).

B. Left panel: Variant 1. Middle: Variant 2. Right panel: Variant 3. Explanation see text.

C. Left panel: The CS ostium measured in anterior-posterior direction. Transversal plane. Right panel: The CS ostium in superior-inferior direction. Coronal plane.

D. Measurement of the distances between the different tributaries of the cardiac venous drainage system. Abbreviations as above.

ant = anterior, AP = pulmonary artery, Ao = aorta, LA = left atrium, LV = left ventricle, RA = right atrium, RV = right ventricle

Anatomic observations: The anatomy of the coronary sinus and its tributaries was studied in relation to the crux cordis. The tributaries of the cardiac venous system (**Figure 1A**) were identified on volume rendered reconstructions. Hereafter, the course of the veins was evaluated in 3 orthogonal planes and using multiplanar reformatting (MPR). Each patient was designated to one of 3 groups of variable anatomy (modified after Von Ludinghausen, **Figure 1B**)⁵.

Variant 1: Continuity of the cardiac veins at the crux cordis. The small cardiac vein connects to the coronary sinus at the crux cordis.

Variant 2: The small cardiac veins and/or the anterior cardiac veins enter the right atrium (RA) independently from the coronary sinus. The posterior interventricular vein (PIV) connects to the coronary sinus at the crux cordis.

Variant 3: Disconnection between the coronary sinus and the PIV. The PIV is connected to the small cardiac vein or enters the RA independently.

Quantative data: The ostium of the coronary sinus was defined as the site where the coronary sinus makes an angle with the RA. Multiplanar reformatting was used to determine the size of the ostium in two directions. (**Figure 1C**). The distance between the ventricular tributaries was measured on volume rendered reconstructions (**Figure 1D**).

Statistical analysis

Continuous data are expressed as mean values and corresponding standard deviations. Dichotomous data are expressed as numbers and percentages. The paired student's T-test was used to evaluate differences in diameters of the ostium of the coronary sinus in anterior-posterior and superior-inferior direction. A p-value < 0.05 was considered significant.

Results

Anatomic observations: The cardiac venous system was visualized in all patients. Whereas the coronary sinus and the PIV were observed in all patients, the posterior vein of the LV (PVLV) and the left marginal vein (LMV) were observed in 36(95%) and 23(61%) patients respectively. A small cardiac vein was present in 17(45%) of patients.

Variants in anatomy: Continuity of the coronary sinus with the small cardiac vein was observed in 11(29%) of patients (*Variant 1*). In 21(55%) patients, the small cardiac vein was not found. In 24(63%) of patients, the PIV connected to the crux cordis (*Variant 2*), and in 3(8%) of patients the PIV was not connected to the coronary sinus at the crux cordis, but entered the RA separately (*Variant 3*). Examples of anatomical variations are demonstrated in **Figure 2**. The vein of Marshall was distinguished in 13(34%) patients. Anatomic observations are summarized in **Table 1**.

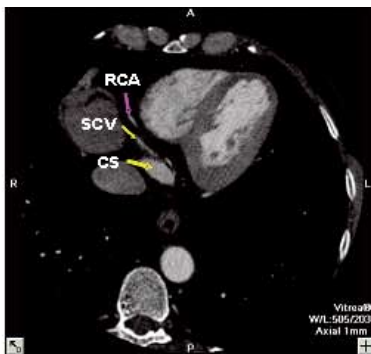
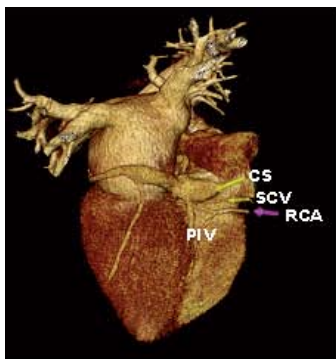
Quantative data: Interindividual variation was observed in the distances between the main tributaries draining the LV. No significant differences were observed in patients with, as compared to patients without heart failure. In 4 patients the distance between the PIV and the PVLV was ≤ 2 cm. Two of these patients also lacked the presence of the LMV. The mean diameter of the LMV was quite small with an average of only 3.9 ± 1.9 mm. The diameter of the LMV was significantly larger in patients with as compared to those without heart failure.

Mean diameter of the ostium of the coronary sinus in the anterior-posterior direction was 12.6 ± 3.6 mm. In the superior-inferior direction, the diameter of the ostium was significantly larger (15.5 ± 4.5 mm, $p < 0.01$), indicating an asymmetrical shape of the ostium with the long axis in the superior-inferior direction. There were no significant differences in diameters of the ostia in patients with, as compared to patients without heart failure ($p = 0.05$). Quantative data are summarized in **Table 2**.

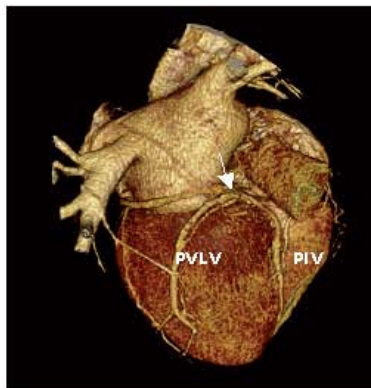
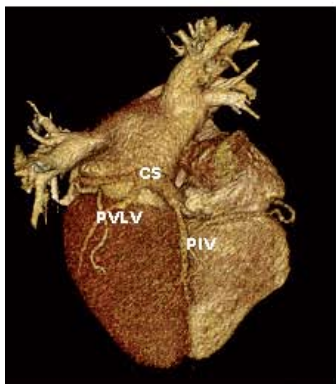
► Figure 2

- A. Variant 1.** Left panel: volume rendered reconstruction. The coronary sinus (CS), posterior interventricular vein (PIV) and small cardiac vein (SCV) are continuous at the crux cordis. The SCV (lower yellow arrow) runs in close association with the right coronary artery (RCA, purple arrow). Right panel: The CS and SCV (yellow arrows) and the RCA (purple arrow) on the transversal plane.
- B. Variant 2.** The CS enters the RA independently from the anterior cardiac veins. Right panel: The ostia of the CS, the PIV and the posterior vein of the left ventricle (PVLV) are confluent and form a large common ostium (arrow).
- C. Variant 3.** Left panel: The PIV is not connected to the coronary sinus, but enters the RA independently, as is also demonstrated on the transversal orthogonal plane on the right panel. The purple arrows indicate the PIV and a right marginal vein (RMV), the yellow arrow indicates the CS.
- D.** MSCT scan of a patient who, besides the PIV, lacks CS tributaries. Although the ostium is rather large, more distal from the ostium the CS narrows, demonstrated on a volume rendered reconstruction (left panel) and on a curved MPR (right panel).

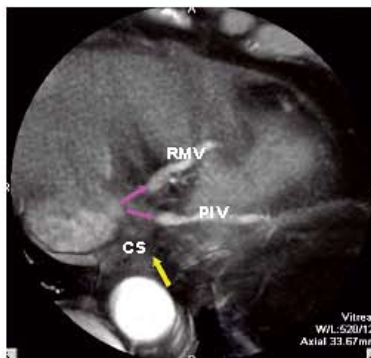
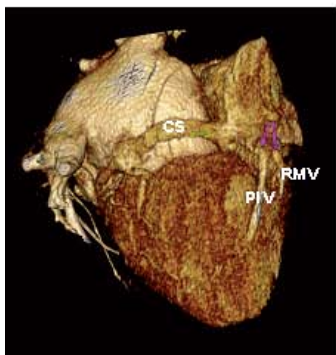
A



B



C



D

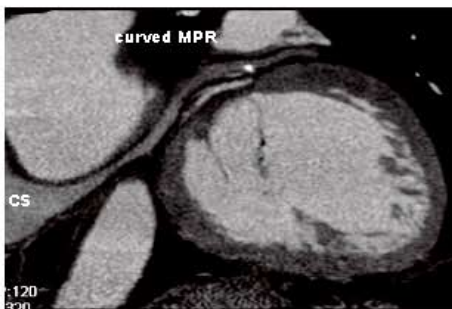


Table 1: Anatomical observations

	No HF	HF
Number of patients	28	10
Coronary sinus	28(100%)	10(100%)
Small cardiac vein	13(46%)	4(40%)
Posterior interventricular vein	28(100%)	10(100%)
Posterior vein of the left ventricle	27(86%)	9(90%)
Left marginal vein	16(57%)	7(70%)
Vein of Marshall	10(36%)	3(30%)
Posterior branches	9(32%)	4(40%)
Variant 1	8(29%)	3(30%)
Variant 2	18(64%)	6(60%)
Variant 3	2(8%)	1(10%)

HF = heart failure

Table 2: Quantative data

	No HF	HF
Ostium CS anterior-posterior (mm)	11.9±3.5	14.4±3.4
Ostium CS superior-inferior (mm)	14.7±4.4*	17.9±4.0*
Diameter LMV (mm)	2.6±1.1	5.4±1.4**
Distance PIV-PVLV (mm)	44.6±17.4 (range 13.9-76.4)	35.9±19.5 (range 6.1-59.6)
Distance PVLV-LMV (mm)	37.7±14.6 (range 14.6-68.3)	45.8±17.9 (range 21.0-64.6)
Distance PVLV-AIV (mm)	77.6±18.3 (range 50.3-122.7)	83.0±29.9 (range 40.3-117.1)
Distance LMV-AIV (mm)	44.9±16.4 (range 17.4-77.2)	46.5±14.1 (range 15.5-57.7)

* p<0.01 as compared to the diameter in anterior-posterior direction

** p<0.01 as compared to patients without HF

CS = coronary sinus, HF = heart failure LMV = left marginal vein, PIV = posterior interventricular vein, PVLV = posterior vein of the left ventricle; AIV = anterior interventricular vein

Discussion

Results of this study demonstrate an interindividual variation of the cardiac venous system in: 1) insertion and continuity of the main tributaries, 2) the number of antero/posterolateral tributaries, and 3) the distance between the main tributaries. To date, only few anatomical reports provide a detailed description of the cardiac venous anatomy⁵. Our study is the first to describe variations in cardiac venous anatomy using MSCT.

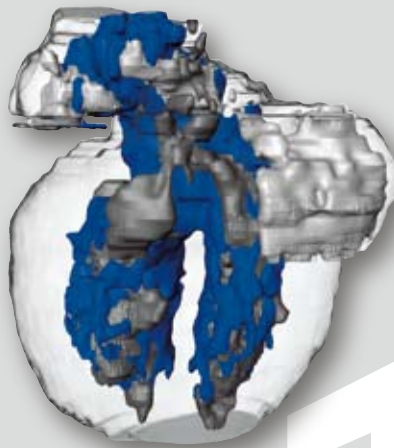
Not only the lack of suitable side branches, but also obstruction and ostial narrowing (by e.g. a Thebesian valve) may complicate LV lead implantation^{1,2,6}. In the current study, a left marginal vein was not observed in 15(39%) patients. In two of these patients, the PVLV already branched within 2 cm from the crux cordis without additional side branches. The small cardiac vein was observed in 45%, slightly more than described by Von Ludinghausen⁵. Particularly the identification of patients who lack the presence of posterolateral branches with a sufficient diameter to allow passage of a catheter or pacemaker lead may have implications for clinical practice. The variation in drainage patterns observed in the current study, largely agree with results of anatomical studies⁵. Observations from the current study also reveal a large variation in distances between the different side branches of the cardiac drainage system (**Table 2**). The finding that the coronary sinus ostium is ovally shaped agrees with observations in other cardiac veins⁷.

The vein of Marshall can be used to mark the border between the coronary sinus and the great cardiac vein⁵. At this site, the valve of Vieussens is often present, which is an important cause of problems advancing the catheter into cardiac veins⁸. In the current study, the vein of Marshall was observed in only 13 patients (34%). This finding is not surprising, since this structure is often obliterated by fibrosis.

Clinical implications: MSCT may be used to identify complex patients who do not have additional side branches on MSCT, and therefore may benefit more from an epicardial lead placement using a minimal invasive surgical approach. In addition, the site of latest LV activation, where the LV lead should ideally be positioned, can be evaluated for the presence of suitable venous anatomy preceding pacemaker implantation. Based on these findings, the clinician can beforehand decide whether a transvenous or a minimally invasive approach for LV lead positioning is preferred.

Reference List

1. Abraham WT, Hayes DL. Cardiac resynchronization therapy for heart failure. *Circulation* 2003;**108**:2596-603.
2. Puglisi A, Lunati M, Marullo AG, Bianchi S, Feccia M, Sgreccia F *et al*. Limited thoracotomy as a second choice alternative to transvenous implant for cardiac resynchronisation therapy delivery. *Eur.Heart J.* 2004;**25**:1063-9.
3. Ansalone G, Giannantoni P, Ricci R, Trambaiolo P, Fedele F, Santini M. Doppler myocardial imaging to evaluate the effectiveness of pacing sites in patients receiving biventricular pacing. *J.Am.Coll.Cardiol.* 2002;**39**:489-99.
4. Ropers D, Baum U, Pohle K, Anders K, Ulzheimer S, Ohnesorge B *et al*. Detection of coronary artery stenoses with thin-slice multi-detector row spiral computed tomography and multiplanar reconstruction. *Circulation* 2003;**107**:664-6.
5. von Ludinghausen M. The venous drainage of the human myocardium. *Adv.Anat.Embryol.Cell Biol.* 2003;**168**:I-104.
6. Vander Salm TJ. Coronary sinus cannulation: a technique to overcome an obstructing thebesian valve. *Ann.Thorac.Surg.* 1993;**56**:1441-2.
7. Wittkampfh FH, Vonken EJ, Derksen R, Loh P, Velthuis B, Wever EF *et al*. Pulmonary vein ostium geometry: analysis by magnetic resonance angiography. *Circulation* 2003;**107**:21-3.
8. Corcoran SJ, Lawrence C, McGuire MA. The valve of Vieussens: an important cause of difficulty in advancing catheters into the cardiac veins. *J.Cardiovasc.Electrophysiol.* 1999;**10**:804-8.



Chapter

10

Mario D. Gonzalez¹
Leonardo J. Contreras¹
Monique R.M. Jongbloed³
Jaime Rivera¹
Timothy P. Donahue¹
Anne B. Curtis¹
Michael S. Bailey¹
Jamie B. Conti¹
Glenn I. Fishman²
Martin J. Schalij³
Adriana C. Gittenberger-de Groot⁴

From the ¹Division of Cardiovascular Medicine, University of Florida College of Medicine, Gainesville, Florida; ²Division of Cardiology, New York University School of Medicine, New York, NY; Departments of ³Cardiology and ⁴Anatomy and Embryology, Leiden University Medical Center, Leiden, the Netherlands.

Left Atrial Tachycardia Originating From the Mitral Annulus-Aorta Junction

Circulation. 2004 Nov;110(20):3187-92

Abstract

Background: At the mitral annulus-aorta (MA-Ao) junction, the left atrium is continuous through the subaortic curtain with the musculature of the anterior mitral leaflet. Under experimental conditions, this region can generate abnormal electrical activity. In patients with left atrial tachycardia, we investigated whether this region could be the source of this arrhythmia.

Methods and Results: In 10 (28%) of 35 consecutive patients with left atrial tachycardia, the arrhythmia originated from the MA-Ao junction. Sustained, self-limited episodes of atrial tachycardia (cycle length, 340 ± 56 ms; duration, 125 ± 69 seconds) were repeatedly induced. Prematurity of the extrastimulus and time to first atrial tachycardia complex were directly correlated ($R=0.66$; $P<0.001$). During tachycardia, bipolar electrograms at the earliest site preceded onset of the P wave by 44 ± 14 ms and were of longer duration and lower amplitude than those recorded from nearby left atrial sites (52 ± 8 versus 24 ± 4 ms, $P<0.001$; and 0.53 ± 0.08 versus 3.45 ± 0.96 mV, respectively; $P<0.001$). Ablation eliminated the tachycardia with no recurrence after a mean follow-up of 24 ± 19 months. A comparative study in mouse embryos demonstrated the presence of the developing specialized conduction system in the MA-Ao region starting at embryonic age 11.5.

Conclusions: The MA-Ao junction can be a frequent source of left atrial tachycardia. This previously unrecognized site of origin may explain why catheter ablation has been less successful in eliminating left versus right atrial tachycardias. Remnants of the developing specialized conduction system could be the underlying substrate of this arrhythmia.

Introduction

Previous reports have documented that left atrial or atrial walls and, rarely, from the mitral annulus or left atrial appendage ¹⁻⁶, yet catheter ablation is less successful at eliminating tachycardias originating from the left atrium than those arising from the right atrium ², possibly because of difficulties in mapping and incomplete information about sites of origin. Although the mitral annulus-aorta (MA-Ao) junction (**Figure 1**) can be the source of arrhythmias under certain experimental conditions ⁷⁻⁹, the present study is the first to show that this region can give rise to atrial tachycardias in humans. In this report, we describe the electrophysiological characteristics of left atrial tachycardias originating from the MA-Ao junction.

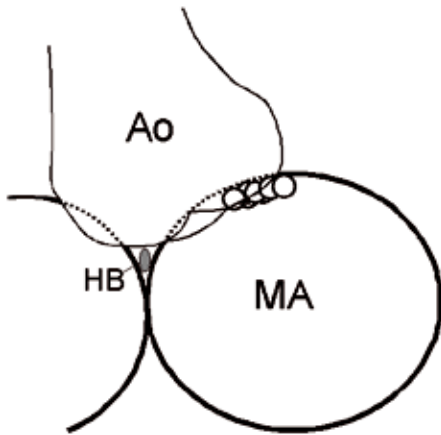


Figure 1

Schematic representation of the MA-Ao junction in the left anterior oblique projection. Dots indicate sites of atrial tachycardia origin in 10 patients. Ao indicates aorta; HB, His bundle; and MA, mitral annulus.

Methods

Patients

We analyzed 35 consecutive patients with structurally normal hearts referred for catheter ablation and in whom mapping of both atria identified a focal left atrial tachycardia. In 10 (28%) of these patients, the tachycardia originated from the MA-Ao junction. These individuals, all women (mean age, 42 ± 16 years), comprised the study population. They had documented paroxysmal atrial tachycardia for a mean of 7 ± 5 years, refractory to a mean of 3 ± 2 antiarrhythmic drugs. Patients complained of recurrent episodes of short-lasting palpitations that occurred several times a day. Five of these patients had a previous ablation attempt of a left atrial tachycardia at another institution. Their echocardiograms were normal, as required by the selection criteria (mean left atrial diameter, 31 ± 5 mm; mean ejection fraction, $57 \pm 3\%$). All patients gave written informed consent, and the University of Florida Institutional Review Board approved this study.

Electrophysiological Study

Patients discontinued antiarrhythmic medications 2 weeks before undergoing electrophysiological study. The procedure was performed with patients in the fasting state under light sedation with intravenous fentanyl and midazolam. Multipolar electrode catheters were introduced percutaneously and positioned into the right atrial appendage, right ventricle, His bundle region, and coronary sinus¹⁰. To record His bundle activation, a 7F deflectable catheter with 4 closely spaced pairs of electrodes was used. A deflectable catheter with 8 pairs of electrodes (5 mm between pairs) was advanced into the coronary sinus, with the most proximal pair of electrodes positioned at the coronary sinus ostium. Bipolar electrograms (30 to 500 Hz) and unipolar electrograms (0.5 to 500 Hz) were displayed and stored using a digital recording system (Bard Electrophysiology). Stimulation was performed at 2 to 3 times diastolic threshold, using pulses of 2-ms duration. Initially, single extrastimuli were introduced at several basic cycle lengths (400 to 600 ms). The coupling interval was decreased in 10-ms steps until atrial refractoriness was reached. If tachycardia could not be induced, rapid stimulation was used (250 to 500 ms). When required, intravenous aminophylline (6 mg/kg over a period of 30 minutes) and/or isoproterenol (1 to 4 $\mu\text{g}/\text{min}$) were given and atrial stimulation was repeated by using extrastimuli first followed by rapid stimulation. The diagnosis of atrial tachycardia was confirmed using these criteria: (1) atrial activation sequence during tachycardia different from that recorded during sinus rhythm; (2) atrial activation sequence during tachycardia different from that obtained during ventricular stimulation with retrograde ventriculo-atrial conduction; (3) A-A-V response after discontinuation of ventricular pacing¹¹; (4) induction of tachycardia independent of a critical prolongation of the A-H interval; (5) transient atrioventricular (AV) block during tachycardia; and (6) inability to obtain concealed entrainment of the tachycardia using ventricular extrastimuli. A left atrial origin of the tachycardia was suspected when

right atrial activation was earliest in the fossa ovalis, Bachmann bundle region, triangle of Koch, or coronary sinus. The morphology of the P wave was analyzed during transient AV block or after ventricular premature beats that did not alter the atrial tachycardia. The A-H interval during tachycardia was compared with that obtained during stable right atrial stimulation at identical cycle length. Access to the left atrium for mapping and ablation was obtained through the transeptal approach, using the electrode catheters as anatomic landmarks¹². A 7F quadripolar ablation catheter with a 4-mm tip electrode was introduced through a preformed 8F sheath (SL1, Daig) and advanced into the left atrium. The earliest bipolar electrogram associated with a negative unipolar deflection was considered the site of atrial tachycardia origin. Electroanatomic mapping was obtained with the Carto system (n=4) or with NavX (n=1). In 5 patients, an echocardiogram (transthoracic, 3; intracardiac, 2) was used to confirm the location of the mapping catheter in relation to the MA-Ao junction.

Radiofrequency Ablation

The earliest activation site was targeted for ablation. Radiofrequency energy (10 to 50 W; maximal temperature, 60°C) was delivered between the tip electrode and a skin patch electrode positioned under the left scapula using an EPT 1000 generator (EP Technologies). The power was progressively increased until a temperature of >50°C was reached or the tissue impedance changed >10 Ω. Atrial stimulation was repeated before, during, and after isoproterenol administration for 60 minutes to confirm elimination of the atrial tachycardia. After the procedure, patients were monitored for 24 hours in a telemetry unit.

Comparative Study of the Developing Conduction System in Mouse Embryos

To test the possibility that remnants of the developing cardiac conduction system may persist in the MA-Ao region, we used a transgenic cardiac conduction system-*lacZ* murine strain capable of delineating the developing and mature cardiac conduction system¹³. Twenty-three embryos of embryonic age (E) 9.5 to 15.5 days were stained for β -galactosidase activity, which produces a blue staining at the sites of expression. Embryos were fixed at room temperature in 5% buffered saline. They were sliced transversely and examined using light microscopy, with attention specifically focused on the region between the aorta and the atrioventricular junction.

Data Analysis

Data are reported as mean \pm SD. Values were analyzed by means of the paired and unpaired Student *t* test. The correlation between extrastimuli coupling intervals and the interval between the extrastimulus and the first tachycardia complex was analyzed by means of Pearson correlation analysis. The χ^2 test was used to compare inducibility by single extrastimuli versus rapid stimulation. A probability value of <0.05 was accepted as statistically significant.

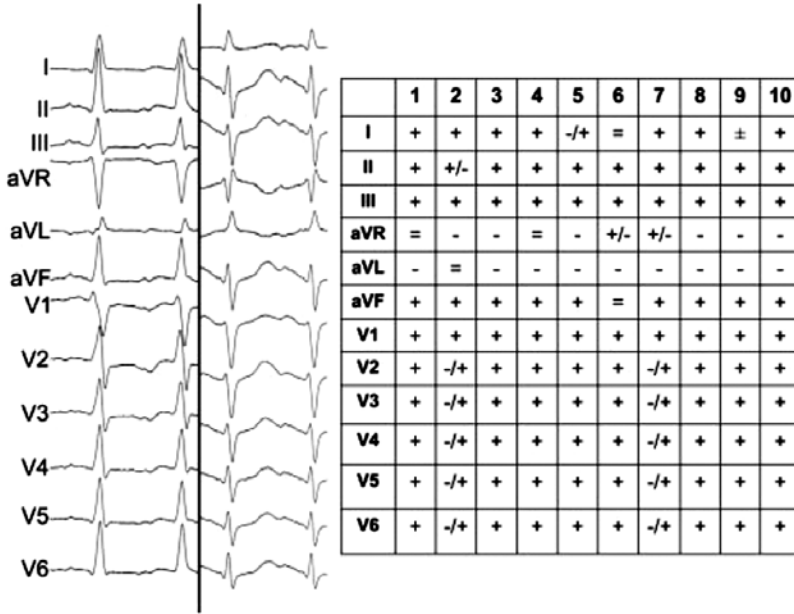


Figure 2
 Representative 12-lead ECGs from 2 patients during atrial tachycardia. P waves were of low voltage and notched. Polarity and morphology of the P wave in 10 patients are depicted in the table on right. -/+ indicates minus/plus; +/- plus/minus; and =, isoelectric.

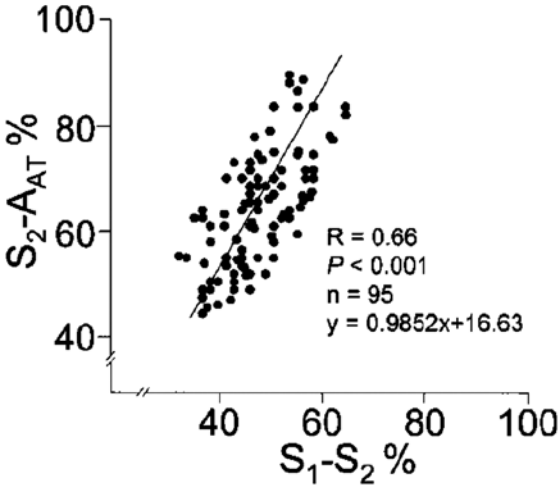


Figure 3
 Linear regression analysis of the relation between the coupling interval of the extrastimulus (S_1-S_2) and the interval between the extrastimulus and the first beat of the tachycardia (S_2-A_{AT}). All values are expressed as percentage (%) of the preceding S_1-S_1 cycle length. A direct correlation between the S_1-S_2 and the S_2-A_{AT} was observed ($P \leq 0.001$, $R = 0.66$).

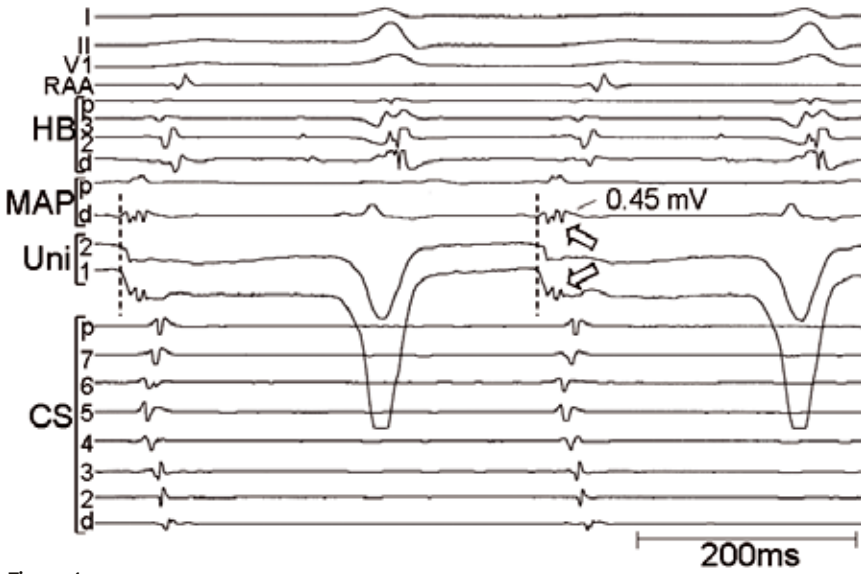


Figure 4
Fractionated, low-amplitude (0.45 mV) bipolar electrograms recorded from distal electrodes of the mapping catheter (MAPd) at the successful ablation site. Unipolar electrogram obtained from the more distal electrode (Uni 1) shows an initial negative deflection that coincides with the onset of the bipolar electrogram, followed by fractionated potentials. CS indicates coronary sinus; HB, His bundle; MAP, mapping catheter; and RAA, right atrial appendage.

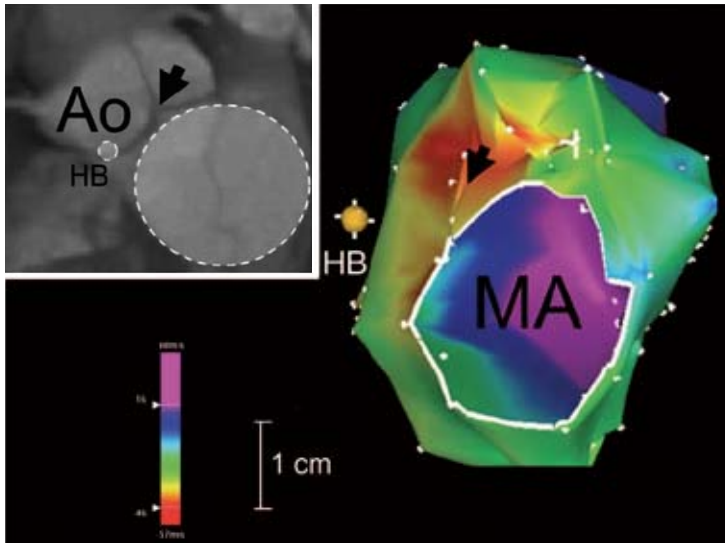


Figure 5
Sequence of left atrial activation using electroanatomic mapping during atrial tachycardia. Left upper insert shows a coronal section across the aorta and mitral annulus of a spiral CT obtained from the same patient. Earliest activation (arrow) site is located at the junction of the mitral annulus with the aorta and approximately 1 cm superior to the site where His bundle (HB) activation was recorded. Ao indicates aorta; MA, mitral annulus; and PV, pulmonary vein.

Results

Characteristics of Atrial Tachycardia

200 In 9 patients, both extrastimuli and rapid stimulation initiated atrial tachycardia; in 1 patient, only rapid stimulation induced it. Isoproterenol administration was required in 7 patients to induce tachycardia, including 2 patients who required both isoproterenol and aminophylline. During tachycardia (cycle length of 340 ± 56 ms), the P waves were of low voltage, broad, and notched, negative in aVL ($n=9/10$) and positive in leads III and V_1 ($n=10$). **Figure 2** depicts the characteristics of the P wave during atrial tachycardia. Sustained (>30 seconds), self-limited episodes of tachycardia ($n=234$) were repeatedly induced in all patients. Rapid stimulation was more successful than single extrastimuli in inducing atrial tachycardia (139 versus 95 episodes, $P<0.05$). The mean duration of atrial tachycardia was 125 ± 69 seconds (range, 30 to 242 seconds). When all episodes initiated by atrial extrastimuli were analyzed, a direct correlation was found between prematurity of the extrastimulus and the elapsing interval to the first tachycardia complex ($P<0.001$; $R=0.66$; **Figure 3**). Activation at the earliest site preceded the P wave by 44 ± 14 ms. Local bipolar and unipolar electrograms (**Figure 4**) at the earliest site were consistent with an area of slow conduction because local potentials were of longer duration and lower amplitude than those recorded from nearby left atrial sites (52 ± 8 versus 24 ± 4 ms, $P<0.001$; and 0.53 ± 0.08 versus 3.45 ± 0.96 mV, $P<0.001$; respectively). Activation at the earliest site preceded atrial activation near the His bundle by 44 ± 13 ms, at the proximal coronary sinus (up to 2 cm from the ostium) by 46 ± 15 ms, and at the right atrial appendage by 71 ± 14 ms. The A-H interval during MA-Ao atrial tachycardia was shorter than that observed during right atrial stimulation at a cycle length identical to that of the tachycardia (87 ± 34 ms versus 123 ± 27 ms, $P<0.05$), consistent with an atrial activation reaching the AV node through a left atrial input¹⁰. **Figure 5** illustrates the sequence of left atrial activation, using electroanatomic mapping during atrial tachycardia.

Atrial tachycardia terminated either spontaneously ($n=126$), because of premature atrial beats ($n=105$), or after administration of intravenous adenosine (6 mg bolus, $n=3$). In 7 patients, spontaneous termination always followed a gradual increase in cycle length ($8 \pm 2\%$ during the last 10 ± 5 cycles, 97 episodes). In 3 patients, termination of the tachycardia followed alternating long-short cycles (29 episodes, **Figure 6**).

Earliest Activation Site During Atrial Tachycardia

The origin of the tachycardia was confirmed through the use of biplane fluoroscopy (**Figure 7**). In the left anterior oblique projection, this site was situated between the 11 and 12 o'clock positions (**Figures 1 and 5**). In the right anterior oblique projection, the tip of the catheter was approximately 1 cm superior to the catheter recording His bundle activation. In 5 patients, an echocardiogram (transthoracic, 3; intracardiac, 2) confirmed that the catheter was in contact with the subaortic curtain or MA-Ao junction (**Figure 8**).

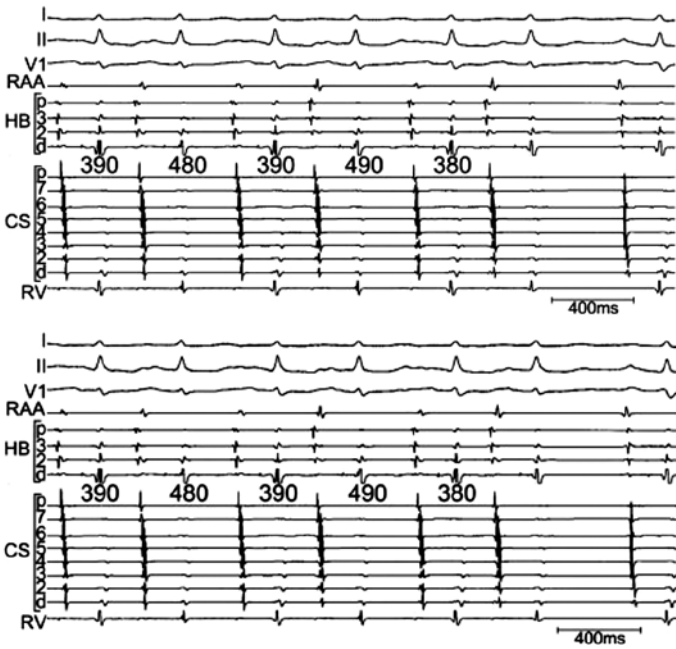


Figure 6
Spontaneous termination of atrial tachycardia preceded by beat-to-beat oscillations in cycle length. CS indicates coronary sinus; HB, His bundle; MAP, mapping catheter; and RAA, right atrial appendage. Values are in milliseconds.

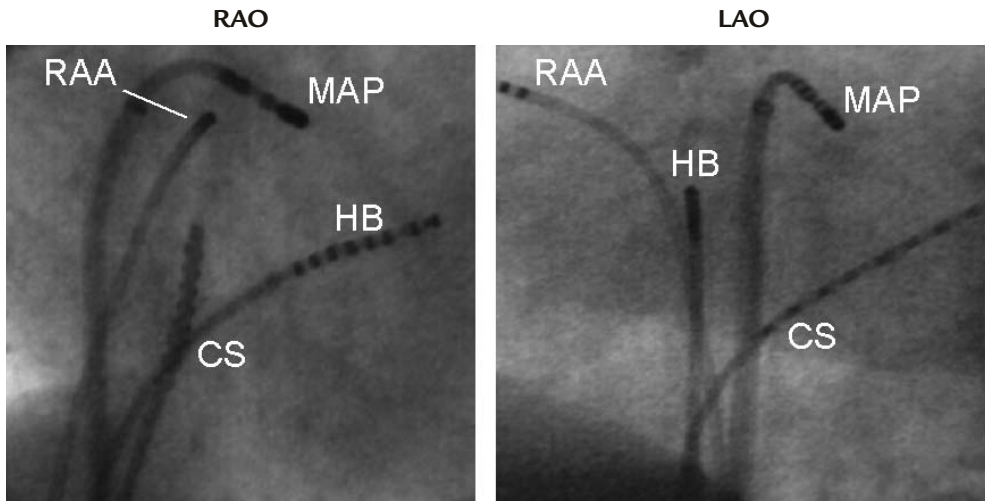


Figure 7
Position of the tip of the mapping catheter at the site of atrial tachycardia origin as viewed from the right anterior oblique (RAO) and left anterior oblique (LAO) projections. The mapping catheter (MAP) has been advanced through a preformed sheath into the left atrium after transseptal puncture and positioned at the MA-Ao junction. CS indicates coronary sinus; HB, His bundle; and RAA, right atrial appendage.

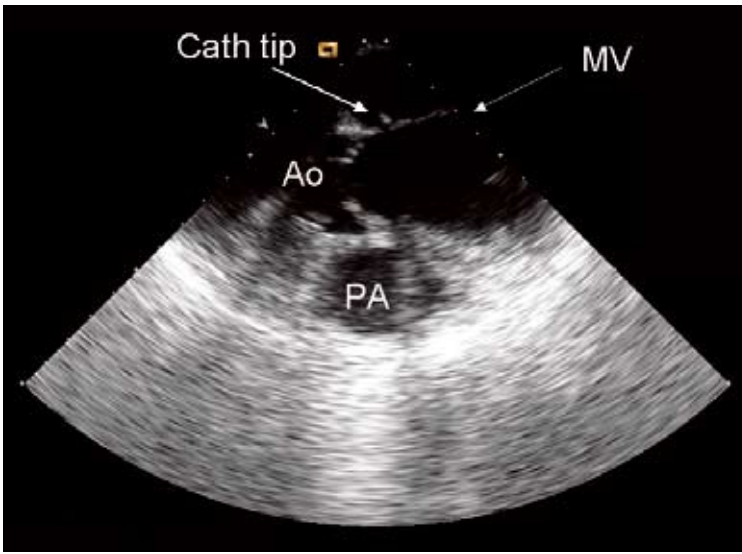


Figure 8

Intracardiac echocardiogram displaying the tip of the catheter recording the origin of the tachycardia. The tip of the catheter (arrow) is in contact with the subaortic curtain, which represents the junction of the aortic cusps and the anterior leaflet of the mitral valve. Ao indicates aorta; MV, mitral valve; and PA, pulmonary artery.

Associated Tachycardias

A concurrent tachycardia was observed in 5 patients: slow fast AV nodal reentrant tachycardia (n=2), fast-slow AV nodal reentrant tachycardia (n=1), and coronary sinus ostium atrial tachycardia (n=2).

Radiofrequency Ablation

Radiofrequency ablation at the earliest atrial activation site eliminated tachycardia in all patients after a mean of 1.4 ± 0.5 (median 1) applications of energy. Termination of atrial tachycardia occurred after a mean of 11 ± 9 (1 to 25) seconds of energy delivery. Atrial tachycardia terminated abruptly in 4, and after transient acceleration, in 6 patients. Mean power, temperature, and impedance were 33 ± 8 W, $49 \pm 3^\circ\text{C}$, and $89 \pm 5 \Omega$, respectively. No changes in AV nodal conduction were found after successful ablation. All associated tachycardias were successfully eliminated. During a follow-up period of 24 ± 19 months on no antiarrhythmic medications, no patients had recurrent tachycardia.

Developing a Murine Cardiac Conduction System

In the earliest stages examined, stage E 9.5 and E 10.5, septation between the aorta and the pulmonary artery had not occurred yet, so the outflow tract still consisted of a common trunk. Also, the AV canal was still a common canal that was situated mainly above the

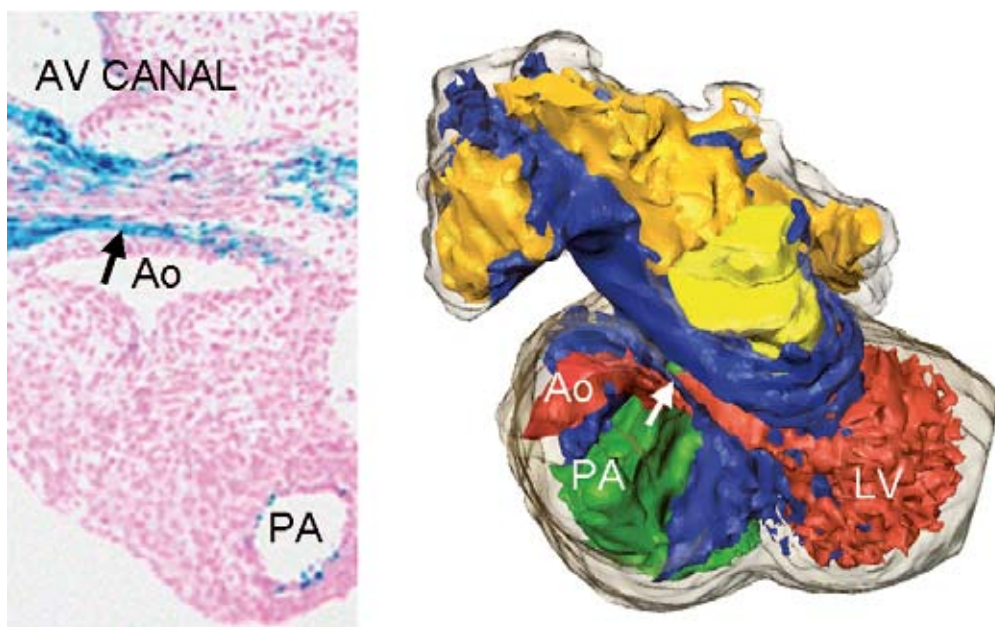


Figure 9

Observations in the *CCS-lacZ* transgenic mouse model. Left panel demonstrates a transverse section through the heart of an embryo of 12.5 days. Immunohistochemical staining was performed with a monoclonal anti-muscle actin- antibody to produce a double staining with *CCS-lacZ*. Slices were counterstained with hematoxylin. *CCS-lacZ* is present in the retroaortic position (arrow), at the junction with the AV canal. Right panel demonstrates a 3D reconstruction obtained from serial microscopic images of the same embryo, demonstrating the same bundle of *lacZ*-positive tissue (arrow). Heart is depicted from a frontal and cranial view. Different cardiac compartments are color-coded: yellow, left atrium; orange, right atrium; red, left ventricle and aorta; green, right ventricle and pulmonary artery; and blue, *CCS-lacZ* staining. Ao indicates aorta; PA, pulmonary artery; and LV, left ventricle.

primitive left ventricle. In these early stages, *CCS-lacZ* was already present at the AV canal, which became continuous with a band of *lacZ* present at the junction with the outflow tract. At stage E 11.5, a separate aorta and pulmonary trunk could be observed and at stage E 12.5 the mitral and tricuspid orifices were situated above the left and right ventricle respectively. Starting at stage E 11.5, the developing conduction system was observed running between the aorta and the mitral annulus (**Figure 9**, left panel). We created 3-D reconstruction of an embryo of age E 12.5 to visualize the distribution of *CCS-lacZ* in the MA-Ao region. In this reconstruction, a bundle of fibers running in the retro-aortic position at the junction with the AV canal is clearly demonstrated (**Figure 9**, right panel). This region corresponds to the site of origin of the atrial tachycardia observed in our patient population. At a later stage (E 15), the staining of the conduction system was markedly reduced indicating regression of this system in older embryos.

Discussion

The present study demonstrates that the MA-Ao junction can be the source of focal atrial tachycardia in patients with structurally normal hearts. This previously unrecognized site of origin might partially explain why catheter ablation has been less successful at eliminating left versus right atrial tachycardias². The presence of fractionated, low-voltage electrograms at the earliest activation site is consistent with a region of slow conduction. On the other hand, the mode of initiation of this tachycardia suggests triggered activity as the mechanism of this arrhythmia. The presence of both abnormal conduction and abnormal automaticity in this region is consistent with previous observations in animal studies⁷⁻⁹.

204

The MA-Ao Junction and the Anterior Mitral Valve Leaflet

The MA-Ao junction is not simply formed by two opposing fibrous annuli. A common structure, the subaortic curtain¹⁴⁻¹⁷, simultaneously supports 2 of the aortic cusps (left coronary and noncoronary) and the anterior leaflet of the mitral valve. In other words, at the MA-Ao junction, the left atrial wall does not join the left ventricular wall but is attached to the aorta. More important, the muscle fibers of the left atrium are continuous with those of the anterior mitral valve leaflet^{7-9,18}. Notably, microelectrode studies have shown that although the leaflet musculature resembles atrial muscle, the action potentials have AV nodal-type characteristics⁷⁻⁹. These unique properties can be explained by calcium dependent cells, responsive to adenosine and similar to AV nodal cells¹⁸. Similar to our findings in humans, experiments in animals have shown that cells from the mitral annulus and the anterior mitral leaflet can give rise to triggered activity under the influence of catecholamines⁷⁻⁹.

Characteristics of MA-Ao Atrial Tachycardia

Despite isoproterenol administration, most episodes of atrial tachycardia were self-limited, either due to spontaneous termination or after atrial premature beats. Therefore, atrial stimulation was frequently required to reinduce the tachycardia to identify the site of origin. In three patients with prolonged episodes of tachycardia, adenosine (6 mg intravenous bolus) terminated the tachycardia. This response as well as the mode of initiation suggests triggered activity. Importantly, there was a consistent relation between the coupling interval of the extrastimulus and the interval between the extrastimulus and the first beat of the tachycardia, consistent with triggered activity¹⁹.

The finding that the A-H interval was shorter during MA-Ao atrial tachycardia than during right atrial stimulation at identical cycle length is consistent with the wavefront entering the AV node using the left-sided input to the A-V node¹⁰.

Previous Studies

Matsuoka and colleagues⁶ described a patient with 2 closely located atrial tachycardias originating from what they called left anteroseptum. Their Figure 2, however, suggests the origin actually might have been the MA-Ao junction. Interestingly, they also described the presence of fractionated potentials in this region, an observation that mirrors our findings. Other authors have also shown that the mitral annulus can be the source of atrial tachycardias^{4 20 21}. The present study extends the findings made by Kistler et al.⁴ in patients with atrial tachycardia arising from the mitral annulus. These authors found that the tachycardia originated close to the mitral-aortic continuity. In our patients, the arrhythmia was shown to originate from the MA-Ao junction itself. The present study suggests that triggered activity may be the underlying mechanism and that remnants of the developing conduction system may be the substrate for this form of atrial tachycardia. The much higher incidence of tachycardias originating from the MA-Ao in our patients when compared with the Kistler study cannot be readily explained. The fact that 50% of our patients were referred after a previous failed ablation may account for the difference. Therefore, our findings represent a selected group of patients and cannot be extrapolated to the general population of individuals with atrial tachycardia.

The MA-Ao Junction and the Developing Conduction System

Previous embryological studies have suggested that the occurrence of atrial arrhythmias at specific anatomic sites may be linked to the presence of the developing conduction tissue at these sites during embryogenesis^{22 23}. In the present comparative murine embryological study, the specialized conduction system was shown to run between the aorta and the AV canal early in the development. At a later stage (E 15), the staining of the conduction system was markedly reduced indicating regression of this system in older embryos. These findings suggest that this tissue may fail to regress in some individuals and give rise to left atrial tachycardia arising from the MA-Ao junction. On the basis of these findings, we hypothesize that the occurrence of atrial tachycardias originating from the MA-Ao region may be due to persistence of the developing conduction system in this region.

Study Limitations

The mode of initiation of this form of atrial tachycardia and the effect of adenosine in two patients suggest triggered activity. However, the response to drugs or programmed electrical stimulation in the clinical electrophysiology laboratory does not necessarily identify the actual mechanism of an arrhythmia. Certainly, microreentry cannot be ruled out as the mechanism of atrial tachycardia in our patients.

206

Clinical Implications

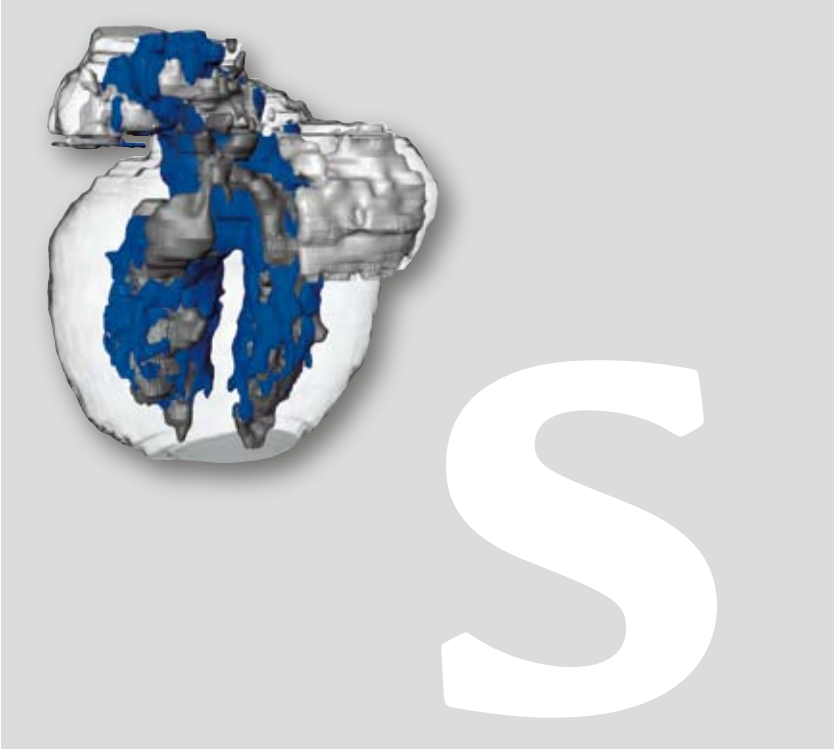
Some patients with atrial tachycardia are refractory to antiarrhythmic agents and require catheter ablation to eliminate the arrhythmia. Previous studies have shown that ablation is less successful at eliminating left atrial tachycardias compared with right atrial tachycardias. Knowledge of the most frequent sites of origin, including the MA-Ao junction, can facilitate successful ablation of these tachycardias.

Acknowledgment

The authors thank Melanie Fridl Ross, MSJ, ELS, for editing assistance. Linda Horne and Deanna Congdon provided excellent secretarial support.

Reference List

1. Chen SA, Chiang CE, Yang CJ, Cheng CC, Wu TJ, Wang SP *et al.* Sustained atrial tachycardia in adult patients. Electrophysiological characteristics, pharmacological response, possible mechanisms, and effects of radiofrequency ablation. *Circulation* 1994;**90**:1262-78.
2. Chen SA, Tai CT, Chiang CE, Ding YA, Chang MS. Focal atrial tachycardia: reanalysis of the clinical and electrophysiologic characteristics and prediction of successful radiofrequency ablation. *J Cardiovasc. Electrophysiol.* 1998;**9**:355-65.
3. Frey B, Kreiner G, Gwechenberger M, Gossinger HD. Ablation of atrial tachycardia originating from the vicinity of the atrioventricular node: significance of mapping both sides of the interatrial septum. *J Am. Coll. Cardiol* 2001;**38**:394-400.
4. Kistler PM, Sanders P, Hussin A, Morton JB, Vohra JK, Sparks PB *et al.* Focal atrial tachycardia arising from the mitral annulus: electrocardiographic and electrophysiologic characterization. *J. Am. Coll. Cardiol.* 2003;**41**:2212-9.
5. Marrouche NF, SippensGroenewegen A, Yang Y, Dibs S, Scheinman MM. Clinical and electrophysiologic characteristics of left septal atrial tachycardia. *J Am. Coll. Cardiol* 2002;**40**:1133-9.
6. Matsuoka K, Kasai A, Fujii E, Omichi C, Okubo S, Teramura S *et al.* Electrophysiological features of atrial tachycardia arising from the atrioventricular annulus. *Pacing Clin. Electrophysiol.* 2002;**25**:440-5.
7. Wit AL, Fenoglio JJ, Jr., Wagner BM, Bassett AL. Electrophysiological properties of cardiac muscle in the anterior mitral valve leaflet and the adjacent atrium in the dog. Possible implications for the genesis of atrial dysrhythmias. *Circ. Res.* 1973;**32**:731-45.
8. Wit AL, Cranefield PF. Triggered activity in cardiac muscle fibers of the simian mitral valve. *Circ. Res.* 1976;**38**:85-98.
9. Wit AL, Fenoglio JJ, Jr., Hordof AJ, Reemtsma K. Ultrastructure and transmembrane potentials of cardiac muscle in the human anterior mitral valve leaflet. *Circulation* 1979;**59**:1284-92.
10. Gonzalez MD, Contreras LJ, Cardona F, Klugewicz CJ, Conti JB, Curtis AB *et al.* Demonstration of a left atrial input to the atrioventricular node in humans. *Circulation* 2002;**106**:2930-4.
11. Knight BP, Zivin A, Souza J, Flemming M, Pelosi F, Goyal R *et al.* A technique for the rapid diagnosis of atrial tachycardia in the electrophysiology laboratory. *J Am. Coll. Cardiol* 1999;**33**:775-81.
12. Gonzalez MD, Otomo K, Shah N, Arruda MS, Beckman KJ, Lazzara R *et al.* Transseptal left heart catheterization for cardiac ablation procedures. *J Interv. Card Electrophysiol.* 2001;**5**:89-95.
13. Rentschler S, Vaidya DM, Tamaddon H, Degenhardt K, Sassoon D, Morley GE *et al.* Visualization and functional characterization of the developing murine cardiac conduction system. *Development* 2001;**128**:1785-92.
14. Cardiac chambers and internal features. In: Williams PL, ed. *Gray's anatomy: The anatomical basis of medicine and surgery.* New York, NY: Churchill Livingstone, 1995:1483-94.
15. Dean JW, Ho SY, Rowland E, Mann J, Anderson RH. Clinical anatomy of the atrioventricular junctions. *J Am. Coll. Cardiol* 1994;**24**:1725-31.
16. Gallagher JJ, Sealy WC, Cox JL. Anatomic substrates of the Wolff-Parkinson-White syndrome. In: Rosenbaum MB, Elizari MV, eds. *Frontiers in cardiac electrophysiology.* The Hague, Netherlands: Martinus Nijhoff Publishers, 1983:689-701.
17. Sonnenblick EH, Napolitano LM, Daggett WM, Cooper T. An intrinsic neuromuscular basis for mitral valve motion in the dog. *Circ. Res.* 1967;**21**:9-15.
18. McGuire MA, De Bakker JM, Vermeulen JT, Moorman AF, Loh P, Thibault B *et al.* Atrioventricular junctional tissue. Discrepancy between histological and electrophysiological characteristics. *Circulation* 1996;**94**:571-7.
19. Rosen MR. Is the response to programmed electrical stimulation diagnostic of mechanisms for arrhythmias? *Circulation* 1986;**73**:II118-II27.
20. Mallavarapu C, Schwartzman D, Callans DJ, Gottlieb CD, Marchlinski FE. Radiofrequency catheter ablation of atrial tachycardia with unusual left atrial sites of origin: report of two cases. *Pacing Clin. Electrophysiol.* 1996;**19**:988-92.
21. Nogami A, Suguta M, Tomita T, Naito S, Taniguchi K, Aonuma K *et al.* Novel form of atrial tachycardia originating at the atrioventricular annulus. *Pacing Clin. Electrophysiol.* 1998;**21**:2691-4.
22. Blom NA, Gittenberger-De Groot AC, DeRuiter MC, Poelmann RE, Mentink MM, Ottenkamp J. Development of the cardiac conduction tissue in human embryos using HNK-1 antigen expression: possible relevance for understanding of abnormal atrial automaticity. *Circulation* 1999;**99**:800-6.
23. Jongbloed MR, Schalij MJ, Poelmann RE, Blom NA, Fekkes ML, Wang Z *et al.* Embryonic Conduction Tissue. *J. Cardiovasc. Electrophysiol.* 2004;**15**:349-55.



Summary and Conclusions

Summary and Conclusions

210

This thesis starts with a **Chapter 1** that provides a general overview of the basics of cardiac development, development of the cardiac conduction system and markers for the developing cardiac conduction system. Predilection sites for the occurrence of clinical arrhythmias are discussed. Furthermore, current treatment strategies and imaging modalities are described. Thereafter, the two main parts of the thesis can be distinguished. In part I of the thesis the developing cardiac conduction system was studied and a developmental origin of clinical adult arrhythmias was hypothesized based on the spatial expression pattern of the marker *CCS-lacZ* in murine embryos. Furthermore, the incorporation of the primitive pulmonary vein in the left atrium was studied in sequential developmental stages in humans. In part II of the thesis, the treatment of clinical arrhythmias that are initiated and/or perpetuated at specific anatomical locations in the heart (particularly the pulmonary veins) guided by imaging techniques for visualisation of the substrate, was described.

Part I

In **Chapter 2** the developing CCS was studied in the murine transgenic *CCS-lacZ* model. The *CCS-lacZ* gene has been shown to be expressed in the developing and mature CCS. We observed *CCS-lacZ* expression not only in putative areas of the adult CCS, such as the sinus node, the AV node, His bundle, left and right bundle branches and Purkinje fibers, but also in specific myocardial areas that are not part of the adult cardiac conduction system. These areas include the left and right venous valves and septum spurium (internodal myocardium), the left and right AV ring, and the retro-aortic root bundle. Furthermore, *CCS-lacZ* expression was observed in a bundle of tissue running in a retro-aortic position between the left and right atrium, corresponding to the site of Bachman's bundle. All of these sites are anatomic regions that correspond to the occurrence of clinical arrhythmias in adults. Interestingly, *CCS-lacZ* expression was also observed in the dorsal wall of the left atrium. This area was continuous with the left venous valve of the sinus venosus. In later stages, expression of *CCS-lacZ* was observed in a cuff of myocardial cells surrounding the pulmonary veins. Results of this study support the hypothesis that the occurrence of cardiac arrhythmias that originate from specific anatomical sites in the heart is not random but may be related to the development of the CCS.

In **Chapter 3** a developmental origin of atrio-ventricular bypass tracts such as present in patients with Mahaim tachycardia, was hypothesized. In early cardiogenesis, the AV canal is situated entirely above the primitive left ventricle, whereas the outflow tract connects to the embryonic right ventricle. During development a right atrioventricular connection, and a connection between the left ventricle and the aorta must be established. This process

of formation of the right ventricular inflow tract was studied in relation to the developing cardiac conduction system in *CCS-lacZ* transgenic mice and it was hypothesized that the outcome of this process may provide a developmental morphological explanation for the occurrence of Mahaim tachycardia. Results of this study demonstrated that starting from embryonic day 11.5 a myocardial groove is formed in the *CCS-lacZ* positive tissue of the primary fold (the border between the embryonic right and left ventricle). Further outgrowth of this groove, concomitant with outgrowth of the right ventricular dorsal wall, resulted in a division of the *CCS-lacZ* positive primary fold tissue in a medial part, the *trabecula septo-marginalis* (that contains the right bundle branch), and a lateral part, the right ventricular *moderator band* that connected medially to the right bundle branch and could laterally be traced all the way to the lateral AV-junction, thus forming a tract bypassing the AV node. Electrophysiological testing was performed in murine embryo's aged 15.5 days in which a section was made in vertical direction through the heart, to divide the heart in a left specimen containing the AV node and the major part of the bundle branches, and a right specimen that contained the right atrium, right ventricle and the right ventricular moderator band. The isolated RA and RV were only myocardially connected at the lateral AV-junction. In 2 out of 8 embryos sequential electrical and mechanical activation of atria and ventricles was demonstrated in both RA/RV and LA/LV preparations. Morphological study of these specimens demonstrated that conduction of the electrical impulse in the right specimen could only have travelled over the lateral AV connection, along the free wall of the RA to the RV, an area corresponding to location of the right ventricular moderator band, and to the site of Mahaim fibers in humans.

In **Chapter 4** the histology of the left atrial wall in relation to the incorporation of the pulmonary veins was studied immunohistochemically in sixteen human embryos and fetuses, one neonate and five adults. Histological staining was performed to distinguish between the different tissues of the wall of the atria and the pulmonary veins. Based on histological criteria, three different compartments could be distinguished in the left atrium: the smooth-walled left atrial body with vessel wall tissue, that after incorporation of the pulmonary veins could not be distinguished from the vessel wall of the pulmonary veins; the trabeculated left atrial appendage, without vessel wall tissue; and a transitional zone in between the left atrial appendage and the left atrial body, which was smooth-walled and lacked vessel wall tissue (and that histologically resembled the sinus venarum tissue in the right atrium). The right atrial appendage, the body of the right atrium and the atrial septum were not lined by vessel wall tissue. It was hypothesized that during development, due to the incorporation process of the pulmonary veins, left sided sinus venosus tissue had shifted towards the transition with the left atrial appendage.

Furthermore, it was observed that the left atrial dorsal wall between the pulmonary veins can be poorly myocardialized or that myocardium can even be absent. It remains to be investigated whether this is correlated with the pulmonary vein incorporation into the left

atrium. The left atrial wall can, because of lack of proper myocardium, be easily damaged. Due to the incorporation process of the pulmonary veins into the left atrium, the inner wall of the left atrium is composed of vessel wall and a histological border between the left atrial body and the pulmonary veins cannot be found.

Part 2

212

In **Chapter 5** multi-slice computed tomography was used for the evaluation of the left atrium and pulmonary veins prior to radiofrequency catheter ablation surrounding the pulmonary veins in 23 patients with atrial fibrillation, and in 11 control patients without atrial fibrillation. In this chapter, a method was constructed to evaluate the atrio-pulmonary venous transition using multi-slice computed tomography. The atrio-pulmonary venous junction was evaluated in 3 different orthogonal planes and using 3-D reconstructions. Measurements in 2 perpendicular planes were performed using multi-planar reformatting. Using this standardized method, large interindividual variations in anatomy were observed. Common ostia of the left and right pulmonary veins were observed 19/23(83%) and 9/23(39%) patients respectively. Additional right pulmonary veins, presumably draining the right middle pulmonary lobe, were observed in 6/23(26%) patients, whereas a left additional vein (presumably draining the lingula area of the left lung) was observed in only 1(4%) patient. Early branching occurred more often in right vs. left pulmonary veins. There were no statistical differences in occurrence of variations between patients and controls in this study. Furthermore, it was demonstrated that pulmonary venous ostia are asymmetrically shaped. Left sided veins were significantly more oval-shaped than right-sided veins. Although size of the ostia tended to be larger in patients with atrial fibrillation than in those without atrial fibrillation, these differences were not statistically significant. Information obtained by multi-slice computed tomography was used to guide radiofrequency catheter ablation aimed outside the ostia of the pulmonary veins.

In **Chapter 6** a review of the application of intracardiac echocardiography in percutaneous interventional procedures is provided. An overview of the history of intracardiac echocardiography is given, as well as the technical requirements. Nowadays low-frequency transducers allow intracardiac echocardiography of the entire heart with an ultrasound catheter positioned solely in the right atrium or right ventricle. Clinical applications of intracardiac echocardiography include: evaluation of intracardiac thrombus, transseptal puncture, closure of atrial septal defect, guidance of interventional electrophysiological procedures (such as radiofrequency catheter ablation of atrial fibrillation, atrial tachycardia, complex atrial flutter and ventricular tachycardia), diagnostic biopsy, and visualisation of the coronary sinus. Doppler capacities allow hemodynamic measurements, such as the evaluation

of flow velocities inside the pulmonary veins prior to and after radiofrequency catheter ablation, for evaluation of the occurrence of acute pulmonary vein stenosis.

Chapter 7 describes the use of intracardiac echocardiography for the evaluation of left atrial and pulmonary vein anatomy in 31 patients admitted for radiofrequency catheter ablation outside pulmonary venous ostia. A method for evaluation of the atrio-pulmonary venous junction is described, using 2-D ultrasound planes. Using this method, a common ostium of the left and right pulmonary veins was observed in 22(71%) and 10(32%) patients respectively. Additional right pulmonary veins were observed in 6(19%) patients. Prior to the procedure, intracardiac echocardiography was used to evaluate the left atrium and left atrial appendage for the presence of thrombus. Two patients were not treated with radiofrequency catheter ablation because of suspicion of intracardiac thrombus with intracardiac echocardiography and in one patient transseptal puncture could not be performed because of an aneurysmatic septum. During the procedure, intracardiac echocardiography was used to guide transseptal puncture, to guide catheters at the pulmonary venous ostia and to continuously monitor the occurrence of acute complications. In the 28 patients treated, mean ostial diameters of right superior pulmonary veins and common ostia of left pulmonary veins were significantly smaller after radiofrequency catheter ablation. For the other veins, ostial diameters were slightly but not significantly smaller. Mean systolic peak flow velocities in pulmonary veins after radiofrequency catheter ablation were not significantly higher in any of the veins, indicating that slight narrowing of pulmonary veins directly after ablation does not have significant hemodynamic consequences.

After evaluation of the left atrium and pulmonary venous anatomy with both multi-slice computed tomography and intracardiac echocardiography, the next step was to perform a head-to-head comparison between both techniques, which is described in **Chapter 8**. In this study, performed in 42 patients, evaluations of both anatomical variations and measurements performed at the pulmonary venous ostia were compared between the 2 techniques. Results of this study demonstrated that the large interindividual variation in pulmonary vein anatomy could be demonstrated with both techniques. However, using multi-slice computed tomography as the gold standard, the sensitivity for detection of additional branches was higher for multi-slice computed tomography. Results of measurements of pulmonary venous ostia suggested an underestimation of ostial size by intracardiac echocardiography, and less accurate determination of the shape of the ostium by intracardiac echocardiography.

In **Chapter 9**, evaluation of the coronary venous system using multi-slice computed tomography is described. The coronary venous system has gained interest in recent years, both in relation to implantation of biventricular pacing devices for cardiac resynchronisa-

tion therapy, and in electrophysiological catheter ablation procedures. In a substantial number of patients cannulation of the coronary sinus and insertion of catheters is not possible due to narrowing of the coronary sinus ostium and lack of suitable side branches. Therefore anatomical information prior to these procedures is mandatory. The coronary venous system was evaluated in 38 patients. As in the pulmonary venous system, large interindividual variation was also observed in the coronary venous system. Anatomical variants were divided in 3 groups, dependent on the continuity of the cardiac venous system at the crux cordis. The most frequently observed variant had a separate insertion of the coronary sinus and the small cardiac vein in the right atrium (24(63%) patients). In 11(29%) patients, there was continuity of the anterior and posterior venous system at the crux cordis. In 3(8%) patients, the posterior interventricular vein (PIV) did not connect to the coronary sinus. Large interindividual anatomical variation in the presence of posterolateral branches and in distances between coronary sinus-tributaries was observed. Whereas the coronary sinus and the PIV were observed in all patients, the posterior vein of the left ventricle (PVLV) and the left marginal vein (LMV) were observed in 36(95%) and 23(61%) patients respectively. Furthermore, measurements of the ostia of the coronary sinus in 2 perpendicular directions using multiplanar reformatting, demonstrated an oval shape of the coronary sinus ostium.

Finally, in **Chapter 10** a correlation was made between anatomy and electrophysiology by correlating data obtained by studying *CCS-lacZ* mutant mice with clinical mapping data in patients with atrial arrhythmias. Thirty-five patients with focal left atrial tachycardia were analysed in this study. In 10 patients, the tachycardia originated from a circumscribed region at the junction between the aorta and the mitral valve. This site of origin of the atrial arrhythmias, the mitral annulus-aorta junction, correlated to the expression pattern of *CCS-lacZ* in murine embryo's, indicative of developing cardiac conduction system. Radio-frequency catheter ablation at this site eliminated the tachycardia with no recurrence after a mean follow up of 24 ± 19 months. It was hypothesised that remnants of the developing cardiac conduction system could be the underlying substrate of this arrhythmia.

Conclusions

- Sites related to the occurrence of clinically relevant cardiac arrhythmias correlate with cells positive for *CCS-lacZ*, indicative of the developing specialized cardiac conduction system.

- After formation of the right ventricular inflow tract, a *CCS-lacZ* positive tract is present that can be traced from the right bundle branch up to the lateral AV ring, corresponding to the site of Mahaim fibers in humans, thus supporting the hypothesis that these tracts may provide a morphological explanation for the occurrence of Mahaim tachycardia.

- Due to the incorporation of the pulmonary veins in the left atrium during development, there is no histological marked border or difference between the wall of the left atrium and the vessel wall of the pulmonary veins

- Multi-slice computed tomography can be used to define the atrio-pulmonary venous junction and accordingly evaluate the ostial insertion of pulmonary veins, the presence of additional pulmonary veins and early branching. Recognition of variations in pulmonary vein anatomy using a standardized method may facilitate radiofrequency catheter ablation around pulmonary venous ostia.

- Using multi-slice computed tomography as the gold standard, the sensitivity for detection of additional pulmonary venous branches is higher for multi-slice computed tomography than for intracardiac echocardiography. 3-D imaging techniques, such as multi-slice computed tomography, are required to demonstrate an asymmetric shape of pulmonary venous ostia.

- Imaging of variations in the coronary venous system is a new application of multi-slice computed tomography that may have implications for improvement of selection of patients for cardiac resynchronisation therapy.

- The junction between the mitral annulus and the aorta is a predilection site for the initiation of atrial tachycardias, and is accessible for catheter ablation.

Future perspectives

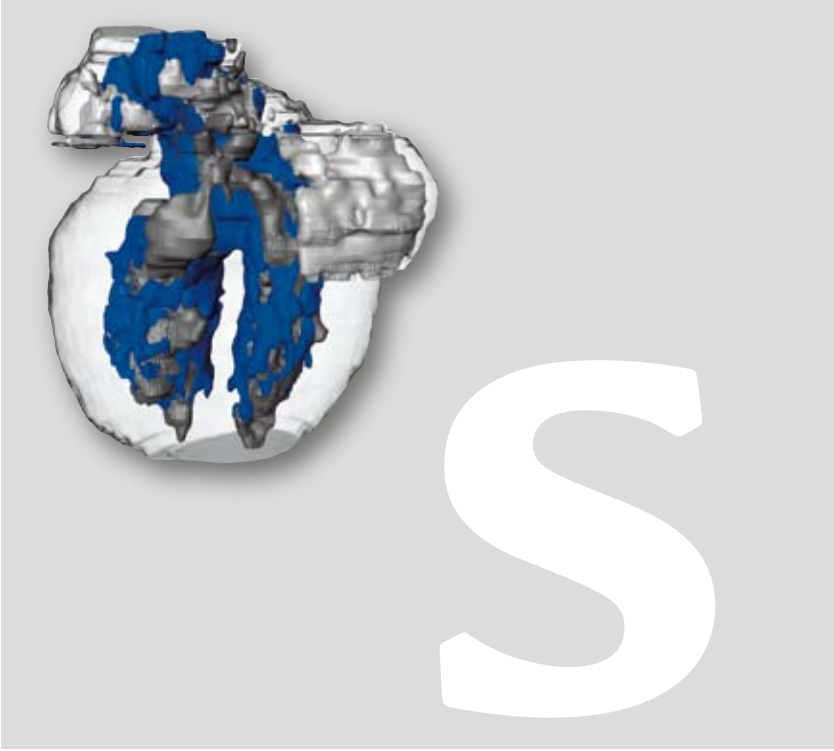
Development of the Cardiac Conduction System (CCS)

To study the developing cardiac conduction system the Leiden Research Group has thus far worked with several markers, such as HNK1 en the marker *CCS-lacZ* that was used in the studies of this thesis. It is clear that the development of the cardiac conduction system is a complex process, that does not involve a single gene, but much more likely is the result of a complex interaction between multiple genes. Future research will be aimed at the exploration and reconstruction of the expression of myocardial and cardiac conduction system markers (such as podoplanin en *Nkx2.5*) and their interaction. Also functional electrophysiological tests will help to clarify the function of different genes and factors involved in cardiac conduction system development. The correlation between anatomy and electrophysiology can be further clarified by studying electrical activation patterns and comparing results between healthy embryos and embryos with cardiac conduction system developmental anomaly.

Furthermore, the question what induces the cardiomyocyte to become either a working myocardial cell or a cardiac conduction system cell still needs further clarification. We have hypothesized in earlier studies that cardiac neural crest cells as well as epicardium derived cells, may have an indirect effect on this process. However, the exact mechanisms driving a cardiomyocyte to become either a working myocardial cell or a conduction cell, are still unclear and will be further addressed in the future.

Imaging in Electrophysiological Interventional Cardiology: The Future is Fusion.

In the clinical research performed in this thesis, multiple imaging techniques have been used parallel to facilitate radiofrequency ablation procedures. Currently, it is possible to fuse the images obtained with multi-slice CT with 3-dimensional mapping systems. Using this integrated approach, on line electrical activation maps can be directly correlated to the patient's anatomy as obtained with multi-slice CT. This new technology not only expands the possibility to integrate anatomy with electrophysiology during the treatment of atrial fibrillation, but also during the ablation of ventricular tachycardia using an endocardial or epicardial approach (Zeppenfeld, Tops et al, *Circulation* 2006-*In Press*). Furthermore, integration of activation maps with high resolution computed tomography imaging may become important in guiding implantation procedures of biventricular pacing devices, as the site of latest ventricular activation can be directly correlated to ventricular anatomy and the presence of suitable coronary veins (for implantation of the left ventricular lead) at this site. Prospective studies comparing the results in patients treated using standard angiography and treated using the integrated imaging approach, are a next step in evaluation of the efficiency of this new technique.



Samenvatting en Conclusies

Samenvatting en Conclusies

Dit proefschrift begint met een **Hoofdstuk 1** waarin een algemeen overzicht wordt gegeven van de ontwikkeling van het hart, de ontwikkeling van het geleidingssysteem, en van de huidige markers die gebruikt worden om het zich ontwikkelende cardiale geleidingssysteem te bestuderen. Verschillende voorkeursplaatsen voor het ontstaan van klinische ritmestoornissen worden besproken. Daarnaast wordt ingegaan op verschillende behandelstrategieën en beeldvormende technieken. Vervolgens worden er twee hoofddelen onderscheiden. In deel I van dit proefschrift werd het zich ontwikkelende cardiale geleidingssysteem bestudeerd. Een oorsprong van klinische volwassen ritmestoornissen werd gehypothetiseerd gebaseerd op het expressiepatroon van de marker *CCS-lacZ* in een embryonaal muismodel. Daarnaast werd de incorporatie van de primitieve pulmonaalvene bestudeerd in verschillende opeenvolgende stadia in de mens. In *deel II* van het proefschrift wordt de behandeling van klinische aritmieën, die worden geïnitieerd en/of onderhouden op specifieke anatomische lokaties in het hart beschreven, waarbij gebruik gemaakt wordt van verschillende beeldvormende technieken.

220

Deel I

In **hoofdstuk 2** werd het zich ontwikkelende geleidingssysteem bestudeerd in het transgene *CCS-lacZ* muismodel. In dit model is in het verleden is aangetoond dat de marker *CCS-lacZ* tot expressie komt in het zich ontwikkelende en volwassen geleidingssysteem. Expressie van *CCS-lacZ* werd niet alleen aangetoond gebieden behorend tot het toekomstige volwassen geleidingssysteem, zoals de sinusknoop, de AV-knoop, de bundel van His, de linker en rechter bundeltakken en de Purkinjevezels, maar ook in specifieke gebieden van myocard die geen deel uitmaken van het volwassen geleidingssysteem van het hart. Deze gebieden includeren de rechter en linker veneuze kleppen en het septum spurium (oftewel het internodale myocard), de linker en rechter AV-ring, en in een retro-aortaal verlopende bundel (de zogenaamde retro-aortic root bundle). Daarnaast werd *CCS-lacZ* expressie geobserveerd in een andere weefselbundel die in een retro-aortale positie verloopt tussen het rechter en het linker atrium, die overeenkomt met de lokatie van Bachmann's bundel. Al deze gebieden zijn anatomisch gecorreleerd aan het voorkomen van klinische ritmestoornissen bij volwassenen. Opvallend was dat *CCS-lacZ* expressie ook werd gezien in de achterwand van het linker atrium. Dit gebied was continu met de linker veneuze klep van de embryonale sinus venosus. In latere stadia werd expressie van *CCS-lacZ* tevens gezien als een uitloper van myocardcellen rondom de longvenen. De resultaten van deze studie ondersteunen de hypothese dat het voorkomen van hartritmestoornissen vanuit specifieke anatomische lokaties in het hart niet willekeurig is, maar gerelateerd zou kunnen zijn aan de ontwikkeling van het geleidingssysteem van het hart.

In **hoofdstuk 3** werd een oorsprong vanuit de ontwikkeling van atrioventriculaire verbindingen, zoals aanwezig bij patiënten met Mahaim tachycardie, gehypothetiseerd. Gedurende de vroege ontwikkeling van het hart is bevindt het atrioventriculaire kanaal zich nog geheel boven de primitieve linker ventrikel, terwijl de uitstroom van het hart aansluit op de primitieve rechter ventrikel. Gedurende de ontwikkeling moet er dus een verbinding ontstaan tussen rechter atrium en rechter ventrikel en er moet een verbinding ontstaan tussen de linker ventrikel en de aorta. De vorming van het rechter ventrikel instroom gebied werd bestudeerd in relatie tot het zich ontwikkelende cardiale geleidingsstelsel in CCS-*lacZ* transgene muizen, waarbij gehypothetiseerd werd dat het resultaat van dit proces een morfologische verklaring vanuit de hartontwikkeling kon geven voor het ontstaan van Mahaim tachycardie. De resultaten van deze studie toonden aan dat vanaf embryonale dag 11.5 een myocardiale groeve wordt gevormd in het CCS-*lacZ* positieve weefsel van de primaire plooï (de grens tussen de embryonale rechter en linker ventrikel). Verdere uitgroei van deze groeve, samen met de uitgroei van de achterwand van de rechter ventrikel, resulteerde in een splitsing van het CCS-*lacZ* positieve primaire plooï weefsel in een mediaal deel, de *trabecula septomarginalis* (die de rechter bundeltak bevat) en een lateraal deel, de *moderator band* van de rechter ventrikel, die mediaal aansloot op de rechter bundeltak en die naar lateraal toe helemaal vervolgd kon worden tot aan de laterale atrioventriculaire overgang. Op deze manier werd een atrioventriculaire verbinding gevormd buiten de AV knoop om. Elektrofysiologische test werden vervolgens uitgevoerd in muizenembryo's van 15.5 dag oud, waarin een snede was gemaakt in verticale richting door het hart, om zo het hart te verdelen in een linker preparaat, die de AV-knoop en het grootste deel van de bundeltakken bevatte, en een rechter preparaat die het rechter atrium, de rechter ventrikel en de moderator band van de rechter ventrikel bevatte. Het geïsoleerde rechter atrium en de rechter ventrikel hadden alleen myocardiale verbinding bij de laterale AV-overgang. In 2 van de 8 embryo's werd achtereenvolgende elektrische en mechanische activatie van de atria en ventrikels waargenomen in zowel de RA/RV als in de LA/LV preparaten. Morfologische studie van deze preparaten toonde aan dat de geleiding van de elektrische impuls in het rechter preparaat alleen kon hebben plaatsgevonden over de laterale atrioventriculaire verbinding langs de vrije wand van het rechter atrium naar de rechter ventrikel: een gebied dat overeenkomt met de lokatie van de moderator band van de rechter ventrikel, en met de lokatie van Mahaim verbindingen in de mens.

In **hoofdstuk 4** werd de histologie van de linker atriumwand in relatie tot de incorporatie van de pulmonaalvenen immunohistochemisch bestudeerd in 16 humane embryo's en foetussen, een neonaat en 5 volwassenen. Histologische kleuringen werden uitgevoerd om onderscheid te kunnen maken tussen de verschillende weefsels van de wand van de atria en de pulmonaalvenen. Gebaseerd op histologische criteria, konden er drie verschillende compartimenten worden onderscheiden in het linker atrium: het gladwandige corpus van het linker atrium met vaatwandweefsel, dat na incorporatie van de pulmonaalvenen niet kon

worden onderscheiden van de vaatwand van de pulmonaalvenen; het getrabeculariseerde linker hartoor, zonder vaatwand weefsel; en een overgangszone tussen het linker hartoor en het lichaam van het linker atrium, dat gladwandig was en geen vaatwand bezat (en histologische het meest leek op het sinus venarum weefsel van het lichaam van het rechter atrium). Het rechter hartoor, het corpus van het rechter atrium en het atriumseptum waren niet bedekt met vaatwand. Er werd gehypotheetiseerd dat gedurende de ontwikkeling, ten gevolge van het incorporatie proces van de pulmonaalvenen, linkszijdig sinus venosus weefsel verplaatst is richting de overgang met het linker hartoor. Verder werd geobserveerd dat de linker atrium achterwand tussen de pulmonaalvenen soms matig van myocard voorzien is zijn of dat het myocard zelfs afwezig kan zijn. Of dit verschijnsel gecorreleerd is met de pulmonaalvene incorporatie in het linker atrium, verdient nader onderzoek. De linker atrium wand kan gemakkelijk worden beschadigd door het ontbreken van voldoende myocard. Ten gevolge van het incorporatieproces van de pulmonaalvenen in het linker atrium bestaat de binnenwand van het linker atrium uit vaatwand en er is geen histologische grens waarneembaar tussen het corpus van het linker atrium en de pulmonaalvenen.

Deel II

In **hoofdstuk 5** werd multi-slice computed tomografie (MSCT) gebruikt voor de evaluatie van het linker atrium en de pulmonaalvenen voorafgaand aan radiofrequente catheter ablatie rondom de pulmonaalvenen in 23 patiënten met boezemfibrilleren en in 11 controle patiënten zonder boezemfibrilleren. In dit hoofdstuk werd een methode ontwikkeld om de atrio-pulmonaal veneuze overgang te evalueren, gebruikt makend van multi-slice computed tomografie (multi-slice CT). De atrio-pulmonaal veneuze overgang werd geëvalueerd in 3 verschillende orthogonale vlakken en met behulp van 3-D reconstructies. Metingen in 2 orthogonale vlakken werden verricht met behulp van de techniek van multi-planar reformatting. Gebruik makend van deze gestandaardiseerde methode, werden grote inter-individuele anatomische variaties geobserveerd. Gemeenschappelijke ostia van de linker en rechter pulmonaalvenen werden gezien in respectievelijk 9/23(83%) en 9/23(39%) van de patiënten. Extra rechter pulmonaalvenen, waarschijnlijk ten behoeve van drainage van de rechter middenkwab, werden gezien in 6/23 (26%) patiënten, terwijl een additionele linker vene (waarschijnlijk het lingula gebied van de linker long drainerend) werd geobserveerd in slechts 1(4%) patiënt. Vroege vertakkingen van longvenen kwamen vaker voor in rechter versus linker pulmonaalvenen. Er werden geen statistisch significante verschillen gevonden in het voorkomen van variaties tussen patiënten en controle personen in deze studie. Daarnaast werd aangetoond dat de ostia van pulmonaalvenen asymmetrisch van vorm zijn. Linkszijdige venen zijn significant meer ovaal gevormd dan rechtzijdige venen. Hoewel de grootte van de ostia een trend naar vergroting in personen met boezemfibrilleren vertoonden, waren de verschillen in grootte tussen beide groepen niet significant. De informatie

verkregen door multi-slice CT werd gebruikt ter begeleiding van radiofrequente catheter ablatie rondom de ostia van de pulmonaalvenen.

Hoofdstuk 6 geeft een overzicht van de toepassingen van intracardiale echocardiografie in percutane interventieprocedures. Een overzicht van de geschiedenis van intracardiale echocardiografie wordt gegeven, evenals de technische vereisten. Tegenwoordig kan met de laagfrequente transducers intracardiale echocardiografie van het gehele hart plaatsvinden met een echocatheter gepositioneerd in het rechter atrium of in de rechter ventrikel. Klinische toepassingen van intracardiale echocardiografie omvatten: evaluatie van de aanwezigheid van intracardiale trombus, transseptale punctie, sluiting van atriumseptum defecten, het begeleiden van electrofysiologische procedures (zoals radiofrequente catheter ablatie van boezemfibrilleren, boezemtachycardie, complexe boezemflutter en ventrikeltachycardie), diagnostische biopsie en visualisatie van de sinus coronarius. Doppler eigenschappen maken hemodynamische metingen mogelijk, zoals de evaluatie van stroomsnelheden in de pulmonaalvenen voorafgaand aan en na radiofrequente catheter ablatie, ter beoordeling van het ontstaan van acute pulmonaalvene stenose.

Hoofdstuk 7 beschrijft het gebruik van intracardiale echocardiografie voor de beoordeling van het linker atrium en pulmonaalvene anatomie bij 31 patiënten die werden opgenomen voor het ondergaan van radiofrequente catheter ablatie rondom de pulmonaalvene ostia. Een methode voor de beoordeling van de atrio-pulmonaal veneuze overgang wordt beschreven, gebruik makend van 2-D echovlakken. Met deze methode werd een gemeenschappelijk ostium van de linker en rechter pulmonaalvenen geobserveerd in 22(71%) and 10(32%) patiënten respectievelijk. Additionele rechter pulmonaalvenen werden geobserveerd in 6(19%) patiënten. Voorafgaande aan de procedure werd intracardiale echocardiografie gebruikt ter beoordeling van het linker atrium en het linker hartoor op de aanwezigheid van een trombus. Twee patiënten werden niet behandeld met radiofrequente catheter ablatie vanwege verdenking op een intracardiale trombus met intracardiale echocardiografie, en in één patiënt kon geen transseptale punctie worden verricht vanwege een aneurysmatisch septum. Gedurende de procedure werd intracardiale echo gebruikt voor het begeleiden van de transseptale punctie, het begeleiden van catheters bij de pulmonaalvene ostia en voor het continu bewaken van het optreden van acute complicaties. In de 28 patiënten die behandeld werden, waren de gemiddelde diameters van de rechter bovenste pulmonaalvenen en van de gemeenschappelijke ostia van de linker pulmonaalvenen significant kleiner na radiofrequente catheter ablatie. De diameters van de ostia van de andere venen waren in geringe mate, doch niet significant kleiner. De gemiddelde piek-systolische stroomsnelheden in de pulmonaalvenen na radiofrequente catheter ablatie waren niet significant hoger in alle venen, erop wijzend dat een lichte vernauwing van de pulmonaalvenen direct na de procedure geen significante hemodynamische consequenties heeft.

Na de beoordeling van het linker atrium en de pulmonaalvene-anatomie met zowel multi-slice CT als met intracardiale echocardiografie, was de volgende stap het uitvoeren van een directe vergelijking tussen beide technieken, hetgeen wordt beschreven in **hoofdstuk 8**. In deze studie, uitgevoerd in 42 patiënten, werden zowel de observatie van het voorkomen van anatomische variaties als de metingen verricht bij de pulmonaalvene ostia vergeleken tussen beide technieken. De resultaten van deze studie laten zien dat er grote interindividuele variatie kan worden aangetoond met beide technieken. Echter, als multi-slice CT gebruikt wordt als de gouden standaard, is de gevoeligheid voor het aantonen van extra pulmonaalvene takken groter voor multi-slice CT dan voor intracardiale echocardiografie. De resultaten van de metingen van de pulmonaalvene ostia suggereren een onderschatting van de grootte van de ostia, en een minder nauwkeurige bepaling van de vorm van het ostium door intracardiale echocardiografie.

In **hoofdstuk 9** wordt de beoordeling van het coronaire veneuze systeem door multi-slice CT beschreven. Het coronair veneuze systeem is de afgelopen tijd toenemend in de aandacht gekomen, zowel in relatie tot de implantatie van biventriculaire pacemakers in het kader van cardiale resynchronisatie therapie, als bij electrofysiologische catheter ablatie procedures. In een aantal patiënten is cannulatie van de sinus coronarius en het opvoeren van catheters niet mogelijk ten gevolge van vernauwing van het sinus coronarius ostium en een gebrek aan geschikte zijtakken. Derhalve kan het verkrijgen anatomische informatie voorafgaand aan deze procedures nodig zijn. Het coronaire veneuze systeem werd geëvalueerd in 38 patiënten. Zoals ook gezien werd in het pulmonaal veneuze systeem, werd er in het coronair veneuze systeem een grote interindividuele variatie in anatomie geobserveerd. Anatomische varianten werden verdeeld in 3 groepen, afhankelijk van de continuïteit van het coronaire veneuze systeem bij de crux cordis. De meest frequent geobserveerde variant liet een aparte inmonding zien van de sinus coronarius en de small cardiac vein (SCV) in het rechter atrium (24(63%) patiënten). In 11(29%) patiënten was er continuïteit van het anteriore en posterioire veneuze system bij de crux cordis. In 3(8%) patiënten, was er geen verbinding van de posterior interventricular vein (PIV) met de sinus coronarius. Grote interindividuele anatomische variaties in de aanwezigheid van posterolaterale takken en in afstanden tussen aftakkingen van de sinus coronarius werden geobserveerd. Terwijl de sinus coronarius en de PIV werden geobserveerd in alle patiënten, werden de posterior vein of the left ventricle (PVLV) en de left marginal vein (LMV) geobserveerd in 36(95%) en 23(61%) patiënten respectievelijk. Daarnaast toonden metingen van de ostia van de sinus coronarius in 2 perpendiculaire richtingen met behulp van multiplanare reformatting, een ovale vorm van het sinus coronarius ostium aan.

Tenslotte werd er in **hoofdstuk 10** een correlatie gemaakt tussen anatomie en electrofysiologie door data verkregen door studie van *CCS-lacZ* muizen te correleren met klinische mapping data bij patiënten met atriale ritmestoornissen. Vijfendertig patiënten met focale

linker atrium tachycardiën werden geanalyseerd in deze studie. In 10 patiënten origineerde de tachycardie uit een circumscripde regio bij de overgang tussen de aorta en de mitralisklep. Deze plaats van herkomst van atriale ritmestoornissen, the mitralis annulus-aorta overgang, correleerde met het expressie patroon van *CCS-lacZ* in muizenembryo's, indicatief voor zich ontwikkelend cardiaal geleidingssysteem. Radiofrequente catheter ablatie op deze plaats bij de tachycardie patiënten elimineerde de tachycardie zonder recidief bij een gemiddelde follow-up van 24 ± 19 maanden. Er werd gehypothetiseerd dat overblijfselen van het zich ontwikkelende cardiale geleidingssysteem het onderliggende substraat zouden kunnen zijn van deze ritmestoornissen.

Conclusies

226

- Anatomische lokaties in het hart die gerelateerd zijn aan het voorkomen van klinisch relevante hartritmestoornissen, correleren met het voorkomen van CCS-lacZ positieve cellen, wijzend op gebieden van zich ontwikkelend cardiaal geleidingssysteem.
- Na vorming van het instroomgebied van de rechter ventrikel, is er een CCS-lacZ positieve verbinding aanwezig die kan worden vervolgd van de rechter bundeltak tot aan de laterale atrioventriculaire ring, die overeenkomt met de anatomische lokatie van Mahaim verbindingen in mensen, hetgeen de hypothese ondersteunt dat deze verbindingen een morfologische verklaring kunnen vormen voor het voorkomen van Mahaim tachycardie
- Ten gevolge van de incorporatie van de pulmonaalvenen in het linker atrium gedurende de ontwikkeling, is er geen histologisch duidelijke overgang of verschil tussen de wand van het linker atrium en de vaatwand van de pulmonaalvenen.
- Multi-slice CT kan worden gebruikt om de atrio-pulmonaal veneuze overgang te definiëren en aldus de ostiale inmonding van de pulmonaalvenen, de aanwezigheid van additionele pulmonaalvenen en vroege vertakkingen te beoordelen. Herkenning van de variaties in pulmonaalvene anatomie met behulp van een gestandaardiseerde methode, kan radiofrequente catheter ablatie rondom pulmonaalvene ostia faciliteren.
- Met gebruik van multi-slice CT als de gouden standaard, is de sensitiviteit voor detectie van additionele pulmonaalvene taken hoger voor multi-slice CT dan voor intracardiale echocardiografie. 3-D beeldvormende technieken, zoals multi-slice CT, zijn nodig voor het aantonen van een asymmetrische vorm van pulmonaalvene ostia.
- Beeldvorming van variaties in het coronair veneuze system is een nieuwe toepassing van multi-slice CT die gevolgen kan hebben voor de verbetering van de selectie van patiënten voor cardiale resynchronisatie therapie.
- Het overgangsgebied tussen de mitralisklep annulus en de aorta is een voorkeursgebied voor het optreden van atriale tachycardieën, en is toegankelijk voor catheter ablatie.

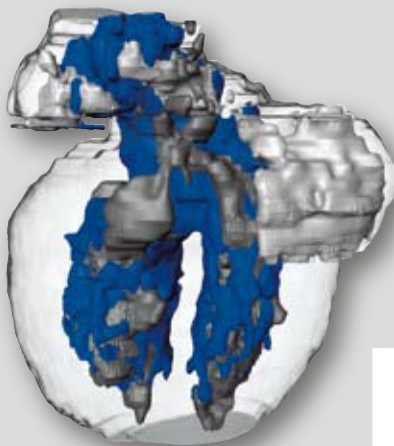
Toekomstperspectieven

Ontwikkeling van het cardiale geleidingssysteem

Voor studie van het zich ontwikkelende cardiale geleidingssysteem heeft de onderzoeksgroep in Leiden tot nog toe gewerkt met verschillende markers, zoals HNK1 en de marker *CCS-lacZ* die gebruikt werd in de studies van dit proefschrift. Het is duidelijk dat de ontwikkeling van het cardiale geleidingssysteem een complex proces is, waarbij niet een gen betrokken is, maar dat veel waarschijnlijker het resultaat is van de complexe interactie tussen verschillende genen. Toekomstig onderzoek zal zich richten op de reconstructie van de expressie van myocardiale en cardiale geleidingssysteem markers (zoals podoplanine en *nkx2.5*) en hun interactie. Daarnaast zullen functionele electrofysiologische tests helpen om de functie van verschillende genen en factoren betrokken bij de ontwikkeling van het geleidingssysteem op te helderen. De correlatie tussen anatomie en electrofysiologie kan verder worden verlicht door studie van elektrische activatiepatronen en het vergelijken van resultaten tussen gezonde embryo's en embryo's met ontwikkelingsanomalieën van het cardiale geleidingssysteem. Een andere vraag die opheldering verdient is wat de cardiomyocyt induceert om zich te ontwikkelen tot ofwel een werkmyocardcel, danwel een cardiale geleidingscel. In onze eerdere studies werd gehypothetiseerd dat cardiale neurale lijst cellen, evenals van het epicardium afgeleide cellen, een indirect effect op dit proces zouden kunnen hebben. Het exacte mechanisme dat ervoor zorgt dat de cardiomyocyt zich ontwikkelt tot een werkmyocardcel of een geleidingscel, is echter onduidelijk en zal in de toekomst nadere aandacht krijgen.

Beeldvorming bij electrofysiologische interventie procedures: "The Future is Fusion"

Bij het klinische onderzoek verricht in dit proefschrift, werden multiple beeldvormende technieken parallel gebruikt ter facilitaire van radiofrequente catheter ablatie procedures. Momenteel is het mogelijk om de beelden verkregen met multi-slice CT, te fuseren met 3-dimensionele mapping systemen. Gebruik makend van deze geïntegreerde benadering, kunnen online activatiemaps direct gecorreleerd worden met de anatomie van de patiënt, verkregen met multi-slice CT. Deze nieuwe technologie breidt niet alleen de mogelijkheden uit om anatomie met electrofysiologie te correleren gedurende de behandeling van boezemfibrilleren, maar ook gedurende de ablatie van ventriculaire tachycardie gebruik makend van een endocardiale of epicardiale benadering (Zeppenfeld, Tops et al, *Circulation* 2006-*In Press*). Daarnaast kan integratie van activatiemaps met hoog-resolutie multi-slice CT belangrijk worden voor het begeleiden van de implantatie van biventriculaire pacemakers, gezien het feit dat de plaats van laatste activatie direct gecorreleerd kan worden aan de ventriculaire anatomie en de aanwezigheid van geschikte coronaire venen (voor de implantatie van de linker ventrikel lead) op deze lokatie. Een volgende stap in de evaluatie van deze techniek is het verrichten van prospectieve studies ter vergelijking van de resultaten bij patiënten behandeld met gebruik van standaard angiografie met de resultaten bij patiënten waarbij gebruik werd gemaakt van de geïntegreerde beeldvorming benadering.



P

List of Publications

List of Publications

Radiofrequency Catheter Ablation of Paroxysmal Atrial Fibrillation; Guidance by Intracardiac Echocardiography and Integration with Other Imaging Techniques

M.R.M. Jongbloed, J.J. Bax, M.S. Dirksen, N.M.S. de Groot, H.J. Lamb, A. de Roos, E.E. van der Wall, M.J. Schalij
Eur J Echocardiogr. 2003; **4**(1):54-58

Noncompaction Cardiomyopathy

M.R.M. Jongbloed, J.J. Bax, M.J. Schalij, E.E. Van der Wall
Netherlands Heart Journal. 2003; **11**(10):416-417

230

Intracardiac Metastasis of a Merkel Cell Carcinoma

M.R.M. Jongbloed, B.L.J. Kanen, M. Visser, H. Niessen, M.J. Flens, R.J.L.F. Loeffeld
J Clin Oncol. 2004; **22**(6):1153-6

Embryonic Conduction Tissue: A Spatial Correlation with Adult Arrhythmogenic Areas. Transgenic CCS-lacZ Expression in the Cardiac Conduction System of Murine Embryos

M.R.M. Jongbloed, M.J. Schalij, R.E. Poelmann, N.A. Blom, M.L. Fekkes, Z. Wang, G.I. Fishman, A.C. Gittenberger-de Groot
J Cardiovasc Electrophysiol. 2004; **15**(3):349-355

Thrombus in the Left Atrial Appendage Detected by Intracardiac Echocardiography

M.R.M. Jongbloed, J.J. Bax, E.E. van der Wall, M.J. Schalij
Int J Cardiovasc Imaging. 2004; **20**(2): 113-116

Radiofrequency Catheter Ablation of Ventricular Tachycardia Guided by Intracardiac Echocardiography

M.R.M. Jongbloed, J.J. Bax, A.E. Borger van der Burg, E.E. Van der Wall, M.J. Schalij
Eur J Echocardiogr. 2004; **5**(1):34-40

Anatomical Observations of the Pulmonary Veins with Intracardiac Echocardiography and Hemodynamic Consequences of Narrowing of Pulmonary Vein Ostial Diameters after Radiofrequency Catheter Ablation of Atrial Fibrillation

M.R.M. Jongbloed, J.J. Bax, K. Zeppenfeld, E.E. van der Wall, M.J. Schalij
Am J Cardiol. 2004; **93**(10):1298-302

The Neural Crest is Contiguous with the Cardiac Conduction System in the Mouse Embryo: A Role in Induction?

R.E. Poelmann, M.R.M. Jongbloed, D.G. Molin, M.L. Fekkes, Z. Wang, G.I. Fishman, T. Doetschman, M. Azhar, A.C. Gittenberger-de Groot
Anat Embryol (Berl). 2004; **208**(5):389-93

Left Atrial Tachycardia Originating From The Mitral Annulus-Aorta Junction

M.D. Gonzalez, L.J. Contreras, M.R.M. Jongbloed, J. Rivera, T.P. Donahue, A.B. Curtis, M.S. Bailey, J.B. Conti, G.I. Fishman, M.J. Schalij, A.C. Gittenberger-de Groot
Circulation. 2004; **110**(20):3187-92

Atrial Fibrillation: Multi-Detector Row CT of Pulmonary Vein Anatomy Prior to Radiofrequency Catheter Ablation – Initial Experience

M.R.M. Jongbloed, M.S. Dirksen, J.J. Bax, E. Boersma, K. Geleijns, H.J. Lamb, E.E. van der Wall, A. de Roos, M.J. Schalij
Radiology. 2005; **234**(3):702-9

Multi-slice Computed Tomography versus Intracardiac Echocardiography to Evaluate the Pulmonary Veins Prior to Radiofrequency Catheter Ablation of Atrial Fibrillation: A Head-to-head Comparison

M.R.M. Jongbloed, J.J. Bax, H.J. Lamb, M.S. Dirksen, K. Zeppenfeld, E.E. van der Wall, A. de Roos, M.J. Schalij
J Am Coll Cardiol. 2005;**45**(3):343-50

Non-invasive Visualization of the Cardiac Venous System Using Multi-Slice Computed Tomography

M.R.M. Jongbloed, H.J. Lamb, J.J. Bax, J.D. Schuijf, A. de Roos, E.E. van der Wall, M.J. Schalij
J Am Coll Cardiol. 2005;**45**(5):749-53

Development of the Right Ventricular Inflow Tract and Moderator Band; Possible Morphological and Functional Explanation for Mahaim Tachycardia

M.R.M. Jongbloed, M.C.E.F. Wijffels, M.J. Schalij, N.A. Blom, R.E. Poelmann, A. van der Laarse, M.M.T. Mentink, Z. Wang, G.I. Fishman, A.C. Gittenberger-de Groot
Circ Res 2005;**96**(7):776-83

Clinical Applications of Intracardiac Echocardiography in Interventional Procedures

M.R.M. Jongbloed, M.J. Schalij, K. Zeppenfeld, P.V. Oemrawsingh, E.E. van derWall, J.J. Bax
Heart. 2005;**91**(7):981-90

Fusion of Multi-Slice Computed Tomography Imaging with Three-Dimensional Electroanatomical Mapping to Guide Radiofrequency Catheter Ablation Procedures

L.F. Tops, J. J. Bax, K. Zeppenfeld, M.R.M. Jongbloed, H.J. Lamb, E.E. van der Wall, M.J. Schalij
Heart Rhythm. 2005 Oct;**2**(10):1076-81.

Histology of Vascular-Myocardial Wall of Left Atrial Body after Pulmonary Venous Incorporation

Y.L. Douglas*, M.R.M. Jongbloed*, A.C. Gittenberger-de Groot, D. Evers, P. Voigt, M.M. Bartelings, M.J. Schalij, T. Ebels, M.C. DeRuiter
Am J Cardiol 2006;**97**(5):662-70

Clinical Applications of Cardiac Multi-Slice Computed Tomography

J.D. Schuijf, M.R.M. Jongbloed, J.W. Jukema, H.J. Lamb, E.E. van der Wall, A. de Roos, and J.J. Bax
Current Medical Imaging Reviews 2005

Contrast Echocardiography as a Useful Additional Diagnostic Tool in Evaluating a Primary Cardiac Tumor

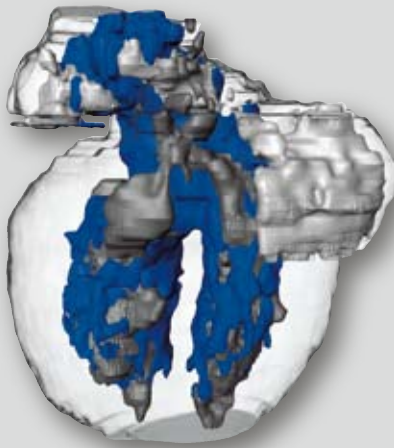
M.C. Haverkamp, A.J. Scholte, E.R. Holman, M.R.M. Jongbloed, E.F. Schippers, A. de Roos, E.E. van der Wall, D. Poldermans D, J.J. Bax, M.J. Schalij
Eur J Echocardiogr. 2005;**6**(5):388-91

Fusion of Multislice Computed Tomography Imaging with Three-Dimensional Electroanatomic Mapping to Guide Radiofrequency Catheter Ablation Procedures.

L.F. Tops, J.J. Bax, K. Zeppenfeld, M.R.M. Jongbloed, H.J. Lamb, E.E. van der Wall, M.J. Schalij
Heart Rhythm 2005;**2**(10):1076-81

Effect of Radiofrequency Catheter Ablation for Atrial Fibrillation on Left Atrial Cavity Size.

Tops LF, Bax JJ, Zeppenfeld K, Jongbloed MR, van der Wall EE, Schalij MJ.
Am J Cardiol. 2006 Apr 15;**97**(8):1220-2



A

Acknowledgements

Acknowledgements

Al er iets is wat ik geleerd heb gedurende de periode van mijn promotie, is het wel de kracht van een goede samenwerking. Graag zou ik hieronder een aantal mensen willen bedanken voor hun steun en bijdrage aan deze promotie.

De medewerkers van het secretariaat Cardiologie: Lya, Talitha, Linda en Saskia, en de research verpleegkundigen Renée, Josien en Saskia: hartelijk dank voor de leuke sfeer en praktische ondersteuning de afgelopen jaren. Het cathkamer personeel wil ik hartelijk danken voor de uitleg en gezelligheid tijdens de (soms langdurige) procedures. De medewerkers van de computergroep: Tom, Hylke, en ook Rens en Henk: bedankt voor jullie crisisinterventies! Alle medeonderzoekers in de tuin dank ik voor de steun en gezelligheid. Joanne Schuijf, ik ben blij dat ik me regelmatig voor vragen op CT-gebied tot jou kon wenden. Laurens Tops, dank je voor het delen van je kennis over de image fusion. Sander Molhoek, hartelijk dank voor het beantwoorden van de vragen over alle praktische dingen die nodig waren om de promotie af te ronden. De kamergenoten op C4, Natasja de Groot, Renée van Wamelen en Philippine Kiès. Natasja, jij bent de eerste die mij wegwijst maakte op de afdeling. Ook voor jou is het eind in zicht! Lieve Renée, jij hebt ons er met jouw warme persoonlijkheid allemaal van tijd tot tijd doorheen gesleept. Phil, onze promotie- en opleidingstrajecten lopen parallel. Het was erg prettig om in de afgelopen jaren van alles met elkaar te kunnen overleggen. De medewerkers van de afdeling Anatomie & Embryologie wil ik hartelijk danken voor de gezellige sfeer en alle steun die ik ondervonden heb. Joke van Bente, het was heel fijn dat ik me altijd tot jou kon wenden voor het maken van afspraken en voor praktische tips. Marco de Ruiter. Beste Marco, ik heb er erg van genoten om met jou te “brainstormen”, ik hoop dat we ook in de toekomst nog zullen samenwerken. Yvonne Douglas, het was heel leuk en stimulerend om met je samen te werken. Het begin van jouw proefschrift is er nu ook! Monica Menink, hartelijk dank voor al je inspanningen, zowel bij het verwerken van alle CCS-*lacZ* hartjes, als bij het uitvoeren van de electrofysiologische metingen. Jan Leeflang, dank voor je hulp bij het verwerken van al het materiaal van de humane harten. Bert Wisse: dank voor je hulp en geduld bij het bewerken van de 3-dimensionele reconstructies op AMIRA en voor je hulp bij het kiezen van de cover figuur. Jan Lens: veel dank voor je enorme inzet en professionaliteit bij het produceren van een groot aantal van de figuren die dit proefschrift rijk is. Ron Slagter en Bas Blankenvoort dank ik voor het maken van de schematische tekeningen in de verschillende hoofdstukken in deel I van het proefschrift.

De medewerkers en de röntgenlaboranten van de afdeling Radiologie dank ik voor de samenwerking en voor de ondersteuning bij het maken van de Multi-Slice CT scans.

Mario Gonzales. Dear Mario, thank you for your enthusiasm. It was very nice to collaborate with you on Chapter 10 of this thesis. I hope we can work together again in the future.

I would like to thank Dr. Glenn Fishman for giving me the opportunity to work at his lab for 6 months. Dina Myers, thank you so much for teaching me so many lab basics. Besides that you have been a wonderful friend and it was a lot of fun exploring New York with you. All other researchers in the “Fishman and Morley lab”: thank you for a fantastic time and the opportunity to learn during all the journal clubs, lab meetings and the daily practice. Lenore Block, thank you for your hospitality and warmth. I admire your critical mind, your spirit and your humor.

Collega's in het Flevoziekenhuis: Marc, Nienke, Sander D, Sander B, Suzanne, Julia, Nadine en Roos: hartelijk dank voor de flexibiliteit als ik voor “de regedingen” van de promotie tijd nodig had. Ser Peters. Ser, je bent een prettige opleider, je schept een sfeer die het prettig maakt om te vragen en te leren. Jij, Jan Baars en Robin Hes zijn zeer prettige supervisors geweest, met veel gevoel voor de patiënten, waardoor ik altijd met plezier naar mijn werk ging. Ik dank jullie en de andere internisten in de maatschap hartelijk daarvoor.

Klaas! Manuel! In de afgelopen jaren hebben jullie altijd naast mij gestaan. Het sprak voor mij vanaf het begin van de promotie al voor zich dat bij ik jullie ook bij de verdediging van mijn proefschrift naast mij wilde hebben staan. Ik ben dan ook erg gelukkig met jullie als paranimfen! Ik hoop dat onze bijzondere vriendschap zich nog vele jaren zal voortzetten.

Lieve Monique, ook jij bent al jaren een grote steun, (waar op aarde je ook verkeerde). Ik bewonder je grenzeloze optimisme, en je enthousiasme werkt iedere keer weer aanstekelijk. Ook Marscha, Tanja en Annemarie dank ik voor de jarenlange vriendschap. Ik kijk altijd erg uit naar onze lunches/diners/thee-afspraken, die altijd weer relativerend werken.

Riet Brouwer. Lieve Riet, zonder jouw steun was ik waarschijnlijk niet in de gelegenheid geweest om überhaupt aan de studie geneeskunde te beginnen. Ik wil je uit de grond van mijn hart bedanken voor alles wat je voor mij gedaan hebt en voor je warme ondersteuning. Ik wens je alle goeds voor de toekomst.

Lieve Arjan, ook jou wil ik bedanken voor de vele jaren van liefdevolle steun, die er zeker toe hebben bijgedragen dat ik uiteindelijk deze weg heb kunnen inslaan.

Mijn ouders. Lieve Frank en Hilly, ik dank jullie voor alle onvoorwaardelijk liefde en voor het feit dat jullie altijd achter mij hebben gestaan en vertrouwen hadden in de keuzes die ik maakte. Ik ben jullie heel dankbaar voor die liefdevolle basis en voor alle steun die ik van jullie, en van Arno en Heike ontvangen heb in de afgelopen jaren. Ward en Annemieke, en Sacha, ik prijs me heel gelukkig met jullie. Gideon, veel dank voor het meedenken. Lieve Evelien en Maarten, de manier waarop jullie mij hebben verwelkomd in jullie gezin is hartverwarmend. Ik ben heel blij dat jullie er zijn!

Lieve Aart, waar zal ik beginnen...



Curriculum Vitae

Curriculum Vitae

238

De auteur van dit proefschrift is geboren op 20 april 1972 in Alkmaar. In 1991 deed zij eindexamen VWO aan het Bonhoeffer College te Castricum. In 1992 startte zij met de studie Geneeskunde aan de Vrije Universiteit in Amsterdam, in 1997 behaalde zij haar doctoraalexamen en in 2000 heeft zij het artsexamen (cum laude) afgelegd. Achtereenvolgens werkte zij daarna als AGNIO neurologie en als AGNIO Interne Geneeskunde, Pulmonologie en Cardiologie. In 2002 begon zij als AGIKO Cardiologie in het Leids Universitair Medisch Centrum (prof. Dr E.E. van der Wall en Prof. Dr. M.J. Schalij). Zij deed klinisch wetenschappelijk onderzoek onder leiding van Prof. Dr. M.J. Schalij en Prof. Dr. J.J. Bax, gericht op de behandeling van hartritmestoornissen door middel van catheter-ablatie begeleid door beeldvormende technieken. Daarnaast verrichtte zij basaal onderzoek onder leiding van Prof Dr. A.C. Gittenberger-de Groot (afdeling Anatomie en Embryologie van het LUMC) met name gericht op het zich ontwikkelende geleidingssysteem van het hart. De resultaten van dit onderzoek staan beschreven in dit proefschrift. In december 2005 won zij hiervoor C.J. Kok prijs. Van oktober 2005 tot en met maart 2006 werkte zij in het laboratorium van Dr. Glenn Fishman aan de New York University mee aan een project betreffende de genetische determinanten van de ontwikkeling van het geleidingssysteem van het hart. Recent heeft zij haar vooropleiding Interne Geneeskunde afgerond in het Flevoziekenhuis te Almere (Opleider Dr. S.H.A Peters). Per 1 april 2006 vervolgt zij haar opleiding Cardiologie in het Leids Universitair Medisch Centrum (Opleider Prof. Dr. E.E. van der Wall). Naast het vervolgen van de klinische opleiding Cardiologie, zal zij zich in de toekomst blijven bezighouden met wetenschappelijk onderzoek.

